Structure Determination and Biochemical Characterization of the Protein Ubiquitin Ligases SCF^{Fbw7} and APC

Dissertation

In fulfillment of the requirements for
the degree of

doctor rerum naturalium (Dr. rer. nat.)

submitted to the
Faculty of Mathematics and Natural Sciences,
Martin-Luther-University Halle-Wittenberg, Germany

by Stephanie Schumann
date of birth, 13.04.1977 in Wippra, Germany

Reviewing Professors
1. Prof. Dr. Milton T. Stubbs
2. Prof. Dr. Nikola P. Pavletich
3. Prof. Dr. Stefan Jentsch

Halle (Saale), 4. October 2007

urn:nbn:de:gbv:3-000012609
[http://nbn-resolving.de/urn/resolver.pl?urn=nbn%3Ade%3Agbv%3A3-000012609]

I dedicate this work to my parents,

Rosemarie and Gerd Oehlmann

Parts of this work are in preparation for publication.

Oehlmann, S., Hao, B., Sowa, M., Harper, W.J., and Pavletich, N.P.. Structure of a Fbw7-Skp1-CyclinE Complex: Multisite-Phosphorylated Substrate Recognition by SCF Ubiquitin Ligases. Mol. Cell, submitted for publication.

Acknowledgements

I would like to thank everyone who provided me with assistance and support during the time in which I completed this thesis. I am most grateful to Nikola Pavletich, who allowed me the opportunity to work on a range of very interesting and challenging projects. I am also thankful for the scientific support that he provided and the freedom that he gave me to explore my own scientific considerations.

I would like to thank the Slaon Kettering Institute for the financial support.

I would also like to thank all of the past and present members of the Pavletich Lab for the helpful discussions, for their support, the parties, the friendly working atmosphere, and for all of the other help that they gave me along the way. I want to especially thank Bing Hao.

I want to thank the staff at the MSKCC Protein Sequencing Facility for the help they gave me in analyzing my protein sequences.

I would like to address a particularly special thank you to David King for helping me with the mass spectroscopy analysis.

I also want to express a particular thank you to my sister, Maren, for encouraging me to complete this thesis.

I am also very thankful to Tino, who supported me in the good times and cheered me up in the bad times, and above all else, for his love. I also want to thank my children, Sophie and Albert, for their long naps.

Last but not least, I would like to thank my parents and my friends for their continual support.

Declaration

I declare that the writing of this thesis was completed independently and without the help of others. All literature used in this work is cited. This thesis has never previously been submitted for a higher degree.

March 2007, Waiblingen Stephanie Schumann

List of Abbrevations

aa	amino acid
AcNPV	*Autographa californica* nuclear polyhedrosis virus
Amp^r	Ampicilin resistent
APC	Anaphase Promoting Complex
APS	ammonium persulfate
ATP	adenosine triphosphate
bp	base pair
BSA	bovine serum albumin
BTB	broad-complex,Tram-track and Bric-a-Brac
BTP	bis tris propane
Cdk	Cyclin dependent kinase
CIP	Calf intestine alkaline phosphatase
c-Myc	myeloctyomatosis
CPD	consensus phosphobinding degron/motif
CTD	C-terminal domain
CV	column volume
DD	dimerization-defective
DMSO	dimethylsulphoxide
DNA	deoxyribonucleic acid
dNTP	deoxyribonucleotides triphosphate
DTT	1,4-dithio-D,L-threitol
E. coli	*Escherichia coli*
EDTA	Ethylen-diamine-tetraacetic acid
ERK	extracellular receptor kinase
FBP	Fbox protein
FPLC	Fast protein liquid Chromatography
GSK3	glycogen synthase kinase-3
GST	Glutathione-S-Transferase
h	human, hour
Hi5	High Five
H2O	distilled water
HPLC	High performance liquid chromatography
IPTG	isopropyl-ß-D-thiogalactopyranoside
ITC	Isothermal Titration Calorimetry
kbp	Kilo base pair
Kd	Dissociation-constant
kDa/MDa	Kilo Dalton/Mega Dalton
L	liter
LiSO4	Lithium sulfate
MCS	multiple cloning site
min	minute
ml	milliliter
mt/mut	mutant
MW	molecular weight
NaCl	sodium chloride
nm	nanometer
NTD	N-terminal domain
OD	optical density
P	phosphate group/passage
PAGE	polyacrylamide gel electrophoresis
PCR	polymerase chain reaction
PEG	polyethylene glycol
pI	isoelectric point
PMSF	phenyl-methane-sulphonylfluoride
RBS	ribosome binding side
rpm	revolutions per minute
RT	room temperature
Sc	*Saccharomyces cerevisiae*
SCF	Skp1-Cul1-Rbx1-Fbox protein
SDS	sodium dodecyl sulfate
sec	second
SF9	*Spodoptera frugiperda*
Skp1	S-phase-kinase-associated protein-1
SOCS	suppressor of cytokine signaling
Sp	*Schizosacchromyces pompe*
TAE	Tris Acetate EDTA
TEMED	N,N,N'N'-tetramethyl-ethylendiamine
TFA	trifluoroacid
U	unit
UPS	Ubiquitin proteasome system
UV-light	ultraviolet light
v/v	volume per volume
w/v	weight per volume
wt	wild type
µl	microliter
λ	wavelength
°C	degree celsius
Δ	internal deletion

List of Figures

List of Tables

1. Introduction

1.1 Eukaryotic cell cycle control and cancer

The central function of the eukaryotic cell cycle is the production of exact replicas of the parent cells. Therefore, the chromosomes have to be duplicated and segregated equally to the mother and daughter cell. The eukaryotic cell cycle can be divided into four phases: In the G1-phase (gap1-phase) cells prepare for DNA-synthesis. During S-phase (synthesis-phase), chromosomes are duplicated. In the G2-phase (gap2-phase) cells prepare for cell division. In M-phase (mitosis) the chromatide of the duplicated chromosomes are segregated and equally distributed to the mother and daughter cells. Furthermore, cytokinesis takes place, resulting in two identical cells (Murray and Hunt, 1993). To conserve the genetic information from one cell generation to the next, the cell has to ensure a faultless completion of each cell cycle phase. Genetic alterations, especially in genes such as those in pro-oncogenes and tumor suppressor genes (Bishop, 1989), products that are involved in growth control, cell cycle regulation and apoptosis (Weinberg, 1989) are found commonly in cancer cells. The central question is: How is the progression of the cell cycle regulated in order to maintain genetic integrity?

One piece of the puzzle was discovered in 1982 by Tim Hunt and coworkers, who identified a protein in rapidly dividing sea urchin embryos that was destroyed during each cell division (Evans et al., 1983). Because of its cyclic expression pattern it was termed Cyclin, and it was suggested that its degradation might be important for cell cycle regulation (Evans et al., 1983). Today we know that the cell cycle dependent degradation of Cyclins and many other cellular proteins is important for the regulation of cellular functions and is mediated by the Ubiquitin-proteasome system.

1.2 Ubiquitin-proteasome system (UPS)

The function of the UPS is to ubiquitinate and to degrade target proteins. For this purpose, the pre-cursor-form of ubiquitin needs to be cleaved by the protease activity of the deubiquitinating enzymes (reviewed by Amerik and Hochstrasser, 2004) resulting in the mature form of ubiquitin, which exposes a conserved C-terminal glycine-glycine motif. Ubiquitin is a highly conserved 76 amino acid protein (Vijay-Kumar et al., 1987), which

exhibits regulatory functions while covalently bound to specific target proteins (Hershko and Ciechanover, 1998). Ubiquitination of a target protein involves a three-step enzymatic cascade (Hershko et al., 1983; Pickart, 2001). First, a free mature ubiquitin is activated by an ubiquitin-activating enzyme (E1), which uses ATP to form an E1-ubiquitin thioester between E1s active site cysteine and the C-terminal glycine residue of ubiquitin. In the second step, the activated ubiquitin is transferred by the formation of a new thioester linkage to an active-site cysteine on the ubiquitin-conjugating enzyme (E2). Finally, the ubiquitin is conjugated by the ubiquitin-protein ligases (E3) to the target protein by forming an isopeptide bond between the C-terminus of ubiquitin and the ε-amino group of a lysine residue on the target protein (Figure 1.1).

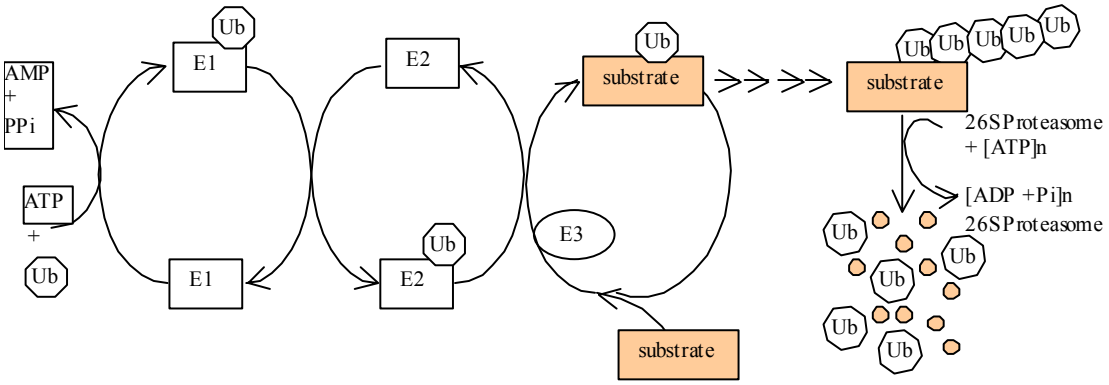

Figure 1.1. The ubiquitin-proteasome system.

Ub, ubiquitin; E1, Ub-activating enzyme; E2, Ub-conjugating enzyme; E3, Ub-ligating enzyme. Substrate is recognized by E3 and polyubiquinated with the ATP-dependent E1-E2-E3 enzyme cascade. The polyubiquitinated substrate is recognized and degraded by the 26S proteasome.

Depending upon how the ubiquitin is transferred to a substrate, the ubiquitin-protein ligases are divided into two main groups. The HECT-type E3 ligases form an ubiquitin thioester intermediate via their cysteine in the active site, and the ubiquitin from E2 before transferring the ubiquitin to the target protein (Schneffner et al., 1994), whereas in the RING-type E3 ligases the ubiquitin is directly transferred from the E2 to the substrate (Borden, 2000; Jackson et al., 2000). Regardless of what kind of mechanism is used for the ubiquitin transfer to the substrate, E3s are important for substrate recognition, substrate ubiquitination as well as for E2 recruitment. E3 ligases induce the formation of a polyubiquitin chain by repeatedly conjugating another activated ubiquitin moiety to the ε-amino group of ubiquitin

Lys48 (Pickart, 2000). The polyubiquitinated target protein is then shuttled, recognized and degraded by the 26S proteasome, a ~2.5 MDa ATP-dependent protease complex consisting of a 20S catalytic core and two 19S regulatory complexes (Hochstrasser, 1996; Hershko, 1997; Coux et al., 1996; Baumeister et al., 1998; Elsasser et al., 2004; Richly et al., 2005; Verma et al., 2004). The degradation of the ubiquitinated protein by the 26S proteasome leads to the release of free reusable ubiquitin (Lam et al., 1997), whereas the protein is cleaved into small peptides (3-23 amino acids) (reviewed by Yao and Cohen, 1999). The small peptides are then either further degraded to single amino acids or are presented to the immune system by the MHC class I molecules (Stoltze et al., 2000).

For general cell cycle progression, two related large oligomeric RING-type E3 ubiquitin ligases have a prominent role, the Anaphase Promoting Complex (APC) and the Skp1-Cul1-Fbox (SCF) complex. Both selectively target and polyubiquitinate proteins that have fulfilled their cellular function and are no longer needed by the cell. Whereas cell cycle regulation by the APC occurs intrinsic of the ligase itself, cell cycle regulation by the SCF is usually mediated by substrate phosphorylation. The proteolysis of the polyubiquitinated target proteins by the 26S proteasome is irreversible, which guides the cell unidirectional through the cell cycle. The E3 ligases APC and SCF, particularly the SCF complexes with the Fbox proteins Fbw7 and Skp2, are very important for the regulation of the cell cycle progression.

1.3 SCF protein ligase

1.3.1 Composition and architecture of the SCF protein ligase

The SCF complex is a multisubunit ubiquitin ligase composed of four subunits: S-phase-kinase-associated protein-1 (Skp1), cullin 1 (Cul1), the RING-box protein-1 (Rbx1) also known as Hrt1 or Roc1 and the Fbox protein (FBP) (Feldman et al., 1997; Skowyra et al., 1997; Kamura et al., 1999; Kipreos et al., 1996; Ohta et al., 1999; Tan et al., 1999). The Skp1, Cul1 and Roc1 subunits are invariant components of the SCF complex, whereas the substrate specificity is determined by the variable part of FBPs. The invariant Fbox domain, which is an ~40 amino acid motif of the FBPs, was first identified in human Cyclin F and termed the family as FBPs (Bai et al., 1996). The Fbox motif interacts with the C-terminus of the adaptor protein Skp1, which links the FBPs to the SCF complex (Deshaies, 1999). FBPs

consist of a very large versatile group of proteins (~70 FBPs in human, Bateman et al., 2004) that interact with substrates through their C-terminal protein-protein interaction domain. The C-terminal protein-protein interacting domains of the FBPs have been classified according to their structural motif and are followed by a numerical identifier (Cenciarelli et al., 1999; Winston et al., 1999; Jin et al., 2004). So far, three FBP-classes have been distinguished between: The FBWs are FBPs with WD40 repeat domains, also known as the Trp-Asp motif. Each WD40 repeat domain consists of ~40 amino acids and forms the first three β-sheets of one blade and the last β-sheet of the next blade. This fold assembles into a WD40 domain structure such as in budding yeast Cdc4, β-Trcp1 and Fbw7. The FBLs are FBPs containing leucine-rich repeats (LRR). This structural motif contains leucine in a regular occurrence and the domain folds in an arc shaped α-β-repeat structure such as in Skp2. All other FBPs belong to the class of FBXs, which exhibit a structure motif varying from WD40 domain or LRR domain structure. Each FBP binds to a specific subset of substrates. FBWs and FBLs recognize mainly phosphorylated substrates, whereas FBXs recognize for example N-glycanylated substrates (reviewed by Cardozo and Pagano, 2004).

A typical quaternary SCF complex is assembled in a C-shaped superstructure, as shown in Figure 1.2. In that SCF^{Skp2} complex (the superscript denotes the FBP Skp2) the

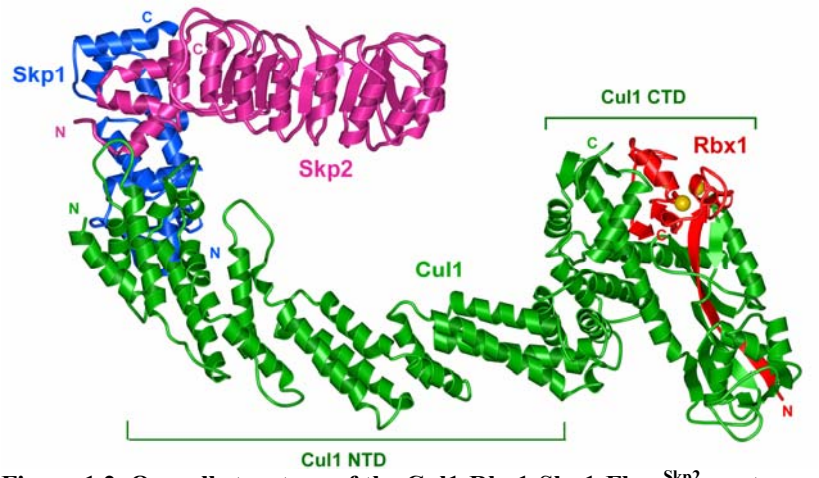

Figure 1.2. Overall structure of the Cul1-Rbx1-Skp1-$Fbox^{Skp2}$ quaternary complex.

Cul1, Rbx1, Skp1 and the $Fbox^{Skp2}$ are colored in green, red, blue and magenta respectively (copied from Zheng et al., 2002).

NTD-part of the scaffold protein Cul1 adopts to a long stalk-like structure and binds with the N-terminal tip of the first repeat to the Skp1-$Fbox^{Skp2}$ complex. Interestingly, the amino

residues Pro113 and Glu 115 of $Fbox^{Skp2}$ helix1, which directly interact with the NTD-part of Cul1 are conserved among most FBPs (Zheng et al., 2002). The CTD-part of Cul1 folds into a globular α/β domain and interacts with the incorporated 16 residue β-strand of Rbx1. Rbx1 is also responsible for E2 recruitment (Zheng et al., 2002; Pickart, 2001).

Modelling the E2 subunit to the SCF^{Skp2} complex (Zheng et al., 2002) shows that the Skp2 C-terminal LRR domain and the active cysteine site of the E2 point to each other. Based on this model, the distance between E2 and Skp2 C-terminal LRR domain is about 50 Å. It has been proposed that the transfer of E2 ubiquitin could overcome the 50 Å distance by the binding of Skp2 substrate p27 to Skp2 C-terminal LRR through p27 phospho-threonine 187. And p27 lysine residues 134, 153, 165 are proposed to be involved in its ubiquitination (Shirane et al., 1999; Zheng et al., 2002). One interesting feature of the SCF structure is the imposed rigidity of Cul1 that has been shown to be crucial for the activity of the SCF complex. The introduction of a flexible linker into Cul1 neither abolished binding of the Skp1-$Fbox^{Skp2}$ complex nor inhibited E2 recruitment by Rbx1, but it disrupted the ability of the SCF complex to ubiquitinate substrates, probably due to incorrect positioning of the donor E2-ubiquitin and acceptor substrate towards each other (Zheng et al., 2002). This model is supported by the finding that deletion or lengthening in budding yeast Cdc4 helices H5 and H6, which link the Fbox and WD40 domain, disrupts the critical orientation of the substrate bound to the WD40 domain towards E2 and abolishes ubiqitination *in vivo* (Orlicky et al., 2003). Furthermore, the finding that the FBP β-Trcp1 acts as a homodimer (Suzuki et al., 1999) has initiated discussion concerning the possibility that the SCF complex may also act in oligomerization states.

In addition to the SCF complex, SCF-like complexes have also evolved. All of the identified SCF-like complexes maintain reaction specificity by utilizing one of the cullin subunits 1 to 7 and Roc1 as their catalytic core and an E2 binding site for direct ubiquitin transfer from E2 to the substrate (Joazeiro and Weissman, 2000). The diversity in SCF-like complexes is achieved by subunits or domains, which mimic the fold of Skp1, as in elongin C and the BTB/POZ domain (Furukawa et al., 2003; Schulman et al., 2000). The adaptor protein elongin C recruits the SOCS-box proteins (SBPs), similar to the FBPs, to the SCF-like complex, which mediate substrate specificity (Zheng et al., 2002; Hilton et al., 1998). Proteins of the BTB/POZ-family combine the properties of Skp1 and FBPs in a single

polypeptide-chain and directly interact with both cullins and specific substrates (Krek, 2003). Surprisingly, all SCF ligases, SCF-like ligases and the single subunit HECT ubiquitin ligases (Huang et al, 1999) show an ~50 Å distance between the donor and acceptor entities (hot zone). The universal adaptation of E3 ligases underlines the importance of this system for the cell and suggests that apart from the different substrate recognition mechanisms, the fundamental process of the ubiquitin transfer to the substrate is likely to be the same.

1.3.2 Function and regulation of the SCF protein ligase

The SCF complexes regulate the ubiquitination of substrates, which primarily led to the G1/S-phase transistion. Such substrates are the regulatory subunits Cyclin E and Cyclin D of Cyclin-dependent kinases (Cdks); the Cyclin kinase inhibitors (CKI) Sic1, p21 and p27 or the Wnt signal transducer β-catenin. Other substrates are the FBPs β-Trcp1, Cdc4 and Emi1, as well as the transcription factor c-Myc (reviewed by Cardozo and Pagano, 2004). Structural and biochemical studies on the SCF complex have elucidated the way in which some substrates bind to their FBPs, how the SCF helps to transfer ubiquitin from the E2 to the substrate and how the SCF activity is regulated.

Studies on the individual FBPs Fbw7, β-Trcp1 and Skp2 elucidated that their C-terminal interacting domain recognizes a specific subset of protein substrates when these substrates are posttranslational modified by phosphorylation. The specific targeting of phosphorylated substrates by their FBPs is a prerequisite for the substrates subsequent ubiquitination and degradation by the UPS. As previously pointed out (Introduction, 1.3.1) the precise arrangement of the individual subunits of the SCF complex is crucially important for the ubiquitin transfer from E2 to the substrate. To gain an insight into how the SCF complex might bridge the proposed ~50 Å distance between the FBP and the opposite E2 active site (Zheng et al., 2000) a recruitment model was proposed, based on differential amino acid spacing between the acceptor lysine and the doubly phosphorylated destruction motif D[pS]GØX[pS] (Ø representing a hydrophobic and X any amino acid) of β-catenin peptides, which is a substrate of the FBP β-Trcp1 (Wu et al., 2003). They found that binding of β-catenins doubly phosphorylated destruction box to β-Trcp1 WD40 domain was unaffected by the varying lengths of the peptides. Interestingly, subsequent ubiquitination assays revealed that the effectiveness of the ubiquitination of the acceptor lysine was strongly

dependent on the lysine to destruction motif spacing. In agreement with random polymer theory (Creighton, 1993 and references therein), it was suggested that one criterion is the amino acid spacing that allows optimal presentation of the acceptor lysine to the E2 active site. Moreover, it seems that SCF catalyses ubiquitination by increasing the effective concentration of the specific lysine at the E2 active site (Wu et al., 2003, Zheng et al., 2002). Another important aspect is the regulation of SCF activity. It has been elucidated that most cullin proteins are covalently modified (neddylated) with the ubiquitin-like molecule Nedd8/Rub1 near the E2 binding site, (Figure 1.3) (Pan et al., 2004; Hori et al., 1999;

Cullins		Neddylation site	
hCUL1	704	EEDRKLLIQAAIVRIMKMR--KVLKHQQLLGEV	734
hCUL2	673	DEDRKMYLQAAIVRIMKAR--KVLRHNALIQEV	703
hCUL3	696	DDDRKHEIEAAIVRIMKSR--KKMQHNVLVAEV	726
hCUL4A	589	FQDRQYQIDAAIVRIMKMR--KTLGHNLLVSEL	619
hCUL4B	825	FQDRQYQIDAAIVRIMKMR--KTLSHNLLVSEV	855
hCUL5	708	VQLRILRTQEAIIQIMKMR--KKISNAQLQTEL	738
hCUL7	1560	LEKRRNLLNCLIVRILKAHGDEGLHIDQLVCLV	1592

Figure 1.3. Alignment of neddylation sites among cullin family members.

The neddylation site is colored in green. The accession numbers of cullins are: hCUL1 (NP_003583); hCUL2 (NP_003582); hCUL3 (NP_003581); hCUL4A (NP_003580); hCUL4B (NP_003579); hCUL5 (NP_003469); hCUL7. Modified from Pan et al., 2004.

reviewed by Deshaies, 1999). *In vitro* ubiquitination assays suggest that the ubiquitin transfer to the substrates is enhanced upon neddylation of Cul1 (Read et al., 2000; Morimoto et al., 2000) and that a mutation on Cul1 neddylation site Lys720 leads to the accumulation of SCF substrates (Ohh et al., 2002). It further has been reported that the cullin proteins are deneddylated by the isopeptidase activity of the COP9 SIGNALOSOME complex (CSN) (reviewed in Cope and Deshaies, 2003). This leads not only to the down regulation of SCF ubiquitination activity, but also to the disassembly of the SCF by Cand1 (Liu et al., 2002; Zheng et al., 2002). Cand1 binds tightly to the Cul1-Roc1 dimer of the deneddylated SCF complex, which leads to the disassembly of the Skp1-FBP dimer and to the inactivation of the SCF ubiquitin ligase (Liu et al., 2002; Zheng et al., 2002). Such an assembly-disassembly mechanism of the SCF is imaginable because at any given stage in the cell cycle there are only limited amounts of Cul1-Roc1 in a cell but a large amount of FBPs (Kipreos and Pagano, 2000; Winston et al., 1999). In addition the proposed autoubiquitination of FBPs in

the absence of their substrates (Galan and Peter 1999; Li et al., 2004; Kus et al., 2004) would be prevented.

1.3.3 The human tumor suppressor Fbw7

Fbw7 (also known as human Cdc4) consists of an N-terminal Fbox domain, a linker domain and a C-terminal WD40 domain. The Fbox domain interacts with the C-terminus of the adapter protein Skp1 and establishes the functional SCF^{Fbw7} ligase (the superscript denotes the FBP Fbw7). The Fbw7 WD40 domain recognizes substrates exhibiting a phosphorylated high affinity consensus phosphobinding degron/motif (CPD, LL[pT]PP) as identified in Cyclin E (Koepp et al., 2001; Moberg et al., 2001; Strohmaier et al., 2001), Notch (Tsunematsu et al., 2004; Gupta-Rossi et al., 2001), c-Jun (Nateri et al., 2004) and c-Myc (Yada et al., 2004) (Figure 1.4). These substrates are ubiquitinated by the SCF^{Fbw7} complex and subsequently degraded by the 26S proteasome. Surprisingly, the large T antigen (LT) of the Simian virus 40 (SV40) contains a CPD, which is recognized by Fbw7 (Welcker and Clurman, 2005).

	P-8				P-4				P0	P+1			P+4	
C-terminal Cyclin E	372-	**S**	P	L	P	**S**	G	L	L	**T**	**P**	P	Q	**S**	G-385
N-terminal Cyclin E	54 -	**A**	D	P	C	**S**	L	I	P	**T**	**P**	D	K	**E**	D-67
Presenilin-1	346-	**R**	K	D	G	**Q**	L	I	Y	**T**	**P**	F	T	**E**	D-359
Notch-1	111-	**G**	G	G	G	**C**	P	W	A	**T**	**P**	T	L	**S**	P-124
C-Myc	50 -	**W**	K	K	F	**E**	L	L	P	**T**	**P**	P	L	**S**	P-63
C-JUN	231-	**T**	V	P	E	**M**	P	G	E	**T**	**P**	P	L	**S**	P-244
SREBP1B	418-	**K**	T	E	V	**E**	D	T	L	**T**	**P**	P	P	**S**	D-431
Consensus		**X**	**X**	**X**	**ΦE**	**X**	**ΦD**	**ΦT**	**ΦE**	**T**	**P**	**X**	**X**	**SE**	**ΦD**

Φ hydrophobic
X not conserved

Figure 1.4. Alignment of Fbw7 substrates.

Accession numbers for Cyclin E, Presenilin-1, Notch-1, C-Myc, C-Jun and SREB1B are NP_476530, P49768, CAG33502, NP_002458, 1404381A, NP_004167. Substrate residues are numbered starting according to the conserved Thr determined as P0. Conserved residues at P0 and P+1 are colored in red, polar and charged residues at P–4 and P+4 positions are colored in yellow, residues at P–8 are colored in gray.

Three isoforms of Fbw7 (Fbw7α, Fbw7β, Fbw7γ) have been identified, each containing a differently spliced 5'-exon joined to the ten-common exons, (Figure 1.5) (Koepp et al., 2001; Strohmaier et al., 2001; Spruck et al., 2002). Further analysis revealed that each isoform exhibits a distinct subcellular distribution. Fbw7α is localized in the nucleoplasma

excluding the nucleoli (Kimura et al., 2003). Fbw7β contains an N-terminal transmembrane domain (Koepp et al., 2001) and is present in the cytoplasm, and Fbw7γ is found in the nucleolars (Welcker et al., 2004a). Although three Fbw7 isoforms have been identified, the invariant exons 2-11 of the Fbw7 isoforms, which comprise the amino acids 171-707 of Fbw7α, are sufficient for substrate recognition and ubiquitination (Welcker et al., 2004a) but it is not clear how Fbw7 recognizes its substrate.

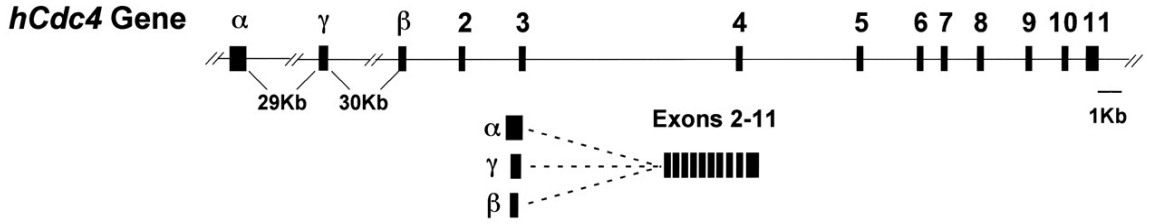

Figure 1.5. Genomic organization of hCdc4 locus localized to chromosome region 4q32.

Alternative splicing joins exons 2-11, which contain the Fbox and WD40 domain, to one of three different 5'-exons (copied from Spruck et al., 2002). The amino acid residues 171-707 of Fbw7α are invariant contained in Fbw7β and Fbw7γ.

Most identified mutations in Fbw7 fall within the ten-common exons and led to primary cancers and genetic instability (Strohmaier et al., 2001; Spruck et al., 2002; Rajagopalan et al., 2004; Moberg et al., 2001). In addition, deletion of Fbw7 causes embryonic lethality in mice (Tetzlaff et al., 2004). A mammalian genetic screen for p53-dependent genes involved in tumor-development (Mao et al., 2004) identified the mouse Fbw7 as a p53-dependent haploinsufficient tumor suppressor gene (Fero et al., 1998; Tang et al., 1998). A haploid insufficient tumor suppressor gene leads to an increased probability to suffer from cancer even without requiring a complete inactivation of the remaining allele. Based on their studies, radiation-induced tumors led to Fbw7 loss of heterozygosity and mutations that were only detected in $p53^{+/-}$ but not in $p53^{-/-}$ mice (Mao et al., 2004). In agreement with this is the finding that Fbw7 is a direct transcriptional target of p53 (Kimaru et al., 2003). Furthermore, preliminary mapping studies localizes Fbw7 to the chromosome region, 4q32. This chromosome region is deleted in 67 % of lung cancers, 63 % of head and neck cancers, 41 % of testicular cancers and 27 % of breast cancers. The chromosome region 4q32 might therefore correlate with high tumor aggressivness (reviewed in Guardavaccaro and Pagano, 2004).

1.3.3.1 Cyclin E a substrate of SCF^{Fbw7}

Human Cyclin E1 was first identified as a G1 Cyclin due to its capability to complement the budding yeast G1 Cyclins (Cln) (Koff et al., 1991; Lew et al., 1991). Later, a second E-type Cyclin was identified, termed Cyclin E2 that shares a 61 % identity with Cyclin E1 (Lauper et al., 1998; Zariwala et al., 1998). Biochemical and structural data revealed that Cyclin E1 consists of several conserved, functionally important domains. It contains an N-terminal nuclear localization sequence (NLS) that transports Cyclin E and the Cyclin E-Cdk2 complex to the nucleus via the importin-α/importin-β nuclear import pathway. Cdk2 lacks an NLS and depends on the interaction with Cyclin E to reach the nucleus (Jackman et al., 2002; Moore et al., 2002; Diehl and Sherr, 1997). Cyclin E also contains a ~200 amino acid stretch highly conserved among Cyclins and necessary for Cdk2-binding and activation, termed the Cyclin box. The C-terminus of Cyclin E exhibits a PEST sequence (residue 370-385), which has been implicated in Cyclin E degradation by the UPS (Lew et al., 1991; Strohmaier et al., 2001; Koepp, et al., 2001).

E-type Cyclins are activators of Cdk2. The Cdk2-Cyclin E complex phosphorylates proteins are involved in cell cycle progression, such as Rb, p27, Cdc25A; examples of proteins involved in centrosome duplication are nucleophosmin and CP110, and examples of proteins involved in gene expression control are the E2F-5. These actions allow cells to enter and to progress through S-phase (reviewed in Moroy and Geisen, 2004). However, recent findings from knock out mouse embryos (Geng et al., 2003; Parisi et al., 2003) showed that Cyclin E is dispensable for cell cycling and therefore challenge the view that Cdk2-Cyclin E is a major key player in the G1/S-phase transition (Sherr, 1993; reviewed by Morgan, 1997). Nevertheless, Cyclin E is essential for re-entering the cell cycle from the quiescent G0-phase and for endoreplication (Geng et al., 2003; Ohtsubo et al., 1995; Parisi et al., 2003; Su and O'Farrell, 1998). Furthermore, new Cdk2-independent roles for Cyclin E are also emerging. It was demonstrated, for example, that Cyclin E mutants defective in binding and activating Cdk2 are able to malignantly transform rat embryonic fibroblast in cooperation with Ras (Geisen and Moroy, 2002). In addition, Cyclin E1 binds with amino acid residue 230-249 to the centrosomes and promotes DNA-synthesis in a Cdk2-independent manner (Matsumoto and Maller, 2004). Moreover, Cyclin E might also be necessary for the cell cycle independent role in specifying neuronal fate within neuroblast lineages (Berger et al., 2005).

It is known that elevated levels of Cyclin E led to premature entry into S-phase (Ohtsubo et al., 1993), genetic instability (Spruck et al., 1999; Rajagopalan et al., 2004) and has also been implicated in many human tumors such as breast carcinomas, bladder cancer and melanomas (Keyomarsi et al., 1995; Harwell et al., 2000; Kawamura et al., 2004; Bales et al., 2005). Moreover, Fbw7 mutations or missing inactivation of Cyclin E by the CKIs result in the upregulation of Cyclin E as well (Strohmaier et al., 2001; Rajagopalan et al., 2004). In addition, in ovarian and breast cancer patients, an increased Cyclin E level significantly correlates with an increase in tumor aggressiveness and a poor survival rate (Keyomarsi and Herliczek, 1997; Porter et al., 1997; Keyomarsi et al., 2002). Importantly, Cyclin $E1^{-/-}E2^{-/-}$ mouse embryonic fibroblast cell lines are resistant to oncogenic transformation (Parisi et al., 2003). However, the exact mechanism remains to be elucidated. Taken together the findings indicate that the deregulation of Cyclin E has a critical role in the initiation of malignancy (Grim and Clurman, 2003; Gladden and Diehls, 2003), and underlines the fact that Cyclin E abundance must be tightly controlled for maintaining a normal cell cycle progression. In cycling cells, Cyclin E abundance peaks near the G1/S-phase transition and is strictly regulated at the levels of transcriptional control by E2F (Hsu et al., 2002; Sim et al., 2004) and via ubiquitin-mediated proteolysis (Strohmaier et al., 2001; Pickart, 2001) which is studied in this thesis.

The SCF^{Fbw7} (Koepp et al., 2001; Moberg et al., 2001; Strohmaier et al., 2001) and the SCF^{Skp2} complex (Nakayama et al., 2000) control the ubiquitin-mediated proteolysis of Cyclin E. It has been suggested that the SCF^{Skp2} ubiquitin ligase interacts and ubiquitinates unphosphorylated free Cyclin E while Cdk2 bound to Cyclin E prevents its ubiquitination, however, the exact mechanism is unclear (Nakayama et al., 2000). The SCF^{Fbw7} dependent degradation of Cyclin E requires binding to the catalytic active Cyclin E-Cdk2 complex and is dependent on Cyclin E phosphorylation (Koepp et al., 2001; Moberg et al., 2001; Welcker at al., 2003). It has therefore been suggested that the SCF^{Fbw7} ubiquitin ligase may play an important role in the termination of Cyclin E-Cdk2 activity. However, *in vitro* ubiquitination assays have shown that the SCF^{Fbw7} complex can also ubiquitinate Cdk2-unbound phosphorylated Cyclin E (Strohmaier et al., 2001).

Mass spectrometry and two-dimensional phosphopeptide mapping analyses have revealed that Cyclin E can be phosphorylated on at least seven sites. Four phosphorylation

sites Ser58, Thr62, Ser75, Ser88 are clustered near the N-terminus, and three Ser372, Thr380, Ser384 are clustered near the C-terminus (Ye et al., 2004; Welcker et al., 2003). The phosphorylation of Cyclin E is controlled by the Cdk2, the glycogen synthase kinase-3 (GSK3) and other unidentified kinase activities. Thr380 is suggested to be the major C-terminal phosphorylation site in Cyclin E and its phosphorylation by Cdk2 or by GSK3 is sufficient for recognition by the WD40 domain (Welcker et al., 2003; Orlicky et al., 2003). The phosphorylation of Ser384 is dependent on an active Cyclin E-Cdk2 complex, indicating a direct involvement of Cyclin E-Cdk2-activity in controlling Cyclin E abundance. Furthermore, it has also been reported that Cyclin E peptides phosphorylated only on Ser384 or Ser372 (responsible kinase unknown) do not interact with Fbw7 (Ye et al., 2004). Moreover, in another experiment in which Cdk2 and the pCMV-Myc-Cyclin E (residues 363-386) vector were co-expressed in insect cells, mass spectrometry analyses by Ye et al., 2004, revealed that the Cyclin E peptides were either doubly or triply phosphorylated. Yet in the context of phosphorylated Thr380, the additional phosphorylation either at residue Ser372 or Ser384 did not enhance binding with Fbw7 (Ye et al., 2004). Therefore, it seems that within the context of immobilized Cyclin E peptides *in vitro*, phosphorylation of residue Thr380 appears to be the major determiant in Fbw7 binding to the C-terminal Cyclin E phosphodegron.

The kinases involved in phosphorylating the N-terminal cluster in Cyclin E are less understood. So far, only Ser58 has been able to be identified as being phosphorylated by GSK3. And a mutation in Thr62 to alanine has been identified to prevent Ser58 phosphorylation (Welcker et al., 2003). This might suggest a priming function for Thr62 (Welcker et al., 2003).The function of phosphorylated Ser58 is unknown. Intriguingly, the mutation of residue Thr62 to Ala62 largely diminishes the ability of GSK3 to phosphorylate Thr380, which results in reduced Cyclin E turnover (Ye et al., 2004). The exact mechanism, however, is not understood. Furthermore, the kinases involved in the phosphorylation of Cyclin E residues Thr62, Ser75 and Ser88 are unknown, and a mutation of the residues Ser75 to Ala75 and Ser88 to Ala88 have no impact on Cyclin E turnover by Fbw7 (Welcker et al., 2003; Ye et al., 2004). Interestingly, Cyclin E cleaved by the serine protease elastase results in N-terminal truncated forms that initiate at amino acid residue 40 or 65 (Porter et al., 2001; Geisen and Moroy, 2002). Both truncated forms are hyperactive, show substantially reduced

p21 binding and reduced apoptosis, and led to an increased tumor progression and metastasis potential (Bales et al., 2005; Akli et al., 2004). Initiating at amino acid residue 65, Cyclin E is especially aggressive.

However, it is still unknown how Fbw7 recognizes Cyclin E.

1.3.3.2 C-Myc a substrate of SCF^{Fbw7}

The proto-oncogene c-Myc contains two regions characteristic of transcription factors, an N-terminal transactivation domain (TAD) and a C-terminal basic helix-loop-helix (bHLH)-leucine zipper domain. The bHLH-leucine zipper domain is known to mediate dimerization and is important for binding to a specific DNA-hexanucleotide element (5'-CACGTG-3'), the E-box motif (Blackwood et al., 1991; Nair et al., 2003). In quiescent cells, c-Myc is a very unstable and almost undetectable. After specific mitogen stimulation however, the c-Myc protein becomes stabilized and its expression level is induced (Gomez-Roman et al., 2003). C-Myc stabilization leads to its heterodimerization with the bHLH-leucine zipper Max domain. The c-Myc-Max heterodimer binds to the E-box motif (Blackwood et al., 1991; Nair et al., 2003) and regulates the transcription of genes involved in cell proliferation such as translation initiation factors elF4E, cell cycle such as Cyclin D, Cdk4, Cdk2, and apoptosis such as p53 or $p19^{ARF}$ (Iritani et al., 1999; Johnston et al., 1999; Prendergast, 1999). Furthermore, c-Myc represses the transcription of p21, p27 (Boxer et al., 2001; Mateyak, et al., 1999; Coller et al., 2000) and therefore allows cells to enter G1-phase (Philipp et al., 1994; Guo et al., 2000). After G1 entry c-Myc abundance needs to be reduced for an orderly cell cycle progression. Elevated c-Myc levels have been associated with high proliferation rates and are found in many malignant tumors (Nesbit et al., 1999). Furthermore, c-Myc mutations around the hotspot residues Glu39, Thr58, Ser62 and Phe138 lead to its stabilization (Salghetti et al., 1999; Bahram et al., 2000; Grandori et al., 2000; Sears et al., 1999).

Ciechanover et al., 1991 and others, have shown that c-Myc is degraded by the UPS and that its turnover depends on two conserved boxes within the TAD, the c-Myc box 1 (MB1, residue 41-66) and the c-Myc box 2 (MB2, residue 128-143) (Grandori et al., 2000; Salghetti et al., 2000). Furthermore, the two FBPs Fbw7 and Skp2 have been implicated in c-Myc degradation (Yada et al., 2004; Kim et al., 2003). It is proposed that SCF^{Skp2}-dependent

degradation of c-Myc requires the binding of MB2 and bHLH-leucine zipper domain, but the regulation mechanism is presently unclear (von der Lehr et al., 2003; Kim et al., 2003). Moreover, MB1 and MB2 have been demonstrated to be recognition sites for regulatory proteins like p21 and TATA box-binding protein (reviewed by Oster et al., 2002). SCF^{Fbw7} induced degradation of c-Myc is thought to be dependent on the phosphorylation of MB1 residues Thr58 and Ser62 (57-P[pT]PPL[pS]P-63) (Yade et al., 2004). At first, mitogen stimulation leads to synthesis of c-Myc as well as Ras-activation. Ras activates the extracellular receptor kinase (ERK) cascade, which leads to MB1 phosphorylation on Ser62 that is required for the subsequent phosphorylation of Thr58. Another function of Ras is the negative regulation of GSK3 activity that inhibits the phosphorylation of c-Myc residue Thr58. Early in G1, this leads to a transiently stable c-Myc protein, which is only phosphorylated on residue Ser62 (Sears, et al., 2000; Yeh et al., 2004). In G1, Ras-activity declines, allowing GSK3 dependent c-Myc phosphorylation on residue Thr58, leading to c-Myc destabilization. Recent studies by Yeh et al., 2004, found that ubiquitinated c-Myc is only phosphorylated on residue Thr58, suggesting that dephosphorylation of residue Ser62 might be required prior to c-Myc ubiquitination. Furthermore, data from Yeh et al., 2004, suggests that the dephosphorylation of residue Ser62 could be regulated by the Pin1 prolyl isomerase (PPI) and protein phosphatase 2 (PP2). However, transfection experiments with c-Myc wild type and c-Myc mutants Thr58Ala, Ser62Ala, Thr58Ala/Ser62Ala in proteasome inhibited HEK293T cells showed that only wild type c-Myc interacted with Fbw7 (Yade et al., 2004). Yet it is unclear if the c-Myc mutant Ser62Ala is phosphorylated on Thr58, since phosphorylation on Ser62 seems to be required for subsequent phosphorylation on Thr58. In addition, Welcker et al., 2004b found that a c-Myc peptide phosphorylated on Thr58 and Ser62 binds to Fbw7. In agreement with these findings, an *in vitro* ubiquitination assay with His_6-c-Myc phosphorylated on Thr58 and Ser62 revealed that c-Myc is ubiquitinated by the SCF^{Fbw7} (Yade et al., 2004). Moreover, after 26S proteasome inhibition, c-Myc colocalizes with the isoform Fbw7γ within the nucleolus (Welcker et al., 2004a), suggesting that c-Myc turnover depends on isoform Fbw7γ. This fits nicely with the observation of Welcker et al., 2005 who found that the large T antigen of SV40 binds, sequesters and mislocalizes the nucleolar Fbw7γ isoform to the nucleoplasm. This reduces Fbw7γ abundance in the nucleolar and causes increased Cyclin E-Cdk2 activity. Furthermore, Thr58 phosphorylation seems to

be critical in c-Myc degradation, since all v-myc genes in transformed retroviruses display a Thr58 mutation (Papas et al., 1985).

1.3.4 ScCdc4, a homolog of Fbw7

ScCdc4 was identified in 1997, and is the first FBP shown to assemble with scSkp1 and the cullin family member Cdc53 (counterpart of Cul1 in yeast) to an SCF complex (Feldman et al., 1997; Skowyra et al., 1997). ScCdc4, which is homologous to Fbw7, consists of an N-terminal Fbox domain, a linker domain and a C-terminal WD40 domain. The Fbox and WD40 domains of scCdc4 are necessary and sufficient to target phosphorylated substrates for ubiquitination (reviewed in Deshaies, 1999; Skowyra et al., 1997). Such substrates comprise of the Cdk-inhibitor Sic1 (Feldman et al., 1997; Verma et al., 1997), the replication initiator Cdc6 (Drury, et al., 1997; Perkins et al., 2001), the polarization factor Far1 (Henchoz et al., 1997; Blondel et al., 2000), the transcription factors Gcn4 (Meimoun et al., 2000) and Tec1 (Chou et al., 2004). Recently, the structure of the scSkp1-scCdc4 complex bound to a singly phosphorylated C-terminal Cyclin E peptide (377-GLL[pT]PPQSG-385, Nash et al., 2001) was solved (Orlicky, et al 2003, Figure 1.6),

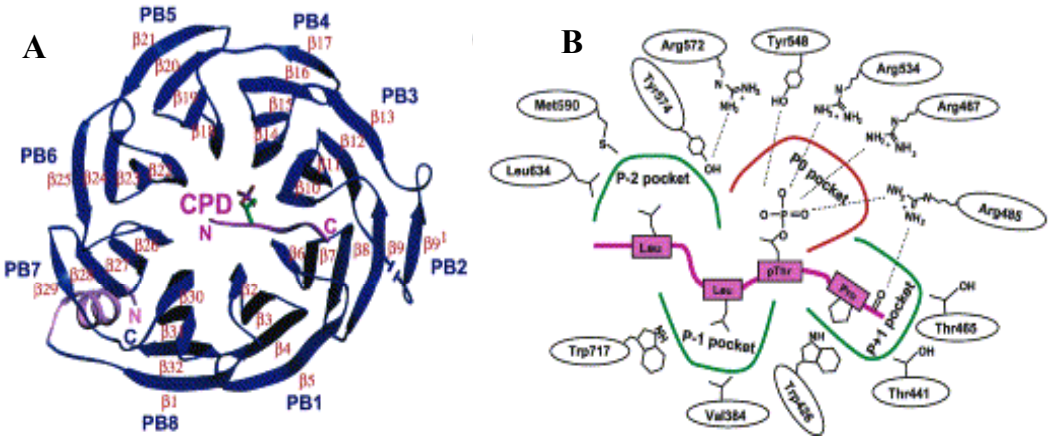

Figure 1.6. ScCdc4 WD40 domain bound to a singly phosphorylated Cyclin E peptide.

A) Ribbons representation of the WD40 domain of Cdc4 (blue) bound to the singly phosphorylated Cyclin E peptide, $CycE^{pT380}$ (purple). The phosphorylated Thr is shown in ball and stick representation. The β-propeller blades of Cdc4 WD40 domain are denoted PB1 to PB8.
B) Schematic scCdc4 binding pocket interactions with the singly phosphorylated Cyclin E peptide. Figures copied from Orlicky et al., 2003.

although Cyclin E is not a physiological substrate for scCdc4. In that structure, the scCdc4 WD40 domain folds into an 8-bladed β-propeller and demonstrates that the phosphorylated C-terminal Cyclin E peptide is stably tethered at the top of the narrow central channel by key residues of the WD40 domain, similar to that of FBWs such as clathrin (ter Haar et al., 2000) and β-Trcp1 (Wu et al., 2003) and their corresponding substrates. Furthermore, all Cdc4 proteins identified thus far exhibit a conserved tryptophane and arginine-triad in their WD40 domains (in scCdc4, Trp426, Arg467, Arg485 and Arg534), which is essential for binding to phosphorylated substrates.

1.3.4.1 Sic1 a substrate of scSCF^{Cdc4}

Sic1, which is a substrate of scCdc4, contains twenty lysine residues, nine Cdk consensus sites, and a C-terminal Cdk1-inhibitory domain (Verma et al., 1997; Hodge and Mendenhall, 1999). Sic1 is an inhibitor of the yeast B-type Cyclin-Cdk1 (Clb5-Cdc28 or Clb6-Cdc28) complexes and blocks the S-phase-Cdk1 activity, which is necessary for the onset of DNA-replication and entry into S-phase (Schwob et al., 1994). Molecular modeling experiments based on the crystal structure of the mammalian Cdk2-Cyclin A-p27 trimer (Russo et al., 1996) have suggested that the p27-inhibitory domain and the Sic1-inhibitory domain share, in addition to a very low primary sequence similarity to p27, functional and structural similarities (Barberis et al., 2005). For example, it has been shown that a sic1-deletion strain can be rescued by an over-expression of the p27 gene in *S. cerevisiae* (Barberis et al., 2005). Moreover, Clb5 (yeast B-type Cyclin) interacts with the human p27-inhibitory domain in a yeast two-hybrid system (Cross and Jacobson, 2000). Interestingly, the mammalian S-phase inhibitor p27 is targeted for ubiquitination by Skp2, an LRR containing FBP (Harper, 2001). The yeast S-phase inhibitor Sic1 is recognized for ubiquitination by scCdc4, a WD40 domain containing FBP, and its human homolog Fbw7 targets the positive cell cycle regulator Cyclin E for ubiquitination.

Entry into S phase requires ubiquitin-dependent degradation of Sic1 by the scSCF^{Cdc4} complex (Nash et al., 2001). Mutagenesis studies by Nash et al., 2001, have revealed that Sic1 has to be phosphorylated on at least five to six of its nine Cdk-consensus sites (Figure 1.7.) by the yeast G1-Cyclin-Cdk1 (Cln1, Cln2 or Cln3 in complex with Cdc28) complexes for entry into S-phase. It has been shown that deletion of all three-yeast G1-Cyclin genes

leads to an inviable yeast strain. The reason for the inviability might be a permanent G1 arrest due to a lack of the yeast G1-Cyclins necessary for the phosphorylation of Sic1 (Schneider et al., 1996; Tyers, 1996). Additional deletion of the Sic1-gene restores the yeast strain viability (Schneider et al., 1996; Tyers, 1996) and underlines the importance of yeast G1-Cyclins in mediating Sic1 phoshorylation, thereby promoting a timely and irreversible G1/S-phase transistion. As shown in the scCdc4-C-terminal CycE^{9pT380} structure (Figure 1.6)

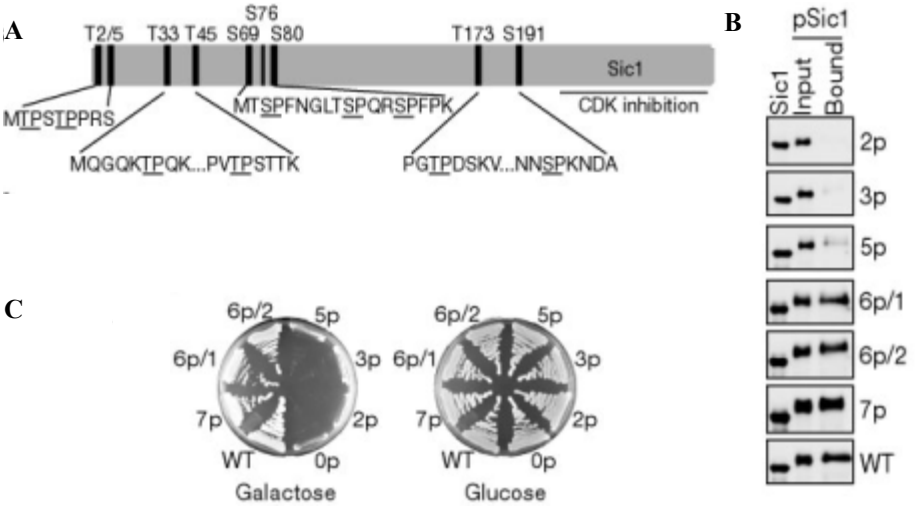

Figure 1.7. Contribution of Cdk phosphorylation sites to Sic1 recognition, ubiquitination and degradation.

A) Consensus SP/TP Cdk phosphorylation sites in Sic1 (underlined).
B) and **C)** Phosphorylation of a minimum of six sites on Sic1 is required for interaction with Cdc4 *in vitro* and for the degradation of Sic1 *in vivo*. Phosphorylated sites are indicated as follows: 2p = T45, S76; 3p = T33, T45, S76; 5p = T2, T5, T33, T45, S76; 6p/1 = T2, T5, T33, T45, S69, S76; 6p/2 = T2, T5, T33, T45, S76, S80; 7p = T2, T5, T33, T45, S69, S76, S80. *GAL1-SIC1* strains were incubated for 2 days at 30 C. Figure copied from Nash et al., 2001.

(Orlicky et al., 2003) the C-terminal CycE^{9pT380} peptide is capable of interacting with the scCdc4 WD40 domain in a phosphorylation dependent manner and suggests a conserved binding mechanism for Sic1 and Cyclin E (Won et al., 1996). However, it has been reported that Sic1 is a very different type of substrate compared to Cyclin E (Introduction, 1.3.3.1). Whereas Cyclin E and other known phosphorylated substrate peptides such as β-catenin and IκB interact with one high affinity phosphodegron to their WD40 domains (Ye et al., 2004; Wu et al., 2003), Sic1 relies on five to six of its nine low affinity phosphodegrons for interacting with the scCdc4 WD40 domain (Verma et al., 1997; Nash et al., 2001). The minimal high affinity C-terminal Cyclin E phosphodegron that is efficient for recognition has

been determined as LL[pT]PP. Yet all nine phosphodegrons in Sic1 are non-optimal, due either basic residues at their P+2 toP+5, a lack of hydrophobic residues at P–1 and P–2, or the replacement of the preferred phosphorylated threonine to a serine at P0. A structural analysis of the scCdc4 WD40 domain surface revealed only one obvious phosphate-binding pocket. Therefore, Orlickly et al., 2003, proposed a binding model, in which multiple low affinity phosphodegrons dance on the single scCdc4 phosphate-binding pocket. According to that model it seems that the high local concentration of Sic1s multiple low affinity phosphodegrons ensure that another Sic1 phosphodegron binds to the phosphate-binding pocket of scCdc4 before Sic1 could diffuse away. It has been reported that the ubiquitinated Sic1 bound to the Cdc28-Clb5 or Cdc28-Clb6 complex is degraded 200 times faster by the 26S proteasome than free ubiquitinated Sic1. This suggests that the 26S proteasome actively disassembles the ubiquitinated Sic1-Cdc28-Clb5 complex prior to Sic1 degradation rather than degrading free ubiquitinated Sic1 that spontaneously dissociates from the complex (Verma et al., 2001). Interestingly, the replacement of a single non-optimal $Sic1^{T45}$ phosphodegron with a single optimal C-terminal $CycE^{19pT380}$ phosphodegron was sufficient to efficiently ubiquitinate Sic1 *in vitro* (Nash et al., 2001). However, if the non-optimal $Sic1^{43\text{-}PVpTPS\text{-}47}$ phosphodegron was changed to the determined optimal $Sic1^{43\text{-}LLpTPP\text{-}47}$ then Sic1 was no longer efficiently ubiquinated *in vitro*, which led to a permanent growth arrest *in vivo* (Nash et al., 2001). Intriguingly, analogous exchanges of the non-optimal $Sic1^{74\text{-}LTpSPQ\text{-}78}$ phosphodegron to the optimal $Sic1^{74\text{-}LLpTPP\text{-}78}$ phosphodegron resulted in effective Sic1 ubiquitination *in vitro* and Sic1 degradation *in vivo* (Nash et al., 2001). In a separate study, Sic1 yeast strains mutated in the six N-terminal lysines (K0N-GFP), the fourteen C-terminal lysines (K0C-GFP), or all twenty lysines (K0-GFP) were tested for endogenous Sic1 turnover. Whereas the turnover of the K0C-GFP mutant was similar to that of WT-GFP, the K0N-GFP mutant was stable up to 180 min. In addition, the K0N-GFP mutant showed a similar G1 arrest, like the K0-GFP mutant. Moreover, adding any one of the six N-terminal lysine residues to the K0N-GFP mutant restores Sic1 turnover. This finding indicates that the N-terminal- but not the C-terminal lysines are required for Sic1 turnover (Petroski and Deshaies, 2003). Although *in vivo*, each of the six single N-terminal lysine were efficient in Sic1 turnover, *in vitro* experiments revealed equal capability to ubiquitinate Sic1, yet surprisingly different Sic1 half-lives were observed, varying between 1 min for wt-Sic1 and 5

min for the Sic1 residue Lys84. This finding implies that not all polyubiquitin chains are equally efficient in Sic1 turnover (Petroski and Deshaies, 2003).

1.4 APC protein ligase

1.4.1 Composition of the APC

APC was discovered a) as a mitosis and Cyclin B specific ubiquitin ligase in clam and xenopus egg extracts (King et al., 1995; Sudakin et al., 1995) and b) through the isolation of budding yeast mutants that are defective in the degradation of mitotic Cyclins (Irniger et al., 1995). To highlight its importance in the anaphase onset, Irniger et al., 1995 and King et al., 1995, called it 'anaphase promoting complex' (APC), whereas Sudakin et al., 1995, called it 'cyclosome' (C) to point out its role in the Cyclin degradation pathway. APC is a large multiprotein complex that contains at least eleven core subunits and additional regulatory subunits such as Cdc20, Cdh1 or Ama1 (Yu et al., 1998; Grossberger et al., 1999; reviewed by Page and Hieter, 1999). Little is currently known about how APC subunits work together to form a functional E3 ligase. Similarly, the exact mechanism of how the APC regulatory molecules modulate E3 activity is not clear. Table 1.1 gives an overview of the known APC subunits in yeast and vertebrates as well as their structural motifs. A comparison of yeast versus vertebrate subunits reveals that the APC has similar composition in all eukaryotes. An exception is the subunit APC7 (Yu et al., 1998), which is specific to vertebrates, and the subunit APC9, which is solely found in *S. cerevisiae* (Zachariae et al., 1998).

Table 1.1. APC subunits of yeast and vertebrates (Table modified from Castro et al., 2005).

Core subunits	***S. cerevisiae***	***S. pompe***	***Vertebrates***	**Motif**
	APC1	Cut4	APC1/Tsg24	Rpn1/2 homology
	APC2	-	Apc2	Cullin homology
	Cdc27	Nuc2	APC3Cdc27	TPR-motif
	APC4	Cut20/Lid1	APC4	-
	APC5	-	APC5	-
	Cdc16	Cut9	APC6/Cdc16	TPR-motif
	-	-	Apc7	TPR-motif
	Cdc23	Cut23	APC8/Cdc23	TPR-motif
	APC9	-	-	-
	Doc1	APC10	APC10	Doc domain, IR-motif
	APC11	APC11	APC11	Ringfinger domain
	Cdc26	Hcn1	Cdc26	-
	Swm1	APC13	-	-
	-	APC14	-	-
	Mnd2	APC15	-	-
Activators	***S. cerevisiae***	***S. pompe***	***Vertebrates***	**Motif**
	Cdc20	Slp1	Cdc20/p^{55cdc}	WD40 domain, IR-motif
	Cdh1/Hct1	Srw1/Ste9	Cdh1	WD40 domain, IR-motif
	Ama1	-	-	WD40 domain

APC1 APC1 is the largest subunit of the complex and was first identified from Xenpus egg extracts (Peters et al., 1996). Homologs of APC1 have been described in several organisms (Zachariae et al., 1996; Yamashita et al., 1996; Engle et al., 1990; Starborg et al., 1994). So far, no functions of APC1 have been identified, but it is speculated that it might serve as a docking module for the assembling of the APC (Lupas et al., 1997). Furthermore, APC1 is hyperphosphorylated in mitosis (Peters et al., 1996; Jorgensen et al., 2001) and sequence analyses reveal that APC1 shares a β-sheet/α-helix-sequence-repeat structure motif with Rpn1 and Rpn2 from the 19S regulatory cap of the 26S proteasome. Rpn1 and Rpn2 recruit shuttle proteins like Rad23 and Rpn10 with their polyubiquitinated substrates to the 26S proteasome (reviewed by Hartmann-Petersen and Gordon, 2004), leading to speculation that APC1 might fulfill a similar function.

APC2 and APC11 APC2 has a C-terminal cullin homology motif similar to the Cdc53/Cul1 subunit of the SCF. APC11 contains a zinc binding Ringfinger motif, like the Rbx1 of the SCF, and is responsible for recruiting the E2 subunit to the APC. The C-terminal

cullin domain of APC2 directly associates with APC11. It has been demonstrated in *in vitro* experiments that the APC2-APC11 complex is sufficient to catalyze ubiquitination in the presence of either UbcH10 or Ubc4 (E2 enzymes) (Gmachl et al., 2000; Leverson et al., 2000; Harper et al., 2002; Tang et al., 2001). Tang et al., 2001, showed that only the APC2-APC11 complex binds to UbcH10 and ubiquitinates substrates, whereas APC11 binds independently of APC2 to Ubc4 to ubiquitinate substrates. Ubiquitination assay with native immunoprecipitated human holo-APC that was depleted of APC2 and APC11 showed no ubiquitination activity, whereas the complex that was reconstituted with co-expressed APC2-APC11 showed ubiquitination activity (Vodermaier et al., 2003). This result confirms that APC2 and APC11 are the main two subunits involved in the ubiquitination reaction. Recently, L. Song determined an ~80 amino acid C-terminal structure of yeast APC2, which adopts a winged-helix fold and can be superimposed on the wing-helix-B of Cul1 (Zheng et al., 2002). This suggests that APC2 might have scaffolding properties like Cdc53 in the SCF complex. Due to the sequence homology of APC2-APC11 with Cul1-Rbx1 complex and their involvement in the ubiquitin transfer, the APC is also known as the distant cousin of the SCF.

APC3, APC6, APC7 and APC8 The Subunits APC3, APC6, APC7 and APC8 contain tetratrico-peptide-repeat (TPR) motifs (Lamb et al., 1994; Tugendreich et al., 1995), which are predicted to promote protein-protein interactions (Das et al., 1998). TPR motifs are present in a wide range of proteins involved in cell cycle regulation, transcriptional control or protein folding (Goebl and Yanagida, 1991). Furthermore, the primary sequences of APC3 and APC7 are highly related, suggesting that they possibly originated from a single gene and might therefore have similar functions. In vertebrates, Cdc16, Cdc23 and Cdc27 are phosphorylated in mitotic extracts and are dephosphorylated in interphase extracts (Peters et al., 1996). Moreover, a conserved C-terminal isoleucine-arginine (IR)-motif in Doc1 and APC activators Cdc20 and Cdh1 has been implicated in mediating binding to the APC3 and APC7 subunits (Passmore et al., 2003; Vodermaier, et al., 2003; Wendt et al., 2001). For APC7, it was further determined that the TPR-motifs within amino acids 298 to 569 are sufficient for binding to the C-terminal IR-motif (Vodermaier, et al., 2003). This raises the possibility that the phosphorylation states of the TPR-containing APC subunits are responsible for regulating APC activity by inducing Cdc20, Cdh1 (Vodermaier and Peters,

2004) and Doc1 association (Wendt et al., 2001). The TPR subunits are also found to be essential for viability in yeast (Lamb et al., 1994), probably because they are necessary for APC activation. It is also tempting to speculate that for the TPR-containing subunits APC6 and APC8, which are unable to interact with the IR-tail, other binding-factors will be found. Moreover, the loss of APC7 expression in breast carcinomas seems to be an indicator for a poor prognostic outcome (reviewed by Park et al., 2005).

APC4 and APC5 The APC4 and APC5 subunits do not have any significant sequence homology to any identified protein. Therefore, nothing is known about their possible role within the APC. It was recently demonstrated that a stable subcomplex, comprising of the subunits APC4, APC5, APC1, APC2 and APC11 can be purified from native immunopurified human holo-APC by utilizing a Source Q KCl-gradient (Vodermaier et al., 2003). In ubiquitination assay, this subcomplex interacted with an E2, and assembling a polyubiquitin chain, but it was unable to conjugate the polyubiquitin chain to the substrate. This was probably due to the missing TPR-containing APC subunits, which interact with the activator proteins (Vodermaier et al., 2003). Furthermore, studies by Koloteva-Levine et al., 2004, showed that APC5 associates with the pre-initiation DNA complex, implying an additional APC-independent role for APC5 in the control of gene expression.

APC9 The APC9 subunit is unique for *S. cerevisiae* (Zachariae et al., 1998), and a homology search revealed no known structural motifs. APC9 is not essential for survival, but entry into anaphase is delayed in an apc9 deletion strain, and pull down experiments with APC9 mutants showed drastically reduced binding of Cdc27/APC3 (Zachariae et al., 1998). This suggests that APC9 might be important for Cdc27/APC3 binding.

APC10 The APC10 subunit is termed Doc1 in *S. cerevisiae*. APC10 was first identified in *S. cerevisiae* from a genetic screen aimed to isolate mutants defective in degrading mitotic Cyclins (Hwang and Murray, 1997). Orthologs of APC10 have been found in *S. pompe* and humans (Kominami et al., 1998; Grossberger et al., 1999). The crystal structures of budding yeast and human APC10 have been solved (Wendt et al., 2001; Au et al., 2002), and structure analysis of the jellyroll-shaped Doc domain have indicated that this domain might be involved in binding ligands such as sugars, phospholipids, DNA and proteins (Wendt et al., 2001; Carroll et al., 2002; Passmore et al., 2003). The Doc domain has also been found in the subunit Cul7 of another SCF-Rbx1-like E3 ligase, and it has been

suggested that it might perform a similar function (Dias et al., 2002). Recent studies showed that the Doc domain is indeed important for substrate D-box recognition and that it is critical for efficient substrate proteolysis and mitotic progression *in vivo* (Carroll et al., 2005). Mutation of four amino acids in the ligand-binding interface of Doc1 resulted in a significant accumulation of G2/M cells, comparable with doc1 deletion strains (Carroll et al., 2005; Hall et al., 2003). This indicates that the Doc1 subunit is involved in the recognition of D-box containing APC substrates. Doc1 also increases the processivity of substrate ubiquitination by enhancing the binding affinity of the substrate to the APC (Carroll et al., 2002). A C-terminal IR-motif in APC10 additionally mediates binding to the APC3 (Wendt et al., 2001) and APC7 subunits (Vodermaier, et al., 2003), similar to the activator proteins Cdc20 and Cdh1. It is also known that APC10 binds directly to APC11 (Tang et al., 2001).

Cdc26 Cdc26 orthologs have been described in yeast (Yamada et al., 1997) and vertebrates (Gmachl et al., 2000), and amino acid sequence analysis revealed no known structure motifs. Cdc26 seems to be important for maintaining the integrity of the APC, because APC purification with cdc26 deletion strains caused reduced binding of the APC subunits APC3, APC6 and APC9 (Zachariae et al., 1998).

APC13, APC14 and APC15 The APC13, APC14 and APC15 subunits were first identified in *S. pompe* (Yoon et al., 2002). The orthologs Swm1 and Mnd2 were also found in *S. cerevisiae* (Hall et al., 2003) but not in vertebrates. Swm1 and Mnd2 are essential for progression through meiosis (Ufano et al., 1999; Rabitsch et al., 2001). In mitosis, however, swm1- and mnd2-deletion strains exhibit only minor delays in anaphase entry (Hall et al., 2003), indicating that Swm1 and Mnd2 play only a minor role in mitosis. Hall et al., 2003, further suggest that Mnd2 and Swm1 aid in APC stability. It was further demonstrated with the use of the rapid translation system (RTS) that Mnd2 can be co-purified with Cdc23/APC8, APC5 and APC1 and Swm1 can be co-purified with Cdc23/APC8 and APC5 (Hall et al., 2003).

The introductory description of the individual APC subunits summarizes the current knowledge of the complex. It shows how little is known about the APC a) on the individual subunit level, and b) on how the APC subunits assemble into a functional E3 ligase. Recently, Passmore et al., 2005, have shed some light on APC subunit stoichiometries.

Surprisingly, this revealed that the APC contains only one copy of subunit APC1 but two or three copies of the other APC subunits. In addition, they showed that APC forms a dimer, which ubiquitinates Pds1 7 times faster than the monomeric APC (Passmore et al., 2005). Moreover, Gieffers et al., 2001, Dube et al., 2005 and Passmore et al., 2005, were able to obtain a more detailed insight into the overall monomeric APC structure by performing cryo-electron microscopy. The 20 Å 3D model of the APC comprises an asymmetric structure with a water-lined channel and many grooves and cavities. Ni-NTA-Gold labeling revealed that the water-lined channel of the APC is surrounded by the helical TPR motifs of the APC subunits (Passmore et al., 2003). A cryo-electron microscopy study of the *Xenopus* APC with and without its cofactor Cdh1 localized the APC2 subunit by antibody labeling, and that suggested the ubiquitination reaction likely takes place on the outer surface of APC (Dube et al., 2005).

1.4.2 Function and regulation of the APC

APC was initially identified as the ubiquitination factor for the anaphase inhibitor Pds1/Securin, which promotes the metaphase/anaphase transition, and for Cyclin B, which results in mitotic exit. Since then, many other APC substrates have been discovered, such as a) the protein kinases Plk1, Cdc5, Aurora A, Aurora B and Nek2A, b) the regulatory subunits of protein kinases the A- and B-type Cyclins, c) the APC cofactor Cdc20, d) the Cdc6 regulator of DNA-replication, e) the phosphatase Cdc25A, and f) the Fbox protein Skp2 (reviewed by Peters, 2002; reviewed by Castro et al., 2005).

The main cell cycle functions of the APC are initiation of anaphase, mitotic exit and G1 maintenance. APC regulates these cell cycle activities through binding to the activator proteins Cdc20 and Cdh1 (Passmore, et al., 2003; Vodermaier, et al., 2003). Binding is regulated by the reversible phosphorylation of APC subunits and APC activators, by the mitotic checkpoint complex (MCC), and by ubiquitination of the APC activators. Moreover, the activators Cdc20 and Cdh1 associate with the APC at different cell cycle stages and recruit substrates to the APC, depending on the presence of either one or two rather poorly defined amino acid sequence elements in their substrates, the destruction-box (D-box, consensus of RxxLxxxxN) and the KEN-box (KEN-box, composed of an amino acid consensus KEN) (Glotzer et al., 1991; Pfleger and Kirschner, 2000). APC^{Cdc20} (the

superscript denotes the activator protein Cdc20) recognizes substrates with a D-box element (Murray et al., 1989; Glotzer et al., 1991), whereas APC^{Cdh1} (the superscript denotes the activator protein Cdh1) recognizes substrates that contain a D-box and a KEN-box (reviewed by Peters, 2002; Glotzer et al., 1991; Pfleger et al., 2000). APC^{Cdc20} is active during meta- and anaphase, a time where the Cyclin B-Cdk1 complex phosphorylates several APC subunits (Rudner and Murray, 2000). Whether phosphorylation of the activator Cdc20 is essential for APC^{Cdc20} activation is still unclear. On the one hand, Kotani et al., 1999, reported that Cdc20 phosphorylation by Cdk1 is necessary for APC activation, whereas Yudkovsky et al., 2000, found that Cdc20 phosphorylation by Cdk1 inhibits APC activity. A third group claims that Cdc20 phosphorylation has no effect on APC activity (Kramer et al., 2000). More experiments have to be performed to understand how Cdc20 activates APC. The main ubiquitination targets for APC^{Cdc20} are Pds1/Securin and Cyclin B (Morgan, 1999; Harper et al., 2002). Prior to APC^{Cdc20} activation, Bub1 and other proteins ensure that all chromosomes are properly attached to the mitotic spindle at the kinetochore before sister chromatids are separated (Cleveland et al., 2003). Unattached chromosomes inhibit APC^{Cdc20} activity and delay the onset of anaphase (Rieder et al., 1994) by the formation of the MCC (containing BubR1-Bub3-Mad2-Cdc20) and also by an inhibitory Cdc20 phosphorylation through Bub1, thereby keeping APC in an inactive state (Tang et al., 2004; Yu, 2002; Bharadwaj et al., 2004). After all chromosomes are attached to the kinetochore, Cdc20 activates the APC and starts to ubiquitinate the inhibitory subunit Securin of the Securin-Separase complex. This leads first to the release of the inactive phosphorylated Separase. Thereafter, Separase gets dephosphorylated and activated once the Cyclin B of the Cyclin B-Cdk1 complex is ubiquitinated by the APC^{Cdc20}. The activated Separase cleaves the Scc1 cohesion complex, resulting in the separation of sister chromatides from each other and guides the cell towards anaphase and mitotic exit (reviewed in Nasmyth, 2001; Hauf et al., 2001; Clute and Pines, 1999). At the end of mitosis, the Cdk activity is very low, and additional Cdh1 dephosphorylation by the phosphatase Cdc14 leads to Cdh1 association and activation of the APC (Lukas et al., 1999; Shirayama et al., 1999; Stegmeier et al., 2002). APC^{Cdh1} is responsible for the ubiquitination of the activator protein Cdc20 and the mitotic Cyclins during mitotic exit and the G1-phase, thereby keeping the Cdk activity at a low level (Cross, 2003). This is necessary as the formation of pre-initiation complexes at the origins of

DNA-replication can only be achieved at low Cdk activity (Yu and Sicinski, 2004; King et al., 1996; Stillman, 1996). At the end of the G1-phase Cdk activity increases, which leads to Cdh1 phosphorylation and APC^{Cdh1} inactivation (Amon et al., 1994; Huang et al., 2001). This limits DNA-replication to a single occurrence per cell cycle (Yu and Sicinski, 2004; King et al., 1996; Stillman, 1996).

1.5 Interconnection of SCF and APC protein ligases

SCF and APC possess overlapping ubiquitination activities in the G1-phase of the cell cycle, mainly executed by APC^{Cdh1} and SCF^{Skp2}-Cks1 (superscript denotes complex of FBP Skp2). G1, APC^{Cdh1} keeps the Cdk level low by targeting Skp2 and Cks1 for ubiquitination (Bashir et al., 2004). The consequences are a) that the Cyclin E-Cdk2 and Cyclin A-Cdk2 complexes are kept in the inactive form by binding to their inhibitor p27, which is a substrate of SCF^{Skp2}-Cks1 (Pagano et al., 1995; Ganoth et al., 2001), and b) that RB stays in the dephosphorylated active form and represses the E2F transcription factors (Weinberg, 1995). After mitogen stimulation, in mid-G1 c-Myc leads to the transcription of genes encoding Cyclin D, which activates Cdk4 and Cdk6. Accumulation of the Cdk4-Cyclin D and the Cdk6-Cyclin D complexes initiates Rb phosphorylation, with the consequence of liberating the E2F transcription factor. In addition, the Cdk4-Cyclin D and Cdk6-Cyclin D complexes sequester p27 without inhibiting its own kinase activity. This reduces the inhibitory effect of p27 on the Cyclin E-Cdk2 and Cyclin A-Cdk2 complexes (reviewed by Galderisi et al., 2003; Cheng et al., 1999). The active E2F transcription factor allows transcription of genes required for DNA-replication and cell cycle progression, including Emi1, Cyclin A, Cyclin B, Cyclin E and Fbw7 (Hsu et al., 2002; Sim et al., 2004). Rb is phosphorylated by Cdk2-Cyclin E complex and Rb causes the complete E2F activation. Moreover, it is thought that Cdk2-Cyclin E activity is initially achieved by cytoplasmic export of its p27 inhibitor (Sherr and Roberts, 1999; Ang and Harper, 2004). The Cyclin A-Cdk2 complex phosphorylates Cdh1, which leads to its dissociation from the APC^{Cdh1} complex and causes APC inactivation (Peters, 2002). Additionally, the anaphase inhibitor Emi1 aids in inactivating APC^{Cdh1} by binding to unbound Cdh1 (Hsu et al, 2002). The inactive APC no longer possess the ability to ubiquitinate Skp2 and Cks1. This leads to the assembly of SCF^{Skp2}-Cks1, which targets the protein kinase inhibitor p27 for ubiquitination and drives the cell to higher Cdk2 activity

(Pagano et al., 1995; Ganoth et al., 2001). This and other regulations guide the cell towards the G1/S-phase transition.

1.6 Aim of this thesis

The introduction has shown that the SCF and APC E3 ligases are crucial for the regulation of the cell cycle. Little is known about how the SCF^{Fbw7} recognizes and ubiquitinates its specific substrates, and even less is known about how the APC fulfills this function. To gain a better insight in these biological mechanisms, this thesis focuses on:

A) The crystal structure determination of the following Fbw7-Skp1 complexes:
   - Fbw7-Skp1 complex,
   - Fbw7-Skp1-$CycE^{31pS372/pT380/pS384}$ complex,
   - Fbw7-Skp1-$CycE^{14pT62}$ complex and
   - Fbw7-Skp1-c-$Myc^{19pT58/pS62}$.

B) The elucidation of Fbw7-Cyclin E binding mechanism.

C) The elucidation of the scCdc4-Sic1 binding mechanism.

D) The purification and biochemical characterization of subunits of the APC complex.

2. Materials and Methods

2.1 Materials

2.1.1 Commercial suppliers

Unless otherwise stated, all chemicals were purchased from Merck, Sigma-Aldrich, Difco, Serva, Fluka, Hampton Research and Boehringer Mannheim. Enzymes were purchased from New England Biolabs (NEB), Roche, Stratagene and Sigma-Aldrich. Inhibitors were purchased from Serva. Antibiotics were purchased from Roche and Invitrogen. Consumed materials were purchased from BioRad, Fisher, Hampton Research, Millipore, NEB and Pharmacia Biotech.

2.1.2 Vectors

The vectors in (Table 2.1) are ampicillin resistant (Amp^r). For vector-maps refer to Figure 7.1, Appendix.

Table 2.1. Vector characteristics of vectors used in the insect and *E. coli* expression systems.

Baculovirus transfer vector	**Expression system**	**Promotor**	**features**	**Created by**
pMage	Insect cells	Polyhedrin	GST-tagged, thrombin site	Pharmingen
pAcG2T	Insect cells	Polyhedrin	GST-tagged, thrombin site	Pharmingen
pVL1392	Insect cells	Polyhedrin	None-tagged	Pharmingen
pVL1393	Insect cells	Polyhedrin	None-tagged	Pharmingen
pVLSO	Insect cells	Polyhedrin	GST-tagged, thrombin site	me
Bacterial vector	**Expression system**	**Promotor**	**features**	**Created by**
pABLO	*E. coli*	Tac	GST-tagged, thrombin site, RBS, 2.MCS	in the lab
pABLOmut	*E. coli*	Tac	GST-tagged, thrombin site, RBS, 2.MCS	me

2.1.3 Bacterial and viral strains

The *Escherichia coli (E. coli)* strain DH5α (Novagen) was used for vector amplification and *E. coli* strain BL21(D3) (Novagen) was utilized for recombinant protein expression. The BaculoGold Baculovirus DNA strain *Autographa californica nuclear polyhedrosis virus (AcNPV)* (Pharmingen) was used for generating the recombinant baculovirus.

2.1.4 Insect cell lines

High Five (Hi5) cell line

Hi5 cells were derived from *Trichoplusia ni egg* cell homogenates (Pharmingen). This cell line is highly susceptible to infection with *AcNPV*, and was used with several Baculovirus expression vectors (Table 2.1). The Hi5 cells were cultivated in suspension- and in monolayer cultures and were utilized for protein expression.

Spodoptera frugiperda (SF9) cell line

The SF9 cell line was cloned in 1983 from the parent line IPLB-Sf21 AE, which was derived from pupal ovarian tissue of the fall army-worm (Pharmingen). This cell line is highly susceptible to infection with *AcNPV* and was used with several Baculovirus transfer vectors (Table 2.1). SF9 cells were cultivated in monolayer culture and were used for virus production.

2.1.5 Media

for *E. coli* strains

LB-Agar: 10 g/L Trypton/Peptone, 10 g/L NaCl, 5 g/L yeast extract, 15 g/L agar

LB-Medium: 10 g/L Trypton/Peptone, 10 g/L NaCl, 5 g/L yeast extract

for insect cell lines

Monolayer culture media: 500 ml Graces insect media, 50 ml Fetal bovine serum, 2.25 ml Penicillin/Streptomycin/L-glutamine-Mix

Suspension culture media: 1 L SF900 II SFM media, 10 ml Penicillin/Streptomycin-Mix

Cryo preservation media: SF900 II SFM media, 10 ml Penicillin/Streptomycin-Mix, 10 % sterile DMSO

2.1.6 Buffers and solutions

Unless otherwise stated, all buffers and solutions were made using water of MilliQ quality. Buffers and solutions not listed below are described together with the method for which they were used.

Acrylamide stock solution
30 % (v/v) acrylamide, acrylamide:bis-acrylamide ratio 37.5:1

Agarose gel loading buffer (6 x)
0.25 % (w/v) BromoPhenol Blue, 0.25 % (w/v) Xylene Cyanol Blue, 50 % (w/v) Glycerol

Ammonium persulphate (APS)
10 % (w/v) APS

Coomassie destain
40 % (v/v) methanol, 10 % (v/v) acetic acid

Coomassie stain
40 % (v/v) methanol, 10 % (v/v) acetic acid, 0.1 % (w/v) Coomassie Brilliant Blue R-250

Cryoprotection solution I
1.4 M LiSO4, 0.1 M BTP pH 8.5, 0.2 M NaCl

Cryoprotection solution II
1.8 M LiSO4, 0.1 M BTP pH 8.5, 0.2 M NaCl

Cryoprotection solution III,
2.2 M LiSO4, 0.1 M BTP pH 8.5, 0.2 M NaCl

Dialysis buffer
100 mM BTP pH 6.8, 0.2 M NaCl, 2 mM DTT

Elution buffer
50 mM Tris pH 8.0, 0.2 M NaCl, 5 mM DTT, 20 mM reduced Glutathione

HPLC Buffer
Buffer A: 0.1 % TFA
Buffer B: 100 % Acetonitrile, 0.1 % TFA

Lysis buffer
50 mM Tris pH 8.0, 0.2 M NaCl, 5 mM DTT, 0.5 mM PMSF, 1 µM Leupeptin, 1 µM Pepstatin A, 0.3 µM Aprotinin

SDS-PAGE loading buffer (5 x)
625 mM Tris/HCl pH 6.8, 25 % (w/v) sucrose, 10 % (w/v) SDS, 0.1 % (w/v) bromophenol blue, 10 % (v/v) β-mercaptoethanol

SDS-PAGE running buffer
25 mM Tris/HCl pH 8.3, 0.1 % (w/v) SDS, 192 mM glycine

TAE (50 x)
242 g Tris Base, 57.1 ml Acetic Acid (glacial), 37.2 g EDTA, add to 1 L H2O

TFB1-buffer
30 mM KoAc, 100 mM RbCl2, 10 mM CaCl2, 50 mM MnCl2, 15 % (v/v) glycerol, adjust pH to 5.8 with acetic acid, sterile filtration

TFB2-buffer
10 mM MOPS, 75 mM CaCl2, 10 mM RbCl2, 15 % (v/v) glycerol, adjust pH to 6.5 with HCl, sterile filtration

Transfer buffer
10 mM CAPS pH 11, 10 % (v/v) methanol

Wash buffer
50 mM Tris pH 8.0, 0.2 M NaCl, 5 mM DTT

2.1.7 Kits

The Maxiprep-, the Miniprep-, the PCR-purification- and the DNA-extraction kits were all purchased through Qiagen. The BaculoGold Baculovirus DNA-transfection kit was purchased through Pharmingen. The crystallization screening kits, the Hampton Screen I/II, the MPD-Screen, the AmSO4-Screen, the PEG/Ion-Screen, the PEG-Screen, the Additive Screen I-III and the Detergent-Screen I-III were purchased through Hampton Research. Unless otherwise stated, all of the kits were used used strictly in accordance with the manufacturers instructions.

2.2 Methods

2.2.1 Polymerase chain reaction (PCR)

2.2.1.1 General PCR-protocol

PCR enables the rapid and specific amplification of DNA-sequences. The oligonucleotides used for PCR were custom-made by Genelink. A typical PCR-reaction contained 10 µl of 10 x polymerase buffer, 3 µl of 10 mM dNTPs, 1 µM of the 5'- and 3'-primers, 5 to 100 ng of template, 1 to 5 U of polymerase. Distilled water was also added to the final volume of 100 µl. The PCR-amplification program started with a 1 min denaturation step at 94 to 98 °C, followed by 10 to 30 sec primer annealing, which was performed 5 to 10 °C below the melting point of the primer. The next step in the cycle was primer extension at 72 to 75 °C for 1 to 10 min. After 30 cycles, a single primer extension of DNA-fragments

was performed for 10 min at 72 to 75 °C. The quality of the amplified DNA-fragments was analyzed by agarose gel electrophoresis and purified using the PCR-purification kit (Material, 2.1.7).

2.2.1.2 PCR-screening

PCR-screening was used to screen transformed bacterial colonies if they contained the vector with the desired insert by using vector- or gene-specific 5'- and 3'-primers. Single transformed bacterial colonies were selected from the LB-agar-plate and transferred into a PCR-tube containing 20 µl of the pre-pipetted PCR-reaction mixture. PCR was performed immediately and checked by agarose gel electrophoresis.

2.2.1.3 Overlapping-PCR

Overlapping-PCR was performed to incorporate a point mutation into the 2nd-phosphate-binding pocket of the scCdc4$^{271-779}$ DNA-fragment as well as for internal DNA-sequence deletions in the scAPC4 gene. The mutated 5'- and 3'-primers were derived from the position at the native template DNA and changed to the novel DNA-primer sequence bearing the desired mutation or internal deletion. Furthermore, native 5'- and 3'-primer were designed that comprised the whole native template DNA. At first, two DNA-fragments were amplified with the native template DNA, one with the primer pair native 5'- and mutated 3'-primer and the other with the primer pair mutated 5'- and native 3'-primer. The result was two short DNA-fragments bearing the same introduced mutation/deletion, either at the 5'- or the 3'-end of the DNA-fragment. The next PCR was performed with the two mutated 5'- and 3'-DNA-fragments as a template, which overlapped (annealed) in the region where the mutation was introduced. As result of this PCR the amplified DNA bears the desired mutation/deletion inside the DNA-sequence.

2.2.1.4 Side-directed mutagenesis

Side-directed mutagenesis PCR was performed for introducing a point mutation in the second multiple cloning site (MCS) of the pABLO vector. The mutated 5'- and 3'-primers were designed to cover approximately 20 base pair (bp) on each side of the respective point mutation to guarantee specific annealing. The whole vector-DNA was amplified by utilizing

the *pfu* polymerase. On completion of the PCR, the methylated mother vector-DNA was digested for 2 h at 37 °C with the restriction enzyme *Dam*, which specific cuts methylated-DNA. PCR-purification of the newly synthesized mutated vector-DNA (Material, 2.1.7) and transformation then followed.

2.2.2 Cloning

2.2.2.1 Digestion of DNA

DNA-digestion of the PCR-fragments and the vector-DNA was performed with appropriated restriction endonucleases using the buffer system, with time and temperature as recommended by the manufacturer, NEB. To prevent religation of the digested linearized vector-DNA, the 5'-phosphate groups were removed by treatment with Calf intestinal phosphatase (CIP). CIP is compatible with the NEB buffer 2 to 4 used by the restriction enzymes. One unit of CIP is directly added to 2.5 µg linearized vector-DNA digestion mix and incubated for 1 h at 37 °C. The analysis of the PCR-fragments and the vector-DNA digestion by agarose gel electrophoresis then followed and digested DNA-fragments were excised and purified with the DNA-extraction kit (Material, 2.1.7).

2.2.2.2 Ligation with T4 ligase

For the ligation of digested DNA-fragments the molar ratio of insert-DNA to linearized vector-DNA was varied in a ratio of 1 to 1 up to 5 to 1, typically using 100 µg of vector. The DNA-fragments were ligated using 1 µl of T4 ligase in a total reaction volume of 20 µl following the instructions of the manufacturer (NEB). The ligated vector-DNA mix was used for transforming bacterial cells without further purification.

2.2.2.3 Preparation of competent *E. coli* cells

A small amount ~10 µl of frozen competent *E. coli* cells were added to a flask containing 200 ml of LB-Medium with no antibiotic and incubated at 37 °C and 250 rpm. When the bacterial culture reached an OD_{600} value of approximately 0.5, the flask was removed from the shaker and cooled on ice. After 10 min, the bacteria culture was transferred to a pre-chilled 250 ml centrifuge tube and the cells were harvested by centrifugation at 3.5 K, 4 °C for 10 min. The cell pellet was re-suspended in 80 ml ice cold

TFB1-buffer (Material, 2.1.6) and incubated on ice for 5 min. The cells were once again the cells were harvested by centrifugation at 3.5 K, 4 °C for 10 min. That new cell pellet was re-suspended in 8 ml ice cold TFB2-buffer (Material, 2.1.6) and the cells were dispensed as 75 µl aliquots into micro-centrifugation tubes, shock-frozen in liquid nitrogen, and stored at -80 °C until further use.

2.2.2.4 Transformation of *E. coli* cells

Competent *E. coli* cells were thawed in hand and 75 µl was mixed with 20 µl of the ligated vector-DNA mix or 100 ng vector-DNA. The mixtures were kept on ice for 30 min, followed by a heat shock for 1 min at 42 °C and then an immediately 2 min incubation on ice. Transformed *E. coli* cells were incubated for 1 h at 37 °C, with 0.3 ml LB-media containing no antibiotics. After this, the *E. coli* cells were spread on LB-Agar plates containing Amp^r. Subsequent to over-night incubation at 37 °C, *E. coli* transformants were visible as colonies. To identify whether transformants contained the gene of interest, PCR-screening and vector digestion were performed from selected bacterial colonies. The PCR as well as the vector digestion were each analyzed using agarose gel electrophoresis.

2.2.2.5 Isolation of vector-DNA

Transformed *E. coli* cultures were grown over-night at 37 °C and 240 rpm. The next day, 5 ml (200 ml) cell culture was harvested by centrifugation at 3.5 K for 10 min and DNA was purified with the DNA-Miniprep kit (DNA-Maxiprep kit) (Material, 2.1.7). Maxiprep purification was necessary when large DNA amounts were required, such as with the generation of recombinant Baculovirus.

2.2.2.6 Agarose gel electrophoresis

Agarose gel electrophoresis was performed to separate DNA-fragments according to their size. The agarose concentration of the gels varied from 0.8 to 2.0 % depending on the size of DNA-fragments to be analyzed. The agarose was melted in 1 x TAE buffer (Material, 2.1.6) and 0.5 µg/ml Ethidium bromide was added before pouring the gel. Ethidium bromide is an organic dye with a plane structure that intercalates into DNA. It gets excited with UV-light (254 to 366 nm) and emits light of the orange-red spectrum (590 nm) that visualizes the

DNA-fragments. Samples were mixed with 1/5vol of agarose gel loading buffer (Material, 2.1.6) before loading. Gels were run at 5 V/cm and photographed using the Mitsubishi P90 system. A 100 bp- or 1 kbp ladder from NEB was applied as a size standard.

2.2.2.7 Determination of DNA-concentration

DNA has an UV-light absorption maximum at 260 nm due to the aromatic rings of its bases. Therefore, DNA-concentrations of the samples were determined by measuring the OD at 260 nm using a Perkin Elmar spectrophotometer. An OD_{260} of one equals a concentration of 50 µg/ml DNA.

2.2.2.8 DNA-sequencing

Determination of DNA-sequences was done using the dideoxyribonucleotides triphosphate (ddNTPs) chain termination method from F. Sanger (Sanger et al., 1977). Samples were prepared following the instructions of Genewiz. The DNA-sequencing was performed by Genewiz and the DNA-sequencing results were analyzed with the programs DNA Star and Chromas.

2.2.2.9 Vector design

pABLOmut vector

The pABLOmut vector (Figure 2.1) was derived from the pABLO vector which is capable of simultaneously expressing a GST-fusion and a none-tagged protein (Appendix, Figure 7.1). The purpose of the pABLOmut vector design was to mutate the first restriction site NdeI in pABLOs second MCS which contains the first start codon ATG. By mutating the start codon from ATG to ATC (Appendix, Table 7.1) it was possible to use restriction sites

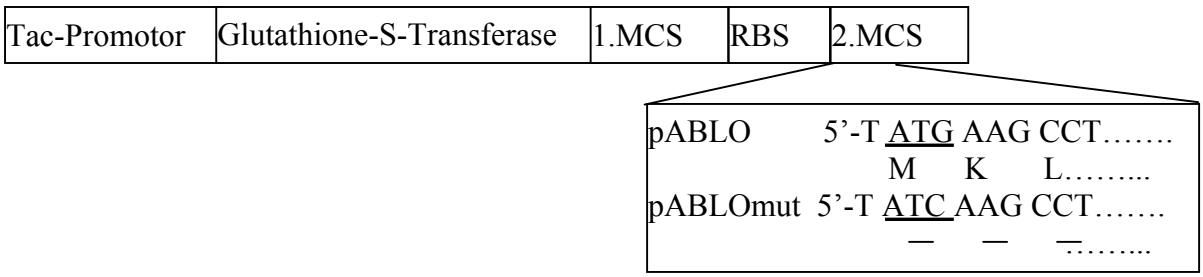

Figure 2.1. Composition of the second MCS of the pABLO and the pABLOmut vector.

downstream of NdeI in the cloning process and to choose the initiation of protein synthesis by incorporating an ATG in the 5'-primer. The vector mutation was performed as described in Method, 2.2.1.4.

pVLSO vector

The pVLSO vector was derived from the none-tagged vector pVL1392, in which the GST-tagged from the vector pMage was cloned in front of pVL1392 MCS. Both vectors were digested with the restriction enzymes EcoRV and Not1, which resulted in two DNA-fragments of each vector on an agarose gel. The smaller DNA-fragment from pMage (5'-EcoRV-GST-Not1-3') and the bigger DNA-fragment from pVL1392 (5'-EcoRV-Not1-3') were excised, purified, ligated and transformed in *E. coli*, and the purified novel vector-DNA was confirmed by DNA-sequencing. The created pVLSO vector contains an N-terminal GST-tagged and misses the first two restriction sites BglII and PstI from the MCS of pVL1392 (Appendix, Figure 7.1).

The designing of the pVLSO vector was performed to simplify the cloning efforts of the APC genes. With the GST-tagged vector pVLSO and the none-tagged vector pVL1392 the same restriction enzymes were used to obtain each APC gene with a single double-digested PCR-product. The pVLSO vector contains the GST-fusion and the pvL1392 vector contains the none-tagged version of the same APC subunit.

2.2.2.10 Cloning of the studied genes and DNA-fragments

The herein studied genes and DNA-fragments were constructed with the methods described above in 2.2.1 to 2.2.2. The composition of the utilized primer pairs and final constructs are found in Table 7.1 and Table 7.2 in the Appendix.

2.2.3 Cell biology methods

2.2.3.1 Cultivation of insect cell lines

Hi5- and SF9 insect cell lines were grown in suspension- and in monolayer cultures. Small-scale cultivation of insect cells can be maintained as monolayer cultures. However, for large-scale insect cell cultivation this is too time-consuming. Therefore suspension cultures are used. To maintain Hi5- (SF9) monolayer cultures, confluent monolayer cultures were

split every 3 days in a ratio of 1 to 5 (1 to 3) into monolayer culture media (Material, 2.1.5). Suspension cultures were maintained by splitting at a cell density of 4 x 10^6 cells/ml back to a density of 5 x 10^5 cells/ml in fresh suspension culture media (Material, 2.1.5).

2.2.3.2 Thawing, freezing and storage of insect cells

Thawing of insect cells

The cell culture vial was thaw in hand and cells were washed twice with 25 ml of suspension culture media. Centrifugation was performed at 1500 rpm for 2 min. After this, the cell pellet was re-suspended in 100 ml suspension culture media and cells were cultivated at 27 °C and 200 rpm. The viability of the cell culture was analyzed every 2 to 3 days and culture was expanded depending on the cell density.

Freezing and storage of insect cells

For freezing insect cells, 300 ml of 2 x 10^6 cells/ml cell culture were centrifuged at 1500 rpm for 2 min and the cell pellet re-suspended in 30 ml cryo preservation media. Aliquots of the cell culture were slowly frozen in the blue-topped isopropanol container and cell culture vials were kept for a day at –80 °C before they were transferred them to the liquid nitrogen tank for long-term storage.

2.2.3.3 Generating and amplification of recombinant Baculovirus

The mixing of a Baculovirus transfer vector (Table 2.1) with the Baculovirus DNA strain *AcNPV*, allows recombination between their homologous sites and transfers the heterologous gene from the Baculovirus transfer vector to the *AcPNV*, resulting in the recombinant Baculovirus.

For generating a recombinant Baculovirus, approximately 2 x 10^6 SF9 cells were seeded onto a 60 mm tissue culture plate, followed by a 5 min incubation period at RT to allow the cells to attach firmly to the tissue culture plate (50 to 70 % confluent). The monolayer culture media was then replaced with 1 ml of Transfection Buffer A (Material, 2.1.7). In the meantime 2 to 5 µg Baculovirus transfer vector containing the gene of interest were mixed with 0.5 µg *AcPNV*, generating the recombinant Baculovirus. After a 5 min incubation period, the sample was mixed with 1 ml of Transfection Buffer B, and was added

drop-by-drop to the tissue culture plate to mix with Buffer A. The SF9 plate was incubated for 4 h at 27 °C before removing the mixture. Cells were washed twice with 3 ml monolayer culture media before once again adding 3 ml monolayer culture media to the SF9 monolayer culture. The plates were then incubated for 4 to 5 days at 27 °C. The supernatant, which included the recombinant passage 1-Baculovirus (P1-virus), was then harvested by centrifugation at 1500 rpm for 5 min and stored in a dark place at 4 °C until further use.

To amplify, recombinant Baculovirus SF9 cells were grown to a confluence of 60 to 80 % on 15 cm tissue culture plates. Up to 2 ml of the monolayer culture media was removed before 0.1 to 1 ml of recombinant P1-virus was added to each plate. Plates were rocked for 1 to 1.5 h at RT, before 20 ml of monolayer culture media was added and the cells were incubated at 27 °C for 3 days. The supernatant (recombinant P2-virus) was then harvested by centrifugation at 1500 rpm for 5 min and stored in a dark place at 4 °C until further use. The amplification process was repeated with the P2-virus and the P3-virus. The P4-virus obtained was used for large-scale recombinant protein production.

2.2.3.4 Protein expression

In insect cells Hi5 monolayer culture

Hi5 monolayer culture cells were used to investigate protein expression levels of proteins of interests with a low passage of recombinant Baculovirus (P2-virus), as amplifying viruses and expanding cells is a very time-consuming process and insoluble expressed proteins cannot be used for further studies.

Therefore, Hi5 monolayer culture cells were grown in 15 cm tissue culture plates to a confluence of 70 to 80 %. Up to 2 ml of the monolayer culture media was removed and the plates were infected with 0.1 to 1 ml of P2-virus. The plates were then rocked for 1 to 1.5 h at RT before 20 ml of monolayer culture media was added to the cells and they were incubated at 27 °C for 3 days. After this, the Hi5 cells were harvested and the cell pellet was stored at –80 °C or used as source of protein purification.

In insect cells Hi5 suspension culture

Hi5 suspension culture cells were used for large-scale protein expression. For that purpose, the P4-virus was necessary.

For a typical 8 L protein expression experiment, 4 x 1 L bottles and 8 x 2.8 L flasks were autoclaved the day before starting the experiment. The next day, 4 x 1 L Hi5 suspension cultures with a density of 4 x 10^6 Hi5 cells/ml were centrifuged at 1500 rpm for 5 min. Each Hi5 cell pellet was re-suspended with 40 ml P4-virus and combined into a 1 L bottle which was rocked for 1 to 1.5 h at RT. After this, the bottle of infected Hi5 cells was divided into eight spinner flasks and to each flask 1 L fresh suspension culture media was added. The infected Hi5 suspension cultures were incubated for 2 to 3 days by 200 rpm at 27 °C. The Hi5 cells were then harvested by centrifugation at 4000 rpm for 10 min. The Hi5 cell pellets were stored at –80 °C or used as source of protein purification.

In *E. coli*

For a typical 12 L *E. coli* protein expression experiment, 12 flasks, each containing 1 L LB-media were autoclaved the day before starting the experiment. In addition, 100 ml LB-Amp^r-media was inoculated with a single colony from a LB-Amp^r-agar plate and incubated over-night at 37 °C by 240 rpm. The next day, the autoclaved LB-media was supplemented with Amp^r and was inoculated with a ratio of 1 to 1000 of the over-night starting culture. The flasks were shaken at 37 °C and 240 rpm until the *E. coli* cell culture density reached an OD_{600} of 0.6 to 0.8 and protein expression was induced with 1 mM IPTG. After induction, the flasks were shaken at RT at 240 rpm for 12 to 18 h. The *E. coli* cell cultures were then centrifugated at 4000 rpm for 10 min. The cell pellets were stored at –80 °C or used as source of protein purification.

2.2.3.5 Cell lysis

Cell lysis is a method that disrupts cells and leads to the release of their proteins into the lysis buffer. Recombinant cell pellets from bacteria- and insect cell cultures were re-suspended in lysis buffer to 30 ml of each L of cell culture (Material, 2.1.6). Cells were lysed three times at 15.000 psi with the Cell disruptor, EmulsiFlex-C5, Avestin. After cell lysis, the homogenate was centrifuged at 40.000 rpm for 1 h (Sorvall, SS34-rotor). The supernatant contains the soluble proteins (the crude extract) and is the source of protein purification.

2.2.4 Chromatographic methods

Purification of GST-fusion proteins

In the glutathione-S-transferase (GST)-fusion system, the target protein is fused to GST-tagged (26 kDa). The GST-tagged has a high binding affinity to glutathione and is therefore a convenient tool to purify GST-fusion proteins from crude extracts. For this purpose the glutathione ligand is coupled via a 10-carbon linker to highly cross-linked 4 % agarose beads, Glutathione 4 B (G4B) and have a binding capacity of approximately 10 mg recombinant GST/ml G4B. The appropriated amount of G4B was added to a gravity column and equilibrated with 5 CV of wash buffer, before the crude extract was applied twice over. After this, the column was washed with 20 CV of wash buffer (Material, 2.1.6). The specific bound GST-fusion protein was eluted with 5 CV of elution buffer (Material, 2.1.6). The free glutathione of the elution buffer competes for the matrix bound GST, in which process the GST-fusion protein is eluted from the beads.

Ion exchange chromatography (IEC)

IEC separates proteins due to their reversible adsorption to a counter charged group immobilized to a matrix (Table 2.2). The extent of tightness to which a protein is bound to an ion exchange matrix depends upon the factors influencing the net charge of the protein such as pH and ionic strength. The adsorpt proteins were separated by gradually increasing the salt-concentration in the mobile phase through which the protein with a low net charge are desorpt and eluted first. After the GST pull down experiment, the ion strength of the protein solution was reduced from 200 mM NaCl to 50 mM NaCl by diluting it in the same buffer, which contains no NaCl. The diluted protein sample was then loaded onto the IEC, equilibrated with 50 mM NaCl, and the proteins were eluted with a NaCl-gradient (50 mM NaCl to1 M NaCl).

Table 2.2. Characteristics of ion exchange matrices.

Ion exchange matrix	Composition	Ion exchange
Source Q	$-CH_2-O-CH_2-CHOH-CH_2-O-CH_2-CHOH-CH_2-N^+(CH_3)_3$	anion
Source S	$-CH_2-O-CH_2-CHOH-CH_2-O-CH_2-CHOH-CH_2-SO_3^-$	cation
Heparin (glycosaminoglycan)	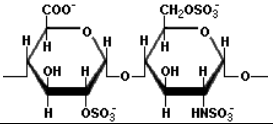	cation

Size exclusion chromatography (SEC)

SEC separates proteins according to their size and shape. The gel filtration matrix contains pores, which allow smaller proteins to distribute in a larger volume than bigger proteins. As a consequence, the smallest protein is the last to elute. In this thesis, the Superdex 200 gel filtration matrix was used. It contains dextran-agarose beads with a pore size of 34 μm and is used to separate proteins of 10-600 kDa (according Pharmacia). To achieve a good level of separation, the protein loading volume never exceeded 2 ml.

Reversed phase Chromatography (RPC)

In RPC, proteins or peptides are bound through hydrophobic interaction to the stationary phase. The stationary phase consists of silicon-based molecules with chlorine as the reactive group, to which a hydrocarbon group is attached. The linear aliphatic hydrocarbon groups of 8 carbons (C8) or 4 carbons (C4) form the hydrophobic phase. A C8-column was used for peptide- and a C4-column for protein purification. After the column was equilibrated with HPLC Buffer A (Material, 2.1.6), the sample was loaded. The acetonitrile-gradient was then started with HPLC Buffer B (Material, 2.1.6) and led to the elution of the proteins, initially with a minimum level of hydrophopic interaction. RPC was used as a sample preparation for mass spec analysis and for peptide purification.

2.2.5 Biochemical methods

2.2.5.1 Thrombin cleavage

All GST-fusion proteins used in this thesis contain the thrombin recognition site Leu-Val-Pro-Arg-Gly-Ser, which links the GST-tag to the protein of interest. Thrombin binds to the thrombin recognition site and cleaves the GST-fusion protein in the GST-protein and the target protein starting with the amino acid sequence Gly-Ser. The amount of thrombin necessary to cleave the GST-fusion protein was dependent on the accessibility of the thrombin recognition site.

2.2.5.2 SDS polyacrylamide gel electrophoresis (SDS-PAGE)

SDS-PAGE was used to separate proteins according to their molecular weight (MW). SDS is an anionic detergent and binds to proteins through hydrophobic interaction. It

complexes proteins in a constant weight ratio and masks the protein charge with SDS own strongly negative charge, resulting in identical charge densities on the surface. Protein samples were prepared by boiling with SDS and DTT containing SDS-PAGE loading buffer, which destroys structure elements as well as it cleaves disulphide bridges of proteins. The MW of the separated proteins was determined through comparison with a SDS-PAGE MW standard (BioRad). The SDS-PAGE was carried out in a Mini ProteanII Cell (BioRad). The percentage of acrylamide used in the SDS-PAGE was dependent on the MW of the investigated protein. After this, protein gels were boiled for 1 min in coomassie staining solution (Material, 2.1.6) and then transferred into the coomassie destaining solution (Material, 2.1.6) until protein bands were clearly visible. For the purpose of record keeping, destained gels were dried with Slab Gel Dryer Model SE II 60 (Pharmacia Biotech). SDS-gels were prepared as outlined (Table 2.3).

Table 2.3. Buffers and solutions for 10 SDS-PAGEs.

50 ml SDS running PAGE				**50 ml SDS stacking PAGE**	
	15 %	18 %			4.3 %
30 % Acrylamide	18.75 ml	22.5 ml		30 % Acrylamide	5.4 ml
2 M Tris pH 8.8	9.4 ml	9.4 ml		1 M Tris pH 6.8	6.8 ml
20 % SDS	0.25 ml	0.25 ml		20 % SDS	0.25 ml
distilled H2O	21.05 ml	17.3 ml		distilled H2O	37.6 ml
TEMED	0.05 ml	0.05 ml		TEMED	0.05 ml
APS 10 %	0.5 ml	0.5 ml		APS 10 %	0.5 ml

2.2.5.3 Limited proteolysis

Limited proteolysis is a powerful method, which determines flexible and unstructured regions in a protein of interest. The limited proteolysis of a protein can be controlled by the amount, time and the specificity of the enzyme used in the experiment. Under constant conditions, the fragmenting pattern of a protein is very characteristic and reproducible. To further analyze the fragmentation pattern, the protein fragments were separated and visualized on an SDS-PAGE. N-terminal sequencing- and mass spec analysis of the protein fragments then followed, which can lead to the identification of the more stable core domains of a protein of interest. Subsequent cloning of the protein, excluding the determined flexible regions, leads to more stable proteins that might be easier to crystallize.

Subtilisin The enzyme Subtilisin belongs to the serine protease family and has no preference in catalyzing the cutting of specific amino acid bonds.

Trypsin The enzyme Trypsin belongs to the serine protease family and preferably cleaves the peptide bonds C-terminal of the amino acids of arginine and lysine.

2.2.5.4 Phosphorylation of proteins

The $Sic1^{1-100}$ protein fragment was phosphorylated by using 1 to 100 molar ratio of Cdk6 bound to the herpesvirus K-Cyclin, prepared as previously described (Jeffrey et al., 2000) in 100 mM HEPES pH 7.0, 200 mM NaCl, 10 mM ATP and 10 mM MgCl2 at RT for 30 min. The phosphorylation sites and levels were verified by electrospray ionization mass spectrometry of reversed phase HPLC-purified tryptic digest.

2.2.5.5 Western blot

To blot proteins from a SDS-PAGE to a Polyvinylidine diflouride membrane (PVDF), a wet transfer was performed in a Mini Trans-Blot Cell (BioRad). The PVDF membrane was submerged in 100 % methanol and was then washed twice with distilled H2O. Before the western blot transfer stack was assembled as outlined in (Figure 2.2), foam pads, Whatman filter paper and PVDF membrane were soaked in transfer buffer (Material, 2.1.6). The transfer was carried out at 300 mA for 2 h at 4 °C.

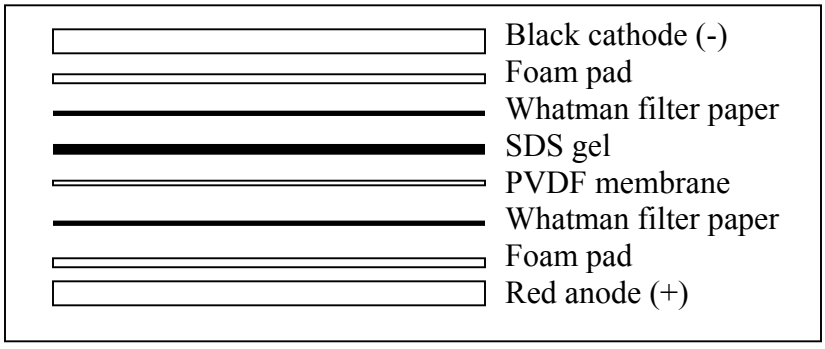

Figure 2.2. Assembly of a western blot transfer stack.

2.2.5.6 Sample preparation for N-terminal protein sequencing

The N-terminal protein sequencing was performed using the solid-phase-Edman-reduction method. In each cycle, the most N-terminal amino acid of the polypeptide chain is

reduced and determined. For this technique proteins need to be bound to a solid phase. Therefore, protein samples were prepared by separation on an SDS-PAGE followed by a western blot. The PVDF membrane of the western blot was stained with Coomassie until blue protein bands were visible and the membrane was air dried. The blue protein bands of interest were excised and the MSKCC Protein Analysis lab performed the N-terminal protein sequencing analysis.

2.2.5.7 Sample preparation for mass spectrometry

Mass spectrometry is a method to identify the exact MW of proteins and requires only ~20 ng of protein. For mass analysis, proteins with a purity of at least 90 % were used. Mass analyses of protein fragments from limited proteolysis were prior-purified by FPLC or HPLC. Protein samples were sent and analyzed by the mass spectrometry facility in Berkeley, California.

2.2.5.8 Dialysis

Dialysis was performed to adjust the buffer conditions of the protein- and peptide solutions used in the ITC-experiments. Protein- and peptide solutions were each filled in a size-appropriated dialysis bag and dialyzed against the dialysis buffer (Material, 2.1.6). The buffer was exchanged for three times with a sample to buffer ratio of 1 to 500.

2.2.5.9 Concentrating of proteins

Protein solutions were concentrated with the ultrafiltration device from Amicon (Millipore) in accordance with the instructions of the manufacturer.

2.2.5.10 Determination of protein concentration

A rough estimation of protein concentrations was achieved via Bradford assay. One microliter of protein solution was diluted into 1 ml Bradford solution, mixed and incubated for 5 min before reading at OD_{595}. It was assumed that a reading of 0.3 equals a protein concentration of 10 mg/ml, lab standard.

More accurate measurements of protein concentrations were determined by the use of the proteins distinct coefficient factors and the reading obtained at OD_{280}.

2.2.5.11 Purification of the studied proteins and protein complexes

Purification of the Fbw7-Skp1 complex

Due to its insolubility in the *E. coli* strain BL21(DE3), the Fbw7$^{232-707}$-Skp1 complex was purified from Hi5 insect cells, whereas the Fbw7$^{263-707}$-Skp1 complex and the Fbw7$^{279-707}$-Skp1 complex were purified from the *E. coli* strain BL21(DE3). All Fbw7-Skp1 complexes were purified using the following protocol: Initially, cells were disrupted and the GST-fusion complex was isolated from the crude extract by GST-affinity chromatography. The eluted GST-fusion complex (50 mM Tris pH 8.0, 200 mM NaCl, 5 mM DTT and 20 mM Glutathione) was then digested with 1 % thrombin over-night. The next day, the protein complex was diluted to 50 mM NaCl, 5 mM DTT, 50 mM Tris pH 8.0, it was loaded onto the Heparin column equilibrated in the same buffer, and the complex was eluted with a linear NaCl-gradient. The peak fractions were pooled and concentrated by ultrafiltration before purification continued by size exclusion chromatography. A maximum of 2 ml of complex was loaded onto an equilibrated Superdex 200 column (20 mM BTP pH 6.8, 5 mM DTT, 200 mM NaCl) and was collected in 0.5 ml fractions. The peak fractions were pooled and stored at –80 ºC until further use.

Purification of the scCdc4-Skp1 complex

The scCdc4$^{111-779}$-Skp1 complex, the scCdc4$^{271-779}$-Skp1 complex as well as the mt-scCdc4$^{S464A/T465V}$-Skp1 complex and the mt-scCdc4$^{R443M/S464A/T465V}$-Skp1 complex were purified from Hi5 insect cells. All scCdc4-Skp1 complexes were purified using the following protocol: Initially, cells were disrupted and the GST-fusion complex was isolated from the crude extract by GST-affinity chromatography. The eluted GST-fusion complex (50 mM Tris pH 8.0, 200 mM NaCl, 5 mM DTT and 20 mM Glutathione) was digested with 5 % thrombin over two nights. Then, the protein complex was diluted to 50 mM NaCl, 50 mM MES pH 6.0, 5 mM DTT and loaded onto a Source S column equilibrated with the same buffer. The elution of the complex then followed, with a linear NaCl-gradient. The peak fractions were pooled and concentrated by ultrafiltration before purification continued by size exclusion chromatography. A maximum of 2 ml of complex was loaded onto an equilibrated Superdex 200 column (100 mM BTP pH 6.8, 5 mM DTT, 200 mM NaCl) and was collected in 0.5 ml fractions. The peak fractions were pooled and stored at –80 ºC until further use.

Purification of APC4

GST-fusion of full-length scAPC4, spAPC4 and hAPC4 were purified from Hi5 insect cells and the APC4 fragments were purified either from *E. coli* strain BL21(DE3) or from Hi5 insect cells. All APC4 subunits and APC4 protein fragments were purified using the following protocol: Initially, cells were disrupted and the GST-fusion complex was isolated from the crude extract by GST-affinity chromatography. The eluted GST-fusion complex (50 mM Tris pH 8.0, 200 mM NaCl, 5 mM DTT and 20 mM Glutathione) was digested with 0.1-1 % thrombin over-night. Then, the protein complex was diluted to 50 mM NaCl, 50 mM Tris pH 8.0, 5 mM DTT and loaded onto a Source Q column equilibrated with the same buffer. The elution of the complex with a linear NaCl-gradient then followed. The peak fractions were pooled and concentrated by ultrafiltration before purification continued by size exclusion chromatography. A maximum of 2 ml of complex was loaded onto an equilibrated Superdex 200 column (50 mM Tris pH 8.0, 5 mM DTT, 200 mM NaCl) and was collected in 0.5 ml fractions. The peak fractions were pooled and stored at –80 ºC until further use.

Purification of all other APC subunits and fragments

The purification of all other APC subunits is identical to the described purification protocol for APC4. However, the buffer composition of the final size exclusion chromatography was different for hAPC7 (10 mM BTP 6.8, 200 mM NaCl, 6 mM DTT) and hAPC2$^{554-822}$-hAPC11 (20 mM Tris pH 7.8, 200 mM NaCl, 5 mM DTT).

Purification of Sic1-100

The His-Sic1$^{1-100}$ protein fragment was purified by Bing Hao from the *E. coli* strain BL21(DE3).

2.2.6 Isothermal titration calorimetry (ITC)

ITC is a method that measures the thermodynamic properties of an intermolecular protein-protein interaction in the equilibrium by directly measuring the heat evolved during the association of a ligand with its binding partner (Figure 2.3). In a single experiment, the values of the association constant (K_a), the stoichiometry (n) and the enthalpy of binding (ΔH_b) are determined. The free energy and entropy of binding can be determined from (K_a) (Pierce et al., 1999).

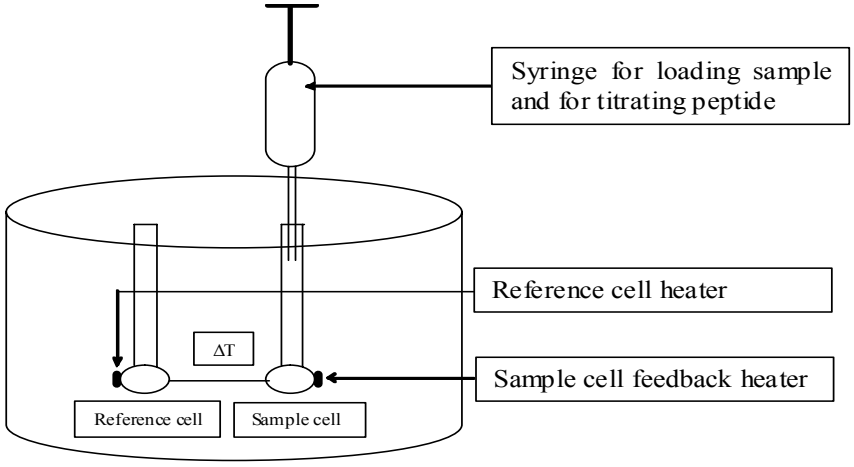

Figure 2.3. ITC instrument.

It consists of two identical cells (reference cell containing water, sample cell the probe) composed of a highly efficient thermal conducting material surrounded by a jacket in which water of constant temperature is circulating. During an injection of a titrant into the sample cell the feedback heat detector senses and adjusts the temperature difference between the cells through a time dependent input of power (µcal/sec).

Prior to the binding studies of the Fbw7-Skp1 and scCdc4-Skp1 complex with their phosphorylated peptides Cyclin E and Sic1, the complexes and peptides were dialyzed in the same dialysis buffer and beaker (Material, 2.1.6). The final dialysis buffer was used for concentration adjustments. Before the ITC experiments, all samples were centrifuged and degassed for 5 min. ITC was performed on the MCS ITC unit from Microcal. The sample cell was filled with a 17 to 50 µM solution of the complex and was titrated to saturation with the 0.8 to 1 mM peptide solution contained in the syringe. Each ITC experiment was performed with 25 injections of 5 µl peptide solution at 2 min intervals and 25 ºC as described (Min et al., 2002). The data was analyzed using the program MicroCal Origin

version 7.0. All dissociation constants (K_d) represent a mean of two or three independent determinations.

2.2.7 Protein crystallization

In effort to find conditions that allow a protein of interest to crystallize, a trail and error approach is applied with the screening of many different crystallization conditions. If a potential promising protein crystallization condition is found, then a screening around that condition is performed with varying parameters such as protein concentration, buffer and salt condition, temperature and drop size.

2.2.7.1 Hanging drop vapor diffusion method

In the hanging drop vapor diffusion method, the hanging drop (2-10 µl) was equilibrated against a much larger reservoir volume of precipitant solution (0.5 ml) in an enclosed chamber (Figure 2.4). The hanging drop was performed on a cover slide by mixing protein and reservoir solution in a 1 to 1 volume ratio. After the setup, the concentration of both solutions in the hanging drop will be half. During the equilibration process, water vapor diffuses through the vapor phase from the hanging drop, which contains a high vapor pressure, to the reservoir solution, which contains a low vapor pressure.

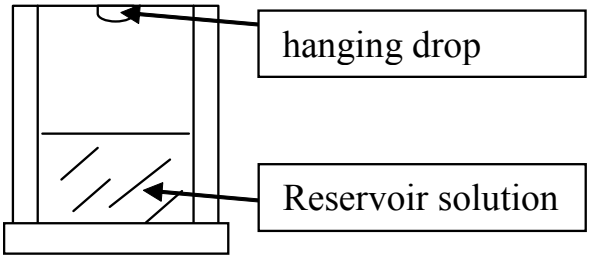

Figure 2.4. Protein crystallization with the hanging drop vapor diffusion method.

The loss of water from the hanging drop decreases its volume and leads to an increase of all the concentrations of the nonvolatile components in the hanging drop, which drives the system towards supersaturation (metastable-, labile- and precipitation zone) (Figure 2.5). When supersaturation reaches the labile zone and micro protein crystals are formed, the macromolecule solution concentration decreases as the macromolecules become part of the growing crystal. Crystal growth stops when the hanging drop and reservoir solution have the

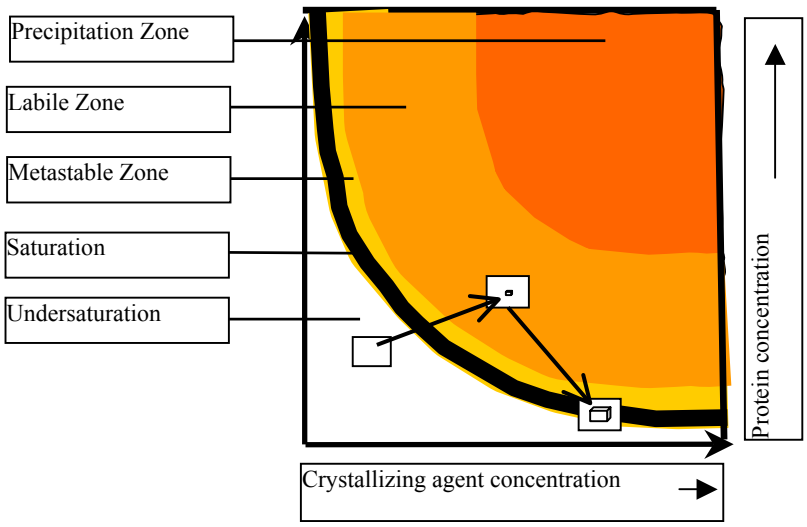

Figure 2.5. Phase diagram of a protein solution under crystallization condition.

same vapor pressure (McPherson, 1998). For the protein crystallization experiments, screening kits from Hampton Research and home-made screening kits were used. For improving crystal quality Additive-Screen I-III and Detergent-Screen I-III were tested (Hampton Research).

2.2.7.2 Co-crystallization

Co-crystallization is a method used to obtain crystals of protein-peptide complexes. For co-crystallization experiments of Fbw7-Skp1 with their specific phosphorylated Cyclin E or c-Myc peptides, the dimer was mixed with the peptides in a 1 to 2 molar ratio and used for setting up the co-crystallization experiments with the hanging drop vapor diffusion method.

2.2.8 X-ray crystallography

A detailed description of the physical principles of X-ray crystallography is beyond the scope of this work. For an introduction on the theoretical background as well as on the theory of the applied methods, the following book is recommended (McPhearson, 1998).

2.2.8.1 Crystal-preparation and x-ray data collection

To collect x-ray data in the -170 ºC nitrogen-stream, the protein crystals need to be cryoprotected to avoid damage to the crystal lattice due to the formation of ice. The transfer of protein crystals to a cryoprotectant was performed in three steps, where only the

concentration of the cryoprotectant such as glycerol, PEG or LiSO4 is increased. The ability of a cryoprotectant to cryoprotect a protein crystal has to be determined for each crystallization condition separately using a trail and error approach. The cryoprotection of the Fbw7-Skp1 crystals in the presence and absence of peptides was performed as follows: A crystal was picked up with a loop from a hanging drop and placed for 30 sec in the cryoprotection solution I (Material, 2.1.6) before transferring the crystal to the cryoprotection solution II, which only increased the concentration of the cryoprotectant, LiSO4 to 1.8 M. After 30 sec, the crystal was transferred to a cryoprotection solution III, where only the concentration of the cryoprotectant LiSO4 was increased to 2.2 M. The cryoprotected crystal was then picked up by a loop, flash frozen and stored in liquid nitrogen until data collection was performed.

X-ray data collection is the last experimental step in crystallography. It includes mounting the crystals on a goniometer head in an x-ray beam and measuring the intensity and pattern of the diffraction spots using an automated detector. The synchroton data of the Fbw7-Skp1 crystals in the presence and absence of peptides were collected at the National Synchroton Light Source (NSLS) at Brookhaven, NY, and at the Advanced Photon Source (APS) in Argonne, IL.

2.2.8.2 Structure determination

To determine the protein structure from the reflection intensities of the collected data frames, the intensities need to be Fourier-transformed in an electron-density map. To achieve this, it is necessary to know the phase of each reflection. However, the phase information of each reflex is lost during data collection. Three major techniques have evolved to solve the phase problem: multiple isomorphous replacement (MIR), multiple anomalous dispersion (MAD) and molecular replacement (MR). In this thesis, MR solved the phase problem of Fbw7-Skp1.

MR is the method of choice when the target protein has homology to a protein whose structure has already been determined. In the case of Fbw7 as the search model, the structures of scCdc4 (Orlicky et al., 2003), β-Trcp1 (Wu et al., 2003) and Skp1 (Schulman et al., 2000) were used. The patterson-search was performed with the program AmoRE, which

searches for an orientation and position of the search model that can be fitted into the diffraction data. The patterson-solution was optimized by rigid body refinement.

2.2.8.3 Model building and refinement

After the phase problem was solved, an electron-density map was calculated and visualized with the program O. Model building is an iterative process, comprising of the manual fitting of molecule parts in the electron-density map, as the map gradually becomes interpretable. After each fitting cycle, the new structure-factors are calculated and the new calculated phases are used with the original reflection intensities to calculate a better interpretable electron-density map. In principle, refinement involves the adjusting of the positions and temperature factors of all the atoms in the model, as well as the building of water molecules, ions and other ligands. The quality of the refinement is evaluated by the R-factor, which is a value of agreement between the observed structure-factor amplitudes (F_{obs}) and those calculated from the model (F_{calc}). To prevent the structure from being over-refined, an unbiased R_{free}-factor was calculated during the refinement process using about 5 % of the data randomly omitted from the refinement. The electron-density maps of the four Fbw7-Skp1 structures in the presence and absence of peptide were refined with the CNS program (Bruenger et al., 1998) until their R-factor yielded around 25 %.

3. and 4. Results and Discussion

3.1 Cloning, expression, purification and characterization of the Fbw7-Skp1 complex

The Fbw7 protein was studied to identify how the Fbw7 WD40 domain recognizes its phosphorylated substrates. It was necessary to co-express Fbw7 with Skp1, because Fbw7 by itself is insoluble, when expressed recombinantly. The studied Fbw7$^{232-707}$-Skp1, Fbw7$^{263-707}$-Skp1 and Fbw7$^{279-707}$-Skp1 complexes are comprised of the invariant Fbw7-exons among the Fbw7α, Fbw7β and Fbw7γ isoforms and contain an Fbox, Linker and WD40 domain (Introduction, Figure 1.5). The boundaries for the three truncated Fbw7 proteins were chosen according to a secondary structure prediction of the Fbw7 protein, and preserve the ability of Fbw7 to bind with its N-terminal Fbox domain to Skp1 and with its WD40 domain to phosphorylated substrates (Figure 3.1). These Fbw7-Skp1 complexes were expressed in either the *E. coli* strain BL21(DE3) or Hi5 insect cells. Both systems are suitable for producing high quantities of recombinant proteins, a necessity for protein crystallization.

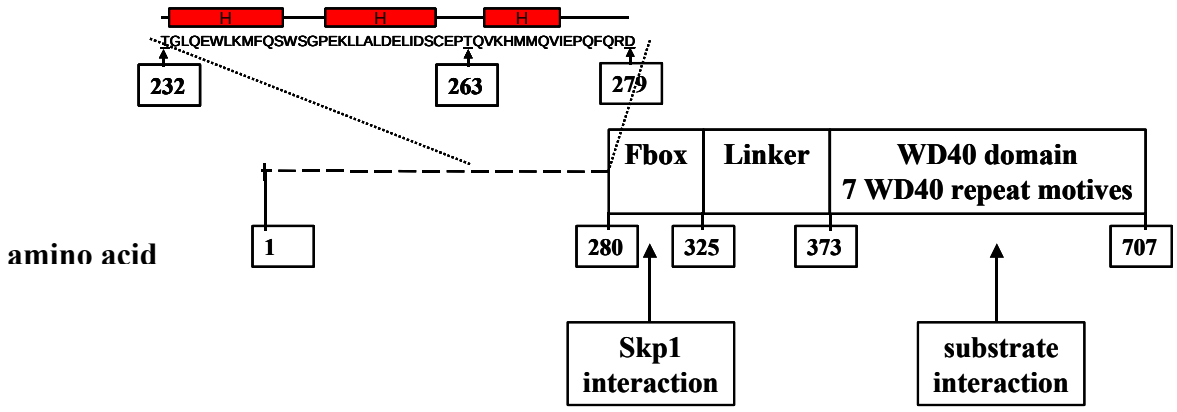

Figure 3.1. Predicted domain structure of Fbw7.

Shown is a schematic representation of the organization of main functional domains in Fbw7. Three constructs comprising the amino acid residues 232-707, 263-707 and 279-707 of Fbw7 were chosen for biochemical characterization and crystallization.The red boxes denote the predicted Fbw7 helices.

3.1.1 Cloning and expression of the Fbw7-Skp1 complex in *E. coli*

The Fbw7 gene was cloned into the pAcG2T vector previously by Brenda Schulman. The truncated Fbw7 fragments comprising the amino acids 232 to 707, 263 to 707 and 279 to 707 of the Fbw7 gene were subcloned into the pABLOmut vector. The Skp1 gene, previously constructed by Brenda Schulman, contains two internal deletions of the amino acids 39 to 43

and 71 to 82. This facilitates Skp1 crystallization as reported in (Schulman et al., 2000). The Skp1 gene was subcloned into the pABLOmut vector as a dicistronic message with the GST-Fbw7 fusion-coding region in front of Skp1 (Appendix, Table 7.1 and Table 7.2). The co-expression of the recombinant proteins in *E. coli* strain BL21(DE3) was started after induction with 1mM IPTG (Method, 2.2.3.4).

3.1.2 Cloning and expression of the Fbw7-Skp1 complex in insect cells

The Fbw7 gene was cloned into the pAcG2T vector previously by Brenda Schulman. The C-terminal amino acids 232 to 707, 263 to 707 and 279 to 707 of the Fbw7 gene were subcloned into the GST-tagged transfer vector pAcG2T (Appendix, Table 7.1 and Table 7.2). The none-tagged transfer vector pVL1393_Skp1 was constructed by Brenda Schulman and contains two internal deletions of Skp1 amino acids 39 to 43 and 71 to 82 as reported in (Schulman et al., 2000). Homologous Baculovirus recombination, recombinant Baculovirus amplification and co-expression of the Fbw7 and Skp1 protein in Hi5 insect cells then followed (Methods, 2.2.3.3 and 2.2.3.4).

3.1.3 Purification and characterization of the Fbw7-Skp1 complexes

All Fbw7-Skp1 complexes were purified using the following protocol: Initially, cells were lysed and the complex was purified by glutathione affinity chromatography. The GST-tag of Fbw7 was then cleaved by thrombin. Subsequently, the complex was purified via a

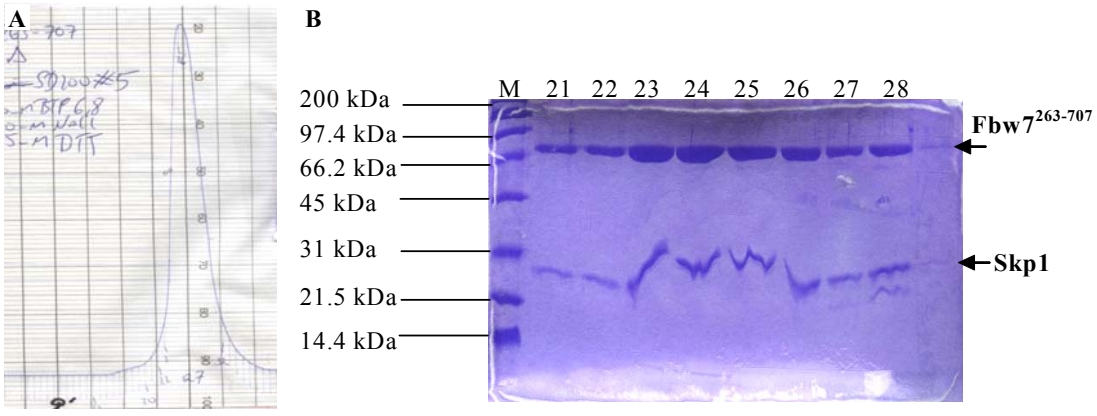

Figure 3.2. Purification of the Fbw7$^{263-707}$-Skp1 complex.

A) The chromatogram shows the SD200 elution profile of the Fbw7$^{263-707}$-Skp1 complex, flow rate 0.5ml/min, elution buffer (200 mM NaCl, 5 mM DTT, 20 mM BTP pH 6.8).
B) SD200 protein fractions were separated by SDS-PAGE and stained with Coomassie blue.

Heparin column and the purification finished using an SD200 column (Method, 2.2.4; Figure 3.2). The Fbw7$^{279-707}$-Skp1 and Fbw7$^{263-707}$-Skp1 complexes show comparable protein expression levels in insect cells and bacteria, and behave similarly during protein purification. As a result of time constraints, expression in *E. coli* strain BL21(DE3) was preferred for the purification of these constructs. Only the Fbw7$^{232-707}$-Skp1 complex was purified from insect cells due to its insolubility in *E. coli* strain BL21(DE3).

Surprisingly, the comparison of the SD200 elution profiles of the different Fbw7-Skp1 complexes showed significant differences. The peak fraction of Fbw7$^{263-707}$-Skp1 complex eluted at an apparent MW of 67 kDa consistent with a monomeric Fbw7$^{263-707}$-Skp1 complex, whilst the Fbw7$^{232-707}$-Skp1 complex, which contains only 31 additional amino acids, eluted at an apparent MW of 130 kDa, which corresponds to a dimeric Fbw7$^{232-707}$-Skp1 complex (data not shown). This suggested that the N-terminal 31 amino acids of the Fbw7$^{232-707}$-Skp1 complex might be involved in the dimerization of the Fbw7-Skp1 complex. However, analytical centrifugation of the three Fbw7-Skp1 complexes showed that the Fbw7$^{279-707}$-Skp1 complex and the Fbw7$^{263-707}$-Skp1 complex are monomers under the

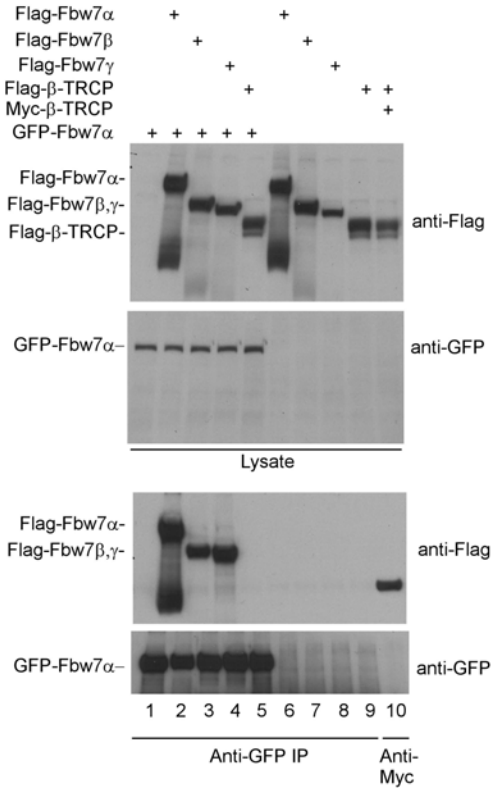

Figure 3.3. Dimerization of Fbw7.

Lysate of GFP-Fbw7α was incubated with Flag-Fbw7α, Flag-Fbw7β and Flag-Fbw7γ and visualized with anti-Flag and anti-GFP. Data was provided by Wade Harper.

conditions tested, whereas the Fbw7$^{232-707}$-Skp1 complex aggregates. Therefore, it is uncertain if Fbw7$^{232-707}$ N-terminal 31 amino acids are involved in dimerization. Furthermore, an *in vitro* pull down assay, which was provided by our collaborator, Wade Harper, shows that all three full-length Fbw7 isoforms dimerize with matrix bound GFP-Fbw7α (Figure 3.3).

3.2 Cloning, expression, purification and characterization of the scCdc4-Skp1 complex

The scCdc4 protein, which is a homolog of Fbw7, was studied to elucidate how the scCdc4 WD40 domain recognizes its phosphorylated substrate Sic1.

3.2.1 Cloning and expression of the scCdc4-Skp1 complex in insect cells

The scCdc4 fragments, coding for the C-terminal amino acids 111 to 779 and 271 to 779, were subcloned into the GST-tagged transfer vector pAcG2T and the full-length scSkp1 was subcloned into the none-tagged transfer vector pVL1392. The three constructs were a kind gift by Brenda Schulman. The two scCdc4$^{S464A/T465V}$ and scCdc4$^{R443M/S464A/T465V}$ mutants coding for the scCdc4 amino acids 271 to 779 were obtained by overlapping-PCR from the pAcG2T_scCdc4$^{271-779}$ construct and were subcloned into the GST-tagged transfer vector pAcG2T (Appendix, Table 7.1 and Table 7.2). Following homologous recombination and recombinant Baculoviruses amplification, proteins were co-expressed in Hi5 insect cells (Methods, 2.2.3.3 and 2.2.3.4).

3.2.2 Purification and characterization of the scCdc4-Skp1 complexes

The purification of the complex started with cell lysis, followed by glutathione affinity chromatography, cleavage of the GST-tag with thrombin, anion exchange chromatography and finally, SD200 size exclusion chromatography (Figure 3.4). Analytical ultra centrifugation with the scCdc4$^{111-779}$-Skp1 and the scCdc4$^{271-779}$-Skp1 complexes revealed that the scCdc4$^{271-779}$-Skp1 complex exists as a monomer, whereas the scCdc4$^{111-779}$-Skp1 complex forms a dimer (data not shown). This suggested that scCdc4 N-terminal amino acid sequence 111 to 270 that precede the Fbox domain is involved in dimerization.

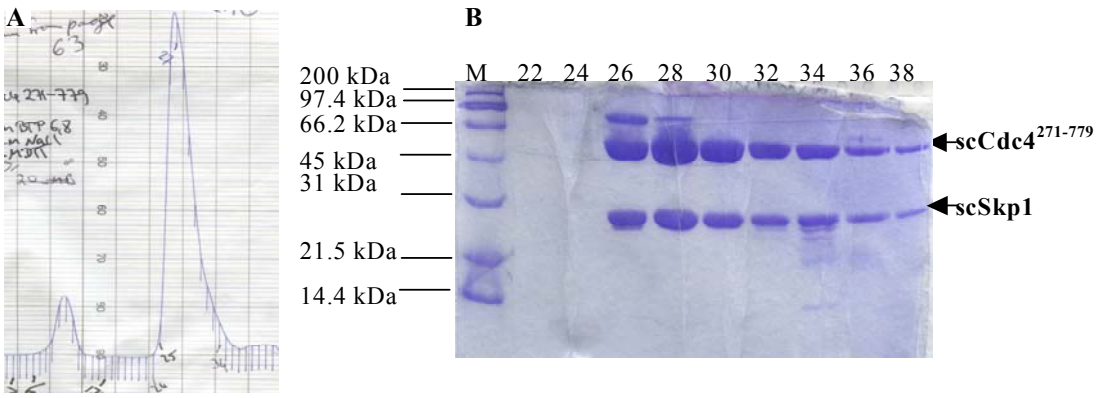

Figure 3.4. Purification of the scCdc4$^{271-779}$-Skp1 complex.

A) The chromatogram shows the elution profile of scCdc4$^{271-779}$-Skp1 complex after SD200, flow rate 0.5ml/min, elution buffer (200 mM NaCl, 5 mM DTT, 20 mM BTP pH 6.8).
B) SD200 protein fractions were separated by SDS-PAGE and stained with Coomassie blue.

3.3 Binding studies of Fbw7-Skp1 with phosphorylated Cyclin E peptides

Previous biochemical data has demonstrated that the recognition of Cyclin E by Fbw7 is dependent upon the phosphorylation of the C-terminal Cyclin E residue Thr380 (Strohmaier et al., 2001; Koepp et al., 2001) or the N-terminal Cyclin E residue Thr62 (Welcker et al., 2003; Ye et al., 2004) at the position 0 (P0). Interestingly, it has also been reported that the C-terminal Cyclin E residues Ser372 at the position –8 (P-8) (Koepp et al., 2001; Ye et al., 2004) and Ser384 at the position +4 (P+4) (Welcker et al., 2003) are also phosphorylated, and that they support binding to Fbw7. The function of the by GSK3 phosphorylated N-terminal Cyclin E residue Ser58 at the position –4 (P-4) is unknown (Welcker et al., 2003; Ye et al., 2004). The alignment of several Cyclin E orthologs (Figure 3.5) reveals that in their N-terminal and C-terminal degrons, all orthologs contain a conserved threonine or serine at P0. Furthermore, the proposed phosphorylated C-terminal Cyclin E residue Ser372 at P-8 and N-terminal residue Ser58 at P-4 are not highly conserved among Cyclin E orthologs. All C-terminal Cyclin E orthologs, however (Figure 3.5), and most Fbw7 substrates (Introduction, Figure 1.4) contain a serine at P+4. In addition, most orthologs contain a phospho-mimicking residue in their N-terminal Cyclin E region at P+4. It is hence possible that the phosphorylation at P+4 is of general significance.

Binding studies with ITC thus aim to clarify how the phosphorylation of the C-terminal Cyclin E residues Ser384 and Ser372 influences binding to the Fbw7 WD40

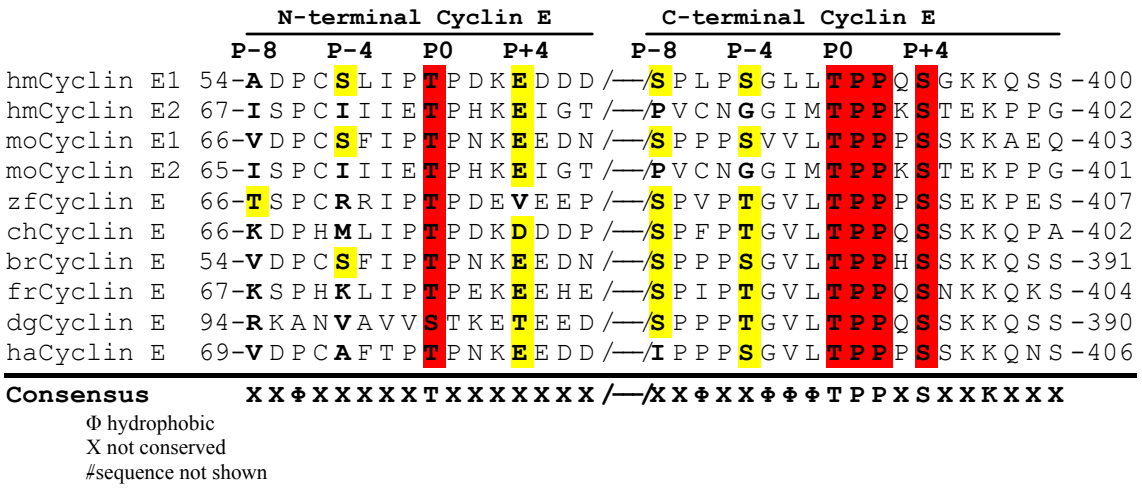

Figure 3.5. Sequence alignment of Cyclin E orthologs.

Used accession numbers for human, hmCyclin E1 (A40270); human, hmCyclin E2 (096020); mouse, moCyclin E1 (NP_031659); mouse, moCyclin E2 (NP_033960); zebrafish, zfCyclin E (P47794); chicken, chCyclin E (P49707); brown rattus, brCyclin E (BAA03116); frog, frCyclin E (Q91780); dog, dgCyclin E (XP_541724); hamster, haCyclin E (AAL03941). Substrate residues are numbered according to the conserved Thr determined as P0. 100 % conserved residues are colored in red, polar and charged residues are colored in yellow.

domain. Four different C-terminal Cyclin E peptides were synthesized, all containing a phosphate group at residue Thr380 at P0 and varied in the number and position of the phosphorylated serines (Table 3.1). ITC data showed that C-terminal CycE^{31pT380} peptide,

Table 3.1. Cyclin E peptides used in ITC experiments with the Fbw7$^{263-707}$-Skp1 complex.

CycE-Peptides	peptide sequence				K_d to Fbw7-Skp1 (µM)
		P-8	P0	P+4	
CycE^{31pT380}	360-AKKAMLSEQNRA	S PLPSGLL	**[pT]**PPQ	S GKKQSS-390	49 ± 31
CycE$^{31pT380/pS384}$	362- KAMLSEQNRA	S PLPSGLL	**[pT]**PPQ**[pS]**GKK	-387	0.07 ± 0.11
CycE$^{29pS372/pT380}$	360-AKKAMLSEQNRA**[pS]**PLPSGLL		**[pT]**PPQ	S GKKQ -388	no ITC signal
CycE$^{31pS372/pT380/pS384}$	360-AKKAMLSEQNRA**[pS]**PLPSGLL		**[pT]**PPQ**[pS]**	GKKQSS-390	0.13 ± 0.03

C-terminal Cyclin E (CycE) peptides with phosphorylated sites in bold and all CycE peptides are N-terminal acetylated. Phosphorylation position is indicated above. Dissociation-constant (K_d) values of the peptides to Fbw7-Skp1 complex were measured at 25ºC and are an average of three independent sets of ITC readings, ± indicates the standard deviation.

solely phosphorylated on residue Thr380, had a K_d of 49 µM to Fbw7. Interestingly, the introduction of a second phosphorylation at residue Ser384 (CycE$^{31pT380/pS384}$) had a K_d of 0.07 µM to Fbw7. This revealed that the doubly phosphorylated C-terminal CycE$^{31pT380/pS384}$ peptide binds 700 times better to Fbw7 than the singly phosphorylated C-terminal CycE^{31pT380} peptide. The C-terminal CycE$^{31pS372/pT380/pS384}$ peptide phosphorylated on the residues Ser372, Thr380 and Ser384 bound with a K_d of 0.13 µM to Fbw7 and is comparable to the doubly phosphorylated C-terminal CycE$^{31pT380/pS384}$ peptide. Surprisingly, if the C-

terminal CycE^{31pT380} peptide contained a further phosphate group at residue Ser372 (CycE$^{31pS372/pT380}$), no ITC signal was obtained when added to the Fbw7-Skp1 complex.

The ITC data has revealed that doubly phosphorylated C-terminal CycE$^{31pT380/pS384}$ peptide is a much better Fbw7 substrate than the singly phosphorylated C-terminal CycE^{31pT380} peptide, and suggests a 2nd-phosphate-binding pocket in Fbw7. Moreover, the comparable binding of the doubly phosphorylated C-terminal CycE$^{31pT380/pS384}$ peptide and the triply phosphorylated C-terminal CycE$^{31pS372/pT380/pS384}$ peptide suggest that the phosphorylation of Cyclin E on residue Ser372 does not contribute to Fbw7 binding. Therefore, the function of phosphorylated residue Ser372 is not clear. Yet according to the literature, it is proposed that Fbw7 binds to C-terminal CycE$^{31pS372/pT380}$. However, in the *in vitro* Fbw7 pull down assay, Ye et al., 2004, used a one amino acid shorter CycE$^{30pS372/pT380}$ peptide and visualized the binding to Fbw7 by silver staining, a method much more sensitive than ITC, which may explain the contrasting results.

3.4 Crystallization and data collection of the Fbw7-Skp1 complexes

To elucidate the structural basis on how phosphorylated substrates are recognized by Fbw7 I was determined to crystallize the Fbw7-Skp1 complex by itself and in combination with several peptides. The triply phosphorylated C-terminal CycE$^{31pS372/pT380/pS384}$ peptide was chosen to identify how the phosphorylated residues Thr380, Ser384 and Ser372 bind to Fbw7. Crystallization was also performed with a singly phosphorylated N-terminal CycE^{14pT62} peptide because the phosphorylated residue Thr62 has also been implicated in the binding to Fbw7 (Ye et al., 2004, Welcker et al., 2004). The doubly phosphorylated c-Myc$^{19pT58/pS62}$ peptide was additionally chosen because biochemical data has not clarified clearly how c-Myc$^{19pT58/pS62}$ binds to Fbw7. It is reported that doubly phosphorylated c-Myc$^{19pT58/pS62}$ is prone to degradation by the UPS and has been shown to bind to Fbw7 (Koepp et al., 2001; Yade et al., 2004). However, Yeh et al., 2004, showed that ubiquitinated c-Myc is only phosphorylated on residue Thr58 (Introduction, 1.3.3.2). Table 3.2 shows the sequences of the phosphorylated peptides as used in crystallization. Crystallization of the Fbw7-Skp1 complex in the presence or absence of a peptide was performed at RT using the hanging drop vapor diffusion method (Method, 2.2.7.1), utilizing equal volumes of the reservoir solution and the Fbw7-Skp1 complex or Fbw7-Skp1-substrate peptide complex.

Table 3.2. Substrate peptides used in crystallization with the Fbw7$^{263-707}$-Skp1 complex.

CycE-Peptides	**peptide sequence**	**P-8**	**P0**	**P+4**	
CycE$^{31pS372/pT380/pS384}$	360-AKKAMLSEQNRA**[pS]**PLPSGLL**[pT]**PPQ**[pS]**GKKQSS-390				
CycE^{14pT62}	55-		DPCSLIP**[pT]**PDKEDD		-68
Myc-Peptide					
Myc$^{19pT58/pS62}$	51-		KKFELLP**[pT**]PPL**[pS]**PSRRSGL-69		

Bold brackets in the peptide sequences depict phosphorylated residues. Numbers above the sequences indicate the position of phosphorylation sites based on the pT380, pT62 and pT58 determinant as 0.

3.4.1 Crystallization of the Fbw7-Skp1 complex in the absence of substrate peptides

For the crystallization of the Fbw7-Skp1 complex without peptide, the truncated Fbw7$^{279-707}$ and Fbw7$^{263-707}$ proteins were used. At first crystals were obtained of the Fbw7$^{279-707}$-Skp1 complex (15 mg/ml), using 20 mM Tris pH 8, 0.4 M NaCl and 1.4 M AmSO4 in the reservoir solution (Figure 3.6A). The best crystals (~100 µm x 40 µm x 40 µm) were harvested after 3-5 days, and cryoprotected with reservoir solution supplemented with 30 % glycerol. Unfortunately, the crystals diffracted only to 4.5 Å, and showed twinning therefore no data sets were collected. Optimization attempts of the crystallization condition by streak seeding and additive screening showed no improvement, and other promising crystallization conditions of the Fbw7$^{279-707}$-Skp1 complex did not lead to crystals. Initial screening of the

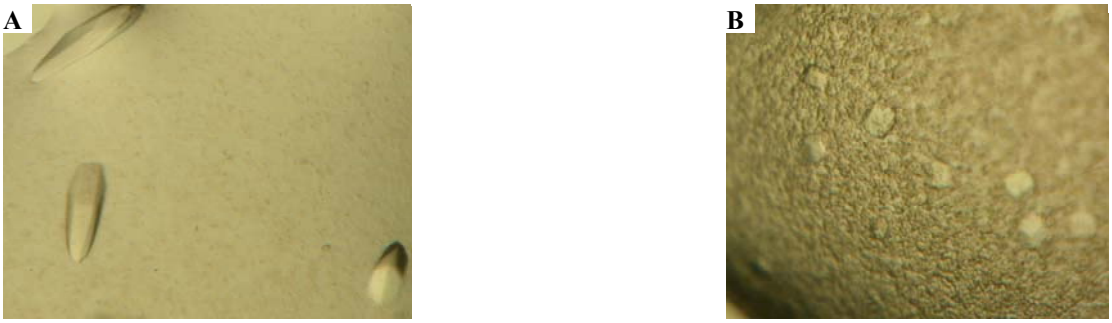

Figure 3.6. Crystals of the Fbw7-Skp1 complex in the absence of substrate peptides.

A) Fbw7$^{279-707}$-Skp1 (15 mg/ml) crystallized with 1.4 M AmSO4, 0.4 M NaCl, 20 mM Tris pH 8 at 20 °C.
B) Fbw7$^{263-707}$-Skp1 (50 mg/ml) crystallized with 1.2 M LiSO4, 0.1 M Hepes pH 7.5, 7.5 % glycerol at 20 °C.

Fbw7$^{263-707}$-Skp1 complex showed granular precipitates with AmSO4 and LiSO4 but no crystals. Increasing the protein concentration to 50 mg/ml, and fine-tuning of LiSO4 concentration to 1.2 M LiSO4, 0.1 M Hepes pH 7.5 and 7.5 % glycerol led to small (~40 µm x 40 µm x 40 µm) crystals after 3-5 days (Figure 3.6B). The crystals were cryoprotected by

increasing the concentration of LiSO4 to 2.2 M (Method, 2.2.8.1) and were flash frozen until data collection was performed.

3.4.2 Crystallization of the Fbw7-Skp1 complex in the presence of substrate peptides

The co-crystallization of the Fbw7$^{263-707}$-Skp1 complex (thereafter, Fbw7-Skp1 complex) in combination with either, the triply phosphorylated C-terminal CycE$^{31pS372/pT380/pS384}$ peptide, the singly phosphorylated N-terminal CycE^{14pT62} peptide, or an N-terminal doubly phosphorylated c-Myc$^{19pT58/pS62}$ peptide was performed. Prior to the crystallization trials, the Fbw7-Skp1 complex was mixed with the Cyclin E or c-Myc peptides at a 1 to 2 molar ratio (Method, 2.2.7.2). Luckily, crystals were obtained from all three ternary Fbw7-Skp1-substrate peptide complexes (Figure 3.7). Best ternary Fbw7-Skp1-C-terminal CycE$^{31pS372/pT380/pS384}$ crystals were obtained at a protein concentration of 50mg/ml and a reservoir solution containing 1.4 M LiSO4 and 0.1 M Bicine pH 9 at 20 °C (Figure 3.7A). The Fbw7-Skp1-N-terminal CycE^{14pT62} crystals were optimal at a protein concentration of 15 mg/ml and a reservoir solution containing 1.12 M LiSO4 and 0.1 M Hepes pH 7.5 at 20 °C (Figure 3.7C). The Fbw7-Skp1-c-Myc$^{19pT58/pS62}$ crystals were optimal at a protein concentration of 50 mg/ml and a reservoir solution of 1.4 M LiSO4 and 0.1 M Tris pH 8.0 at 20 °C (Figure 3.7B). The crystals of the ternary complexes were cryoprotected

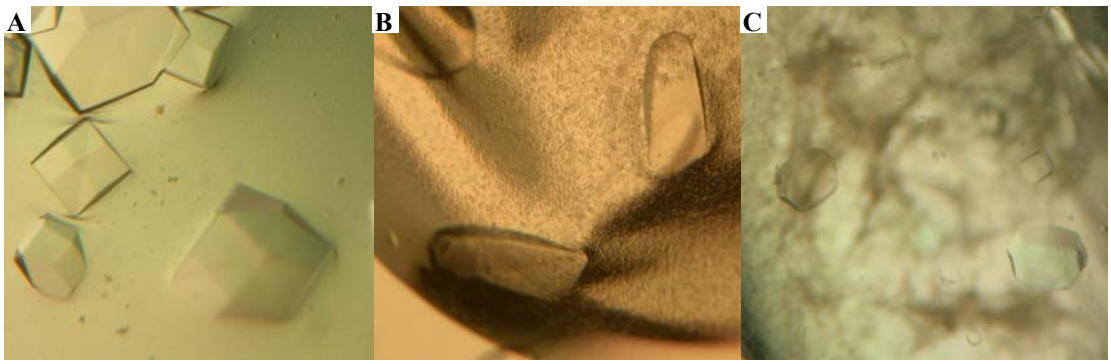

Figure 3.7. Crystals of the Fbw7-Skp1 complex in the presence of substrate peptides.

A) Fbw7-Skp1-CycE$^{31pS372/pT380/pS384}$ (50 mg/ml) crystallized with 1.4 M LiSO4, 0.1 M Bicine pH 9 at 20 °C.
B) Fbw7-Skp1-c-Myc$^{19pT58/pS62}$ (50 mg/ml) crystallized with 1.4 M LiSO4, 0.1 M Tris pH 8.0 at 20 °C.
C) Fbw7-Skp1-CycE^{14pT62} (15 mg/ml) crystallized with 1.12 M LiSO4, 0.1 M Hepes pH 7.5 at 20 °C.

by increasing the concentration of LiSO4 to 2.2 M and were then flash frozen in liquid nitrogen until data collection was performed (Method, 2.2.8.1).

3.4.3 Data collection of the Fbw7-Skp1 crystals

Data sets for the Fbw7-Skp1-N-terminal CycE^{14pT62} complex were collected at the 8BM beamline of the Advanced Photon Source (APS) at Argonne National Laboratories, to a resolution of 2.5 Å. Figure 3.8 shows a typical diffraction image from the data collection of a Fbw7-Skp1-N-terminal CycE^{14pT62} crystal recorded with a charge-coupled device (CCD) detector. Data sets for the Fbw7-Skp1 complex and the ternary complexes of Fbw7-Skp1-C-terminal CycE$^{31pS372/pT380/pS384}$ and Fbw7-Skp1-c-Myc$^{19pT58/pS62}$ were collected at Brookhaven National Laboratory Synchroton Light Source (BNL) at beam-line X9A to a resolution of 2.9 Å, of 2.6 Å and of 2.8 Å respectively.

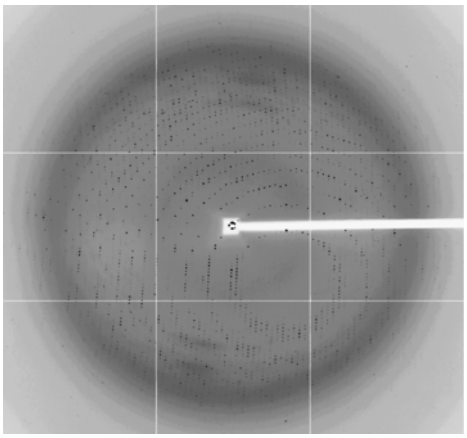

Figure 3.8. Diffraction image of the Fbw7-Skp1-N-terminal CycE^{14pT62} crystal.

Image was recorded on a CCD detector at the APS synchrotron beamline 8BM. The resolution of the outer rim of the image is 2.5 Å.

Data sets of all ternary Fbw7-Skp1-peptide complexes were processed using the HKL suite of data processing programs (Otwinowski et al., 1997). All crystals belong to space group $I4_122$ and have one molecule in the asymmetric unit. Table 3.3 summarizes the statistics from the crystallographic analysis.

3.5 Structure determination of the Fbw7-Skp1 complexes

The structures of the Fbw7-Skp1 complex, the Fbw7-Skp1-C-terminal CycE$^{31pS372/pT380/pS384}$ complex, the Fbw7-Skp1-N-terminal CycE^{14pT62} complex and the Fbw7-Skp1-c-Myc$^{19pT58/pS62}$ complex were determined by MR using the program AMORE (CCP4). As search models, the WD40 domain of the scCdc4-Skp1 structure (Orlicky et al., 2003) and the Skp1 and Fbox domain of the ß-Trcp1-Skp1 structure (Wu et al., 2003) were used. The structures of the Fbw7-Skp1 complexes were build with the program O and improved by several rounds of manual rebuilding and refinement by the program CNS (Brunger et al., 1998; Jones et al., 1991), until the R_{free} converged to 25 to 27 %. The Cyclin E and c-Myc peptides were built into the $2F_o$-F_c and F_o-F_c maps in program O and refined using CNS (Brunger et al., 1998; Jones et al., 1991) (Table 3.3).

Table 3.3. Summary of crystallographic analysis.

	Fbw7-Skp1	**Fbw7-Skp1-CycE$^{31pS372/pT380/pS384}$**	**Fbw7-Skp1-CycE^{14pT62}**	**Fbw7-Skp1-c-Myc$^{19pT58/pS62}$**
Beamline	BNL X9A	APS 8BM	BNL X9A	BNL X9A
Space group	$I4_122$	$I4_122$	$I4_122$	$I4_122$
Resolution (Å)	100.0–2.9	100.0-2.6	100.0-2.5	100.0-2.8
Nr. of measured reflections	226,048	279,053	267,794	168,872
Nr. of unique reflections	29,166	44,674	50,357	35,176
I/Σ(I)	18.4 (6.5)	14.4 (5.1)	22.9 (6.9)	17.7 (4.8)
Completeness (%)	99.6 (100.0)	97.6 (99.0)	98.7 (99.7)	96.1 (97.5)
R_{sym} (%)[b]	9.3 (34.4)	9.1 (36.3)	5.8 (28.7)	7.0 (33.2)
Refinement				
Resolution range (Å)	20.0–2.9	20.0–2.6	20.0–2.6	20.0–2.6
Number of reflections	28,352	42,657	49,288	34,500
Total protein atoms	4,554	4,650	4,643	4,648
Water molecules	119	178	201	135
R_{cryst}/R_{free} (%)[c]	23.6/26.8	23.3/26.6	22.6/25.1	22.4/25.5
Rmsd Bond lengths (Å)	0.008	0.007	0.009	0.007
Rmsd Bond angles (deg.)	1.5	1.6	1.7	1.5
Rmsd *B*-factors (Å^2)	2.5	1.6	2.6	1.6

[a]Numbers in parentheses represent the statistics for the shell comprising the outer 10 % (theoretical) of the data.
[b]$R_{sym} = \Sigma|I - \langle I \rangle| / \Sigma I$, where I is the integrated intensity of a given reflection.
[c]$R_{cryst} = \Sigma|F(obs) - F(calc)| / \Sigma F(obs)$, $R_{free} = R_{cryst}$ calculated using 3.5 % to 6.9 % random data omitted from the refinement.

The refined Fbw7-Skp1 structures contain residues 265 to 338 and 441 to 706 of Fbw7 and residues 1 to 37, 44 to 68 and 84 to 159 of Skp1. Furthermore, interpretable electron densities were obtained for the C-terminal CycE$^{31pS372/pT380/pS384}$ peptide residues 373 to 385, the N-terminal CycE^{14pT62} peptide residues 58 to 65, and the c-Myc$^{19pT58/pS62}$ peptide residues 54 to 61. Residues with no interpretable electron density are believed to be disordered in the crystals and were excluded from the refined models. The refined models were evaluated by Procheck (Laskowski et al., 1993). The Ramachandran plot of the Fbw7-Skp1 structures without peptide (Figure 3.9) reveals that nearly all residues (98.8 %) are in the allowed region and comparable results are obtained for the Fbw7-Skp1-substrate peptide structures.

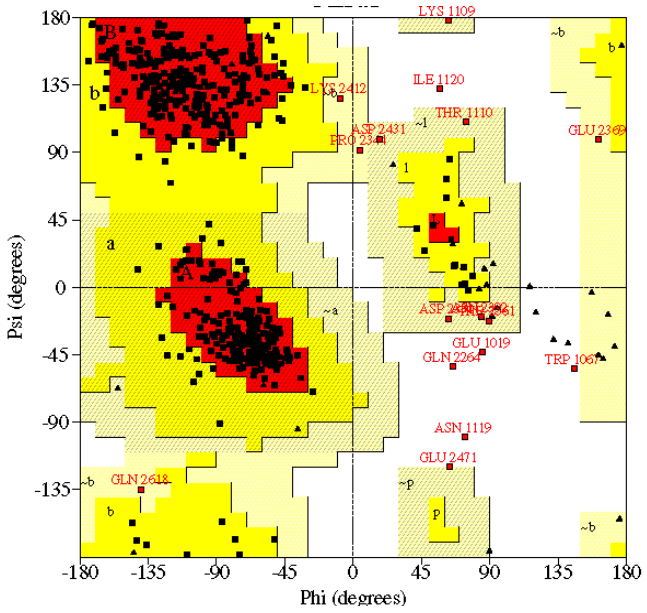

Residues in most favored region [A, B, L]	439	85.4%
Residues in additional allowed regions [a, b, l, p]	66	12.7%
Residues in generously allowed regions [~a, ~b, ~l, ~p]	9	1.7%
Residues in disallowed regions	6	1.2%
Number of non-glycine and non-proline residues	520	10
Number of end-residues (excl. Gly and Pro)	193	
Number of glycine residues (shown as triangles)	42	
Number of proline residues	19	
Total number of residues	774	

Figure 3.9. Ramachandran plot for the refined model of the Fbw7-Skp1 complex in the absence of substrate.

Most favored regions are colored red, additionally allowed regions yellow and disallowed regions white.

3.6 Overall Structure of the Fbw7-Skp1-substrate peptide complex

The described Fbw7-Skp1 structure lacks the N-terminal 264 amino acids of Fbw7 with an unknown function, but is sufficient to bind to C-terminal CycE$^{31pS372/pT380/pS384}$, N-terminal CycE^{14pT62} and c-Myc$^{19pT58/pS62}$ phosphorylated substrate peptides. The Fbw7-Skp1-substrate peptide structures show a curved C-like shape, with Skp1 and the phosphorylated substrate peptide facing in opposite directions. All four Fbw7-Skp1 structures fold in the presence and absence of the peptides identically. The ternary Fbw7-Skp1-CycE$^{31pS372/pT380/pS384}$ complex is representatively shown for all structures in Figure 3.10.

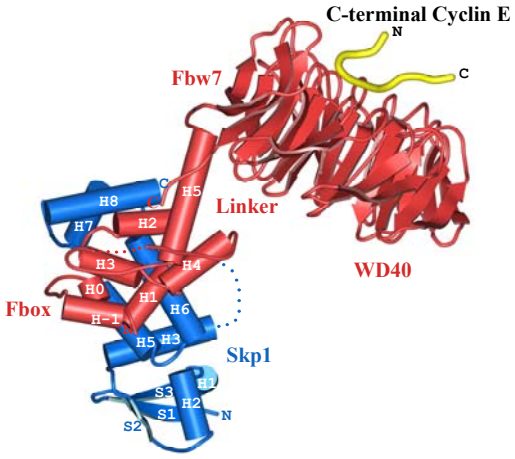

Figure 3.10. Overall structure of the ternary Fbw7-Skp1-C-terminal Cyclin E peptide complex.

Ribbons representation shows Skp1 (blue), Fbw7 Fbox, Linker and WD40 domain (red) and phosphorylated C-terminal Cyclin E, CycE$^{31pS372/pT380/pS384}$ (yellow). Dotted lines represent disordered regions. The secondary structure elements for Skp1 and the Fbox and linker domains of Fbw7 are labeled.

The more detailed structure description of the ternary Fbw7-Skp1-substrate peptide complex that follows starts with the description of the Skp1 structure and continues with the description of the three main regions of the Fbw7 structure, the N-terminal Fbox domain (residues 280 to 324), the linker domain (residues 325 to 366) and the WD40 domain (residues 367 to 701). The intermolecular interactions of Fbw7 to its binding partner Skp1 are also described. Note, the Fbw7 helix –1, (H-1, residues 265 to 279) that precedes the Fbox domain is described together with the Fbox domain, and the WD40 tail (residues 702 to 706) is described together with the linker domain. The binding of the three phosphorylated substrate peptides to Fbw7 WD40 domain is explained in Results and Discussion, 3.7.

3.6.1 Skp1 structure

Skp1 contains a mixed topology of eight helices and three strands (Figure 3.11). The interaction of the Fbox-Skp1 interface involves Skp1 C-terminal helices H5 to H8 and Fbw7 Fbox domain helices H0 to H3 and is described in Results and Discussion, 3.6.3. Structurally important for the Skp1 C-terminal fold are the hydrophobic residues Leu93, Leu100, Leu103, Ala107, Leu115, Leu116, Val118, Val123, Ile127 and Phe139 that cluster Skp1 helices H5 to H7. Residue Arg136 resides at the opposite site of Skp1 helix H7 and its side chain forms a hydrogen bond network, together with the side chain of residue Asn143 of helix H7 extension and the side chain of residue Glu150 of helix H8 that connects the Skp1 helices H7 and H8.

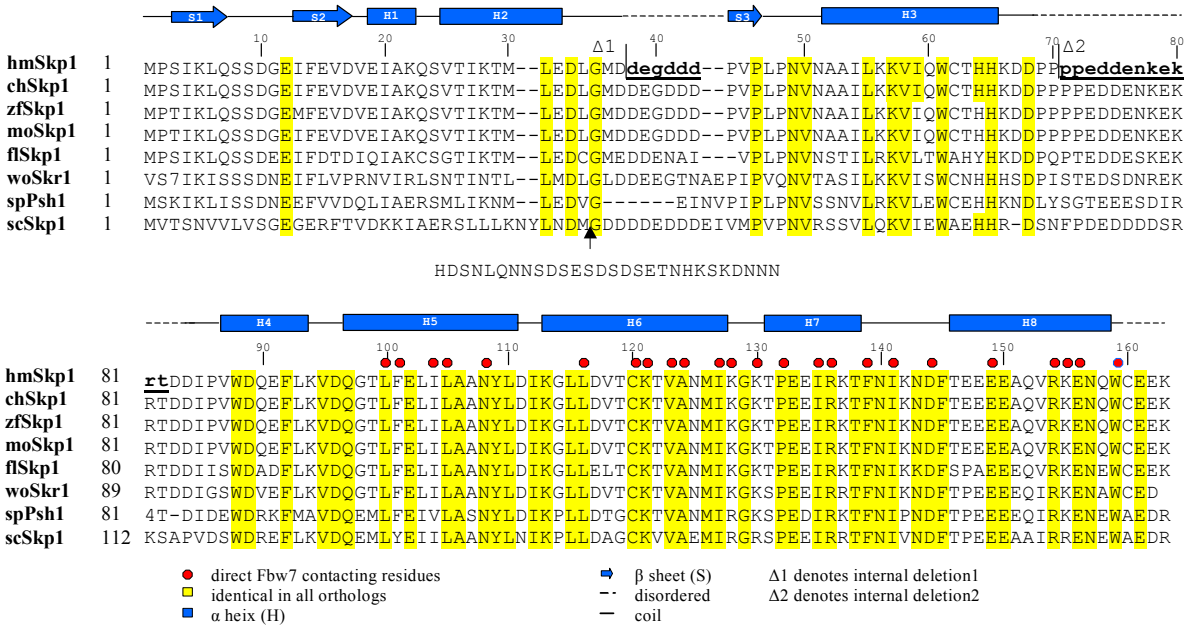

Figure 3.11. Sequence alignment of hmSkp1 with other orthologs.

Secondary structure elements of hmSkp1 are shown above the primary sequence. Human, hm (AAC50241), chicken, ch (XP_414636), zebrafish, zf (AAH59536), mouse, mo (AAH02115), fly, fl (AAF45538), worm, wo (AAL34093), S. pompe, sp (AAD37024) and S. cerevisiae, sc (NP_010615).

3.6.1.1 Comparison with other Skp1 C-terminal structures

The superimposition of the C-terminal helices H5 to H8 of the Skp1 and budding yeast Skp1 (scSkp1) structures, as reported in the Fbox-Skp1 structures of, scCdc4-Skp1 (Orlicky et al., 2003), Skp2-Skp1 (Schulman et al., 2000), β-Trcp1-Skp1 (Wu et al., 2003)

and Fbw7-Skp1 reveals that the Skp1 helices H5 and H6 are identically folded in all compared structures. In the Skp1-Skp2 structure, however, a slight structural shift occurred in Skp1 helices H7 and H8 and is imposed due to the adjacent different linker structures that follow the Fbox domains (Figure 3.12). Furthermore, in the scCdc4-Skp1 and the β-Trcp1-Skp1 structures, the C-terminal part of Skp1 helix H8 and residue Trp159 of the helix H8 extension are disordered and significantly fewer interactions are formed with the Fbox protein. Yet mutagenesis studies with scSkp1 revealed that Skp1 helix H8 and residue Trp159 are important for Skp1 function *in vivo*. A mutation of the residue Trp190 in scSkp1, that corresponds to Skp1 residue Trp159, to alanine or the deletion of scSkp1 helix H8 are incapable of complementing the temperature sensitivity of the *skp1-11* deletion strain (Schulman et al., 2000).

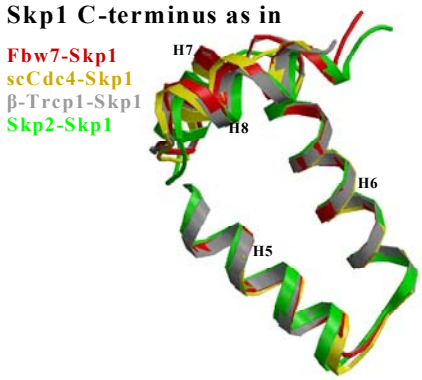

Figure 3.12. Superimposition of Skp1 C-terminal structure domain to other orthologs.

Superimposition of Skp1 C-terminal helices H5-H8 as found in the structure with Fbw7 (red), scCdc4 (yellow), β-Trcp1 (gray) and Skp2 (green).

3.6.2 Fbw7 Fbox domain structure

The Fbox domain of Fbw7 is a helical structure that consists of six helices H-1, H0 to H3, and the N-terminal part of helix H4 (Figure 3.13). In the Fbox structure helix H3 packs antiparallel with the helices of H-1 and H2 and is stabilized by an orthogonal antiparallel helix pair consisting of H1 and H0. The N-terminus of helix H4 is inserted between the two antiparallel helix pairs of H1 and H0, and H2 and H3.

Important for the Fbw7 Fbox domain fold is the conserved residue Pro285 that breaks Fbw7 helix H0 and H1 and the conserved hydrogen bond interaction involving the side chain

of residue Asp279 between the helices of H-1 and H0 and the side chain of residue Trp311 of helix H3. The anchoring of the N-terminal part of helix H4 to the Fbox domain is ensured by a hydrophobic network consisting of conserved or conservative substituted residues among Fbw7 orthologs, and involves the helix H2 residues Pro298, Leu301 and Leu302, and the N-terminal helix H4 residues Leu320, Trp321 and Lys324. Also important for the stability of Fbw7 Fbox domain are the residues Val265 and Ile272 of helix H-1 and the residue Pro274 of loop L-1 that interact with the residues Trp311 and Ile313 of helix H3.

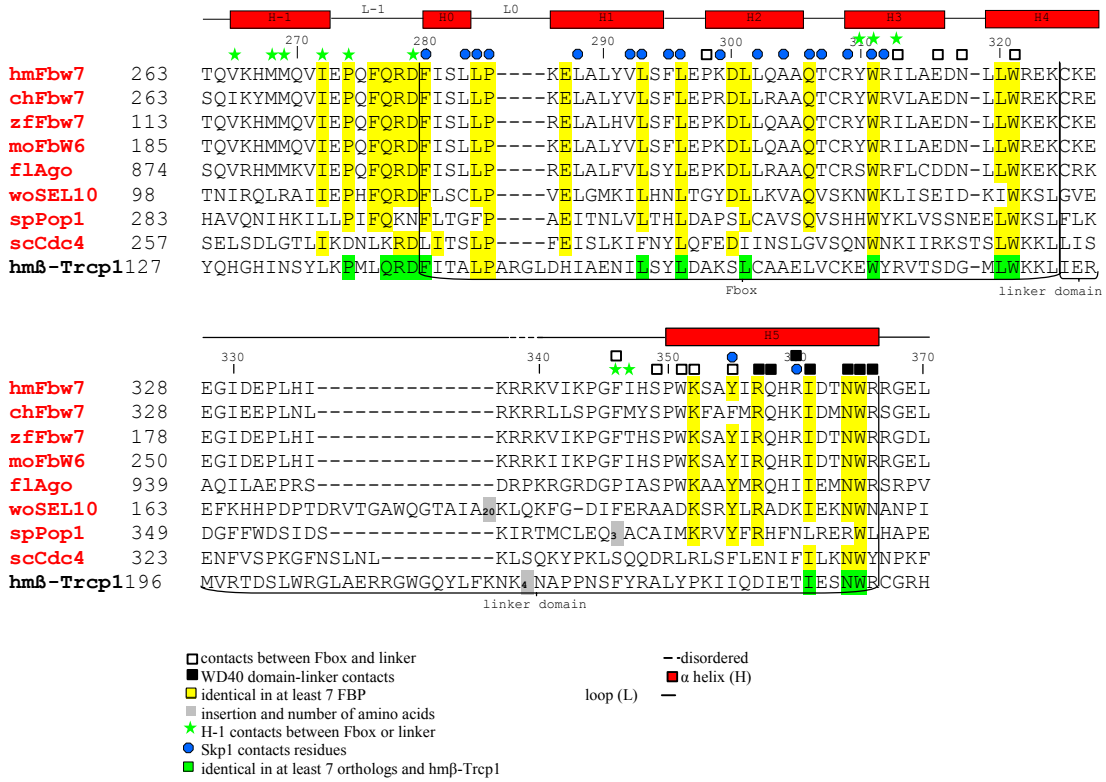

Figure 3.13. Sequence alignment of Fbw7 Fbox and linker domain with others.

Secondary structure elements of Fbw7 Fbox and linker domain are shown above the primary sequence. Fbw7, human, hm (AAL07271), chicken, ch (XP_417265), zebrafish, zf (XP_692667), mouse, mo (AAL40930), fly, fl (AAG22247), worm, wo (Q93794), S. pompe, sp (CAA69671) and S. cerevisiae, sc (NP_116585) are shown in (red) and hmβ-Trcp1 (CAA74572) in black.

3.6.2.1 Comparison with other Fbox domain structures

Comparing the Fbw7 Fbox structure by superimposing it with the earlier reported Fbox domains of the structures scCdc4-Skp1 (Orlicky et al., 2003), Skp2-Skp1 (Schulman et al., 2000) and β-Trcp1-Skp1 (Wu et al., 2003) reveals that the Fbox domain of Fbw7 retains in the same overall Fbox fold (Figure 3.14). Yet several Fbox differences are apparent. Most interesting is that the Fbw7 Fbox structure contains an additional N-terminal helix H-1 that

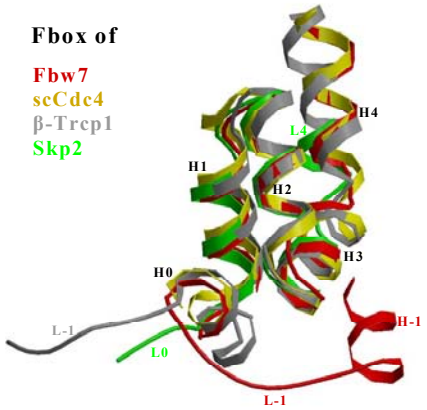

Figure 3.14. Superimposition of Fbw7 Fbox structure with others.
Superimposition of Fbox domains of Fbw7 (red), scCdc4 (yellow), β-Trcp1 (gray) and Skp2 (green).

together with the loop L-1 folds towards Fbw7 Fbox domain and interacts with helix H3. The binding to helix H3 involves one hydrogen bond interaction between the side chain of residue Asp279 of loop L-1 and the side chain of residue Trp311 of helix H3 as well as hydrophobic interactions involving the helix H-1 residues Met268, Met269 and Ile272, the loop L-1 residue Pro274 and the residues Tyr310 and Ile313 of helix H3. Interestingly, all compared Fbox domains contain at the residue Asp279 of Fbw7 L-1 loop either an aspartate or a serine, which brings their L-1 loop and helix H3 in close distance. However, in β-Trcp1 the loop L-1 bends to the opposite site of Fbw7 loop L-1 and most of the corresponding L-1 residues in scCdc4 and Skp2 Fbox structure are disordered. Moreover, the compared scCdc4, β-Trcp1 and Skp2 Fbox structures do not reveal information about the corresponding Fbw7 H-1 residues, as those residues were absent in the proteins employed for crystallization. Secondary structure analysis of the primary sequences of scCdc4, β-Trcp1 and Skp2 predicts that scCdc4 and β-Trcp1 contain the helix H-1 but Skp2 does not. It is thus possible that the

inclusion of the predicted scCdc4 and β-Trcp1 helix H-1 residues might lead to helix H-1 localization similar to that of Fbw7.

A second difference amongst these Fbox domains involves the H0 helix. While Fbw7 Fbox N-terminus retains an H0 helix similar to that of scCdc4 and β-Trcp1, Skp2 exhibits an L0 loop at this position.

A third difference results from the six C-terminal Fbox residues. Although the Fbox C-terminus superimposes well with the compared Fbox structures, their residues adapt to different secondary structures due to their packing with different linker domains. The last six Fbox C-terminal residues of the WD40 domain containing FBPs structures of Fbw7, scCdc4 and β-Trcp1 form the N-terminal part of helix H4 that continues as the first helix of the linker domain. However, in the LRR domain containing Skp2 Fbox structure, the same sequence forms the loop L4 and interacts with the LRR-like linker (Wu et al., 2003; Orlicky et al., 2003).

3.6.3 Fbw7 Fbox-Skp1 interface

The Fbw7 Fbox-Skp1 interaction is of a bipartite nature, where Skp1 helices H5 to H7 bind to one side of the Fbox domain helices H0 to H3, and Skp1 helix H8 binds to the opposite site, virtually clamping the Fbw7 Fbox domain in between (Figure 3.10). The interface of Fbw7 Fbox-Skp1 structure is mainly hydrophobic and buries ~3462Å^2 of solvent-accessible surface. The Fbw7 Fbox helices H0 to H2 bind to Skp1 helices H5, H6 and H7 only by hydrophobic main chain and side chain interactions. This involves the Fbox residues Phe280, Leu283, Leu284, Pro285, Leu288, Val292, Leu293, Phe295, Leu296, Lys299, Leu302 and Ala304 and the Skp1 residues Phe101, Leu100, Val123, Ile104, Leu105, Asn108, Leu116, Cys120, Lys121, Val123, Ala124, Ile127, Lys128, Lys130 and Phe139. The Fbox residues that follow helix H2 bind to Skp1 helix H7 by hydrophobic interaction and to Skp1 helix H7 loop extension and helix H8 mainly through hydrogen bond interactions. This involves the Fbox residues Gln306, Thr307, Arg309, Trp311 and Arg312, which contact the Skp1 residues Arg154, Arg136, Pro132, Glu149, Asp144, Phe139, Ile127, Ile135, Ile141 and Glu156. Figure 3.13 (Figure 3.11) depicts the numerous residues of the Fbox domain (of Skp1) involved in hydrophobic and hydrogen bond interactions with Skp1 (with the Fbox domain).

Analyzing the Fbw7 residues involved in Fbox-Skp1 interface and comparing them with the residues of the Fbox domains of Skp2, β-Trcp1 and scCdc4 reveals that all four Fbox domains use conserved residues or conservative substitutions at similar positions to interact with Skp1 (Figure 3.15). Moreover, the derived Fbox consensus reveals that the most invariant Fbox residues, proline between helix H0 and H1, leucine between helix H1 and H2 and tryptophane of helix H3 interact to Skp1.

Furthermore, the comparison of the Skp1 residues that interact to the Fbox proteins Fbw7, Skp2 and scCdc4 (Figure 3.16) reveals that Skp1 residues interact with their Fbox domains at similar positions. Moreover, Skp1 C-terminal helices H5 to H8 shares with other Skp1 orthologs a ~70 % sequence identity. This indicates that the interaction between Skp1 and Fbox proteins is an evolutionary-conserved function of Skp1.

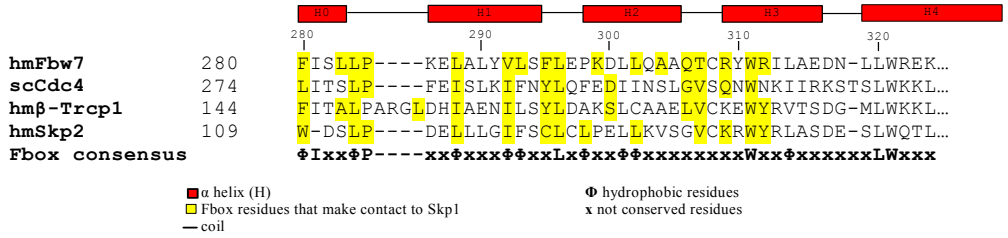

Figure 3.15. Comparison of Fbox residues that mediate contact to Skp1.

Sequence alignment of hmFbw7 Fbox domain with other homologs. Secondary structure elements of hmFbw7 Fbox domain are shown above the primary sequence, accession numbers used as in Figure 3.13, hmSkp2 (AAK31593). Hmβ-Trcp1 and hmSkp2 residues that make contact to Skp1 are as reported by Wu et al., 2003. Derived Fbox consensus sequence is shown below the aligned Fbox proteins.

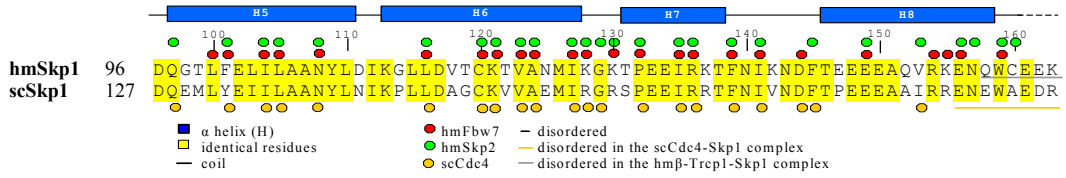

Figure 3.16. Comparison of Skp1 and scSkp1 residues that mediate contact to several Fbox domains.

Sequence alignment of hmSkp1 C-terminus with scSkp1. Secondary structure elements of hmSkp1 C-terminus are shown above the primary sequence, accession numbers used as in Figure 3.11. Skp1 residues that make contact to hmFbw7, hmSkp2 or scCdc4 are marked in red, green and orange respectively. Skp1 contacts to hmSkp2 as reported by Schulman et al., 2000.

3.6.4 Fbw7 linker domain structure

Fbw7 C-terminus of helix H4 and the helix H5 form together the linker domain (Figure 3.17) that adapt into a stalk-like structure and separates Fbw7 WD40 domain from the Fbox domain. The N-terminal linker structure is stabilized through a hydrophobic network that is started with Fbox residue Trp321 of the N-terminus of helix H4 (Results and Discussion, 3.6.2). This hydrophobic network is continued by hydrophobic interaction between Fbox residues Pro298 of helix H2 and residue Trp321 of helix H4 with the linker

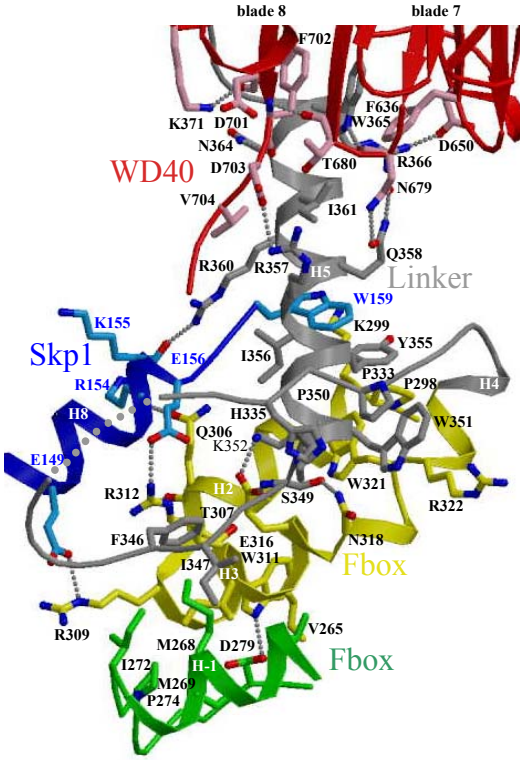

Figure 3.17. Close-up view of Fbw7 linker domain.

The linker interface involves intermolecular contacts to Skp1 and intramolecular contacts to Fbw7 Fbox and WD40 domain. Secondary structures and side chains of Skp1 (blue), of Fbox (yellow), of Fbox H-1 (green), of WD40 (red) and of linker (gray) are shown. Dotted line represent a disordered region in the linker domain. Gray dashes represent hydrogen bonds.

residue Tyr355 of helix H5, and a stacking interaction of Fbox residue Trp321 with the aliphatic part of the linker residue Lys352 of helix H5. Furthermore, Trp351, the neighboring residue of Lys352, exposes its side chain to the opposite site of the linker helix H5, and extends the hydrophobic network by clustering with the residues Pro333 and His335 between helix H4 and H5, and residue Pro350 of helix H5. Moreover, side chains of the linker

residues Lys352 and Ser349 are involved in two hydrogen bond interactions with the side chains of the Fbox residues Glu316 of helix H3 and Asn318 between the helices H3 and H4. Furthermore, the linker residues Phe346 and Ile347 between helices H4 and H5, cluster with the Fbox domain residues Met268, Met269, Ile272 and Pro274 of helix H-1 and residue Ile313 of helix H3.

The C-terminal part of the linker helix H5 is anchored between blade 7 and blade 8 of Fbw7 WD40 domain. The insertion of helix H5 C-terminus into the WD40 domain is mediated through hydrophobic stacking interactions between blade 8 residue Phe702, helix H5 residue Trp365 and blade 7 residue Phe636, as well as electrostatic and hydrogen bond interactions involving residues Trp365 and Arg366 of helix H5, the residue Asp650 of blade 7 and Asn679 of blade 8. Moreover, the side chain of residue Asn679 of blade 8 forms two hydrogen bonds with the side chain of the linker residue Gln358 of helix H5.

In summary, the described networks of hydrophobic and hydrogen bond interactions led to the stable anchoring of the linker N-terminal parts of helix H4 and H5 to Fbw7 Fbox domain and the linker C-terminal part of helix H5 to Fbw7 WD40 domain.

Fbw7 linker stability is further ensured by hydrophobic and hydrogen bond interactions between Fbw7 WD40 domain C-terminal tail residues 702 to 706 and Skp1 helix H8. The WD40 domain C-terminal tail contributes two hydrogen bonds and involves the residues Phe702 and Asp703, and the side chains of the residues Arg357 and Asn364 of the linker helix H5. In addition, the aliphatic part of the WD40 domain C-terminal tail residue Val704 interacts with the aliphatic part of residue Arg360 and Ile361 of linker helix H5. Skp1 helix H8 mediates two hydrophobic and one hydrogen bond interactions with linker helix H5. The hydrogen bond interaction involves the backbone carbonyl group of residue Lys155 of Skp1 helix H8, and the guanidinium group of the linker residue Arg360 of helix H5. The hydrophobic interaction involves the side chain of Skp1 residue Trp159 of helix H8, the side chain of the linker residue Tyr355 of helix H5 and the aliphatic part of Fbox residue Lys299 of helix H2. However, the alignment of the Fbw7 linker domain sequence with the sequences of Fbw7 orthologs and paralogs reveals that the linker is the least conserved domain among Fbox proteins (Figure 3.13).

3.6.4.1 Comparison with other linker domain structures

The Fbw7 linker domain structure was compared with the earlier reported linker domains of the structures of scCdc4-Skp1 (Orlicky et al., 2003), Skp2-Skp1 (Schulman et al., 2000) and β-Trcp1-Skp1 (Wu et al., 2003). It demonstrates that although Fbw7 linker structure contains a two-helix domain, the Fbw7 homolog scCdc4 structure contains a three-helix globular domain and Fbw7 paralog β-Trcp1 contains a four-helix globular domain. The LRR domain, containing Fbox protein Skp2, contains a linker domain, which consists of helices and strands (Figure 3.18). Yet despite the structural diversity of the linker domain, only the first and the last linker helices of the compared FBPs, which are analogous to Fbw7 linker domain helices H4 and H5, are important for the highly conserved interactions necessary for the linkage and orientation of the FBPs Fbox and WD40 domain and underlines its importance for SCF function.

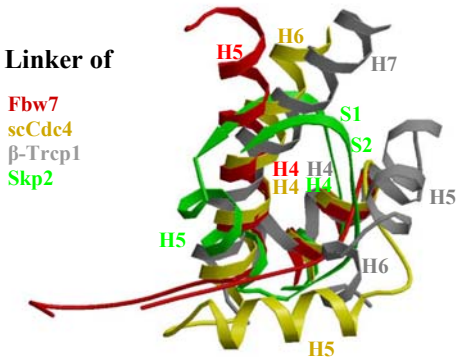

Figure 3.18. Superimposition of Fbw7 linker structure with others.

Superimposition of Fbw7 linker domain (red), scCdc4 (yellow), β-Trcp1 (gray) and Skp2 (green).

The C-terminal tail of Fbw7 WD40 domain is variable in length among Fbw7 orthologs and other WD40 domain containing FBPs. The interface of the WD40 C-terminal tail and the linker domain are hence different. Unfortunately, the WD40 C-terminal tail residues of Fbw7 homolog scCdc4 were deleted prior to crystallization, and the WD40 C-terminal tail residues of Fbw7 paralog β-Trcp1 are disordered in the structure. To my knowledge, Fbw7 is the first WD40 domain-containing FBP to show that its linker domain is stabilized by hydrophobic and hydrogen bond interactions with the WD40 C-terminal tail. A similar mode of binding has been reported for the LRR domain-containing FBP Skp2 (Schulman et al., 2000). However, Skp2 C-terminal LRR tail interacts with its Fbox domain, whereas the Fbw7 C-terminal WD40 tail interacts with the linker domain.

In addition, the interactions between Fbw7 linker domain and Skp1 helix H8 are not present in the other compared WD40 domain containing β-Trcp1-Skp1 and scCdc4-Skp1 structures. Yet the FBP Skp2, which contains a different linker region due to its LRR domain, interacts with Skp1 helix H8. However, in case of scCdc4 and β-Trcp1 linker domain, residues of their additional linker helices contribute to their linker stability. Therefore, one might conclude that the additional helices in scCdc4 and β-Trcp1 fulfill the same linker stability function as the side chains of the Fbw7 linker residues of helix H5.

3.6.5 Fbw7 WD40 domain structure

Fbw7 WD40 domain consists of eight WD40 repeat motifs that fold into an β-propeller (Wall et al., 1995). Each WD40 repeat motif, also known as β-sheet (S) or blade, consists of four antiparallel strands in an A, B, C and D order. The eight sheets are arranged around the β-propeller central axis with the A-strands forming the inner channel and the D-strands the outer rim (Figure 3.19A). A key characteristic of the WD40 domain fold is that its first N-terminal strand, which is S8D in Fbw7, belongs to the last sheet of the WD40 domain (Figure 3.20). To complete Fbw7 sheet S8, the N-terminal S8D strand has to be folded with the C-terminal S8A, S8B and S8C strands. This then leads to the closing of the WD40 domain structure.

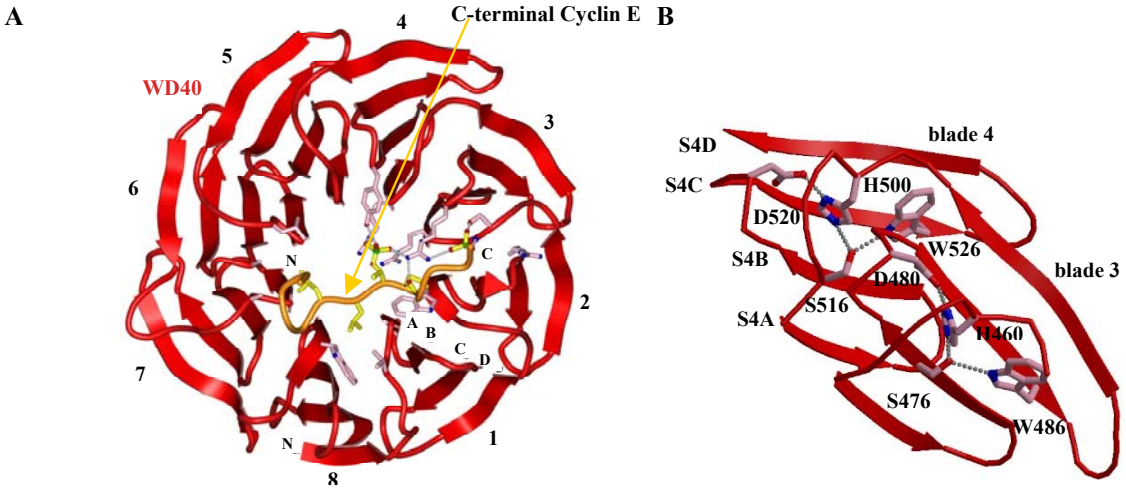

Figure 3.19. Close-up view of Fbw7 WD40 domain.

A) Shows Fbw7 WD40 domain with the eight blades numbered 1 to 8. The four strands of each blade are labeled A to D according to the convention of Wall et al., 1995. WD40 domain is colored in red and some important side chains in pink, C-terminal Cyclin E is colored in yellow and some side chains in light yellow.
B) Shows Fbw7 WD40 blades 3 and 4 in similar orientation as in A.
Figures were prepared with Molscript (Kraulis, 1991).

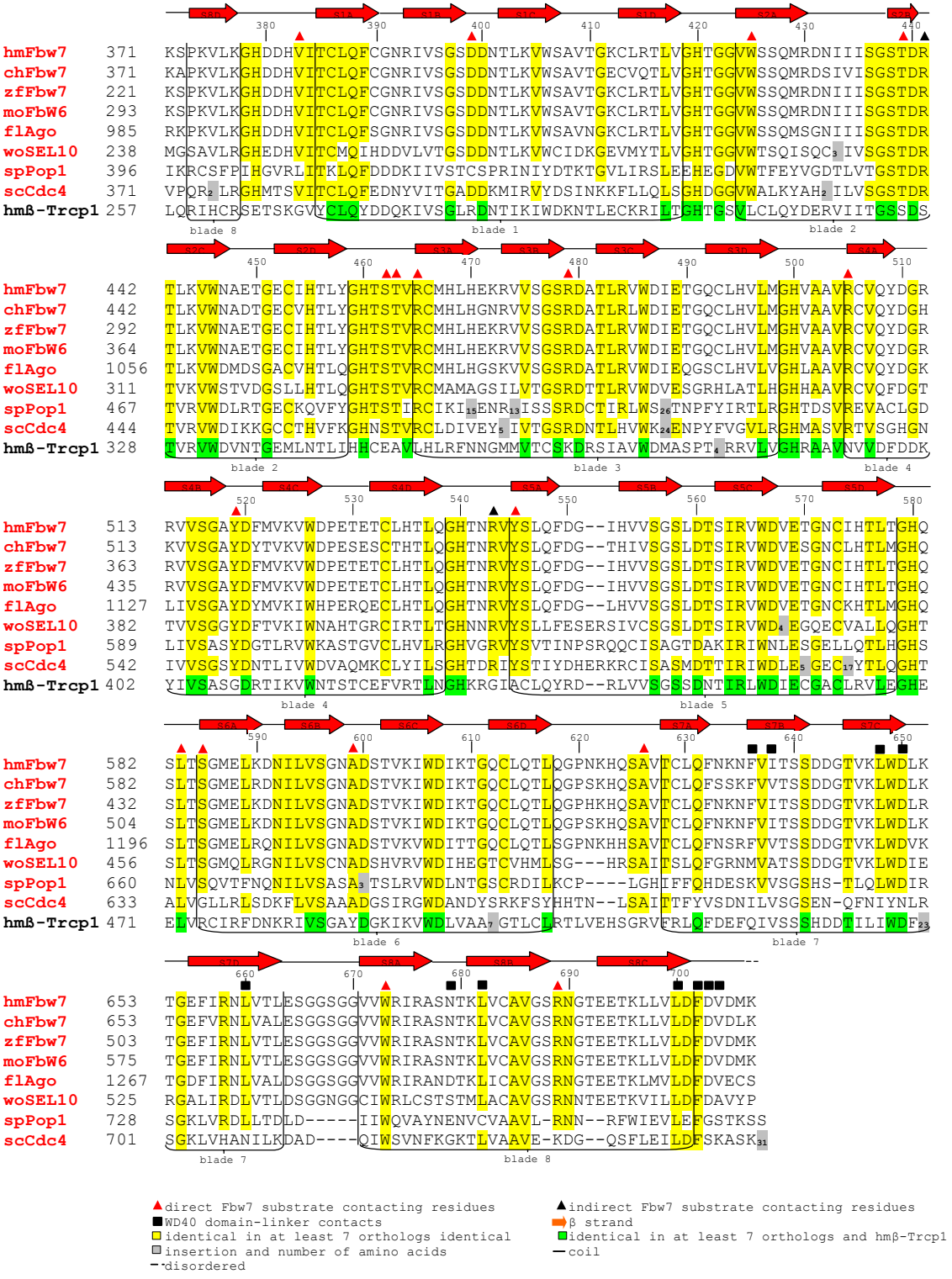

Figure 3.20. Sequence alignment of Fbw7 WD40 domain with others.

Secondary structure elements of Fbw7 WD40 domain are shown above the primary sequence. Accession numbers and color code as in Figure 3.13. Fbw7 residues of the WD40 domain that directly interact with the studied Fbw7 substrates CycE$^{31pS372/pT380/pS384}$, CycE^{14pT62}, c-Myc$^{19pT58/pS62}$ are indicated by red triangles, those who indirectly contribute by black triangles.

The classic WD40 motif is comprised of a conserved triad of hydrogen bonds. It starts with a tryptophane side chain imine group at the strand SC, and involves the side chains of a serine/threonine at strand SB, a histidine between the strands SD and SA, and an aspartate between the strands SB and SC (Figure 3.19B). Based on this classic WD40 motif, seven repeats were predicted for Fbw7 WD40 domain. The last WD40 repeat motif of Fbw7 does not comprise the classic hydrogen bond triad and instead uses the conserved Trp365 of linker helix H5. The Trp365 imine group forms a hydrogen bond with the carbonyl group of residue Asn679 of blade 8. The residue neighboring Asn679 is Thr680, and the backbone carbonyl group of Thr680 forms a hydrogen bond contact to the backbone amide group of Phe702, while Phe702 neighboring residue Asp701 forms a hydrogen bond between its backbone carbonyl group and the side chain of Lys371 (Figure 3.17).

In addition, Fbw7 WD40 domain stability is further ensured by stacking interactions and involves the residues Phe636, Phe702 and Trp365. The Fbw7 WD40 domain has an overall thickness of ~30 Å and measures ~40 Å diameter at the top face, and ~50 Å at the bottom face, measured using Cα atoms only. The β-propeller central water-lined channel is narrowest near the top face (~8 Å versus ~10 Å at the bottom). The top face of Fbw7 WD40 domain binds directly to the phosphorylated substrate peptides N-terminal CycE^{14pT62}, C-terminal CycE$^{31pS372/pT380/pS384}$ and c-Myc$^{19pT58/pS62}$. These Fbw7-substrate peptide interactions are described in detail in Results and Discussion, 3.7.

3.6.5.1 Comparison with other WD40 domain structures

Structural comparison of the 8-bladed Fbw7 WD40 domain with the earlier reported 8-bladed WD40 domain of scCdc4 (Orlicky et al., 2003) and the 7-bladed WD40 domain of β-Trcp1 (Wu et al., 2003) shows that the β-strands of their blades superimpose very well and more variations are seen in the flexible loops connecting the β-strands (Figure 3.21). The structural conservation of their WD40 blades is also reflected in the root-mean-square deviation (rmsd) of only 1.4 Å over 308 scCdc4 WD40 domain Cα atoms. The superimposition of the β-Trcp1 WD40 domain gives an rmsd of only 2.0 Å due to its having only 7 blades compared to 8 blades for Fbw7 and scCdc4 WD40 domain.

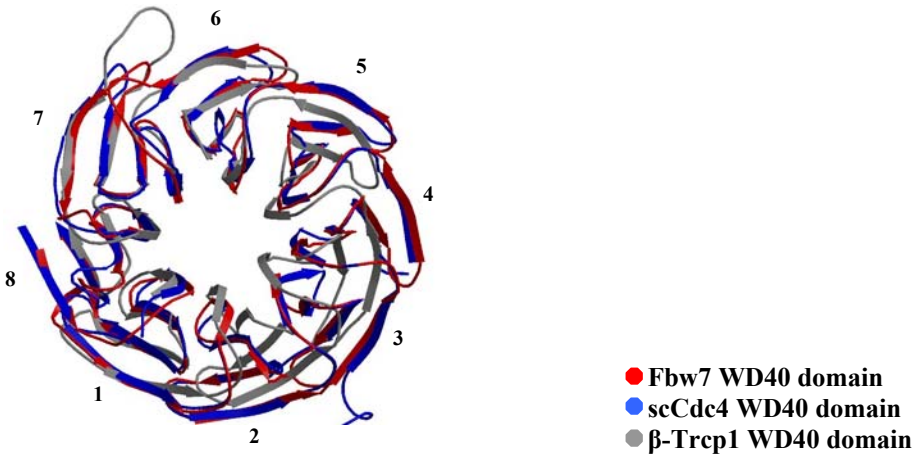

Figure 3.21. Superimposition of Fbw7 WD40 domain structure with others.

Superimposition of Fbw7 WD40 domain in red, scCdc4 WD40 domain in blue and β-Trcp1 in gray. Number 1 to 8 denotes Fbw7 blades.

3.6.6 Model of the SCF^{Fbw7}-E2 complex bound to C-terminal Cyclin E

The structure of the Fbw7-CycE$^{31pS372/pT380/pS384}$-Skp1 complexes modeled onto the SCF complex (Figure 3.22) is based on superimposing the Fbox-Skp1 structure parts of the Fbw7-CycE$^{31pS372/pT380/pS384}$-Skp1 structure onto the Fbox-Skp1 structure parts of the

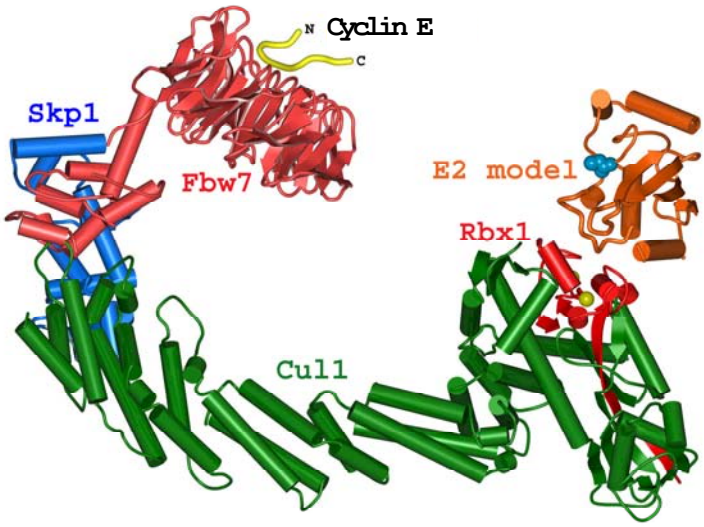

Figure 3.22. Model of SCF^{Fbw7}-E2 complex bound to Cyclin E.

The E2 was docked based on the composite structure of the SCF^{Skp2} (Zheng et al., 2002) and the Ring-type E3 c-Cbl bound to the UbxH7 E2 (Zheng et al., 2000). Fbw7, C-terminal Cyclin E (CycE$^{31pS372/pT380/pS384}$), Skp1, Cul1, Rbx1 and the E2 model are colored in dark red, yellow, blue, green, red and orange. The E2 active site cysteine, which would be attached to the ubiquitin C terminus through a thioester bound, is shown in space-filling representation and is colored cyan.

reconstructed SCF^{Skp2}-E2 complex (Zheng et al., 2002). From the SCF^{Fbw7}-E2 model it is apparent that the WD40 domain of Fbw7 faces the E2 binding site for the ubiquitin transfer with its bound substrate $CycE^{31pS372/pT380/pS384}$. An approximate distance of 50 Å was determined from the structured N- and C-terminal ends of the $CycE^{31pS372/pT380/pS384}$ peptide to the E2 active site cysteine. Similar results were obtained from the SCF-E2 models with the Fbw7 homolog scCdc4 structure (Orlicky et al., 2003) and the paralog ß-Trcp1 structure (Wu et al., 2003).

3.7 Phosphorylated substrate peptides bind to Fbw7 WD40 domain

In the Fbw7-Skp1 complex, the phosphorylated C-terminal $CycE^{31pS732/pT380/pS384}$, N-terminal $CycE^{14pT62}$ and c-$Myc^{19pT58/pS62}$ peptides bind across the top face of Fbw7 WD40 domain. Comparing the three Fbw7 WD40 domain-substrate peptide structures by superimposing them onto Fbw7 WD40 domain structure in the absence of substrate reveals a rmsd of only ~0.8 Å over 336 WD40 domain Cα atoms (Figure 3.23). This indicates that no conformational change occurred in the Fbw7 WD40 domain due to the binding of the

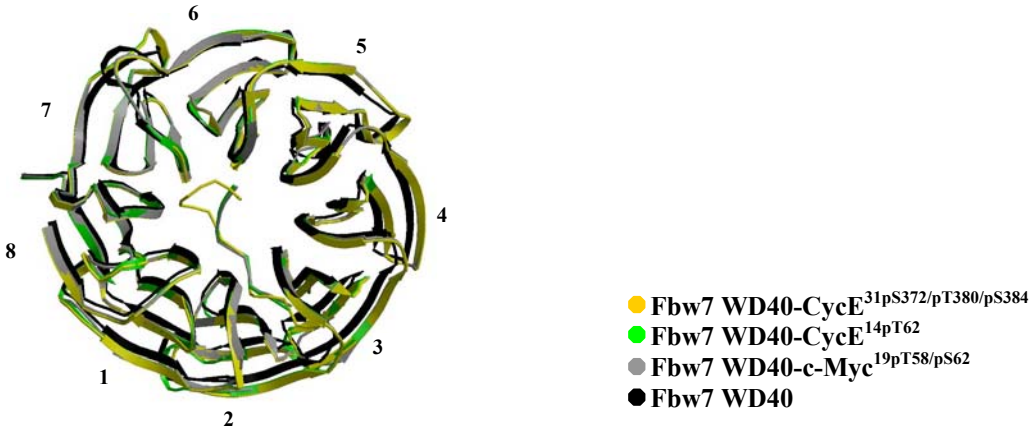

Figure 3.23. Superimposition of Fbw7 WD40 domain structures in the presence and absence of substrate peptides.

Shown is the superimposition of the Fbw7 WD40 domain structures in the absence (black) and presence of the substrate peptides C-terminal $CycE^{31pS372/pT380/pS384}$ (yellow), N-terminal $CycE^{14pT62}$ (green), c-$Myc^{19pT58/pS62}$ (gray). Number 1 to 8 denotes Fbw7 blades. WD40 domain superimposes with an rmsd of ~0.8 Å over 336 WD40 domain Cα atoms.

different substrate peptides. Furthermore, all substrate peptides bind to the same Fbw7 WD40 domain position. The recognition of phosphorylated substrate peptides by Fbw7 WD40

domain is first described by the C-terminal CycE$^{31pS372/pT380/pS384}$ peptide (Figure 3.25). After this, in the close-up of the three superimposed Fbw7 WD40 domain-substrate peptide interfaces (Figure 3.26), the observed binding differences of the c-Myc$^{19pT58/pS62}$ and N-terminal CycE^{14pT62} peptides are described.

3.7.1 Interaction of the Fbw7 WD40 domain with C-terminal Cyclin E

The C-terminal CycE$^{31pS372/pT380/pS384}$ peptide residues starting at P-3 to P+1 dip in an extended conformation across the water-lined channel of the Fbw7 WD40 domain. In addition, the N-terminal residues of the CycE$^{31pS372/pT380/pS384}$ peptide at P-7 to P-4 fold into a turn-like structure, whereas its C-terminal residues at P0 to P+5 form a left-handed helix-like structure. The intermolecular contacts between the CycE$^{31pS372/pT380/pS384}$ peptide and the Fbw7 WD40 domain are centered on its phosphorylated residues Thr380 at P0 and Ser384 at P+4. Furthermore, due to the left-handed helix-like structure of the CycE$^{31pS372/pT380/pS384}$ residues at P0 to P+5 the phosphorylated residues Thr380 and Ser384 reside close to each other and face the same side of the Fbw7 WD40 domain (Figure 3.25; Table 3.4). The CycE$^{31pS372/pT380/pS384}$ third phosphate group at residue Ser372 is disordered, as it has no interpretable electron density. The phosphorylated Thr380 at P0 binds to Fbw7 residue Tyr519 and to the arginine-triad composed of Arg465, Arg479 and Arg505. A surface representation of the top face of the Fbw7 WD40 domain (Figure 3.24) shows, that the arginine-triad at Fbw7 blade 3 and 4 form an area of very high positive electrostatic potential.

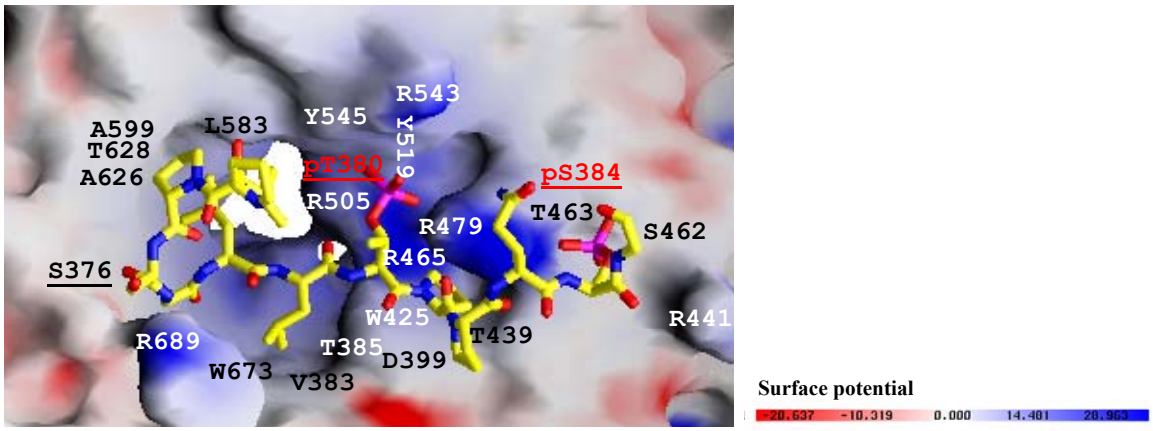

Figure 3.24. Surface representation of the top face of Fbw7 WD40 domain bound to C-terminal Cyclin E.

The surface is colored accordingly to the electrostatic potential (-20.6kT to +29kT) calculated in the absence of the C-terminal Cyclin E peptide with the program GRASP.

The guanidinium groups of the arginine-triad form together with the hydroxyl group of Tyr519 a network of electrostatic and hydrogen bond interactions that coordinates the phosphate group of the substrate at the P0 (Figure 3.25). This 1st-phosphate-binding pocket is conserved in all Fbw7 homologs. The binding is additionally stabilized by stacking interactions mediated by the phenol ring of the surrounding residue Tyr519, the aliphatic parts of the arginine-triad and residue Arg543. In addition the guanidinium groups of Fbw7 residues Arg465 and Arg479 mediate hydrogen bonds to backbone carbonyl groups of the C-terminal portion of Cyclin E. Arg465 interacts with the substrate peptide backbone carbonyl group at P–1 and Arg479 binds to the substrate peptide backbone carbonyl groups at P+1 and P+2. Moreover, Trp425, another invariant residue among Fbw7 orthologs, resides opposite to the 1st-phosphate-binding pocket and packs coplanar with the side chain of Cyclin E residue Pro381 at P+1. Pro382 at P+2 points towards a spacious hydrophobic groove and directs the peptide upwards, and its backbone carbonyl group interacts with Arg479. The residue Gln383 at P+3 continues to bend the substrate peptide upwards and stacks its side chain on top of Arg479, leaving its upper side solvent exposed.

The main chain of Ser384, the second phosphorylated residue of Cyclin E at P+4, extends parallel towards blade 3, whereas the Ser384 phosphorylated side chain binds to a shallow binding pocket on Fbw7 WD40 domain blade 2 and blade 3. In that pocket, the phosphate group of Ser384 binds directly to the guanidinium group of residue Arg479, the hydroxyl groups of Ser462 and Thr463, and to the backbone amide group of Thr463 (Table 3.4). Together these residues form Fbw7 2nd-phosphate-binding pocket. This 2nd-phosphate-binding pocket is primarily formed by the most invariant loop among Fbw7 WD40 domain orthologs, which is located between the strands S2D and S3A (Figure 3.20). If no phosphorylated residue is bound to Fbw7 2nd-phosphate-binding pocket, then this pocket is solvent-exposed. In the structure in the absence of the substrate peptide, this Fbw7 pocket binds to a sulfate molecule from the crystallization buffer. Surprisingly, Arg479 is part of the 1st and the 2nd-phosphate-binding pocket of Fbw7 WD40 domain. The adjacent residue Gly385 at P+5 bends away from the β-propeller and does not contribute additional contacts. The Cyclin E residue Leu379 at P-1 faces towards a hydrophobic groove formed by Fbw7 WD40 domain residues Trp425 and Val383. Cyclin E residue Leu378 at P-2, together with Leu374 at P-6 and Pro375 at P-5 reside in the opposite side of the β-propeller and bind to

another hydrophobic groove formed by Fbw7 side chains of Leu583, Ala626 and Ala599. In addition, the Cyclin E side chain of Leu374 extends that hydrophobic network by interacting with the γ-methyl group of phosphorylated Thr380 and might explain why replacement of Thr380 with Ser380 decreases the binding affinity of a Cyclin E peptide by a factor of seven (Nash et al., 2001). Cyclin E residue Gly377 at P-3 is located at a position with no space for a side chain as the side chains of the residues Arg689 and Trp673 occupy the space.

Additional interactions involve Ser376 at P-4, which binds to a 3rd-Fbw7 substrate-binding pocket. The hydroxyl group of Ser376 forms a direct electrostatic interaction with the guanidinium group of Arg689 of blade 8. Interestingly, an alignment of human Cyclin E with other Cyclin E orthologs reveals that apart from the human and mouse Cyclin E2 all other C-terminal Cyclin Es but not N-terminal Cyclin Es destruction motifs, contain a serine, a threonine or a glutamate at P-4 and mainly a glycine at P-3 (Figure 3.5). However, the

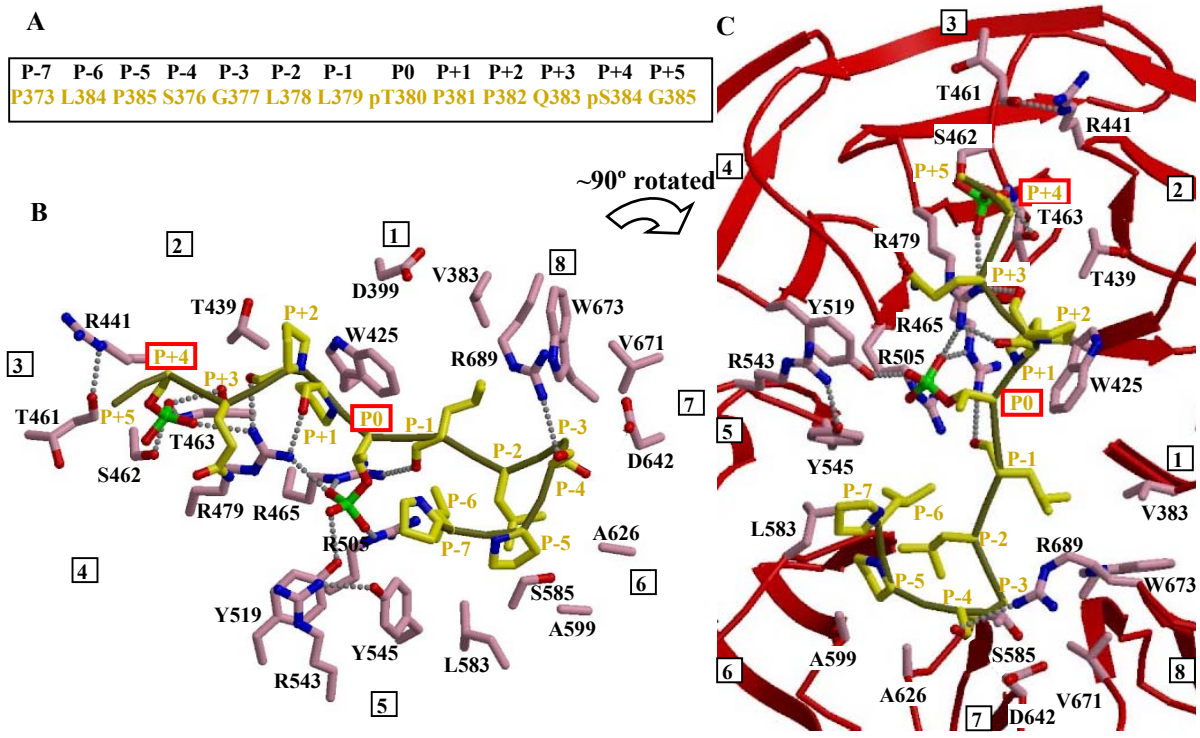

Figure 3.25. Phosphorylated C-terminal Cyclin E binds to the top face of the Fbw7 WD40 domain.

A) Shows residues of the C-terminal CycE$^{31pS372/pT380/pS384}$ peptide as recognized from electron density maps. **B)** and **C)** Close-up view of the interface between the Fbw7 WD40 domain and the C-terminal Cyclin E peptide. The Fbw7 WD40 domain is shown in red, with its side chains in pink, and the C-terminal Cyclin E peptide is shown in dark yellow, with its side chains in yellow. Gray dashes represent hydrogen bonds.

alignment with other Fbw7 substrates (Introduction, Figure 1.4) reveals that the residues at P-3 and P-4 are not conserved. This indicates that Fbw7 3rd-substrate-binding pocket is specific for C-terminal Cyclin E. The following residue, Pro373 at P-5, extends away from the β-propeller and no interactions are observed.

The ternary complex was crystallized with the triply phosphorylated C-terminal CycE$^{31pS372/pT380/pS384}$ peptide, which also included a phosphate group on residue Ser372 at P-8 that has been implicated to be involved in substrate-binding (Koepp et al., 2001; Ye et al., 2004). Yet, in the crystal structure, no clear electron density is visible at this position.

3.7.2 Comparison of Fbw7-C-terminal Cyclin E interaction with other peptides

The comparison of the three Fbw7-substrate structures containing the C-terminal CycE$^{31pS372/pT380/pS384}$, the N-terminal CycE^{14pT62} and the c-Myc$^{19pT58/pS62}$ peptides (Figure 3.26) reveals that the networks of hydrogen bonds and van der Waals contacts between the four substrate residues at P-2, P-1, P0 and P+1 are maintained in all the structures and seems to be required for initiating binding to Fbw7. Compared to C-terminal CycE$^{31pS372/pT380/pS384}$, however, the N-terminal CycE^{14pT62} and the c-Myc$^{19pT58/pS62}$ peptides bind only with their phosphorylated residue at the P0 to Fbw7 1st-phosphate-binding pocket. Outside their phosphorylated residue at P0, the N-terminal CycE^{14pT62} and c-Myc$^{19pT58/pS62}$ peptides bind distinctly to Fbw7 (Table 3.4).

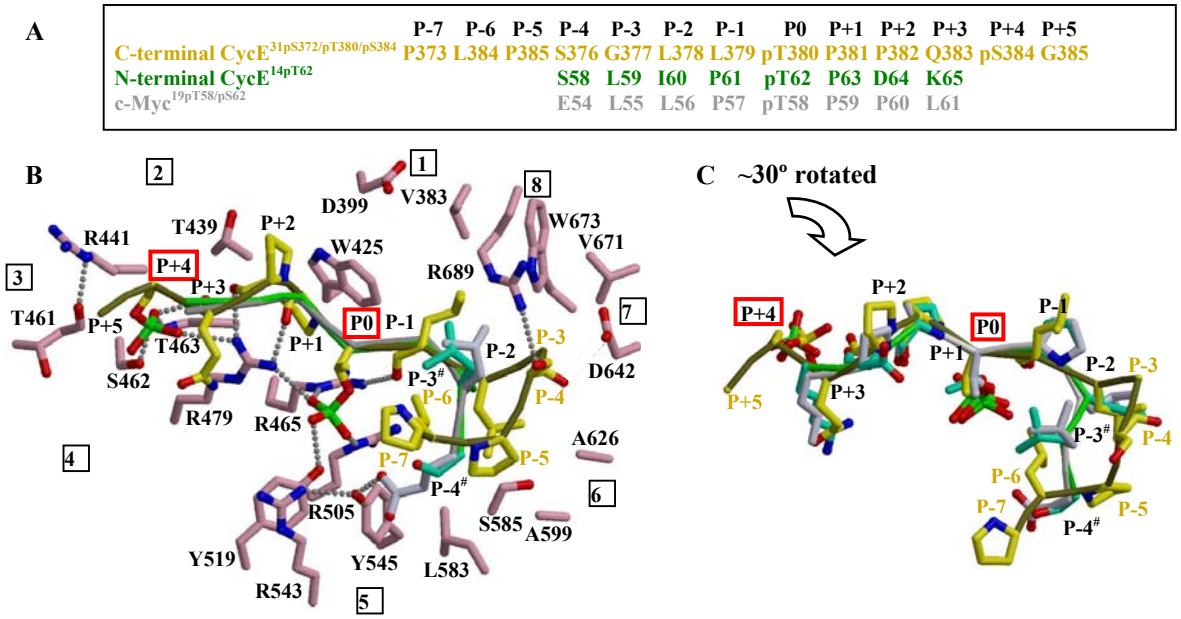

Figure 3.26. Superimposition of the Fbw7-substrate peptide interfaces.

A) Shows residues of the substrate peptides C-terminal CycE$^{31pS372/pT380/pS384}$ (yellow), N-terminal CycE^{14pT62} (green) and c-Myc$^{19pT58/pS62}$ (gray) as recognized from electron density maps.
B) Shows interface residues of Fbw7-Skp1-C-terminal CycE$^{31pS372/pT380/pS384}$ colored in pink and the three substrate peptides are colored as in A. The substrate peptide positions in black are invariant. Substrate peptide positions in black and denoted as P$^{\#}$ show the distinct binding of N-terminal CycE^{14pT62} and c-Myc$^{19pT58/pS62}$ peptides and the positions in yellow show the distinct binding of C-terminal CycE$^{31pS372/pT380/pS384}$peptide.
C) Close-up view of the superimposed C-terminal CycE$^{31pS372/pT380/pS384}$, N-terminal CycE^{14pT62} and c-Myc$^{19pT58/pS62}$ peptides.

3.7.2.1 N-terminal Cyclin E peptide

The N-terminal CycE^{14pT62} peptide binds with its phosphorylated Thr62 at P0 to Fbw7 1st-phosphate-binding pocket, and is very informative, since it contains an Asp64 at P+2, where most Fbw7 substrates contain a hydrophobic side chain. Another exception is Lys65 at P+3, a side chain believed to be disfavored for binding at this position as found in a spot array using a C-terminal CycE^{13pT380} and Gcn^{11pT165} peptide permutated in each position (Nash et al., 2001). However, the side chains of Asp64 and Lys65 adopt conformations very similar to the corresponding residues of the C-terminal Cyclin E peptide (Figure 3.26C). Furthermore, in the N-terminal CycE^{14pT62} peptide the Fbw7 2nd-phosphate-binding pocket is solvent-exposed and occupied by a sulfate molecule from the crystallization condition. At P-3, the N-terminal CycE^{14pT62} peptide contains the large side chain of Leu59, which prevents the peptide from coming close to Trp673 and Arg689 of blade 8, as observed in the C-

terminal Cyclin E peptide. Instead, the aliphatic side chain of Leu59 is pushed away from blade 8 by the charged side chain of residue Arg689. This shifts the course of the peptide backbone towards the opposite side of the Fbw7 WD40 domain. As a consequence, the N-terminal Cyclin E peptide exposes the side chain of Ser58 at P-4$^{\#}$ directed towards Fbw7 blade 5, and Fbw7 side chains of Arg543 and Tyr545 are directed towards the hydroxyl group of Ser58. Yet, no interactions have been observed. Even so, the Fbw7 residues Arg543 and Tyr545 are highly conserved among Fbw7 orthologs and it has been reported that the N-terminal Cyclin E residue Ser58 at P-4$^{\#}$ is phosphorylated by GSK3 (Welcker et al., 2003; Ye et al., 2004). Therefore, it might be possible that a phosphate group at P-4$^{\#}$ could bridge the distance to the side chain of Tyr545. Yet, in the Fbw7-Skp1-N-terminal CycE^{14pT62} structure as well as in the Fbw7-Skp1 structure without peptide no sulfate molecule from the crystallization buffer was bound at P-4. Furthermore, the binding groove is surrounded by the two hydrophobic residues Leu583 and Leu559. In addition, an alignment of the N-terminal sequences of Cyclin E with other Cyclin E orthologs (Figure 3.5) and other Fbw7 substrates (Introduction, Figure 1.4) reveals that the N-terminal CycE^{14pT62} residue Ser58 at P-4 is not conserved.

3.7.2.2 C-Myc peptide

The Fbw7-Skp1 complex has also crystallized with the c-Myc$^{19pT58/pS62}$ peptide, which contains two phosphate groups, one on Thr58 at P0 and the other on Ser62 at P+4. However, the interface of the Fbw7-c-Myc$^{19pT58/pS62}$ structure yielded only an interpretable electron density for the phosphorylated Thr58, which binds to Fbw7 1st-phosphate-binding pocket (Figure 3.26B). This result supports Yeh et al., 2004, who find that c-Myc ubiquitination by the SCF^{Fbw7} does not require the phosphorylation of Ser62 (Introduction, 1.3.3.2). Moreover, the side chain of Leu55 of c-Myc$^{19pT58/pS62}$ at P-3 shifts the peptide backbone, similar to the N-terminal Cyclin E peptide, to the opposite side of Fbw7 WD40 domain, in order to accommodate the Leu55 side chain. Surprisingly, c-Myc Glu54 at P-4$^{\#}$, which positions its side chain identically to N-terminal Cyclin E residue Ser58, engages in a hydrogen bond interaction with residue Tyr545 and represents the 4th-binding pocket in Fbw7. Residue Tyr545 forms a direct hydrogen bond interaction with the guanidinium group of residue Arg543. The residues Tyr545 and Arg543 are highly conserved among Fbw7

orthologs and reside at the outer rim of the Fbw7 1st-phosphate-binding pocket and are connected to it by stacking interactions.

Table 3.4. Potential hydrogen bonds between the peptides and the WD40 domain of Fbw7 and scCdc4.

Peptide	P-7	P-6	P-5	P-4	P-3	P-2	P-1	P0	P+1	P+2	P+3	P+4	P+5
CycE$^{31pS372/pT380/pS384}$	P373	L374	P375	S376	G377	L378	L379	pT380	P381	P382	Q383	pS384	G385
CycE^{14pT62}				S58#	L59	I60	P61	pT62	P63	D64	K65		
c-Myc$^{19pT58/pS62}$				E54#	L55	L56	P57	pT58	P59	P60	L61		
CycE^{9pT380}						L378	**L379**	**pT380**	**P381**	**P382**	Q383	S384	G385
H-bonds between Fbw7 and peptide side chains or main chains				R689			R465	R465 R479 R505 Y519	R479	R479		S462 T463 R479	
							R465	R505 Y519 R465	R479	R479			
				Y545			R465	R465 R479 R505 Y519	R479	R479			
H-bonds between scCdc4 and peptide side chains or main chains							R467	R467 R485 R534 Y548	R479		R485		

Hydrogen bonds of the C-terminal CycE$^{31pS372/pT380/pS384}$, N-terminal CycE^{14pT62} and c-Myc$^{19pT58/pS62}$ peptides to Fbw7 are colored in yellow, green and gray and the hydrogen bonds between the C-terminal CycE^{9pT380} peptide and scCdc4 are colored in blue. Hydrogen bonds to the peptide backbones are underlined, hydrogen bond cut of is ≤3.48Å. Phosphorylated residues are indicated by small p and numbers above the sequences indicate the positions of the residues based on pT380 determent as 0. In bolt electron density was interpreted for both C-terminal CycE^{9pT380} peptides of the scCdc4 dimer complex in the asymmetric unit. # denotes the peptide residue at P-4 that faces towards Fbw7 WD40 blade 5 instead of blade 8.

3.7.3 Conclusion to Fbw7-substrate interaction

In conclusion, the structures show a remarkable complexity on how Fbw7 selectively binds to its substrates. The structures elucidate that the Fbw7 1st-phosphate-binding pocket resides at the arginine-triad and residue Tyr519 at blade 3 and 4. Surprisingly, the presented Fbw7-Skp1-CycE$^{31pS372/pT380/pS384}$ structure shows that Fbw7 contains a 2nd-phosphate-binding pocket on blade 2 and 3. Binding assays with a different phosphorylated C-terminal Cyclin E peptide have shown that the C-terminal Cyclin E peptide phosphorylated on P0 and P+4 binds simultaneously to the two Fbw7 phosphate-binding pockets and increases the substrate-binding affinity to Fbw7 cooperatively (Table 3.1). Interestingly, residue Arg479 is part of both Fbw7 phosphate-binding pockets. Furthermore, along with the two Fbw7 phosphate-binding pockets, Fbw7 contains two additional binding pockets that interact with

the substrate residues at P-4 or P-4$^{\#}$ (Figure 3.26B). Which of the two additional binding pockets are reached depends on whether the substrate contains a side chain at P-3 or not. If the substrate contains no side chain at P-3, then a hydrophilic substrate side chain at P-4 will interact to Fbw7 binding pocket on blade 8. A substrate that does contains a side chain at P-3, however, will shift the course of the substrate backbone to Fbw7 opposite side and exhibits the substrate side chain at P-4$^{\#}$ towards blade 5. A substrate residue that is mimicking a phosphorylated side chain at P-4$^{\#}$ will interact to Fbw7 binding pocket on blade 5. However, substrate recognition by Fbw7 depends on substrate phosphorylation. Therefore, the two additional Fbw7 binding pockets are of minor importance.

3.8 Cyclin E turnover by SCF^{Fbw7}

Cyclin E contains two regions, the N-terminal CycE^{14pT62} and the C-terminal CycE$^{31pT380/pS384}$ regions, that after phosphorylation are recognized by the SCF^{Fbw7} ligase. Furthermore, it has been shown that wt-Fbw7 exists as a dimer (Figure 3.3). Therefore, it seems possible that the phosphorylated N-terminal and C-terminal Cyclin E regions each bind to one WD40 domain of the SCF^{Fbw7} ligase dimer, which may lead to an increased Cyclin E turnover. In support of this, our collaborator Wade Harper has performed an *in vivo* degradation assay with phosphorylated Cyclin E and wt-Fbw7α as well as with Fbw7α caring a single point mutation in the putative N-terminal dimerization region (DD-Fbw7α), which strongly reduces the ability of the matrix bound GFP-DD-Fbw7α to pull down Flag-DD-Fbw7α (Figure 3.27A). Figure 3.27B shows that wt-Fbw7α degrades Cyclin E much faster compared to DD-Fbw7α. This implies that the dimerization of Fbw7α increases the turnover of phosphorylated Cyclin E. Moreover, this is consistent with the findings by Bales et al., 2005 and Akli et al., 2004, that an N-terminaly truncated Cyclin E starting at amino acid 65 shows hyperactivity.

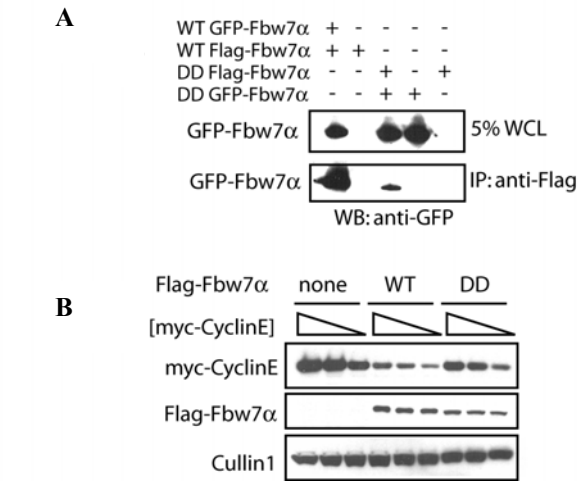

Figure 3.27. *In vivo* degradation assay of phosphorylated Cyclin E by Fbw7.

A) Shows the dimerization of wild type Fbw7α (WT-Fbw7α) and is largely reduced in the dimerization-defective (DD-Flag-Fbw7α).
B) Shows, that phosphorylated Cyclin E is degraded faster by WT-Fbw7α than DD-Fbw7α.
Data was provided by Wade Harper.

3.9 The scCdc4-Skp1-CycE^{9pT380} complex structure

As described in the Introduction, 1.3.4, Orlicky et al., 2003, solved the to Fbw7 homologous structure scCdc4 bound to a singly phosphorylated C-terminal CycE^{9pT380} peptide (377-GLLpTPPQSG-385), although it is not a physiological substrate of scCdc4. The asymmetric unit in the crystals contains two molecules of the scCdc4-Skp1-C-terminal CycE^{9pT380} complex. For both complexes, discernable electron density was unambiguously modeled for the four C-terminal Cyclin E residues Leu379, phosphorylated Thr380, Pro381 and Pro382 at P-1 to P+2. However, only one complex had interpretable electron density for the additional C-terminal Cyclin E residues Leu378 at P-1 and Gln383, Ser384 and Gly385 at P+3 to P+5. In the scCdc4-Skp1-C-terminal CycE^{9pT380} structure, the phosphorylated Thr380 at P0 binds to the scCdc4 residue Tyr548 and to the residues of the invariant arginine-triad of Arg467, Arg485 and Arg534. These residues form the 1st-phosphate-binding pocket of scCdc4 (Table 3.4). Additionally, the side chains of the residues Arg467 and Arg485 form hydrogen bond interactions to the backbone carbonyl groups of the peptide residues at P-1, P+1 and P+2 and stabilize the substrate-binding. Moreover, Pro381 at P-1 forms stacking interactions with the invariant Trp426.

In addition, mutational studies on the scCdc4 WD40 domain surface and subsequent binding to its physiological substrate, the phosphorylated Sic1 has revealed that a single exchange of scCdc4 WD40 domain surface residues Arg467Ala, Arg485Ala, Arg534Ala or Trp426Ala abolished the binding to phosphorylated Sic1, whereas an exchange of Trp717Asn, Arg443Ala, Lys402Ala, Tyr574Phe or Val384Asn did not have an effect at all (Nash et al., 2001; Orlicky et al., 2003). The scCdc4 mutants that did abolish binding of the phosphorylated Sic1 flank scCdc4 substrate phospate-binding pocket at P0 or P+1. From the structural and mutagenesis studies Orlicky et al., 2003 concluded that scCdc4 and its homolog Fbw7 contain only one-phosphate-binding pocket.

3.9.1 Comparison of Fbw7 and scCdc4-substrate interacting interface

The superimposition of Fbw7 WD40 domain structures in the absence and presence of the triply phosphorylated C-terminal CycE$^{31pS372/pT380/pS384}$, the singly phosphorylated N-terminal CycE^{14pT62} and the doubly phosphorylated c-Myc$^{19pT58/pS62}$ peptides onto the scCdc4 WD40 domain structure bound to a singly phosphorylated CycE^{9pT380} peptide (Figure 3.28), reveals that Fbw7 and scCdc4 bind substrates at the same WD40 domain position.

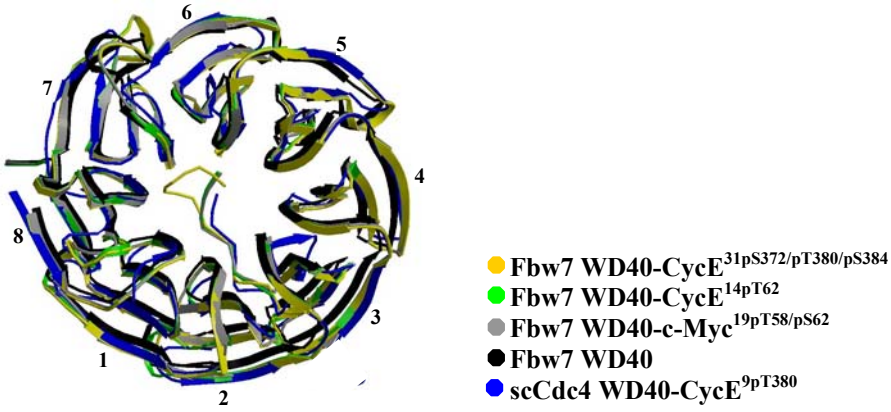

Figure 3.28. Superimposition of Fbw7 and scCdc4 WD40 domain with and without substrate peptides.

Superimposition of the Fbw7 WD40 domain without (black) and with the phosphorylated peptides C-terminal CycE$^{31pS372/pT380/pS384}$ (yellow), N-terminal CycE^{14pT62} (green) and c-Myc$^{19pT58/pS62}$ (gray) onto scCdc4 WD40 domain with the singly phosphorylated C-terminal CycE^{9pT380} peptide (blue).

The comparison of the buried accessible surface areas of the peptides bound to Fbw7 and scCdc4 structures reveals that the thirteen visible residues of the C-terminal CycE$^{31pS372/pT380/pS384}$, the eight visible residues of the C-terminal CycE^{9pT380}, the eight visible

residues of the N-terminal CycE^{14pT62} and the eight visible residues of the c-Myc$^{19pT58/pS62}$ peptides bury a solvent-accessible surface area of 1304 Å^2, 871 Å^2, 897 Å^2 and 1002 Å^2 respectively. It reveals that the thirteen residues of C-terminal CycE$^{31pS372/pT380/pS384}$, which binds with two phosphorylated residues to the Fbw7 WD40 domain, covers a larger solvent accessible area compared to the eight visible C-terminal CycE^{9pT380}, N-terminal CycE^{14pT62} and c-Myc$^{19pT58/pS62}$ peptide residues, that only bind with one phosphorylated residue to either Fbw7 or scCdc4. Moreover, it shows that the eight residues of c-Myc$^{19pT58/pS62}$ that additionally interact with the side chain of residue Glu54 at P-4$^{\#}$ (Figure 3.26B) bury a larger solvent accessible surface than the C-terminal CycE^{9pT380} and N-terminal CycE^{14pT62} peptides (Table 3.5).

Table 3.5. Buried interface surface areas between Fbw7 or scCdc4 and their substrate peptides.

	C-terminal CycE^{9pT380}	C-terminal CycE$^{31pS372/pT380/pS384}$	N-terminal CycE^{14pT62}	c-Myc$^{19pT58/pS62}$
buried contact area in Fbw7	---	**1304 Å^2**	**897 Å^2**	**1002 Å^2**
buried contact area in scCdc4	**871 Å^2**	---	---	---

Buried interface surface areas between Fbw7 (scCdc4) and the substrate peptides are in Å^2.

Furthermore, their WD40 domains are folded in a very similar fashion with an rmsd of 1.3 to 1.4 Å over 308 WD40 domain Cα atoms. The Fbw7 and scCdc4 WD40 domains are best superimposed on their β-strands with only one obvious structural difference being observed in a loop region of blade 8. In Fbw7, the loop between strand S8B and S8C is three residues bigger than in scCdc4 (Figure 3.20). As a consequence, the Fbw7 loop bends closer

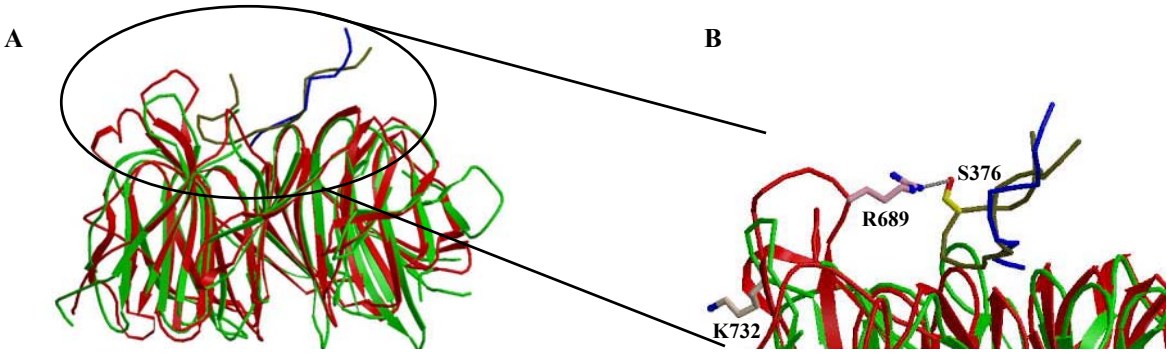

Figure 3.29. Superimposition of Fbw7 and scCdc4 WD40 domain bound to C-terminal Cyclin E.

A) Superimposition of scCdc4 WD40 domain (green) bound to singly phosphorylated C-terminal CycE^{9pT380} (blue) to Fbw7 WD40 domain (red) bound to triply phosphorylated C-terminal CycE$^{31pS372/pT380/pS384}$ (yellow).
B) Close-up view depicts the only structural difference between Fbw7 and scCdc4 WD40 domain.

to the C-terminal Cyclin E peptide and the side chain of Fbw7 residue Arg689 forms a hydrogen bond interaction to the side chain of residue Ser376 at P-4. In contrast to the side chain of residue Arg689 of Fbw7, the corresponding side chain of residue Lys732 in scCdc4 points away from the peptide (Figure 3.29).

3.9.1.1 Comparison of Fbw7 and scCdc4 WD40 domain surface

The Fbw7 WD40 domain surface was identified to be involved in substrate-binding and has been compared to the scCdc4 WD40 domain surface (Figure 3.30). It reveals that the substrate-binding interface of Fbw7 and scCdc4 WD40 blades 2 to 5 is invariant. The WD40 blades 2 to 5 include the highly conserved 1st and 2nd-phosphate-binding pockets at P0 and P+4, the invariant tryptophane at P+1, as well as the additional binding pocket on blade 5 (Figure 3.26B). The substrate-binding interfaces of Fbw7 and scCdc4 WD40 blades 1, 6, 7 and 8 are not highly conserved and show slight structural differences.

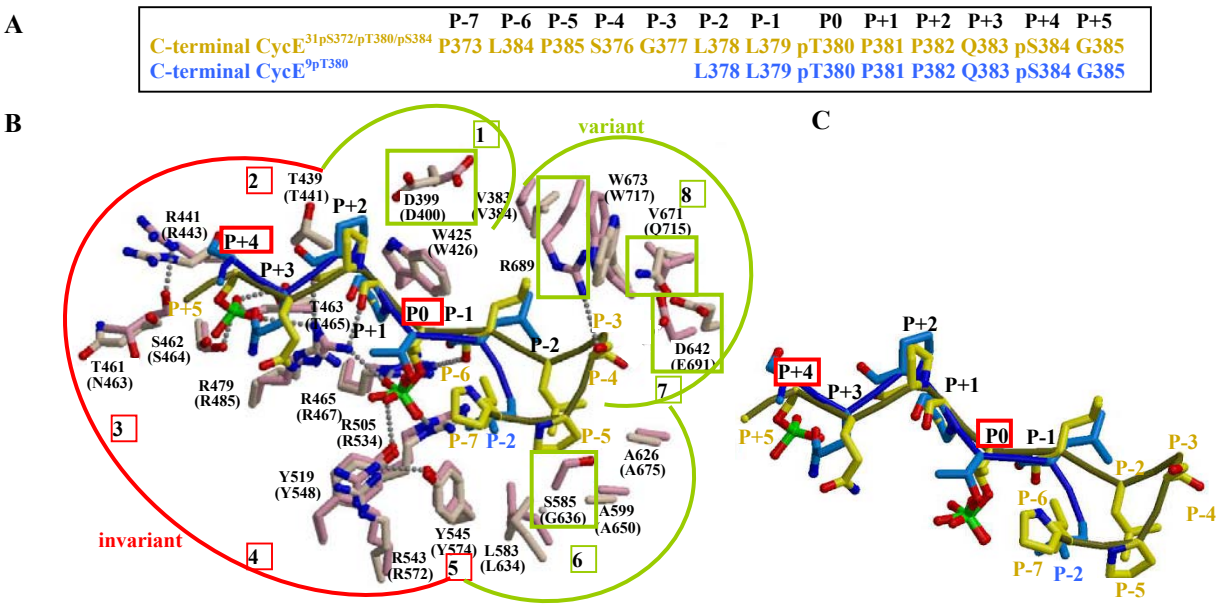

Figure 3.30. Superimposition of the interfaces of Fbw7 and scCdc4 bound to C-terminal Cyclin E.

A) Shows residues of the C-terminal CycE$^{31pS372/pT380/pS384}$ and C-terminal CycE^{9pT380} peptides as recognized from the electron density maps.
B) Top view of scCdc4 bound to singly phosphorylated C-terminal CycE^{9pT380} peptide superimposed to Fbw7 bound to doubly phosphorylated C-terminal CycE$^{31pS372/pT380/pS384}$ peptide. Their invariant WD40 blades are marked in red and the variant WD40 blades in green, the residues in the green boxes differ among the WD40 domains. Invariant peptide positions are marked in black, and in yellow for C-terminal CycE$^{31pS372/pT380/pS384}$ and blue for C-terminal CycE^{9pT380} when distinct.
C) Close-up view of the superimposed C-terminal CycE^{9pT380} and C-terminal CycE$^{31pS372/pT380/pS384}$ peptides.

blade 1

The substrate residue at P+2 binds to a groove at blade 1 that is surrounded by a threonine, an aspartate and a tryptophane. This binding groove differs between the Fbw7 and scCdc4 WD40 domains in the orientation of the side chain of an aspartate. In Fbw7, the side chain of Asp399 forms a hydrogen bond interaction with His382 and faces away from the peptide. ScCdc4 has Thr382 instead of Fbw7 His382 and forms no hydrogen bond with residue Asp400. Therefore, in scCdc4, the side chain of Asp400 faces towards the peptide and reduces the space for substrate residue side chains at P+2. However, it seems unlikely that the different orientated aspartates will significantly change the binding affinity of the substrate, because in all analyzed interfaces the substrate residue side chains at P+2 fit well to the same location in the structure.

blade 6

The Fbw7 binding groove on blade 6 consists of the residues Ala626, Ala599, Leu583 and Ser585. The scCdc4 binding pocket differs in the Fbw7 position of residue Ser585, in which scCdc4 has Gly636. Therefore, the scCdc4-binding groove at blade 6 is slightly deeper and more hydrophobic than in Fbw7. However, the binding groove is only relevant if the substrate contains no side chain at P-3. This is described in the next paragraph.

blade 7 and 8

Fbw7 and scCdc4 blade 8 interact with one hydrogen bond to a hydrophilic substrate side chain at P-4 if the substrate residue contains no side chain at P-3.

P-3 The substrate residue at P-3 is in Fbw7 surrounded by the residues Arg689 and Trp673 of blade 8. ScCdc4 contains, at the Fbw7 residue Trp673, the residue Trp717, whose side chain is 180º rotated. As a consequence, the side chain of residue Trp717 faces deeper into the central channel of scCdc4 β-propeller. In addition, Arg689, which in Fbw7 faces towards the substrate, is in scCdc4 replaced by Lys732 and faces away from the β-propeller (Figure 3.29). Moreover, the side chain of Fbw7 residue Arg689 is involved in expelling substrate side chains at P-3, since there is no space to accommodate it at blade 8. However, it seems possible that in scCdc4, the side chain of residue Gln715, which in Fbw7 is exchanged to residue Val671, acts in a similar fashion to Fbw7 residue Arg689.

P-4 The binding of a substrate residue at P-4 to blade 8 is only relevant if the substrate contains no side chain at P-3, then the substrate backbone can come in close to Fbw7 Trp673 and Asp642, as well as to scCdc4 Trp717 and Glu691 of blade 7 and 8. As a consequence, if the substrate side chain at P-4 contains a hydroxyl group, then it can interact with Fbw7 residue Arg689 of blade 8. In scCdc4, residue Gln715, which is in close proximity to Fbw7 residue Arg689, might form a hydrogen bond interaction in a similar matter.

The analysis of Fbw7 and scCdc4 variable WD40 domain structure surface has revealed that it is unlikely that their WD40 domain surface differences will significantly contribute to different substrate-binding affinities.

3.9.1.2 Comparison of the superimposed C-terminal Cyclin E peptides

Comparing the C-terminal CycE$^{31pS372/pT380/pS384}$ and C-terminal CycE^{9pT380} peptides bound to Fbw7 and scCdc4 WD40 domains (Figure 3.30C) reveals that their peptide residues Pro382, Pro381, the phosphorylated Thr380 and Leu379 at P+2 to P-1 superimpose well in both WD40 domains. The following last visible C-terminal CycE^{9pT380} peptide residue in scCdc4 is Leu378 at P-2, which is significantly shifted compared to Fbw7 C-terminal CycE$^{31pS372/pT380/pS384}$ peptide residue Leu378 at P-2. It is most likely that the shift of Leu378 occurs due to the absence of Pro375 and Leu374 in the C-terminal CycE^{9pT380} peptide, which in the C-terminal CycE$^{31pS372/pT380/pS384}$ peptide cluster together with Leu378 and bind to the hydrophobic binding groove at blade 6. The C-terminal Cyclin E peptide residues Gln383, Ser384 and Gly385 at P+2 to P+5 are visible in both structures. However, only Ser384 of the C-terminal CycE$^{31pS372/pT380/pS384}$ peptide contains a phosphate group at P+4 and binds to Fbw7 2nd-phosphate-binding pocket. Whereas in scCdc4 the side chain of Gln383 is significantly shifted towards the position of the phosphorylated Ser384 of the C-terminal CycE$^{31pS372/pT380/pS384}$ peptide and leads to a weak hydrogen bond interaction with suboptimal geometry to the side chain of scCdc4 Arg485 (Orlicky et al., 2003). This suggests that in the scCdc4 WD40 domain the side chain of C-terminal CycE^{9pT380} residue Gln383 at P+3 attempts to mimic the phosphorylated C-terminal CycE$^{31pS372/pT380/pS384}$ residue Ser384 at P+4. Furthermore, the shift of the side chain of Gln383 at P+3 also leads to a shift of Ser384 at P+4 and Gly385 at P+5 in the scCdc4 structure.

Moreover, a comparison of the interface of the singly phosphorylated C-terminal CycE^{9pT380} peptide bound to scCdc4 (Figure 3.30) to the interfaces of the singly phosphorylated N-terminal CycE^{14pT62}, the doubly phosphorylated c-Myc$^{19pT58/pS62}$ and triply phosphorylated CycE$^{31pS372/pT380/pS384}$ peptides bound to Fbw7 (Figure 3.26), reveals (A) that the N-terminal CycE^{14pT62} and c-Myc$^{19pT58/pS62}$ peptides contain a sulfate molecule at their solvent exposed 2nd-phosphate-binding pocket at P+4, whereas the C-terminal CycE^{9pT380} peptide does not (Figure 3.30), although all Fbw7 and scCdc4 ternary complex crystals were obtained from a condition that contained sulfate; that the three-substrate peptides bound to Fbw7 place their side chain at P+3 in a similar position (Figure 3.26). In the scCdc4 structure, the side chain of Gln383 at P+3 is shifted and partly occupies the space of scCdc4 2nd-phosphate-binding pocket at P+4 by forming a weak hydrogen bond interaction with Gln383, with a suboptimal geometry to the guanidinium group of scCdc4 Arg485 (Figure 3.30). Therefore, no sulfate molecule can bind to the 2nd-phosphate-binding pocket in scCdc4. Yet, Fbw7 and scCdc4 2nd-phosphate-binding pockets are highly conserved, however, so it seems obvious that the addition of a phosphate group to the C-terminal CycE^{9pT380} peptide at P+4 should result in binding identical to scCdc4 like the C-terminal CycE$^{31pT380/pS384}$ peptide to Fbw7.

3.9.2 Comparison of Fbw7 and scCdc4 Cyclin E binding mechanism

Structural analyses of Fbw7 and scCdc4 WD40 domain have revealed that the major substrate-binding area, which contains the two-phosphate-binding pockets, is identical in both (Figure 3.30). Therefore, it was tempting to speculate that scCdc4 binds cooperatively to substrates phosphorylated at P0 and P+4 like Fbw7. However, the current belief is that scCdc4 contains only one-phosphate-binding pocket (Orlicky et al., 2003). Therefore, binding studies with an identical set of phosphorylated C-terminal Cyclin E peptides were used to investigate the substrate-binding mechanisms of Fbw7 and scCdc4. Table 3.6 compares the measured binding affinities of the phosphorylated C-terminal Cyclin E peptides to scCdc4 and to Fbw7.

Table 3.6. Binding affinities of the phosphorylated C-terminal Cyclin E peptides to the Fbw7-Skp1 and scCdc4-Skp1 complex.

CycE-Peptides	K_d (μM) with Skp1-Fbw7	K_d (μM) with scCdc4-Skp1
$CycE^{31pT380}$	49 ± 31	3.8 ± 0.4
$CycE^{31pT380/pS384}$	0.07 ± 0.11	0.093 ± 0.03
$CycE^{29pS372/pT380}$	no ITC signal	2.5 ± 1
$CycE^{31pS372/pT380/pS384}$	0.13 ± 0.03	0.12 ± 0.01

N-terminus of the peptides is acetylated. Dissociation-constant (K_d) values are average of three individual sets of ITC readings. ± indicates the standard deviation of three independent experiments.

The binding assays reveal that the C-terminal $CycE^{31pT380}$ peptide, which is only phosphorylated at residue Thr380 at P0, binds weakly to scCdc4, with a K_d of 3.8 μM. Remarkably, the C-terminal $CycE^{31pT380/pS384}$ peptide, which is additionally phosphorylated at residue Ser384 at P+4 binds to scCdc4 with a K_d of 0.093 μM. This reveals that the doubly phosphorylated C-terminal $CycE^{31pT380/pS384}$ peptide binds ~40 times better than the singly phosphorylated C-terminal $CycE^{31pT380}$ peptide. The triply phosphorylated C-terminal $CycE^{31pS372/pT380/pS384}$ peptide, which contains an additional third phosphate group at residue Ser372 at P-8, binds to scCdc4 with a K_d of 0.12 μM. Comparison of the doubly phosphorylated C-terminal $CycE^{31pT380/pS384}$ peptide with the triply phosphorylated C-terminal $CycE^{31pS372/pT380/pS384}$ peptide reveals that the K_d values are the same within the experimental error. This indicates that the phosphorylated residue Ser372 is not involved in substrate-binding to scCdc4.

A comparison of the scCdc4 and Fbw7 Cyclin E binding affinities reveals that the two phosphate groups at the P0 and P+4 positions of the $CycE^{31pT380/pS384}$ peptide bind cooperatively to Fbw7 and scCdc4. It proves that scCdc4 contains two-phosphate-binding pockets, to which doubly phosphorylated C-terminal Cyclin E peptide binds. The added phosphate group at P-8 does not increase the binding affinity to Fbw7 and scCdc4. Moreover, doubly phosphorylated $CycE^{31pT380/pS384}$ peptide shows a comparable K_d of 0.07 μM to Fbw7 and 0.09 μM to scCdc4. This emphasizes that the doubly phosphorylated $CycE^{31pT380/pS384}$ peptide is a perfect substrate for scCdc4 and underlines that their substrate-binding mechanism is very similar.

3.9.3 Amino acid sequence analysis of scCdc4 substrate Sic1

Binding studies have shown that the two phosphate groups of the C-terminal CycE$^{31pT380/pS384}$ peptide bind cooperatively to Fbw7 and scCdc4 phosphate-binding pockets. Structural data had previously shown that only the 1st-phosphate-binding pocket at P0 requires a phosphorylated threonine or serine residue that is followed by a proline residue at P+1 (Orlicky et al., 2003), but our identified 2nd-phosphate-binding pocket at P+4 does not. However, the current opinion states that scCdc4 recognizes its substrate Sic1 (S-phase inhibitor) only after Sic1 phosphorylation on at least 5 to 6 of its 9 ThrPro/SerPro Cdk consensus sites (Nash et al., 2001; Orlicky et al., 2003). Therefore, the amino acid sequence of Sic1 was analyzed to see if Sic1 ThrPro/SerPro Cdk consensus sites are surrounded by a second Cdk consensus site or another phosphorylated residue at P+4 or P+3. Surprisingly, the amino acid sequence analysis of Sic1 suggested three potential phosphorylated clusters within the N-terminal 80 amino acids (Figure 3.31).

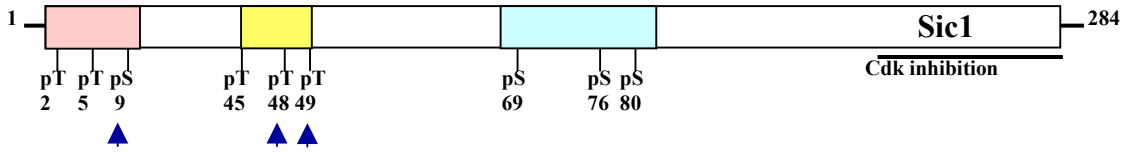

Figure 3.31. Schematic representation of Sic1 with three multi phosphorylated clusters.

Shown are three phosphorylated clusters within the Sic1 protein. Blue arrows mark the phosphorylated Sic1 residues that do not conform to the Cdk consensus.

The first cluster contains the Cdk consensus site residues Thr2 and Thr5 as well as the phosphorylatable residue Ser9, which would match the spacing of P+4. The second cluster contains the Cdk consensus site residue Thr45 and the phosphorylatable residues Thr48 and Thr49 at P+3 and P+4. The third cluster contains the Cdk consensus site residues Ser76 and Ser80 at a spacing of P+4 and the nearby Cdk consensus site residue at Ser69.

3.9.4 Binding studies of scCdc4-Skp1 with phosphorylated Sic1 peptides

To test if Sic1 that is phosphorylated on P0 and P+4 binds to scCdc4 two-phosphate-binding pockets, different phosphorylated Sic1 peptides were designed from three regions within Sic1 amino acid sequence (Figure 3.31.). All Sic1 peptides contain a phosphorylated Cdk consensus site at P0, and except for Ser9 and Thr48, another Cdk consensus site at P+4. Ser9 and Thr48 have been shown to be phosphorylated *in vitro* by Ime2 and Cln-Cdc28,

respectively (Sedgwick et al., 2006; Verma et al., 1997). In the doubly phosphorylated Sic1$^{15pT45/pT48}$ peptide, the second phosphate group was added on residue Thr48 at P+3 instead of residue Thr49 at P+4, because residue Thr48 but not residue Thr49 is conserved among Sic1 orthologs (data not shown). Additionally, the Sic1 Cdk consensus site residues Thr2 at P-3 and Ser69 at P-7 were chosen for phosphorylation. Furthermore, it has been shown that the N-terminal 100 amino acids of Sic1 (Sic1$^{1-100}$), which contains the three identified phosphorylated clusters, are necessary and sufficient to specify Cdc34-dependent ubiquitination (Verma et al., 1997). To test whether the addition of more than two phosphorylated Sic1 Cdk consensus sites increased Sic1 binding affinity to scCdc4, the N-terminal Sic1$^{1-100}$ protein fragment was purified and *in vitro* phosphorylated (Method, 2.2.5.4) (Figure 3.32).

Sic-Peptides		P-7	P-3	P0	P+3	P+4	scCdc4-Skp1 K_d (µM)
Sic1$^{13pT2/pT5}$	1-		M**[pT]**PS	**[pT]**PP	R	T RGTR	-13 **30 ± 8**
Sic1^{11pT5}	1-		T PS	**[pT]**PP	R	T RGT	-12 **17 ± 5**
Sic1$^{11pT5/pT9}$	2-		T PS	**[pT]**PP	R	**[pT]**RGT	-12 **4 ± 1**
Sic1^{15pT45}	36- KP S	QNL	V PV	**[pT]**PS	T	T K	-50 **No ITC signal**
Sic1$^{15pT45/pT48}$	36- KP S	QNL	V PV	**[pT]**PS	**[pT]**	T K	-50 **7 ± 4**$^{\#}$
Sic1^{17pS76}	66-GMT S	PFN	G LT	**[pS]**PQ	R	S PF	-82 **49 ± 4**
Sic1$^{17pS76/pS80}$	66-GMT S	PFN	G LT	**[pS]**PQ	R	**[pS]**PF	-82 **2.6 ± 0.3**
Sic1$^{17pS69/pS76/pS80}$	66-GMT **[pS]**	PFN	G LT	**[pS]**PQ	R	**[pS]**PF	-82 **3 ± 1**
Sic1$^{1-100pT2/pT5/pT33/pT45/pS69/pS76/pS80}$				**4.2±0.4**			

Figure 3.32. Binding affinities of Sic1 peptides to scCdc4-Skp1 complex.

Shows the phosphorylated Sic1 peptides colored according to the three derived clusters within Sic1 (Figure 3.31), additional the N-terminal Sic1$^{1-100}$ protein fragment was in vitro phosphorylated (Method, 2.2.5.4). Superscript denote phosphorylated residues. Binding affinities were measured at 25 ºC and at 37 ºC$^{\#}$. Dissociation-constant (K_d) values are average of three individual sets of ITC readings, ± indicates the standard deviation, bold brackets depict phosphorylated residues.

The binding assays were partly completed by Bing Hao and reveal that the Sic1 peptides only phosphorylated at P0 bind weakly to scCdc4. For example, Sic1 phosphorylated on residue Ser76 binds to scCdc4 with a K_d of 49 µM, Sic1 phosphorylated on residue Thr5 binds to scCdc4 with a K_d of 17 µM, and for Sic1 phosphorylated on residue Thr45 no ITC signal was measured. Surprisingly, the addition of a second phosphate group to the Sic1 peptides at P+4 increases the binding affinity to scCdc4. The doubly phosphorylated Sic1$^{17pS76/pS80}$ peptide binds with a K_d of 2.6 µM, 18 times better than the singly

phosphorylated Sic1^{17pS76} peptide, and the doubly phosphorylated Sic1$^{11pT5/pS9}$ peptide binds with a K_d of 4 μM, 4 times better than the singly phosphorylated Sic1^{11pT5} peptide. The triply phosphorylated Sic1$^{17pS69/pS76/pS80}$ peptide, in which an additional phosphate group was added to residue Ser69, binds with a K_d of 3 μM. This reveals that the binding affinities of the doubly phosphorylated Sic1$^{17pS76/pS80}$ and triply phosphorylated Sic1$^{17pS69/pS76/pS80}$ peptides are comparable, and indicates that the phosphorylated residue Ser69 does not contribute to substrate-binding. Similarly, the doubly phosphorylated Sic1$^{13pT2/pT5}$ peptide, in which a second phosphate group was added to Thr2, reveals a K_d of 30 μM, which is 2-fold weaker than the singly phosphorylated Sic1^{11pT5} peptide. This reveals that the phosphorylated residue Thr2 does not contribute to substrate-binding. Furthermore, the doubly phosphorylated Sic1$^{15pT45/pT48}$ peptide binds at 37 ºC with 7 μM to scCdc4, but gives no ITC signal at 25 ºC. In addition, the *in vitro* phosphorylated Sic1$^{1-100}$ binds to scCdc4 with a K_d of 4.2 μM. Comparing the binding affinity of the phosphorylated Sic1$^{1-100}$ with the other phosphorylated Sic1 peptides reveals that the phosphorylated Sic1$^{1-100}$ binds comparably to the doubly phosphorylated Sic1$^{pS76/pS80}$ peptide, the doubly phosphorylated Sic1$^{15pT45/pT48}$ peptide and to the doubly phosphorylated Sic1$^{11pT5/pS9}$ peptide. This indicates that Sic1$^{1-100}$ uses only two of its seven phosphorylated Cdk consensus sites to bind to scCdc4.

The binding assays with the Sic1 peptides show that the doubly phosphorylated Sic1$^{17pS76/pS80}$, Sic1$^{11pT5/pS9}$ and Sic1$^{15pT45/pT48}$ peptides as well as the phosphorylated Sic1$^{1-100}$ bind to the two-phosphate-binding pockets in scCdc4 and this is consistent with the presented structural results. In addition, the binding assay with the Sic1 peptides reveals that two specific phosphorylated Sic1 residues with a spacing of P+4 or P+3 are enough for efficient Sic1 recognition by scCdc4. Furthermore, the binding assay with Sic1$^{1-100}$, which has been *in vitro* phosphorylated on its seven Cdk consensus sites, shows that the addition of more than two-specific phosphate groups to Sic1 does not increase the binding to scCdc4. This results contrasts with the Nash et al., 2003 finding that Sic1 needs to be phosphorylated on at least six Cdk consensus sites in order to be recognized by scCdc4.

In addition, it has been shown that scCdc4 acts as a dimer (Results and Discussion, 3.2.2), therefore it might be possible that the phosphorylated N-terminal region and C-terminal region of Sic1 each bind to one scSCF^{Cdc4} ligase complex of the scSCF^{Cdc4} ligase

dimer, and that might further increase the efficiency of Sic1 turnover by the scSCF^{Cdc4} ligase as shown for Cyclin E turnover by the scSCF^{Fbw7} ligase (Figure 3.27).

3.9.4.1 Analysis of the binding affinities of doubly phosphorylated Sic1 and Cyclin E peptides to the scCdc4-Skp1 complex

The K_d of the doubly phosphorylated C-terminal CycE$^{31pT380/pS384}$ peptide bound to scCdc4 is 0.09 μM, whereas the doubly phosphorylated Sic1$^{11pT5/pS9}$ and Sic1$^{17pS76/pS80}$ peptides bind with a K_d of 4 μM and 2.6 μM, respectively, to scCdc4. Thus, compared to the doubly phosphorylated Sic1$^{11pT5/pS9}$ and Sic1$^{17pS76/pS80}$ peptides, the doubly phosphorylated C-terminal CycE$^{31pT380/pS384}$ peptide binds to scCdc4 30 to 40 times stronger. Analyzing the residue composition of the doubly phosphorylated C-terminal Cyclin E and Sic1 peptides identifies that the Sic1 peptides are suboptimal substrates for scCdc4. For example, the Sic1 second phosphate group at P+4 is surrounded by a positively charged arginine at P+3 and either by an arginine or a proline at P+5, whereas the C-terminal CycE$^{31pT380/pS384}$ peptide contains a negatively charged glutamate at P+3 and a glycine at P+5. Furthermore, earlier mutational studies in which C-terminal CycE^{13pT380} was varied in each position revealed that C-terminal Cyclin E disfavors basic residues at P+2 to P+5 (Nash et al., 2001). However, in the N-terminal CycE^{14pT62} peptide, the basic side chain of Lys65 at P+3 adapts similar to the P+3 residue of the CycE$^{31pS372/pT380/pS384}$ peptide.

3.10 Mutagenesis of Fbw7 and scCdc4 2nd-phosphate-binding pocket

3.10.1 Binding studies of Sic1 with the scCdc4 mutants

To further support the finding that scCdc4 contains two-phosphate-binding pockets, residues of scCdc4 that would make up the 2nd-phosphate-binding pocket were mutated. Two scCdc4 mutants were made. In the double scCdc4$^{S464A/T465V}$ mutant, Ser464 and Thr465 were replaced with alanine and valine. In the triple scCdc4$^{S464A/T465V/R443M}$ mutant Arg443, which surrounds scCdc4 2nd-phosphate-binding pocket was additionally replaced by methionine. The replacement of Arg443 to methionine was chosen because the guanidinium group of Arg443 is involved in the formation of a hydrogen bond interaction to the carboxyl group of Asn463. This interaction seems important for fixing the position of the nearby scCdc4 residues Ser464, Thr465 and Arg467 that are involved in substrate-binding. The third residue

Arg485 of scCdc4 2nd-phosphate-binding pocket was not mutated, because Arg485 is also important for scCdc4 1st-phosphate-binding pocket. Furthermore, previous scCdc4 mutational studies have already shown that a mutation of Arg485 to alanine abolishes the binding to phosphorylated Sic1 (Nash et al., 2001; Orlicky et al., 2003). In addition, the binding of the phosphorylated $Sic1^{1-100}$ protein fragment to the scCdc4 mutants was tested. Table 3.7 shows the K_d values of the phosphorylated Sic1 and C-terminal Cyclin E peptides to the scCdc4 mutants and compares it to wt-scCdc4.

Table 3.7. Sic1 and Cyclin E peptides used in ITC with wild type and mutated scCdc4 2nd-phosphate-binding pocket.

Peptides	ScCdc4-Skp1 Kd (µM)	scCdc4-Skp1 S464A/T465V Kd (µM)	scCdc4-Skp1 R443M/S464A/T465V Kd (µM)
$Sic1^{13pT2/pT5}$	30 ± 8	30 ± 8	27 ± 6
$Sic1^{11pT5}$	17 ± 5	25 ± 5	51 ± 12
$Sic1^{11pT5/pS9}$	4 ± 1	12 ± 2	43 ± 14
$Sic1^{15pT45}$	No ITC signal	No ITC signal	No ITC signal
$Sic1^{15pT45/pT48}$	4 ± 1#	17 ± 3#	40 ± 5#
$Sic1^{17pS76}$	49 ± 4	60 ± 9	82 ± 17
$Sic1^{17pS76/pS80}$	2.6 ± 0.3	33 ± 7	19 ± 6
$Sic1^{17pS69pS76/pS80}$	3 ± 1	20 ± 4	19 ± 3
$CycE^{9pT380}$	3.8 ± 0.4	1.3 ± 0.3	2.3 ± 0.5
$CycE^{31pT380/pS384}$	0.9 ± 0.03	0.29 ± 0.05	2.4 ± 0.6
$Sic1^{1-100}$	4.2 ± 0.4	Not determined	19 ± 2

Binding affinities were measured at 25 ºC and at 37 ºC#. Dissociation-constant (K_d) values are average of three individual sets of ITC readings, ± indicates the standard deviation.

The binding studies reveal that the doubly phosphorylated $Sic1^{11pT5/pS9}$, $Sic1^{17pS76/pS80}$ and C-terminal $CycE^{31pT380/pS384}$ peptides bind to the double $scCdc4^{S464A/T465V}$ mutant with a K_d of 12 µM, 33 µM and 0.29 µM, respectively. The same peptides bind to the triple $scCdc4^{S464A/T465V/R443M}$ mutant with a K_d of 43 µM, 19 µM and 2.4 µM, respectively, and to wt-scCdc4 with a K_d of 4 µM, 2.6 µM and 0.09 µM. This reveals that the doubly phosphorylated $Sic1^{11pT5/pS9}$, $Sic1^{17pS76/pS80}$ and $CycE^{31pT380/pS384}$ peptides bind to the double $scCdc4^{S464A/T465V}$ mutant 3 to 10 times weaker, and to the triple $scCdc4^{S464A/T465V/R443M}$ mutant 7 to 25 times weaker than to wt-scCdc4.

The lower binding affinities of the doubly phosphorylated Sic1 and C-terminal Cyclin E peptides to the scCdc4 mutants support that scCdc4 contains a 2nd-phosphate-binding pocket. However, the double $scCdc4^{S464A/T465V}$ mutant is less effective in lowering the

binding affinities to the peptides than the triple scCdc4$^{S464A/T465V/R443M}$ mutant. This is probably due to the fact that the mutated residue Thr465Val of the scCdc4$^{S464A/T465V}$ double mutant is still able to make a hydrogen bond between its main chain carboxyl group and the main chain amide group of Arg485. In the triple scCdc4$^{S464A/T465V/R443M}$ mutant, the additional mutation of Arg443Met would eliminate a hydrogen bond between the residues Met443 and Asn463. This would lead to the destabilization of scCdc4s most invariant loop between the strands S2D and S3A that contains the mutated residues Ser464Ala, Thr465Val and nearby residue Arg467. Due to the possible displacement of that loop, (A) no hydrogen bond interaction between Arg485 and Val465 will be formed and (B) the residues Arg467 and Arg485 might not be able to form strong hydrogen bonds, neither to the substrate phosphate group at P0 an P+4, or to the substrate main chain carbonyl groups at P-1 to P+2. The 2nd and the 1st-phosphate-binding pocket destabilizing effects of the triple scCdc4$^{S464A/T465V/R443M}$ mutant might explain its lower binding affinity. Furthermore, the singly and doubly phosphorylated Sic1^{11pT5}, Sic1$^{11pT5/pS9}$, CycE^{31pT380} and CycE$^{31pT380/pS384}$ peptides show comparable binding affinities to the triple scCdc4$^{S464A/T465V/R443M}$ mutant, indicating that the triple scCdc4$^{S464A/T465V/R443M}$ mutant is unable to interact to the substrate second phosphate group at P+4.

The phosphorylated Sic1$^{1-100}$ binds to wt-scCdc4 with a K_d of 4.2 µM and to the triple scCdc4$^{S464A/T465V/R443M}$ mutant with a K_d of 19 µM. This reveals that the triple scCdc4$^{S464A/T465V/R443M}$ mutant binds to Sic1$^{1-100}$ five times less efficiently than wt-scCdc4. Comparing the K_d of the phosphorylated Sic1$^{1-100}$ to the other phosphorylated Sic1 peptides reveals that the phosphorylated Sic1$^{1-100}$ binds similar as the doubly phosphorylated Sic1$^{17pS76/pS80}$ peptide to the scCdc4 mutants. This indicates that Sic1 binds with two phosphate groups to scCdc4 two-phosphate-binding pockets.

3.10.2 Binding and degradation studies of Cyclin E by Fbw7 mutants

To further support the finding that Fbw7 contains two-phosphate-binding pockets, four Fbw7 mutants (mt-Fbw7) were made and tested for their ability to bind and to degrade phosphorylated Cyclin E (Figure 3.33). Mutating Fbw7 residue Arg479 was not pursued because it is needed in both the 1st and 2nd-phosphate-binding pockets of Fbw7.

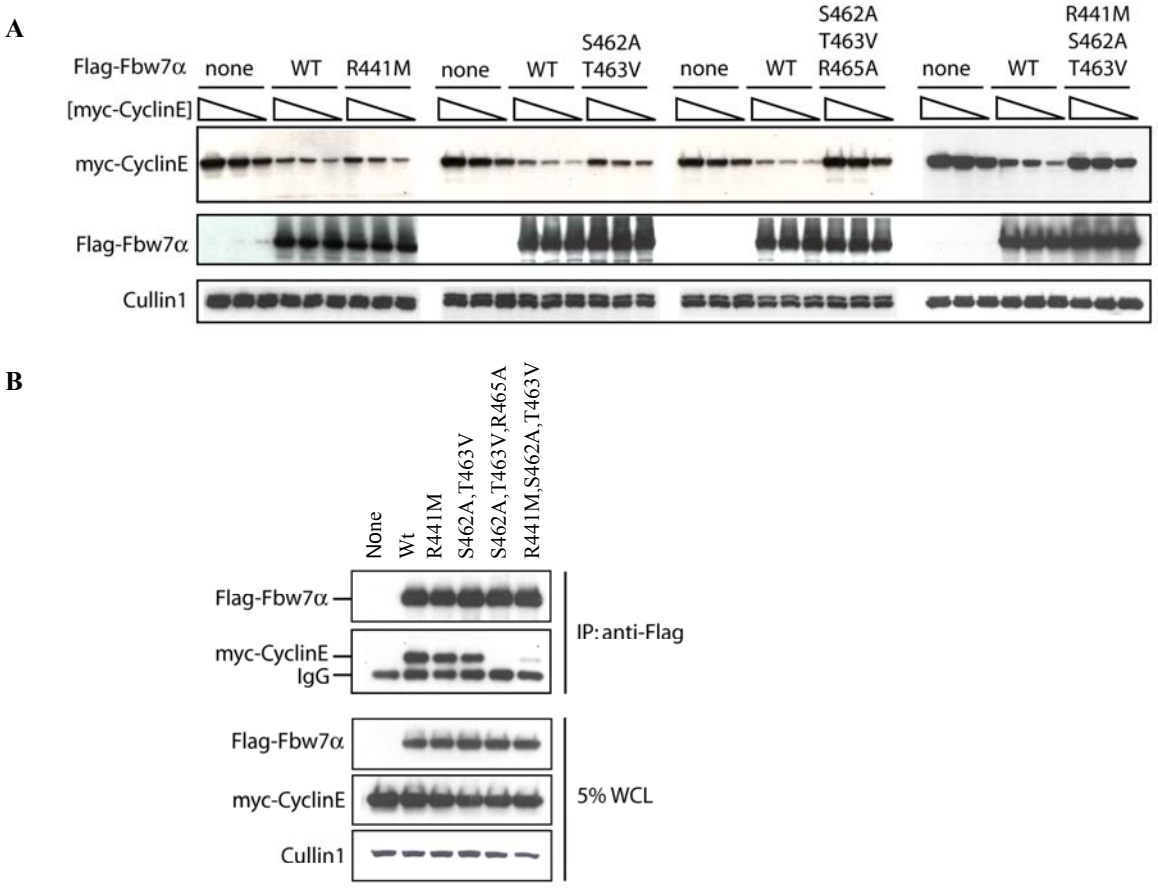

Figure 3.33 Binding and degradation studies of Cyclin E with the Fbw7 mutants, mutated in the 2nd-phosphate-binding pocket.

A) *In vivo* degradation of phosphorylated myc-Cyclin E by mutants of Flag-Fbw7α. Vectors expressing Myc-tagged Cyclin E and the indicated Flag-Fbw7α mutants were transfected together with Cdk2 into 293T cells. After 36 h, cells were lysed and immunoblots were probed with either anti-Flag or anti-Myc antibodies.
B) Binding assay of phosphorylated myc-Cyclin E by mutants of Flag-Fbw7α. Vectors expressing Myc-tagged Cyclin E and the indicated Flag-Fbw7α mutants were transfected together with pCMV-Cul1^{DN} into 293T cells. After 36 h, cells were lysed and immunoblots were probed with either anti-Flag or anti-Myc antibodies.
Data was provided by Wade Harper.

In the mt-Fbw7^{R441M}, residue Arg441 was mutated to methionine. Compared to wt-Fbw7, this mutant shows only a slight reduction in its ability to degrade phosphorylated

Cyclin E *in vivo*. The double mt-Fbw7$^{S462A/T463V}$, in which the residues Ser462 and Thr463 of the 2nd-phosphate-binding pocket were mutated to Ala462 and Val463, show a bigger reduction in Cyclin E turnover compared to the mt-Fbw7^{R441M}. In the triple mt-Fbw7$^{R441M/S462/T463}$, in which the residues Arg441, Ser462 and Thr463 were mutated, a further reduction in the degradation efficiency of phosphorylated Cyclin E is shown. Furthermore, the triple mt-Fbw7$^{S462A/T463V/R465A}$ in which in addition to Ser462 and Thr463 also Arg465 of Fbw7 1st-phosphate-binding pocket was mutated, reveals that the mt-Fbw7$^{S462A/T463V/R465A}$ is unable to turnover phosphorylated Cyclin E. This is consistent with the mutagenesis studies on scCdc4 WD40 domain surface, where mutation of Arg467 to alanine leads to mt-scCdc4 that is unable to interact with phosphorylated Sic1 (Orlicky et al., 2003; Nash et al., 2001).

In conclusion, the Cyclin E degradation assay with the Fbw7 mutants reveals that mutation of the 2nd-phosphate-binding pocket interferes with the degradation of Cyclin E. This supports that Fbw7 contains two-phosphate-binding pockets. However, Cyclin E degradation is not completely abolished and can be explained by residue Arg479, which was not mutated and is important for the interaction to both substrate phosphate groups. The data was provided by Wade Harper.

3.11 Fbw7-Cyclin E and scCdc4-Sic1 binding model

Structural data have shown that Fbw7 binds either to the doubly phosphorylated C-terminal CycE$^{31pT380/pS384}$ or to the singly phosphorylated N-terminal CycE^{14pT62} peptide. Analogous biochemical studies have shown that scCdc4 binds to the doubly phosphorylated Sic1$^{11pT5/pS9}$, the doubly phosphorylated Sic1$^{15pT45/pT48}$ and to the doubly phosphorylated Sic1$^{17pS76/pS80}$ peptides. In addition, ITC studies have shown that although the addition of a single phosphate group at P0 is enough for inducing binding to Fbw7 and scCdc4, only the doubly phosphorylated Cyclin E and Sic1 peptides bind with a high binding affinity to their respectively FBW proteins. Furthermore, the binding assays with Sic1$^{1-100}$ phosphorylated on seven Cdk consensus sites reveal that Sic1$^{1-100}$ binds comparably to the three doubly phosphorylated Sic1 peptides and indicates that Sic1$^{1-100}$ also uses two phosphate groups simultaneously to binds to scCdc4. However, this is in contrast to the studies by Nash et al., 2001, they reported that Sic1 needs to be phosphorylated on at least five to six of its nine Cdk

consensus sites in order to be recognized by scCdc4. Moreover, the two-phosphate-binding pockets described in this thesis for Fbw7 and scCdc4 is in contrast to the current believed one-phosphate-binding pocket model for Fbw7 and scCdc4 as established by Orlicky et al., 2003. (Figure 3.34).

The monomeric form of Fbw7 and scCdc4 binds to one doubly phosphorylated substrate region. As shown by pull down experiments of Fbw7 and ultra centrifugation of scCdc4, it has been revealed that both exist as a dimer. Therefore, it seems possible that their dimeric form binds to two doubly phosphorylated regions of their substrates (Figure 3.34). In addition, an *in vivo* Cyclin E degradation assay with wt-Fbw7 and mt-Fbw7 having a single-point mutation in the putative dimerization region reveals that wt-Fbw7 degrades Cyclin E much faster than mt-Fbw7. However, more biochemistry is needed to solidify it.

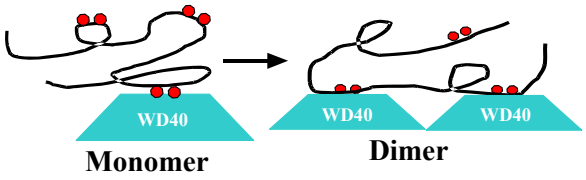

Figure 3.34. Fbw7 and scCdc4 two-phosphate-binding pocket model.

3.12 Biological implication

The identification of the two-phosphate-binding pocket mechanism of Fbw7 and scCdc4 leads to a better understanding of how the substrate turnover is regulated by the SCF^{Fbw7} and $scSCF^{Cdc4}$ ligases. Although, a single phosphate group at the Cyclin E or Sic1 P0 residue is enough for inducing binding to Fbw7 and scCdc4, the addition of a second phosphate group with a spacing of P+3 or P+4 is required to achieve a high substrate-binding affinity necessary for an efficient turnover of Cyclin E and Sic1.

Moreover, this work implicates for the first time that the SCF ligase acts as a dimer. This broadens the picture of the SCF-function and opens the door to discover whether SCF-ligases generally form a dimer and if all substrates contain two or more SCF-binding regions.

4.1 Cloning, expression, purification, characterization and crystallization of the APC subunits

The APC is a multisubunit complex consisting of at least 11 subunits. Apart from the structure determination of the human and budding yeast subunit APC10 (Wendt et al., 2001, Au et al., 2002), no other structural information exists about the other APC subunits (Introduction, 1.4). Therefore, the individual APC subunits of the APC were studied in order to gain an improved insight into their functions. The primary objective was the cloning, purification, characterization and crystallization of the budding yeast APC (scAPC) subunits. In addition, certain human APC (hAPC) and fission yeast APC (spAPC) subunits were also studied. Furthermore, the scAPC and hAPC subunits APC2 and APC11 were also studied as a complex.

4.1.1 Cloning and expression of the APC subunits

The scAPC subunits 1, 4, 6, 8, 9 were amplified from the *S. cerevisiae*-genomic DNA-library, Novagen. Several other scAPC and hAPC subunits were earlier cloned into vectors suitable for expression in insect cells and obtained by Langzhou Song (Appendix, Table 7.2). The spAPC4 gene was obtained by H.Yoon. The coding sequences of the scAPC, hAPC, and spAPC genes or of their fragments were either subcloned into a GST-tagged transfer vector pVLSO or the commercially available GST-tagged transfer vectors pMagE and pAcG2T, or the none-tagged transfer vector pVL1392 (Material, 2.1.2). This was followed by homologous recombination, recombinant Baculovirus amplification and protein expression in Hi5 insect cells (Method, 2.2.3.4).

In addition, several DNA-fragments of the scAPC4 gene were subcloned into the bacterial expression vector, pABLOmut. Furthermore, the boundaries of the hAPC2$^{497\text{-}822}$ and hAPC2$^{554\text{-}822}$ protein fragments were chosen according to a secondary structure prediction of APC2 orthologs and Cul1. The hAPC2$^{554\text{-}822}$ coding sequence of the hAPC2 gene and the full-length hAPC11 gene were subcloned into the bacterial expression vector pABLO as a dicistronic message with the GST-tagged hAPC2$^{554\text{-}822}$ in front of hAPC11 (Material, 2.1.2). The expression or co-expression of the recombinant proteins in *E. coli* was started after the induction with 1mM IPTG (Method, 2.2.3.4).

4.1.2 Purification, characterization and crystallization of the APC subunits

Purification of the individual GST-tagged APC subunits was performed as followed. The recombinant cell pellet was lysed and purified by glutathione affinity chromatography. Subunits that were soluble were cleaved off the GST-tag with thrombin and further purified by ion exchange and sizing column chromatography (Method, 2.2.5.11). The results of the studied APC subunits, fragments and subcomplexes are summarized in Table 4.1.

Table 4.1. Characterization of the APC subunits.

Protein	MW (kDa) without GST	pI	Solubly expressed	Protein stability	Protein aggregation	Crystallization trails and result
GST-scAPC1	196.1	5.8	yes	no	-	no
GST-scAPC2	100.0	6.5	yes	yes	yes	no
GST-scAPC4	75.3	5.6	yes	yes	no	yes, crystals
GST-scAPC4$^{\Delta 594\text{-}601}$	74.3	5.6	yes	yes	no	yes, no crystals
GST-scAPC4$^{\Delta 594\text{-}610}$	73.2	6.2	yes	yes	no	yes, no crystals
GST-scAPC4$^{594\text{-}652}$	6.7	4.4	yes	no	no	no
GST-scAPC4$^{599\text{-}652}$	6.1	4.3	yes	no	no	no
GST-scAPC4$^{602\text{-}652}$	5.7	4.2	yes	no	no	no
GST-scAPC4$^{611\text{-}652}$	4.7	6.4	yes	no	no	no
GST-scAPC4$^{1\text{-}583}$	67.5	6.0	no	-	-	no
GST-scAPC4$^{1\text{-}600}$	69.4	6.0	no	-	-	no
GST-scAPC$^{1\text{-}110}$	12.8	9.9	yes	no	-	no
GST-scAPC4$^{1\text{-}115}$	13.4	9.6	yes	no	-	no
GST-scAPC4$^{116\text{-}652}$	61.8	5.2	no	no	-	no
GST-scAPC4$^{210\text{-}652}$	51.1	5.5	no	no	-	no
GST-scAPC4$^{1\text{-}210}$	24.4	5.9	no	no	-	no
GST-scAPC5	79.3	5.0	yes	no	-	no
GST-scAPC6	95.0	6.6	no	-	-	no
GST-scAPC8	73.1	5.2	yes	yes	yes	no
GST-scAPC9	30.9	5.4	yes	yes	no	yes, no crystals
GST-scAPC10	32.8	7.5	yes	yes	no	no
GST-scAPC11	18.9	4.6	yes	yes	no	no
GST-scAPC11-APC2	118.8	5.9	yes	yes	yes	no
GST-hAPC2	93.8	5.1	yes	yes	yes	no
GST-hAPC2$^{497\text{-}822}$	37.7	4.8	yes	yes	no	yes, no crystals
GST -hAPC4	92.1	5.3	no	-	-	no
GST-hAPC7	63.2	5.6	yes	yes	no	yes, no crystals
GST-hAPC10	21.3	9.1	yes	yes	no	no
GST-hAPC11	9.8	7.7	yes	yes	no	no
GST-hAPC11-APC2	103.6	5.3	yes	yes	yes	no
GST-hAPC2$^{554\text{-}822}$-APC11	40.9	5.2	yes	yes	no	yes, no crystals
GST-spAPC4	82.6	5.8	yes	yes	no	yes, no crystals
GST-spAPC4$^{1\text{-}145}$	16.7	6.5	no	-	-	no

Protein	MW (kDa) without GST	pI	Solubly expressed	Protein stability	Protein aggregation	Crystallization trails and result
GST-spAPC4$^{146-719}$	66.0	5.5	no	-	-	no
GST-spAPC4$^{1-494}$	56.9	6.5	no	-	-	no
GST-spAPC4$^{495-719}$	25.8	4.7	yes	no	-	no

The purification and characterization of the scAPC, hAPC and spAPC subunits studied, reveals that the subunits scAPC1, scAPC2, hAPC2, scAPC4, spAPC4, scAPC5, hAPC7, scAPC8, scAPC9, scAPC10, hAPC10, scAPC11 and hAPC11 are solubly expressed as a GST-fusion, but that the subunits hAPC4 and scAPC6 are not. Further characterization of the subunits scAPC1 and scAPC5 revealed that they are very unstable. Moreover, analysis of the SD200 elution profiles of the individual subunits scAPC2, hAPC2 and scAPC8 as well as the complexes scAPC2-APC11 and hAPC2-APC11 showed that these subunits and complexes eluted in the void volume of the sizing column, indicating that these APC subunits and complexes are aggregated, possible due to misfolding.

The subunits scAPC4, scAPC9, scAPC10, scAPC11, spAPC4, hAPC7, hAPC10 and hAPC11, the hAPC2$^{497-822}$ protein fragment and the hAPC2$^{554-822}$-APC11 complex were solubly expressed, stable during the course of the purification and did not elute in the void volume of a sizing column.

Large-scale protein purification from Hi5 suspension culture cells were performed for the subunits scAPC4, spAPC4, hAPC7 and scAPC9 as well as the hAPC2$^{497-822}$ protein fragment and the hAPC2$^{554-822}$-APC11 complex (Method, 2.2.5.11). The purified APC subunits, APC fragments and complex were used in crystallization trails.

This approach led to the crystallization of the subunit scAPC4 (Figure 4.1), using 3 %

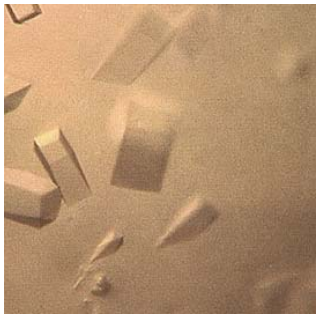

Figure 4.1. Crystals of scAPC4.

ScAPC4 (30 mg/ml) crystallized with 3 % PEG 6 K, 0.2 M NaCl, 100 mM BTP pH 8.5 at 20 ºC.

PEG 6 K, 0.2 M NaCl, 0.1 M BTP pH 8.5 at 20 ºC and 30 mg/ml scAPC4 protein. However, the crystals demonstrated only a limited diffraction up to 6 Å to 8 Å, which meant that no data sets were collected. Optimization attempts of this condition by streak seeding and additive screening and the use of different cryo-condition showed no improvement, and other promising crystallization conditions did not lead to different crystal forms.

4.2 Characterization and crystallization of the APC4 subunits

ScAPC4 orthologs spAPC4 and hAPC4 were additionally studied to find out whether they crystallize in a better-ordered three-dimensional crystalline arrangement than scAPC4. The alignment of the primary sequences of scAPC4, spAPC4 and hAPC4 (Figure 4.2) reveals that they are not very similar. In fact APC4 is the least conserved subunit of APC.

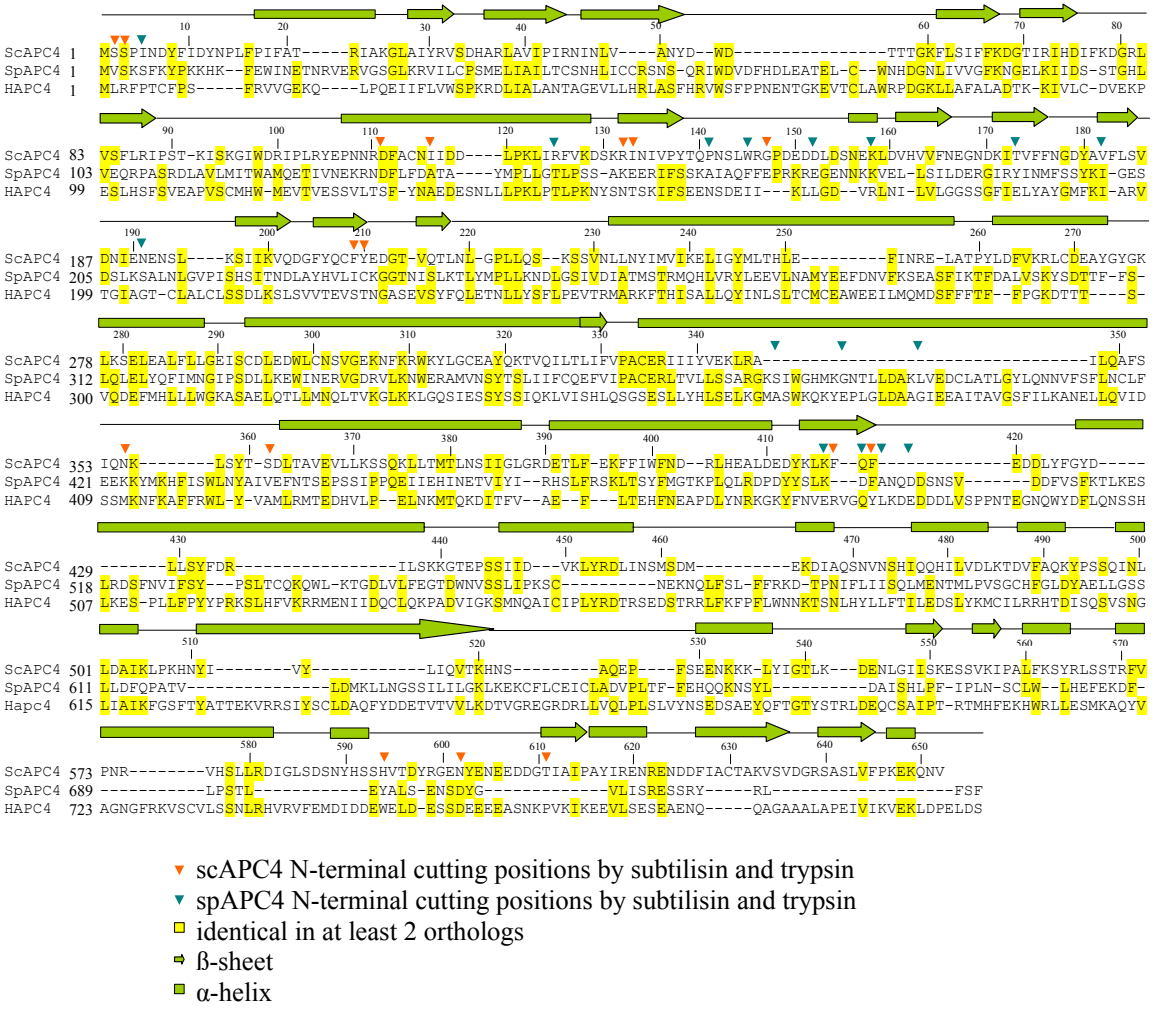

Figure 4.2. Predicted secondary structure alignment of APC4 orthologs.

Predicted secondary structure motifs are depict for scAPC4.

Furthermore, analysis of predicted structure propensity plots suggests that with the exception of one or two flexible regions (Figure 4.3), the APC4 proteins hAPC4, scAPC4

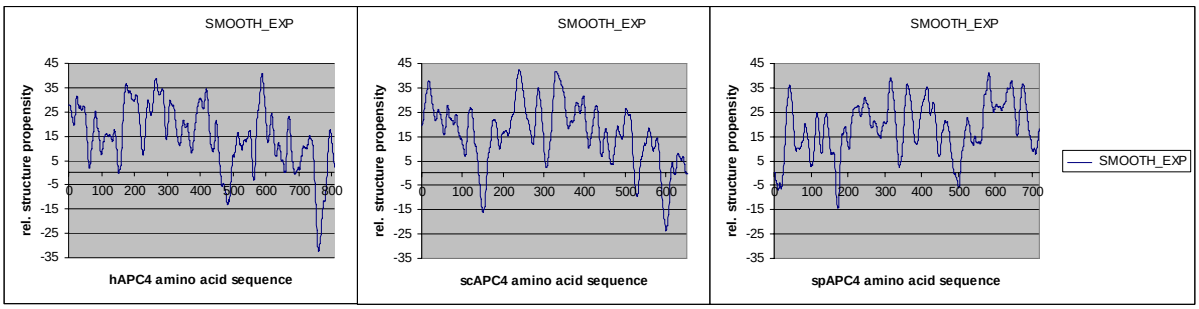

Figure 4.3. Structure propensity plots of APC4 orthologs.

and spAPC4 are structured. HAPC4 contains one predicted C-terminal flexible region between the residues 750 to 800, scAPC4 contains two predicted flexible regions one between residue 120 and 140 and the other one around residue 580 to 610 and spAPC4 contains one predicted flexible region around residue 160 to 180.

ScAPC4 and spAPC4, but not hAPC4, were solubly expressed (Table 4.1). The purifications of scAPC4 and spAPC4 were identical (Method, 2.2.5.11). Moreover, the SD200 elution profiles of scAPC4 and spAPC4 demonstrate that both elute at an apparent molecular weight between a monomer and a dimer (Figure 4.4). Crystallization trials with scAPC4 but not with spAPC4 yielded crystals.

In order to characterize the scAPC4 and spAPC4 protein domain structure in more detail, both proteins were subject to subtilisin and trypsin digestion, N-terminal sequencing and mass spectroscopy. This showed that scAPC4 and spAPC4 have two similar protein regions that are susceptible to subtilisin and trypsin digestion. One protein region is located between scAPC4 residues 111 to 210 and spAPC4 residues 140 to 210, and the second protein region is located between the scAPC4 residues 417 to 419 and spAPC4 residues 494 to 500. Additional scAPC4 proteolytic fragments start with the residues 356 to 361 and the residues 594 to 611. Additional spAPC4 proteolytic fragments start with the residues 382 to 397 (Figure 4.2). Subtilisin and trypsin digests of scAPC4 and spAPC4 were analyzed by mass spectroscopy. However, it proved to be very difficult to get exact masses for the digested scAPC4 and spAPC4 mixtures, because their purification by reverse phase and ion exchange chromatography led in the case of spAPC4 to the elution of the digested mixture in

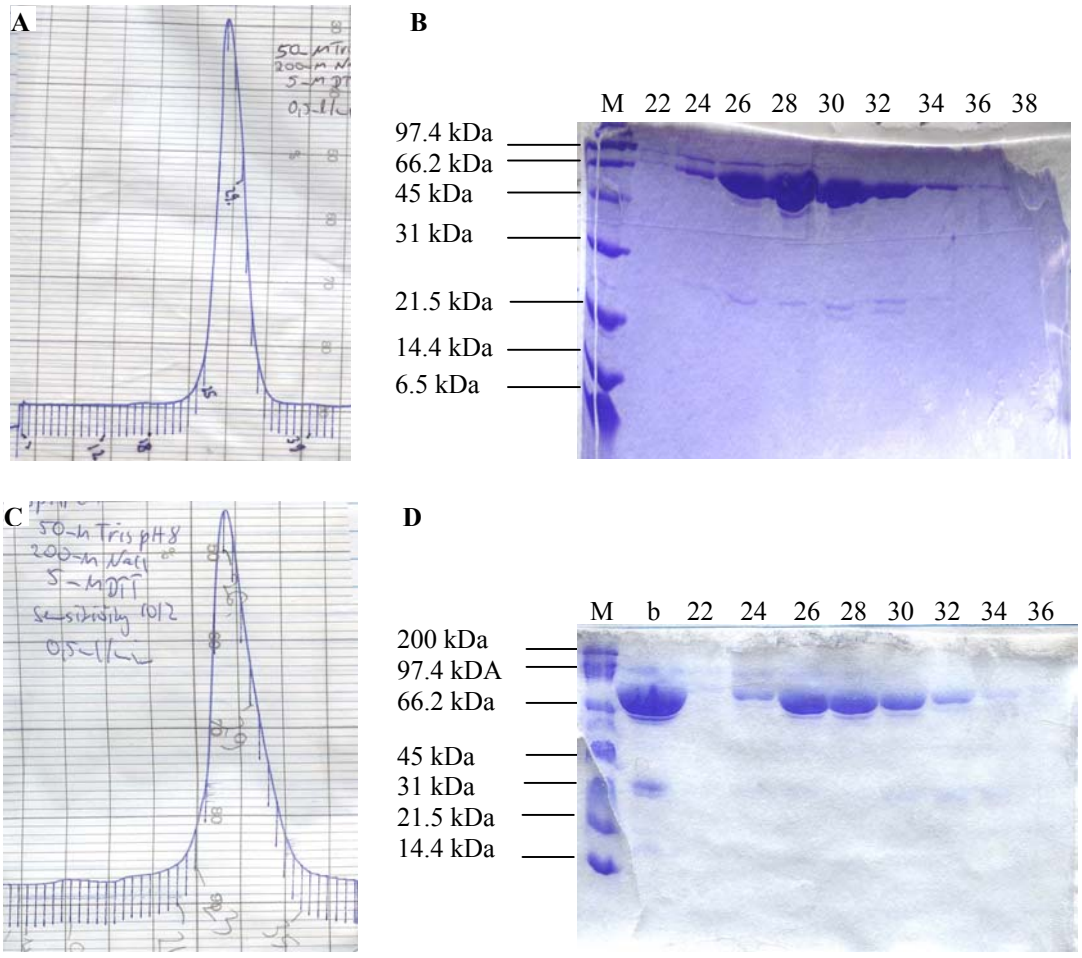

Figure 4.4. Purification of scAPC4 and spAPC4.

A) The chromatogram shows the SD200 elution profile of scAPC4, flow rate 0.5ml/min, elution buffer (200 mM NaCl, 5 mM DTT, 50 mM Tris pH 8.0).
B) SD200 protein fractions were separated by SDS-PAGE and stained with Coomassie blue.
C) The chromatogram shows the SD200 elution profile of spAPC4, flow rate 0.5ml/min, elution buffer (200 mM NaCl, 5 mM DTT, 50 mM Tris pH 8.0).
D) SD200 protein fractions were separated by SDS-PAGE and stained with Coomassie blue.

one peak, and in the case of scAPC4, only to the separation of two small protein peaks from the main peak. Due to the mixed nature of the protein main peaks, it was impossible to obtain exact masses. Exact masses were only obtained for two scAPC4 peaks, and together with the information of the N-terminal sequencing the following protein fragments: scAPC4$^{1\text{-}115}$, scAPC4$^{594\text{-}652}$ and scAPC4$^{602\text{-}652}$ were identified. Nonetheless, several additional APC constructs were designed (Table 4.1), based on the N-terminal sequencing data and the estimation of the sizes of the scAPC4 and spAPC4 protein fragments from the SDS-PAGE. Nearly all tested GST-fusion APC4-fragments were insoluble when expressed in insect cells (Table 4.1). The exceptions were the GST-tagged scAPC4$^{594\text{-}652}$, scAPC4$^{599\text{-}652}$ scAPC4$^{602\text{-}652}$

and scAPC4$^{611-652}$, which were solubly expressed and did not elute in the void volume of the sizing column. However, they tended to get degraded during the course of the purification. Moreover, the scAPC4 protein fragments scAPC4$^{1-583}$ and scAPC4$^{1-600}$, which did not contain the C-terminal scAPC4 residues were insolubly in extracts (Table 4.1). Therefore, two GST-tagged APC constructs scAPC4$^{\Delta 594-601}$ and scAPC4$^{\Delta 594-610}$ were designed, which contain only an internal deletion of scAPC4 C-terminal loop. Surprisingly, both truncated scAPC4$^{\Delta 594-601}$ and scAPC4$^{\Delta 594-610}$ proteins were solubly expressed and behaved similarly to full-length scAPC4 during protein purification. This indicates that the most C-terminal scAPC4 amino residues are needed to solubilize it. Unfortunately, the crystallization attempts of scAPC4$^{\Delta 594-601}$ did not lead to the formation of crystals. In addition, the expression tests with the GST-tagged scAPC4$^{1-110}$, scAPC4$^{1-115}$, spAPC4$^{1-145}$ and spAPC4$^{495-719}$ protein fragments led to the expression of very low amounts of soluble protein. Whereas the GST-tagged scAPC4 protein fragments scAPC4$^{116-652}$, scAPC4$^{210-652}$ and scAPC4$^{1-210}$ as well as the GST-tagged spAPC4 protein fragments spAPC4$^{1-494}$ and spAPC4$^{146-719}$ were insoluble, when expressed in insect cells. The co-expression of two GST-tagged scAPC4 protein fragments scAPC4$^{1-110}$ or scAPC4$^{1-115}$ and scAPC4$^{210-652}$ did also not lead to soluble proteins. The subtilisin digest of scAPC4 was performed several times, and the majority of the times we obtained fragments that started with residue 116. Only once did we obtain a band that started at residue 209 and also 210. Similar results, although not as strong as with subtilisin, were obtained with the trypsin digest of scAPC4, where several distinct scAPC4 protein fragments start with residue 111. As described above, mass spectroscopy resulted in the identification of the protein fragment scAPC4$^{1-115}$. Therefore it well might be that this predicted scAPC4 loop is only cut at the surface.

Unfortunately, extensive subcloning of the scAPC4 protein did not lead to a better crystallizable protein.

4.3 Outlook on the purification of the APC

The approach of studying the individual APC subunits has not proved to be particluarly successful. It is instead necessary to co-express the APC subunits. However, thus far, nobody has succeeded in reconstituting the whole APC. One major pitfall in reconstituting the APC is its complex nature (consists of at least 11 subunits). It hence seems

best to purify the APC from a native cell lysate. This approach has been pursued, however the yield has been inadequate. Moreover, in order to crystallize a protein complex, it is necessary to purify it to homogeneity. It is therefore necessary to purify the APC each time from the same cell cycle phase. However, the synchronization of cells at a scale necessary to obtain enough APC to do protein crystallography has been impractical. Another approach could be to purify subcomplexes of the APC. Indeed, it has been reported that a stable subcomplex, comprised of the subunits APC4, APC5, APC1, APC2 and APC11 can be purified from native immunopurified human holo-APC by utilizing a Source Q with a KCl-gradient (Vodemaier et al., 2003).

In conclusion, much work needs to be done in order to reconstitute and to characterize the APC complex before crystallization of the APC can be attempted. The structural elucidation of the APC is of enormous importance for a better understanding of cellular function. So far, APCs only function has been determined to be an E3 ligase. However, the APC consists of at least 11 subunits, whereas other E3 ligases consist of five or even less subunits. Moreover, the APC1 subunit contains a homology to the proteins Rpn1 and Rpn2, which forms the 19S regulatory cap of the 26S proteasome (reviewed by Hartmann-Petersen and Gordon, 2004). For other APC subunits like APC4, APC5 and APC9, however, no homology to any yet identified protein has been determined. It will therefore be interesting to see if the APC is involved in other cellular functions.

5. Summary/Zusammenfassung

The E3 ligases SCF and APC both selectively target and poly-ubiquitinate proteins that are destined for degradation. Their subsequent proteolysis by the 26S proteasome is irreversible, which guides the cell unidirectionally through the cell cycle. To understand how E3 ligases recognize their substrate(s), it is necessary to characterize the components involved.

In SCF, each of the exchangeable FBPs is responsible for the recognition of a subset of modified substrates. One very important FBP, the Tumor-suppressor Fbw7, is discussed intensively in this thesis. Fbw7 binds with its WD40 domain to phosphorylated substrates like the Cdk2 activator Cyclin E and the transcription factor c-Myc.

In Cyclin E, the phosphorylated C-terminal residues Thr380 (Strohmaier et al., 2001), Ser384 (Welcker et al., 2003) and Ser372 (Koepp et al., 2001) have been implicated in binding to the Fbw7 WD40 domain, yet it has been unclear how the binding occurs. In order to elucidate the binding mechanism of how C-terminal Cyclin E binds to Fbw7, it was necessary to express and purify the Fbw7 in compex with Skp1 due to Fbw7 insolubility on its own. Furthermore, several phosphorylated C-terminal Cyclin E peptides were designed. ITC binding studies with the Fbw7-Skp1 complex and the phosphorylated C-terminal Cyclin E peptides have determined that the C-terminal $CycE^{31pT380}$ peptide solely phosphorylated on Thr380 binds to Fbw7 only weakly with a K_d of 49 μM, whereas the C-terminal $CycE^{26pT380/pS384}$ peptide phosphorylated on Thr380 and Ser384 binds with a K_d of 0.07 μM, 700 times better. The triply phosphorylated C-terminal $CycE^{31pS372/pT380/pS384}$ peptide had a K_d comparable to the doubly phosphorylated C-terminal $CycE^{26pT380/pS384}$ peptide. The ITC binding studies suggest that Fbw7 contains two-phosphate-binding pockets. One pocket seems to be recognized by the phosphorylated C-terminal Cyclin E residue Thr380 at P0, and the other pocket seems to be recognized by the phosphorylated C-terminal Cyclin E residue Ser384 at P+4. Furthermore, the binding studies indicate that the phosphorylated Cyclin E residue Ser372 does not interact with Fbw7.

The model of two-phosphate-binding pockets in the Fbw7 WD40 domain are in contradiction to previously reported biochemical and structural data on scCdc4, which is closely related to Fbw7 (Orlicky et al., 2003; Nash et al., 2001). There, it was reported that scCdc4 WD40 domain contains only one-phosphate-binding pocket. Furthermore, mutational

studies of single residue exchanges on scCdc4 WD40 domain surface and their subsequent pull down experiments with Sic1 phosphorylated on nine Cdk consensus sites were performed. This revealed that the mt-scCdc4 that contain a single residue exchange flanking the one-phosphate-binding pocket abolished binding to phosphorylated Sic1, whereas the other mt-scCdc4 bound to phosphorylated Sic1 like wt-scCdc4. It is for this reason that, Orlicky et al., 2003, suggested scCdc4 and probably Fbw7 only contain one-phosphate-binding pocket to interact with its phosphorylated substrates. To determine if Fbw7 contains one-phosphate-binding pocket, or as suggested by ITC, two-phosphate-binding pockets, and whether the phosphorylated residue Ser372 contributes to Fbw7 binding, the Fbw7-Skp1 complex was co-crystallized with the triply phosphorylated C-terminal CycE$^{31pS372/pT380/pS384}$ peptide. Additionally, Fbw7 was co-crystallized with the singly N-terminal phosphorylated Cyclin E peptide (N-terminal CycE^{14pT62}), because the phosphorylated residue Thr62 has also been implicated to bind to Fbw7 (Ye et al., 2004; Welcker et al., 2004). It was interesting to find out whether or not the N-terminal CycE^{14pT62} peptide binds to the same Fbw7 WD40 domain position as the triply phosphorylated C-terminal CycE$^{31pS372/pT380/pS384}$ peptide. Furthermore, the doubly phosphorylated c-Myc$^{19pT58/pS62}$ peptide was chosen for co-crystallization with Fbw7, because biochemical data has not clarified whether c-Myc binds Fbw7 via its phosphorylation site on residue Thr58 (Yeh et al., 2004) or if binding to Fbw7 requires c-Myc phosphorylation on residues Thr58 and Ser62 (Yade et al., 2004).

The crystal structures of Fbw7-Skp1, Fbw7-Skp1-C-terminal CycE$^{31pS372/pT380/pS384}$, Fbw7-Skp1-N-terminal CycE^{14pT62} and Fbw7-Skp1-c-Myc$^{19pT58/pS62}$ were determined by molecular replacement in a resolution range of 2.6 Å to 2.9 Å. The Fbw7-Skp1-substrate structures were superimposed and analysis of the Fbw7 WD40-substrate structure interfaces revealed that all investigated substrate peptides bound to the same WD40 domain position. The substrates bind via their phosphorylated P0 residue to Tyr519 and to the arginine-triad composed of the residues Arg465, Arg479 and Arg505 of the Fbw7 WD40 domain. Together, these four residues form the 1st-phosphate-binding pocket of Fbw7. Phosphorylated Ser384 at P+4 in the C-terminal CycE$^{31pS372/pT380/pS384}$ peptide binds directly to the Fbw7 WD40 domain residues Arg479, Ser462 and Thr463, which together form the 2nd-phosphate-binding pocket of Fbw7. This proves that Fbw7 contains, as suggested by the ITC binding studies, two-phosphate-binding pockets. In addition, the crystal structure analysis of Fbw7-

Skp1-C-terminal CycE$^{31pS372/pT380/pS384}$ complex revealed no interpretable electron density for the phosphorylated residue Ser372 at P-8, indicating that phosphorylated Ser372 does not contribute to substrate-binding. Structural data of the Fbw7-Skp1-c-Myc$^{19pT58/pS62}$ complex showed that the doubly phosphorylated c-Myc$^{19pT58/pS62}$ peptide binds solely via the phosphorylated Thr58 to Fbw7 1st-phosphate-binding pocket. This implies, that the phosphorylated Ser62 is not involved in substrate-binding.

Next, the Fbw7 WD40 domain structure was superimposed to the earlier elucidated scCdc4 WD40 domain structure (Orlicky et al., 2003) and the WD40 domain surfaces were compared. This revealed that both WD40 domain structures are, with an rmsd of only 1.4 Å over 308 WD40 domain Cα atoms, very similar. Interestingly, blades 2 to 5 of the Fbw7 and the scCdc4 WD40 domain surfaces are invariant and include the identified two-phosphate-binding pockets. This suggests that scCdc4 also contains two-phosphate-binding pockets. To test this possibility, ITC binding studies were performed with the scCdc4-Skp1 complex and the identical set of Cyclin E peptides as used in binding studies with Fbw7. The binding studies elucidated that the singly phosphorylated C-terminal CycE^{31pT380} peptide bound to scCdc4 weakly, with a K_d of 3.8 μM, whereas the doubly phosphorylated CycE$^{26pT380/pS384}$ peptide had a K_d of 0.093 μM and binds 40 times better to scCdc4. Moreover, a comparison of the binding affinities of the doubly and triply phosphorylated peptides (CycE$^{26pT380/pS384}$; CycE$^{31pS372/pT380/pS384}$) revealed, as previously determined for Fbw7, that an additional Cyclin E phosphorylation on Ser372 does not increase its binding to scCdc4. These binding assays showed that scCdc4 contains two-phosphate-binding pockets like Fbw7.

Next, binding studies with scCdc4 and its physiological substrate Sic1 were performed. So far it has been believed that Sic1 needs to be phosphorylated on at least five to six SerPro/ThrPro Cdk consensus sites to be recognized by scCdc4 (Nash et al., 2001; Orlicky et al., 2003). However, sequence comparison of Cyclin E and Sic1 revealed three putative regions within Sic1 that could, like Cyclin E, be phosphorylated at P0 and P+4. Therefore, several Sic1 peptides were designed to identify whether or not Sic1 binds doubly phosphorylated to the two-phosphate-binding pockets of scCdc4. All Sic1 peptides contain a phosphorylated Cdk consensus site at P0. The doubly phosphorylated Sic1 peptides contain an additional Cdk consensus site at P+4 with the exception of the doubly phosphorylated peptides Sic1$^{11pT5/pS9}$ and Sic1$^{15pT45/pT48}$, where the residues Ser9 and Thr48 at P+4 and P+3

do not conform to the Cdk consensus. However, *in vitro* studies on Sic1 have shown that Ser9 and Thr48 are phosphorylated by Ime2 and Cln-Cdc28, respectively (Sedgwick et al., 2006; Verma et al., 1997). The scCdc4 binding studies showed that the singly phosphorylated peptides $Sic1^{11pT5}$ and $Sic1^{17pS76}$ bound to scCdc4 with a K_d of 17 µM and 49 µM, respectively. In contrast, the doubly phosphorylated $Sic1^{11pT5/pS9}$, $Sic1^{15pT45/pT48}$ and $Sic1^{17pS76/pS80}$ peptides bound to scCdc4 with a K_d of 4 µM, 4 µM and 2.6 µM, respectively. Therefore, a second Sic1 phosphorylation site within a distance of P+4 or P+3 increases the binding affinity to scCdc4 significantly. This result indicates that Sic1 binds simultaneously to two-phosphate-binding pockets in the scCdc4 WD40 domain. Moreover, ITC data showed that 1 to 2 phosphorylated Sic1 residues are sufficient for recognition by scCdc4.

To further prove that Fbw7 and scCdc4 contain a 2nd-phosphate-binding pocket, the residues that make up this pocket were mutated to alanine (in Fbw7: Ser462 to Ala462; in scCdc4: Ser464 to Ala464) and valine (in Fbw7: Thr463 to Val 463; in scCdc4 Thr465 to Val 465). Residue Arg479 (Arg485) of the 2nd-phosphate-binding pocket was not mutated, because it is also important for the 1st-phosphate-binding pocket of Fbw7 (scCdc4). In addition, residue Arg441 (Arg443), which surrounds the 2nd-phosphate-binding pocket, was mutated to Met441 (Met443) in Fbw7 (scCdc4).

The pull down assays of the Fbw7 mutants demonstrated that wt-Fbw7, the single mt-$Fbw7^{R441M}$ and the double mt-$Fbw7^{S462A/T463V}$ bound comparable to phosphorylated Cyclin E, whereas the triple mt-$Fbw7^{R441M/S462A/T463V}$ bound to phosphorylated Cyclin E only weakly. Moreover, Cyclin E degradation studies with the SCF^{Fbw7} mutants revealed that in comparison to wt-Fbw7 the single mt-$Fbw7^{R441M}$ only slightly reduced the turnover of Cyclin E. Compared to the single mt-$Fbw7^{R441M}$, the double mt-$Fbw7^{S462A/T463V}$ showed a more pronounced reduction in the turnover of Cyclin E. The triple mt-$Fbw7^{R441M/S462A/T463V}$ was largely incapable to degrade Cyclin E, which is in agreement with its weak binding to Cyclin E. The scCdc4 mutants were tested for their ability to bind to phosphorylated Sic1 peptides. The binding assays revealed that the double mt-$scCdc4^{S464A/T465V}$ and the triple mt-$scCdc4^{S464A/T465V/R443M}$ bound to doubly phosphorylated $Sic1^{11pT5/pS9}$ and $Sic1^{17pS76/pS80}$ peptides three to ten times weaker than wt-scCdc4. In conclusion, the mutational studies on the 2nd-phosphate-binding pocket of Fbw7 and scCdc4 further support that Fbw7 and scCdc4 contain two-phosphate-binding pockets.

Based on the presented biochemical and structural data on the Fbw7 and scCdc4 substrate-binding mechanism, a two-phosphate-binding pocket model was established. Furthermore, pull down assays with two differently tagged full-length Fbw7 and ultra-centrifugation of scCdc4$^{111-779}$ indicated that full-length Fbw7 and scCdc4$^{111-779}$ exist as dimers. Therefore, it seems likely that the two phosphorylated regions in Cyclin E and two phosphorylated regions in Sic1 each bind to one WD40 domain of wt-Fbw7 and wt-scCdc4.

Secondly, subunits of the APC ligase were studied. The APC consists of at least 11 different subunits. Substantial effort was focused on the cloning, characterization and crystallization of the individual subunits. Crystallization was attempted with the following subunits and complexes: hAPC2$^{497-822}$, hAPC2$^{554-822}$-hAPC11, scAPC4, spAPC4, scAPC4$^{\Delta 594-601}$, scAPC9 and hAPC7.

Only the crystallization of full-length scAPC4 was successful and crystals with a limited diffraction of 6 Å to 8 Å were obtained. For the purposes of comparison, the scAPC4 orthologs spAPC4 and hAPC4 were also studied. Unfortunately, full-length hAPC4 was insolubly expressed and crystallization trails with full-length spAPC4 did not lead to crystals. In addition, scAPC4 and spAPC4 were digested by subtilisin and trypsin and the resulting protein fragments were analyzed by N-terminal sequencing and mass spectroscopy to investigate their domain structure. Subcloning and purification of these scAPC4 and spAPC4 protein fragments was then attempted. Except for the four C-terminal scAPC4$^{594-652}$, scAPC4$^{599-652}$, scAPC4$^{602-652}$ and scAPC4$^{611-652}$ protein fragments and the deletions of a C-terminal loop in the scAPC4$^{\Delta 594-601}$ and scAPC4$^{\Delta 594-610}$ proteins, all other APC4 fragments were insoluble when expressed in insect cells.

Die E3 Ligasen SCF und APC erkennen und poly-ubiquitinieren spezifisch modifizierte Proteine welche für den Proteinabbau bestimmt sind. Ihr nachfolgender Abbau im 26S Proteasome ist irreversibel und führt zu einem gerichteten Zellzyklus. Für ein besseres Verständnis über die Substraterkennung der E3 Ligasen wurden einige beteiligte Proteine näher untersucht.

In SCF, erkennt jedes der austauschbaren FBP eine Gruppe spezifisch modifizierter Substrate. Ein sehr wichtiges FBP, der Tumor-suppressor Fbw7, wurde in der vorliegenden

Doktorarbeit umfassend diskutiert. Fbw7 bindet mit seiner WD40 Domäne zu phosphorylierten Substraten wie dem Cdk2 Aktivator Cyclin E und dem Transkriptionsfaktor c-Myc.

Für Cyclin E wurde beschrieben, das die phosphorylierten C-terminalen Aminosäuren Thr380 (Strohmaier et al., 2001), Ser384 (Welcker et al., 2003) und Ser372 (Koepp et al., 2001) an der Bindung zu der Fbw7 WD40 Domäne beteiligt sind. Es war jedoch bisher unklar wie die Substrate zu Fbw7 binden. Um herauszufinden wie das C-terminale Cyclin E Peptid zu Fbw7 bindet, war es notwendig Fbw7 zusammen mit Skp1 zu expremieren und zu reinigen, da Fbw7 alleine unlöslich expremiert wird. Desweiteren wurden vier unterschiedlich phosphorylierte C-terminale Cyclin E Peptide hergestellt und in ITC-Bindungsstudien mit dem Fbw7-Skp1 Komplex untersucht. Diese Studien zeigten, daß das nur an Thr380 phosphorylierte C-terminale $CycE^{31pT380}$ Peptid mit einem K_d von 49 μM nur schwach zu Fbw7 bindete, wohingegen das an Thr380 und Ser384 phosphorylierte C-terminale $CycE^{26pT380/pS384}$ Peptid mit einem K_d von 0.07 μM etwa 700 mal besser bindete. Das dreifach phosphorylierte C-terminale $CycE^{31pS372/pT380/pS384}$ Peptid bindete zu Fbw7 mit einem K_d vergleichbar zu dem zweifach phosphorylierten C-terminalen $CycE^{26pT380/pS384}$ Peptid. Die ITC-Bindungsstudien lassen schlußfolgern, daß Fbw7 zwei-Phosphat-Bindungstaschen besitzt. Die eine Tasche scheint zu der phosphorylierten C-terminalen Cyclin E Aminosäure Thr380 (P0) und die zweite Tasche zu der phosphorylierten C-terminalen Cyclin E Aminosäure Ser384 (P+4) zu binden. Außerdem deuten die ITC-Bindungsstudien an, daß die phosphorylierte C-terminale Cyclin E Aminosäure Ser372 nicht an der Bindung zu Fbw7 beteiligt ist.

Das zwei-Phosphat-Bindungstaschen Modell für Fbw7 WD40 Domäne steht im Widerspruch zu früheren biochemischen und Strukturdaten durchgeführt am zu Fbw7 eng verwandten scCdc4 (Orlicky et al., 2003; Nash et al., 2001). Es wurde berichtet, daß scCdc4 WD40 Domäne nur eine-Phosphat-Bindungstasche besitzt. Desweiteren wurden Mutationstudien durchgeführt, wonach einzelne Aminosäuren an der Oberfläche von scCdc4 WD40 Domäne mutiert wurden und auf Interaktion mit dem an neun Aminosäuren phosphorylierten Sic1 getestet wurden. Dies ergab, daß die mt-scCdc4, welche die eine-Phosphat-Bindungstasche umgeben nicht zu phosphorylierten Sic1 binden konnten. Wohingegen die anderen getesteten mt-scCdc4 wie wt-scCdc4 zu phosphorylierten Sic1

bindeten. Schlußfolgernd schlug Orlicky vor, daß scCdc4 und wahrscheinlich auch Fbw7 nur eine-Phosphat-Bindingstasche enthalten. Für die Ermittlung, ob Fbw7 eine-, oder wie durch ITC-Bindungsstudien vorgeschlagen, zwei-Phosphat-Bindingstaschen enthält, und ob die phosphorylierte Aminosäure Ser372 an der Bindung zu Fbw7 beteiligt ist, wurde das dreifach phosphorylierte C-terminale CycE$^{31pS372/pT380/pS384}$ Peptid zusammen mit dem Fbw7-Skp1 Komplex kristallisiert. Zusätzlich, wurde der Fbw7-Skp1 Komplex zusammen mit dem N-terminalen CycE^{14pT62} Peptid kristallisiert, weil auch die phosphorylierte Aminosäure Thr62 an der Bindung zu Fbw7 verwickelt wurde (Ye, et al., 2004; Welcker et al., 2004). Desweiteren war es interessant herauszufinden, ob das N-terminale CycE^{14pT62} Peptid an die selbe Stelle der Fbw7 WD40 Domäne bindet wie das dreifach phosphorylierte C-terminale CycE$^{31pS372/pT380/pS384}$ Peptid. Weiterhin, wurde das zweifach phosphorylierte c-Myc$^{19pT58/pS62}$ Peptid zusammen mit dem Fbw7-Skp1 Komplex kristallisiert, denn biochemische Untersuchungen haben nicht eindeutig geklärt, ob c-Myc Bindung zu Fbw7 nur die Phosphorylierung an Thr58 erfordert (Yeh et al., 2004) oder ob eine zusätzliche Phosphorylierung an Ser62 notwendig ist (Yade et al., 2004).

Die folgenden Proteinkristallstrukturen Fbw7-Skp1, Fbw7-Skp1-C-terminal CycE$^{31pS372/pT380/pS384}$, Fbw7-Skp1-N-terminal CycE^{14pT62} und Fbw7-Skp1-c-Myc$^{19pT58/pS62}$ wurden bestimmt mit der Methode des molekularen Ersatzes in einer Auflösung von 2.6 Å bis 2.9 Å. Durch die Überlagerung der Fbw7-Skp1-Substrat Strukturen wurde ersichtlich, daß alle untersuchten Substrat-Peptide an die gleiche Stelle der Fbw7 WD40 Domäne binden. Alle Substrate binden mit der phosphorylierten Aminosäure (P0) zu Fbw7 Tyr519 und der Arginine Triade bestehend aus Arg465, Arg479 und Arg505. Diese vier Aminosäuren bilden die erste-Phosphat-Bindungstasche von Fbw7. Das C-terminal CycE$^{31pS372/pT380/pS384}$ Peptid bindet außerdem mit der phosphorylierten Aminosäure Ser384 (P+4) zu den Fbw7 Aminosäuren von Arg479, Ser462 und Thr463, welche zusammen die zweite-Phosphat-Bindungstasche von Fbw7 formen. Damit wurde bewiesen, daß Fbw7, wie zuvor mit den ITC-Bindungsstudien vorgeschlagen, zwei-Phosphat-Bindungstaschen besitzt. Desweiteren ergab die Kristallstruktur vom Fbw7-Skp1-C-terminalen CycE$^{31pS372/pT380/pS384}$ Komplex keine interpretierbare Elektronendichte für die phosphorylierte Aminosäure Ser372 (P-8). Daher ist anzunehmen, daß Ser372 nicht an der Bindung zu Fbw7 beteiligt ist. Weiterhin, ergab die Auswertung der Kristallstruktur vom Fbw7-Skp1-c-Myc$^{19pT58/pS62}$ Komplex, daß

das zweifach phosphorylierte c-Myc$^{19pT58/pS62}$ Peptid nur mit der phosphorylierten Aminosäure Thr58 zur ersten-Phosphat-Bindungstasche von Fbw7 bindet. Dies deutet an, daß die phosphorylierte Aminosäure Ser62 nicht an der Binding zu Fbw7 verwickelt ist.

Nachfolgend wurde die WD40 Domäne von Fbw7 mit der von scCdc4 (Orlicky et al., 2003) verglichen. Die Überlagerung der Proteinstrukturen zeigte, daß sich ihre WD40 Domänen mit einer Standardabweichung von nur 1.4 Å über 308 WD40 Domäne Cα-Atomen sehr ähneln. Interessant ist, daß die Aminosäurekompositionen von Fbw7 und scCdc4 sowie deren Faltung an der Oberfläche der WD40 Domäne im Motive zwei bis fünf identisch sind und in Fbw7 die zwei-Phosphat-Bindungstaschen enthalten. Das legt nahe, daß scCdc4 auch zwei-Phosphat-Bindungstaschen besitzt. Diese Vermutung wurde durch ITC-Bindungsstudien am scCdc4-Skp1 Komplex mit einem Set an phosphorylierten Cyclin E Peptiden wie zuvor auch in ITC-Bindungsstudien mit dem Fbw7-Skp1 Komplex verwendet getestet. Die Bindungsstudien ergaben, daß das einfach phosphorylierte CycE^{31pT380} Peptid mit einem K_d von 3.8 µM nur schwach zu scCdc4 bindete, wohingegen das zweifach phosphorylierte CycE$^{26pT380/pS384}$ Peptid mit einem K_d von 0.093 µM 40 mal besser bindete. Desweiteren zeigte ein Vergleich der scCdc4-Bindungskonstanten der zweifach und dreifach phosphorylierten Cyclin E Peptide (CycE$^{26pT380/pS384}$, CycE$^{31pS372/pT380/pS384}$), daß eine zusätzliche Phosphorylierung an Ser372 die Bindung zu scCdc4 nicht erhöht und ist identisch mit den zuvor ermittelten Daten für Fbw7. Damit wurde gezeigt, daß scCdc4 wie Fbw7 zwei-Phosphat-Bindungstaschen besitzt.

Als nächstes wurden die Bindungskonstanten von scCdc4 mit seinem physiologischen Substrate Sic1 ermittelt. Bis jetzt nahm man an, daß Sic1 an mindestens fünf bis sechs seiner neun SerPro/ThrPro Cdk-Erkennungsseiten phosphoryliert sein muss, um zu scCdc4 binden zu können (Nash et al., 2001; Orlicky et al., 2003). Jedoch, mein Vergleich der Aminosäuresequenzen von Sic1 und Cyclin E ergab, daß Sic1 drei potenzielle Regionen enthält, welche identisch zu Cyclin E an den P0 und P+4 Stellen phosphoryliert werden konnten. Es wurden verschieden phosphorylierte Sic1 Peptide hergestellt um zu überprüfen ob auch Sic1, wie Cyclin E, zweifach phosphoryliert zu den zwei-Phosphat-Bindungstaschen in scCdc4 bindet. Alle Sic1 Peptide enthielten an ihrer P0 Stelle eine, durch Cdk angehängte, Phosphatgruppe. Desweiteren enthielten die zweifach phosphorylierten Sic1$^{13pT2/pT5}$ und Sic1$^{17pS76/pS80}$ Peptide an ihrer P+4 Stelle eine weitere, durch Cdk

angehängte, Phosphatgruppe. Im Gegensatz dazu enthalten die zweifach phosphorylierten Sic1$^{11pT5/pS9}$ und Sic1$^{15pT45/pT48}$ Peptide an Ser9 und Thr48 (P+3- und P+4) keine typische Cdk-Erkennungsseite. Jedoch *in vitro* Studien an Sic1 haben gezeigt, daß Ser9 durch Ime2 (Sedgwick et al., 2006) und Thr48 durch Cln-Cdc28 (Verma et al., 1997) phosphoryliert werden. Die Bindungsstudien zeigten, daß die einfach phosphorylierten Sic1^{11pT5} und Sic1^{17pS76} Peptide mit einem K_d von 17 µM und 49 µM nur schwach zu scCdc4 bindeten. Im Gegensatz dazu bindeten die zweifach phosphorylierten Sic1$^{11pT5/pS9}$, Sic1$^{15pT45/pT48}$ und Sic1$^{17pS76/pS80}$ Peptide mit einem K_d von 4 µM, 4 µM und 2,6 µM viel stärker zu scCdc4. Dies impliziert, daß Sic1 gleichzeitig zu zwei-Phosphat-Bindungstaschen in scCdc4 bindet. Die ITC-Bindungsstudien zeigten außerdem, daß ein ein- bis zweifach phosphoryliertes Sic1 ausreicht, um zu scCdc4 zu binden.

Um weiter zu beweisen, daß Fbw7 und scCdc4 eine zweite-Phosphat-Bindungstasche enthalten, wurden die Aminosäuren der zweiten-Phosphat-Bindungstasche zu Alanine (in Fbw7: Ser462 zu Ala462; in scCdc4: Ser464 zu Ala 464) und Valine (in Fbw7: Thr463 zu Val463; in scCdc4 Thr465 zu Val465) mutiert. Nicht mutiert wurde Arg479 (Arg485) von der zweiten-Phosphat-Bindungstasche, weil diese auch für Fbw7 (scCdc4) erste-Phosphat-Bindungstasche wichtig ist. Zusätzlich wurde Arg441 (Arg443), welche die zweite-Phosphat-Bindungstasche umgibt, mutiert zu Met441 (Met443) in Fbw7 (scCdc4).

Die Substratbindungs- und Substratdegredationsfähigkeit der mt-Fbw7 und der mt-scCdc4 wurden nun mit denen von wt-Fbw7 und wt-scCdc4 verglichen. Die Bindungsstudien demonstrieren, daß wt-Fbw7, die einfache mt-Fbw7^{R441M} und die zweifache mt-Fbw7$^{S462A/T463V}$ vergleichbar gut zu phosphorylierten Cyclin E binden konnten. Wohingegen die dreifache mt-Fbw7$^{R441M/S462A/T463V}$ nur sehr schwach zu phosphorylierten Cyclin E bindete. Desweiteren zeigten die Studien über den *in vivo* Cyclin E Abbau, daß die einfache mt-Fbw7^{R441M} im Vergleich zur wt-Fbw7 den Cyclin E Abbau nur minimal verzögerte. Die zweifache mt-Fbw7$^{S462A/T463V}$ zeigte im Vergleich zur wt-Fbw7 eine stärkere Verzögerung im Cyclin E Abbau. Nahezu unfähig zum Cyclin E Abbau erwies sich die dreifache mt-Fbw7$^{R441M/S462A/T463V}$ was in Übereinstimmung mit seiner schwachen Bindung zu phosphorylierten Cyclin E ist. Die scCdc4 Mutanten wurden auf ihre Bindungsfähigkeit zu unterschiedlich phosphorylierten Sic1 Peptiden getestet. Die Bindungsuntersuchungen ergaben, dass die zweifache mt-scCdc4$^{S464A/T465V}$ und die dreifache mt-scCdc4 $^{R443M/S464/T465V}$

zu dem zweifach phosphorylierten Sic1$^{11pT5/pS9}$ und dem dreifach phosphorylierten Sic1$^{17pS76/pS80}$ Peptiden drei bis zehn mal schlechter als zu der wt-scCdc4 bindeten. Abschließend kann gesagt werden das auch die Mutationsstudien an Fbw7 und scCdc4 zweiten-Phosphat-Bindungstasche unterstützen, daß Fbw7 und scCdc4 zwei-Phosphat-Bindungstaschen besitzen.

Basierend auf den hier vorgestellten biochemischen Erkenntnissen und Strukturdaten über Fbw7 und scCdc4 Substrat-Bindungsmechanismus wurde für sie ein zwei-Phosphat-Bindungstaschenmodel entwickelt. Weiterhin haben Bindungsstudien mit unterschiedlich markierten Fbw7 Proteinen und die Ultrazentrifugation mit dem scCdc4$^{111-779}$ Proteinfragment gezeigt, daß Fbw7 und scCdc4$^{111-779}$ als Dimer existieren. Daher erscheint es möglich, daß die zwei phosphorylierten Regionen in Cyclin E und zwei phosphorylierte Regionen in Sic1 jeweils zu einer WD40 Domäne von dem Fbw7 und scCdc4 Dimer binden.

Im zweiten Teil dieser Arbeit wurden die Untereinheiten der APC Ligase näher untersucht. APC besteht aus mindestens 11 Untereinheiten. Viel Zeit wurde für die Klonierung, die Charakterisierung und die Kristallisation der einzelnen APC Untereinheiten benötigt. Kristallisationsversuche wurden mit den APC Untereinheiten hAPC$^{497-822}$, scAPC4, spAPC4, scAPC4$^{\Delta 594-601}$, scAPC9 und hAPC7 sowie dem hAPC$^{554-822}$-hAPC11 Komplex durchgeführt.

Jedoch, nur die Kristallisation der scAPC4 Untereinheit war erfolgreich. Die scAPC4 Kristalle zeigten eine Streufähigkeit von 6 Å bis 8 Å, welche nicht ausreicht um ein genaues Abbild von dem scAPC4 Protein zu modulieren. Zum Vergleich wurden auch die scAPC4 orthologen Proteine spAPC4 und hAPC4 näher charakterisiert. Es zeigte sich, das die Überexpression der hAPC4 Untereinheit zu einem unlöslich expremierten Protein führte. Im Gegensatz dazu führte die Überexpression der spAPC4 Untereinheit zu einem löslich expremierten Protein. Es gelang jedoch nicht das spAPC4 Protein in die kristalline Form zu überführen. Zusätzlich wurde die Domänenstruktur von den scAPC4 und spAPC4 Proteinen mittels einer enzymatischen Spaltung durch die Enzyme Subtilisin und Trypsin näher untersucht. Die resultierenden scAPC4 und spAPC4 Proteinfragmente wurden mit Hilfe des N-terminalen Proteinabbaus und folgender massenspektrometrischer Untersuchungen identifiziert. Die anschließende Klonierung und Reinigung der scAPC4 und spAPC4

Proteinfragmente ergab, daß nur die vier C-terminalen scAPC4$^{594-652}$, scAPC4$^{599-652}$, scAPC4$^{602-652}$ und scAPC4$^{611-652}$ Proteinfragmente sowie die scAPC4$^{\Delta 594-601}$ und scAPC4$^{\Delta 594-610}$ Proteinfragmente, in welchen eine C-terminale Aminosäureschleife entfernt wurde, löslich expremiert werden konnten.

6. Bibliography

Akli, S., Zheng, P.J., Multani, A.S., et al. (2004). Tumor-specific low molecular weight forms of cyclin E induce genomic instability and resistance to p21, p27, and antiestrogens in breast cancer. Cancer Res. *64*, 3198-3208.

Amerik, A.Y., and Hochstrasser, M. (2004). Mechanism and function of deubiquitinating enzymes. Biochimica et Biophysica Acta *1695*, 189-207.

Amon, A., Irniger, S., and Nasmyth, K. (1994). Closing the cell cycle circle in yeast: G2 cyclin proteolysis initiated at mitosis persists until the activation of G1 cyclins in the next cycle. Cell *77*, 1037-1050.

Ang, X.L., and Harper, W.J. (2004). Interwoven Ubiquitination Oscillators and Control of Cell Cycle Transitions. Sci. STKE *31*, 1-5.

Au, S.W., Leng, X., Harper, J.W., and Barford, D. (2002). Implications for the ubiquitination reaction of the anaphase-promoting complex from the crystal structure of the Doc1/APC10 subunit. J. Mol. Biol. *316*, 955-968.

Bahram, F., von der Lehr, N., Cetinkaya, C., and Larsson, L.G. (2000). C-Myc hot spot mutations in lymphomas result in inefficient ubiquitination and decreased proteasome-mediated turnover. Blood *95*, 2104-2110.

Bai, C., Sen, P., Hofmann, K., Ma, L., Goebl, M., Harper, J.W., and Elledge, S.J. (1996). SKP1 connects cell cycle regulators to the ubiquitin proteolysis machinery through a novel motif, the F-box. Cell *86*, 263-274.

Bales, E., Mills, L., Milam, N., McGahren-Murray, M., Bandyopadhyay, D. et al. (2005). The low Molecular weight Cyclin E Isoforms Augment Angiogenesis and metastasis of Human Melanoma Cells *in vivo*. Cancer Res. *65*, 692-697.

Barberis, M., De Gioia, L., Ruzzene, M., Sarno, S., Coccetti, P. et al. (2005). The yeast cyclin-dependent kinase inhibitor Sic1 and the mammalian $p27^{Kip1}$ are functional homologues with structurally conserved inhibitory domain. J. Biochem. *387*, 639-647.

Bashir, T., Dorrello, N.V., Amador, V., Guardavaccaro, D., and Pagano, M. (2004). Control of the SCF-Skp2-Cks1 ubiquitin ligase by the APC/C-Cdh1 ubiquitin ligase. Nature *428*, 190-193.

Bateman, A., Coin, L., Durbin, R., Finn, R.D., Hollich, V., Griffiths-Jones, S., Khanna, A., Marshall, M., Moxon, S., Sonnhammer, E.L., et al. (2004). The Pfam protein families database. Nucleic Acid Res. *32*, D138-D141.

Baumeister, W., Walz, J., Zuhl, F., and Seemuller, E. (1998). The proteasome: paradigm of a self-compartmentalizing protease. Cell *92*, 367-380.

Berger, C., Pallavi, S.K., Prasad, M., Shashidhara, L.S., and Technau, G.M. (2005). A critical role for Cyclin E in cell fate determination in the central nervous system of Drosophila melanogaster. Nat. Cell Biol. *7*, 56-62.

Bharadwaj, R., and Yu, H. (2004). The spindle checkpoint, aneuploidy, and cancer. Oncogene *23*, 2016-27.

Bishop, J.M. (1989). The molecular genetics of cancer. Science *235*, 305-311.

Blackwood, E.M., and Eisenman, R.N. (1991). Max: a helix-loop-helix zipper protein that forms a sequence-specific DNA-binding complex with Myc. Science *251*, 1211-1217.

Blondel, M., Galan, J.M., Chi, Y., Lafourcade, C., Langaretti, C., Deshaies, R.J., and Peter, M. (2000). Nuclear-specific degradation of Far1 is controlled by the localization of the F-box protein Cdc4. EMBO J. *19*, 6085-6097.

Borden, K.L.B. (2000). RING domains: master builders of molecular scaffolds? Mol. Biol. *295*, 1103-1112.

Boxer, L., and Dang, C. (2001). Translocations involving c-myc and c-myc function. Oncogene *20*, 5595-5610.

Brunger, A.T., Adams, P.D., Clore, G.M., DeLano, W.L., Gros, P., Grosse-Kunstleve, R.W., Jiang, J.S., et al.(1998) Crystallography & NMR system: A new software suite for macromolecular structure determination. Acta Crystallogr. D. Biol. Crystallogr. *54*, 905-921.

Cardozo, T., and Pagano, M. (2004). The SCF ubiquitin ligase: insights into a molecular machine. Mol. Cell Biol. *5*, 739-751.

Carroll, C.W., and Morgan, D.O. (2002). The Doc1 subunit is a processivity factor for the anaphase-promoting complex. Nat. Cell Biol. *4*, 880-887.

Carroll, C.W., Enquist-Newman, M., and Morgan, D.O. (2005). The APC Subunit Doc1 Promotes Recognition of the Substrate Destruction Box. Curr. Biol. *15*, 11-18.

Castro, A., Bernis, C., Vigneron, S., Labbe, J.C., and Lorca, T. (2005). The anaphase-promoting complex: a key factor in the regulation of cell cycle. Oncogene *24*, 314-325.

Cenciarelli, C., Chiaur, D.S., Guardavaccaro, D., Parks, W., Vidal, M., and Pagano, M. (1999). Identification of a family of human F-box proteins. Curr. Biol. *9*, 1177-1179.

Cheng, M., Olivier, P., Diehl, J.A., Fero, M., Roussel, M.F., Robberts, J.M., and Sherr, C.J. (1999). The $p21^{Cip1}$ and $p27^{Kip1}$ CDK "inhibitors" are essential activators of cyclin D-dependent kinases in murine fibroblasts. EMBO J. *18*, 1571-1583.

Chou, S., Huang, L., and Liu, H. (2004). Fus3-Regulated Tec1 Degradation through SCF^{Cdc4} Determines MAPK Signaling Specificity during Mating in Yeast. Cell *119*, 981-990.

Ciechanover, A., DiGiuseppe, J.A., Schwartz, A.L., and Brodeur, G.M. (1991). Degradation of MYCN oncoprotein by the ubiquitin system. Prog. Clin. Biol. Res. *366*, 37-43.

Cleveland, D.W., Mao Y., and Sullivan K.F. (2003). Centromeres and kinetochores: From epigenetics to mitotic checkpoint signaling. Cell *112*, 407-421.

Clute, P., and Pines, J. (1999). Temporal and spatial control of cyclin B1 destruction in metaphase. Nat. Cell Biol. *1*, 82-87.

Coller, H., Grandori, C., Tamayo, P., et al. (2000). Expression analysis with oligonucleotide microarrays reveals that Myc regulates gene involved in growth, cell cycle, signaling, and adhesion. Proc. Natl. Acad. Sci. USA *97*, 3260-3265.

Cope, G.A., and Deshaies, R.J. (2003). COP9 signalosome: A multifunctional regulator of SCF and other cullin-based ubiquitin ligases. Cell *114*, 663-671.

Coux, O., Tanaka, K., and Goldberg, A.L. (1996). Structure and functions of the 20S and 26S proteasomes. Annu. Rev. Biochem. *65*, 801-847.

Creighton, T.E. (1993). Proteins: structures and molecular properties. (New York: W.H. Freeman and Company), 176-179.

Cross, F.R., and Jacobson, M.D. (2000). Conservation and function of a potential substrate-binding domain in the yeast Clb5 B-type cyclin. Mol. Cell Biol. *20*, 4782-4790.

Cross F. R. (2003). Two Redundant Oscillatory Mechanisms in the Yeast Cell Cycle. Dev. Cell *4*, 741-752.

Das, A.K., Cohen, P.W., and Barford, D. (1998). The structure of the tetratricopeptide repeats of protein phosphatase 5: implications for TPR-mediated protein-protein interactions. EMBO J. *17*, 1192-1199.

Deshaies, R.J. (1999). SCF and Cullin/Ring H2-based ubiquitin ligases. Annu. Rev. Biol. *15*, 435-467.

Dias, D.C., Dolios, G., Wang, R., and Pan, Z.Q. (2002). Cul7: a DOC domain-containing cullin selectively binds Skp1.Fbx29 to form an SCF-like complex. Proc. Natl. Acad. Sci. USA *99*, 16601-16606.

Diehl, J.A., and Sherr, C.J. (1997). A dominant-negative cyclin D1 mutant prevents nuclear import of cyclin-dependent kinase 4 (CDK4) and its phosphorylation by CDK-activating kinase. Mol. Cell Biol. *17*, 7362-7374.

Drury, L.S., Perkins, G., and Diffley, J.F.X. (1997). The Cdc4/34/53 pathway targets Cdc6p for proteolysis in budding yeast. EMBO J. *16*, 5966-5976.

Dube, P., Herzog, F., Gieffers, C., Sander, B., Riedel, D., Muller, S.A., Engel, A., Peters, J.M., and Stark, H. (2005). Localization of the coactivator Cdh1 and the cullin subunit Apc2 in a cryo-electron microscopy model of vertebrate APC/C. Mol. Cell *20*, 20867-20879.

Elsasser, S., Chandler-Militello, D., Mueller, B., Hanna, J., and Finley, D. (2004). Rad23 and RPN10 serve as alternative ubiquitin receptors for the proteasome. J. Biol. Chem. *279*, 26817-26822.

Engle, D.B., Osmani, S.A., Osmani, A.H., Rosborough, S., Xin, X.N., and Morris, N.R. (1990). A negative regulator of mitosis in Aspergillus is a putative membrane-spanning protein. J. Biol. Chem. *265*, 16132-16137.

Evans, T., Rosenthal, E.T., Youngblom, J., Distel, D., and Hunt, T. (1983). Cyclin: a protein specified by maternal mRNA in sea urchin eggs that is destroyed at each cleavage division. Cell *33*, 389-396.

Feldman, R.M., Corell, C.C., Kaplan, K.B., and Deshaies, R.J. (1997). A complex of Cdc4p, Skp1p and Cdc53p/cullin catalyzes ubiquitination of the phosphorylated CDK inhibitor SIC1p. Cell *91*, 221-230.

Fero, M.L., Randel, E., Gurley, K.E., Roberts, J.M., and Kemp, C.J. (1998). The murine gene p27Kip1 is haploinsufficient for tumour suppression. Nature *396*, 177-180.

Furukawa, M., He, Y.J., Borchers, C., and Xiong, Y. (2003). Targeting of protein ubiquitination by BTB-Cullin 3-Roc1 ubiquitin ligases. Nat. Cell Biol. *5*, 1001-1007.

Galan, J.M., and Peter, M. (1999). Ubiquitin-dependent degradation of multiple F-box proteins by an autocatalytic mechanism. Proc. Natl. Acad. Sci. USA *96*, 9124-9129.

Galderisi, U., Jori, F.P., and Giordano, A. (2003). Cell cycle regulation and neural differentiation. (2003). Oncogene *22*, 5208-5219.

Ganoth, D., Bornstein, G., Ko, T.K., Larsen, B., Tyers, M., Pagano, M., and Hershko, A. (2001). The cell-cycle regulatory protein Cks1 is required for SCF(Skp2)-mediated ubiqitinylation of p27. Nat. Cell Biol. *3*, 321-324.

Geisen, C., and Moroy, T. (2002). The oncogenic activity of cyclin E is not confirmed to Cdk2 activation alone but relies on several other, distinct functions of the protein. J. Biol. Chem. *277*, 39909-39918.

Geng, Y., Yu, Q., Sicinska, E., Das, M., and Schneider, J.E. (2003). Cyclin E ablation in the mouse. Cell *114*, 431-443.

Gieffers, C., Dube, P., Harris, J.R., Stark, H., and Peters J.M. (2001). Three-Dimensional Structure of the Anaphase-Promoting Complex. Mol. Cell *7*, 907-913.

Gladden, A.B., and Diehl, J.A. (2003). Cell cycle progression without cyclin E/CDK2: Breaking down the walls of dogma. Cancer Cell *4*, 160-162.

Glotzer, M., Murray, A.W., and Kirschner, M.W. (1991). Cyclin is degraded by the ubiquitin pathway. Nature *349*, 132-138.

Gmachl, M., Gieffers, C., Podtelejnikov, A.V., Mann, M., and Peters, J.M. (2000). The RING-H2 finger protein APC11 and the E2 enzyme UBC4 are sufficient to ubiquitinate substrates of the anaphase-promoting complex. Proc. Natl. Acad. Sci. USA *97*, 8973-8978.

Goebl, M., and Yanagida, M. (1991). The TPR snap helix: a novel protein repeat motif from mitosis to transcription. Trends Biochem. Sci. *16*, 173-177.

Gomez-Roman, N., Grandori, C., Eisenman, R.N., and White, R.J. (2003). Direct activation of RNA polymerase III transcription by c-Myc. Nature *421*, 290-294.

Grim, J.E., and Clurman, B.E. (2003). Cycling without CDK2? Trends Cell Biol. *13*, 396-399.

Grossberger, R., Gieffers, C., Zachariae, W., Podtelejnikov, A.V., Schleiffer, A., Nasmyth, K., Mann, M., et al. (1999). Characterization of the DOC1/APC10 subunit of the yeast and the human anaphase-promoting complex. J. Biol. Chem. *274*, 14500-14507.

Guardavaccaro, D., and Pagano, M. (2004). Oncogenic aberrations of cullin-dependent ubiquitin ligases. Oncogene *23*, 2037-2049.

Guo, Q.M., Malek, R.L., Kim, S., Chiao, C., He, M., Ruffy, M., Sanka, K., Lee, N.H., Dang, C.V., and Liu, E.T. (2000). Identification of c-myc responsive genes using rat cDNA microarray. Cancer Res. *60*, 5922-5928.

Gupta-Rossi, N., Le Bail, O., Gonen, H., Brou, C., Logeat, F., Six, E., Ciechanover, A., and Israel, A. (2001). Functional interaction between SEL-10, an F-box protein, and the nuclear form of activated Notch1 receptor. J. Biol. Chem. *276*, 34371-34378.

Hall, M.C., Torres, M.P., Schroeder, G.K., and Borchers,C.H. (2003). Mnd2 and Swm1 Are Core Subunits of the Saccharomyces cerevisiae Anaphase-promoting Complex. J. Biol. Chem. *278*, 16698-16705.

Harper, J.W. (2001). Protein destruction: adapting roles for Cks proteins. Curr. Biol. *11*, R431-R435.

Harper, J. W., Burton, J.L., and Solomon, M.J. (2002). The anaphase-promoting complex: it's not just for mitosis anymore. Genes Dev. *16*, 2179-2206.

Hartmann-Petersen, R., and Gordon, C. (2004). Protein Degradation: Recognition of Ubiquitinylated Substrates. Curr. Biol. *14*, R754-R756.

Harwell, R.M., Porter, D.C., Danes, C., and Keyomarsi, K. (2000). Processing of cyclin E differs between normal and tumor breast cells. Cancer Res. *60*, 481-489.

Hauf, S., Waizenegger, I.C., and Peters, J.M. (2001). Cohesin cleavage by separase required for anaphase and cytokinesis in human cells. Science *293*, 1320-1323.

Henchoz, S., Chi, Y., Catarin, B., Herskowitz, I., Deshaies, R.J., and Peter, M. (1997). Phosphorylation- and ubiquitin-dependent degradation of the cyclin-dependent kinase inhibitor Far1p in budding yeast. Genes Dev. *11*, 3046-3060.

Hershko, A. (1983). Components of ubiquitin-protein ligase system. Resolution, affinity purification, and role in protein breakdown. J. Biol. Chem. *258*, 8206-8214.

Hershko, A. (1997). Roles of ubiquitin-mediated proteolysis in cell cycle control. Curr. Opin. Cell Biol. *9*, 788-799.

Hershko, A., and Ciechanover, A. (1998). The ubiquitin system. Annu. Rev. Biochem. *67*, 425-479.

Hilton, D.J., Richardson, R.T., Alexander, W.S., Viney, E.M., Willson, T.A., Sprigg, N.S., Starr, R., et al. (1998). Twenty proteins containing a C-terminal SOCS box form five structural classes. Proc. Natl. Acad. Sci. USA *95*, 114-119.

Hochstrasser, M. (1996). Ubiquitin-dependent protein degradation. Annu. Rev. Genet. *30*, 405-439.

Hodge, A., and Mendenhall, M. (1999). The cyclin-dependent kinase inhibitory domain of the yeast Sic1 protein is contained within the C-terminal 70 amino acids. Mol. Gen. Genet. *262*, 55-64.

Hori, T., Osaka, F., Chiba, T., Miyamoto, C., Okabayashi, K., Shimbara, N., Kato, S., and Tanaka, K. (1999). Covalent modification of all members of human cullin family proteins by NEDD8. Oncogene *18*, 6829-6834.

Hsu, J.Y., Reimann, J.D., Sorensen, C.S., Lukas, J., and Jackson, P.K. (2002). E2F-dependent accumulation of hEmi1 regulates S phase entry by inhibiting APC(Cdh1). Nat. Cell Biol. *4*, 358-366.

Huang, J.N., Park, I., Ellingson, E., Littlepage, L.E., and Pellman, D. (2001). Activity of the APC(CDH1) form of the anaphase-promoting complex persists until S phase and prevents the premature expression of Cdc20p. J. Cell Biol. *154*, 85-94.

Huang, L., Kinnucan, E., Wang, G., Beaudenon, S., Howley, P.M., Huibregtse, J.M., and Pavletich, N.P. (1999). Structure of an E6AP-UbcH7 Complex: Insights into Ubiquitination by the E2-E3 Enzyme Cascade. Science *286*, 1321-1326.

Hwang, L.M., and Murray, A.W. (1997). A Novel Yeast Screen for Mitotic Arrest Mutants Identifies *DOC1*, a New Gene Involved in Cyclin Proteolysis. Mol. Biol. Cell *8*, 1877-1887.

Iritani, B.M., and Eisenman, R.N. (1999). C-Myc enhances protein synthesis and cell size during B lymphocyte development. Proc. Natl. Acad. Sci. USA *96*, 13180-13185.

Irniger, S., Piatti, S., Michaelis, C., and Nasmyth, K. (1995). Genes involved in sister chromatid separation are needed for B-type cyclin proteolysis in budding yeast. Cell *81*, 269-278.

Jackman, M., Kubota, Y., den Elzen, N., Hagting, A., and Pines, J. (2002). Cyclin A and cyclin E CDK2 complexes shuttle between the nucleus and the cytoplasm. Mol. Cell Biol. *13*, 1030-1045.

Jackson, P.K., Eldridge, A.G., Freed, E., Furstenthal, L., Hsu, J.Y., Kaiser, B.K., and Reimann, J.D.R. (2000). The lore of the RINGs: Substrate recognition and catalysis by ubiquitin ligases. Trends Cell Biol. *10*, 429-439.

Jeffrey, P.D., Tong, L., and Pavletich, N.P. (2000). Structural basis of inhibition of CDK-cyclin complexes by INK4 inhibitors. Genes Dev. *14*, 3115–3125.

Jin, J., Cardozo, T., Lovering, R.C., Elledge, S.J., Pagano, M., and Harper, J.W. (2004). Systematic analysis and nomenclature of mammalian F-box proteins. Genes Dev. *18*, 2573-2580.

Joazeiro, C.A., and Weissman, A.M. (2000). RING Finger Proteins Mediators of Ubiquitin Ligase Activity. Cell *102*, 549-552.

Johnston, L.A., Prober, D.A., Edgar, B.A., Eisenman, R.N., and Gallant, P. (1999). Drosophila myc regulates growth during development. Cell *98*, 779-790.

Jones, T.A., Zou, J.Y., Cowan S.W., and Kjeldgaard, M. (1991). Improved methods for building protein models in electron-density maps and the location of errors in these models. Acta Crystallogr. *47*, 110–119.

Jorgensen, P.M., Gräslund, S., Betz, R., Stahl, S., Larsson, C., and Hoog C.H. (2001). Characterisation of the human *APC1*, the largest subunit of the anaphase-promoting complex. Gene *262*, 51-59.

Kamura, T., Koepp, D.M., Conrad, M.N., Skowyra, D., Moreland, R.J., Iliopoulos, O., Lane, W.S., Kaelin, W.G., Jr., Elledge, S.J., et al. (1999). Rbx1, a component of the VHL tumor suppressor complex and SCF ubiquitin ligase. Science *284*, 657-661.

Kawamura, K., Izumi, H., Ma, Z., Ikeda, R., Moriyama, M. et al. (2004). Induction of centrosome Amplification and chromosome Instability in Human Bladder Cancer Cells by p53 Mutation and Cyclin E Overexpression. Cancer Res. *64*, 4800-4809.

Keyomarsi, K., Conte Jr, D., Toyofuku, W., and Fox, M.P. (1995). Deregulation of cyclin E in breast cancer. Oncogene *11*, 941-950.

Keyomarsi, K., and Herliczek, T.W. (1997). The role of cyclin E in cell proliferation, development and cancer. Prog. Cell Cycle Res. *3*, 171-191.

Keyomarsi, K., Tucker, S.L., Buchholz, T.A., et al. (2002). Cyclin E and survival in patients with breast cancer. N. Engl. J. Med. *347*, 1566-1575.

Kim, S.Y., Herbst, A., Tworkowski, K.A., Salghetti, S.E., and Tansey, W.P. (2003). Skp2 regulates myc protein stability and activity. Mol. Cell *11*, 1177-1188.

Kimura, T., Gotoh, M., Nakamura, Y., and Arakawa, H. (2003). hcdc4b, a regulator of cyclin E, as a direct transcriptional target of p53. Cancer Sci. *94*, 431-436.

King, R.W., Peters, J.M., Tugendreich, S., Rolfe, M., Hieter, P., and Kirschner, M.W. (1995). A 20S complex containing CDC27 and CDC16 catalyzes the mitotic-specific conjugation of ubiquitin to cyclin B. Cell *81*, 279-288.

King, R.W., Deshaies, R.J., Peters, J.M., and Kirschner, M.W. (1996). How Proteolysis Drives the Cell Cycle. Science *274*, 1652-1658.

Kipreos, E.T., Lander, L.E., Wing, J.P., He, W.W., and Hedgecock, E.M. (1996). cul-1 Is Required for Cell Cycle Exit in C. elegans and Identifies a Novel Gene Family. Cell *85*, 829-839.

Kipreos, E.T., and Pagano, M. (2000). The F-box protein family. Genome Biol. *1*, 3002.1-3002.7.

Koepp, D.M., Schaefer, L.K., Ye, X., Keyomarsi, K., Chu, C., Harper, J.W., and Elledge, S.J. (2001). Phosphorylation-dependent ubiquitination of cyclin E by the SCFFbw7 ubiquitin ligase. Science *294*, 173-177.

Koff, A., Cross, F., Fisher, A., Schumacher, J., Leguellec, K., Philippe, M., and Roberts, J.M. (1991). Human cyclin E, a new cyclin that interacts with two members of the CDC2 gene family. Cell *66*, 1217-1228.

Koloteva-Levine, N., Pinchasi, D., Pereman, I. et al. (2004). The APC5 subunit of the Anaphase-Promoting Complex/Cyclosome interacts with Poly(A) binding protein and represses internal ribosome entry site-mediated translation. Mol. Cell Biol. *24*, 3577-3587.

Kominami, K., Seth-Smith, H., and Toda, T. (1998). Apc10 and Ste9/Srw1, two regulators of the APC?cyclosome, as well as the CDK inhibitor Rum1 are required for G1 cell-cycle arrest in fission yeast EMBO J. *17*, 5388-5399.

Kotani, S., Tanaka, H., Yasuda, H., and Todokoro, K. (1999). Regulation of APC activity by phosphorylation and regulatory factors. J. Cell Biol. *146*, 791-800.

Kramer, E.R., Scheuringer, N., Podtelejnikov, A.V., Mann, M., and Peters, J.M. (2000). Mitotic regulation of the APC activator proteins Cdc20 and Cdh1. Mol. Biol. Cell *11*, 1555-1569.

Krek, W. (2003). BTB proteins as henchmen of Cul3-based ubiquitin ligases. Nat. Cell Biol. *5*, 950-951.

Kus, B.M., Caldon, C.E., Andorn-Broza, R., and Edwards, A.M. (2004). Functional Interaction of 13 Yeast SCF Complexes with a Set of Yeast E2 Enzymes *in vitro*. Proteins *54*, 455-467.

Lam, Y.A., Xu, W., DeMartino, G.N., and Cohen, R.E. (1997). Editing of ubiquitin conjugates by an isopeptidase in the 26S proteasome. Nature *385*, 737-740.

Lamb, J.R., Michaud, W.A., Sikorski, R.S., and Hieter, P.A. (1994). Cdc16p, Cdc23p and Cdc27p form a complex essential for mitosis. EMBO J. *13*, 4321-4328.

Laskowski, R.A., Macarthur, M.W., Moss D.S., and Thornton J.M. (1993). Procheck: a program to check the stereochemical quality of protein structures. J. Appl. Crystallogr. *26***,** 283–291.

Lauper, N., Beck, A.R., Cariou, S., Richman, L., Hofmann, K., Reith, W., Slingerland, J.M., and Amati, B. (1998). Cyclin E2: a novel CDK2 partner in the late G1 and S phases of the mammalian cell cycle. Oncogene *17*, 2637-2643.

Leverson, J.D., Joazeiro, C.A.P., Page, A.M., Huang, H., Hieter, P., and Hunter, T. (2000). The APC11 RING-H2 Finger Mediates E2-Dependent Ubiquitination. Mol. Biol. Cell *11*, 2315-2325.

Lew, D.J., Dulic, V., and Reed, S.I. (1991). Isolation of three novel human cyclins by rescue of G1 cyclin (Cln) function in yeast. Cell *66*, 1197-1206.

Li, Y., Gazdoiu, S., Pan, Z.Q., and Fuchs, S.Y. (2004). Stability of homologue of slimb F-box protein is regulated by availability of its substrate. J. Biol. Chem. *279*, 11074-11080.

Liu, J., Furukawa, M., Matsumoto, T., and Xiong Y. (2002). NEDD8 modification of Cul1 dissociates p120(CAND1), an inhibitor of CUL1-SKP1 binding and SCF ligases. Mol. Cell *10*, 1511-1518.

Lukas, C., Sorensen, C.S., Kramer, E., Santoni-Rugiu, E., Lindeneg, C., Peters, J.M., Bartek, J., and Lukas, J. (1999). Accumulation of cyclin B1 requires E2F and cyclin-A-dependent rearrangement of the anaphase-promoting complex. Nature *401*, 815-818.

Lupas, A., Baumeister, W., Hofmann, K. (1997). A repetitive sequence in subunits of the 26S proteasome and 20S cyclosome (anaphase-promoting complex). Trends Biochem. Sci. *22*, 195-196.

Mao, J.H., Peres-Iosada, J., Wu, D., DelRosario, R., Tsunematsu, R., Nakayama, K.I., Brown, K., Bryson, S., and Balmain, A. (2004). Fbxw7/Cdc4 is a p53-dependent, haploinsufficient tumour suppressor gene. Nature *432*, 775-779.

Mateyak, M., Obaya, A., and Sedivy, J. (1999). C-Myc regulates cyclin D-Cdk4 and Cdk6 but effects cell cycle progression at multiple independent points. Mol. Cell Biol. *19*, 4672-4683.

Matsumoto, Y., and Maller, J.L (2004). A centrosomal localization signal in cyclin E required for CDK2-independent S-phase entry. Science *306*, 885-888.

McPherson A. (1998). Crystallization of biological macromolecules. Cold Spring Harbor Laboratory Press.

Meimoun, M., Holtzman, T., Weissman, Z., McBride, H.J., Stillman, D.J., Fink, G.R., and Kornitzer, D. (2000). Degradation of the transcription factor Gcn4 requires the kinase Pho85 and the SCF(CDC4) ubiquitin-ligase complex. Mol. Biol. Cell *11*, 915-927.

Min, J.H., Yang, H., Ivan, M., Gertler, F., Kaelin, W.G.Jr., and Pavletich, N.P. (2002). Structure of an HIF-1alpha -pVHL complex: hydroxyproline recognition in signaling. Science *296*, 1886-1889.

Moberg, K.H., Bell, D.W., Wahrer, D.C., Haber, D.A., and Hariharan, I.K. (2001). Archipelago regulates Cyclin E levels in Drosophila and is mutated in human cancer cell lines. Nature *413*, 311-316.

Moore, J.D., Kornbluth, S., and Hunt, T. (2002). Identification of the nuclear localization signal in Xenopus cyclin E and analysis of its role in replication and mitosis. Mol. Biol. Cell *13*, 4388-4400.

Morgan, D.O. (1997). Cyclin-dependent kinases: Engines, clocks, and microprocessors. Annu. Rev. Cell Dev. Biol. *13*, 261-291.

Morgan, D.O. (1999). Regulation of the APC and the exit from mitosis. Nat. Cell Biol. *2*, E47-E53.

Morimoto, M., Nishida, T., Honda, R., and Yasuda, H. (2000). Modification of cullin-1 by ubiquitin-like protein Nedd8 enhances the activity of SCF(skp2) toward p27(kip1). Biochem. Biophys. Res. Commun. *270*, 1093-1096.

Moroy, T., and Geisen, C. (2004). Cyclin E. Int. J. Biochem. Cell Biol. *36*, 1424-1439.

Murray, A.W., Solomon, M.J., and Kirschner, M.W. (1989). The role of cyclin synthesis and degradation in the control of maturation promoting factor activity. Nature *339*, 280-286.

Murray, A., and Hunt, T. (1993). The cell cycle: an introduction. Oxford University Press.

Nair, S.K., and Burley, S.K. (2003). X-ray structures of Myc-Max and Mad-Max recognizing DNA. Molecular bases of regulation by proto-oncogenic transcription factors. Cell *112*, 193-205.

Nakayama, K., Nagahama, H., Minamishima, Y.A., Matsumoto, M., Nakamichi, I., Kitagawa, K., et al. (2000). Targeted disruption of Skp2 results in accumulation of cyclin E and $p27^{Kip1}$, polyploidy and centrosome overduplication. EMBO J. *19*, 2069-2081.

Nash, P., Tang, X., Orlicky, S., Chen, Q., Gertler, F.B., Mendenhall, M.D., Sicheri, F., Pawson, T., and Tyers, M. (2001). Multisite phosphorylation of a CDK inhibitor sets a threshold for the onset of DNA replication. Nature *414*, 514-521.

Nasmyth, K. (2001). Disseminating the genome: joining, resolving, and separating sister chromatids during mitosis and meiosis. Annu. Rev. Genet. *35*, 673-745.

Nateri, A.S., Riera-Sans, L., Da Costa, C., and Behrens, S. (2004). The ubiquitin ligase SCFFbw7 antagonizes apoptotic JNK signaling. Science *303*, 1374-1378.

Nesbit, C.E., Tersak, J.M., and Prochownik, E.V. (1999). MYC oncogenes and human neoplastic disease. Oncogene *18*, 3004-3016.

Ohh, M., Kim, W.Y., Moslehi, J.J., Chen, Y., Chau, V., Read, M.A., and Kaelin, W.G., Jr. (2002). An intact NEDD8 pathway is required for Cullin-dependent ubiquitylation in mammalian cells. EMBO Rep. *3*, 177-182.

Ohta, T., Michel, J.J., Schottelius, A.J., and Xiong, Y. (1999). Roc1, a homolog of APC11, represents a family of cullin partners with an associated ubiquitin ligase activity. Mol. Cell *3*, 535-541.

Ohtsubo, M., and Robert, J.M. (1993). Cyclin-dependent regulation of G1 in mammalian fibroblasts. Science *259*, 1908-1912.

Ohtsubo, M., Theodoras, A.M., Schumacher, J., Roberts, J.M., and Pagano, M. (1995). Human cyclin E, a nuclear protein essential for the G1 to S phase transition. Mol. Cell Biol. *15*, 2612-2624.

Orlicky, S., Tang, X., Willems, A., Tyers, M., and Sicheri, F. (2003). Structural basis for phosphodependent substrate selection and orientation by the SCF^{Cdc4} ubiquitin ligase. Cell *112*, 243-256.

Oster, S.K., Ho, C.S., Soucie, E.L., and Penn, L.Z. (2002). The myc oncogene: marvelously complex. Advan. Cancer Res. *84*, 81-154.

Pagano, M., Tam, S.W., Theodoras, A.M., Beer-Romero, P., Del Sal, G., Chau, V., Yew, P.R., Draetta, G.F., and Rolfe, M. (1995). Role of the ubiquitin-proteasome pathway in regulating abundance of the cyclin-dependent kinase inhibitor p27. Science *269*, 682-685.

Page, A.M., and Hieter, P. (1999). The anaphase promoting complex: New subunits and regulators. Annu. Rev. Biochem. *68*, 583-609.

Pan, Z.Q., Kentsis, A., Dias, D.C., Yamoah, K., and Wu, K. (2004). Nedd8 on cullin: building an expressway to protein destruction. Oncogene *23*, 1985-1997.

Papas, T.S., Lautenberger, J.A. (1985). Sequence curiosity in v-myc oncogenes. Nature *318*, 237.

Parisi, T., Beck, A.R., Rougier, N., McNeil, T., Lucian, L., Werb, Z., and Amati, B. (2003). Cyclins E1 and E2 are required for endoreplication in placental trophoblast giant cells. EMBO J. *22*, 4794-4803.

Park, K.H., Choi, S.E., Eom, M., and Kang, Y. (2005). Downregulation of the anaphase-promoting complex (APC)7 in invasive ductal carcinomas of the breast and its clinicopathologic relationships. Breast Cancer Res. *7*, R238-R247.

Passmore, L.A., McCormack, E.A., Au, S.W., Paul, A., Willison, K.R., Harper, J.M., and Barford, D. (2003). Doc1 mediates the activity of the anaphase-promoting complex by contributing to substrate recognition. EMBO J. *22*, 786-796.

Passmore, L.A., Booth, C.R., Venien-Bryan, C., Ludtke, S.J., Fioretto, C., Johnson, L.N., Chiu, W., Barford, D. (2005). Structural analysis of the anaphase-promoting complex reveals multiple active sites and insights into polyubiquitylation. Mol. Cell *20*, 855-866.

Perkins, G., Drury, L.S., and Diffley, J.F.X. (2001). Separate SCFCDC4 recognition elements target Cdc6 for proteolysis in S phase and mitosis. EMBO J. *20*, 4836-4845.

Peters, J.M., King, R.M., Hoog, C. and Kirschner, M.W. (1996). Identification of BIME as a Subunit of the Anaphase-Promoting Complex. Science *274*, 1199-1201.

Peters, J.M. (2002). The anaphase-promoting complex: proteolysis in mitosis and beyond. Mol. Cell. *9*, 931-943.

Petroski, M.D., and Deshaies, R.J. (2003). Context of multiubiquitin chain attachment influences the rate of Sic1 degradation. Mol. Cell *11*, 1435-1444.

Pfleger, C.M., and Kirschner, M.W. (2000). The KEN box: an APC recognition signal distinct from the D box targeted by Cdh1. Genes Dev. *14*, 655-665.

Philipp, A., Schneider, A., Vasrik, I., Finke, K., Xiong, Y., Beach, D., Alitalo, K., and Eilers, M. (1994). Repression of cyclin D1: a novel function of MYC. Mol. Cell Biol. *14*, 4032-4043.

Pickart, C.M. (2000). Ubiquitin in chains. Trend Biochem. Sci. *25*, 544-548.

Pickart, C.M. (2001). Mechanisms underlying ubiquitination. Annu. Rev. Biochem. *70*, 503-533.

Pierce, M.M., Raman, C.S., and Nall, B.T. (1999). Isothermal Titration Calorimetry of Protein-Protein Interactions. Methods *19*, 213-221.

Porter, D.C., Zhang, N., Danes, C., et al. (2001). Tumor-specific proteolytic processing of cyclin E generates hyperactive lower-molecular-weight forms. Mol. Cell Biol. *21*, 6254-6269.

Porter, P.L., Malone, K.E., Heagerty, P.J., Alexander, G.M., Gatti, L.A., Firpo, E.J., et al. (1997). Expression of cell-cucle regulators p27Kip1 and cyclin E, alone and in combination, correlate with survival in young breast cancer patients. Nat. Med. *3*, 222-225.

Prendergast, G.C. (1999). Mechanisms of apoptosis by c-Myc. Oncogene *18*, 2967-2987.

Rabitsch, K.P., Toth, A., Galova, M., Schleiffer, A., Schaffner, G., Aigner, E., Rupp, C., Penkner, A.M., et al. (2001). A screen for genes required for meiosis and spore formation based on whole-genome expression. Curr. Biol. *11*, 1001-1009.

Rajagopalan, H., Jallepalli, P.V., Rago, C., Velculescu, V.E., Kinzler, K.W., Vogelstein, B., and Lengauer, C. (2004). Inactivation of hCDC4 can cause chromosomal instability. Nature *428*, 77-81.

Read, M.A., Brownell, J.E., Gladysheva, T.B., Hottelet, M., Parent, L.A., Coggins, M.B., Pierce, J.M., et al. (2000). Nedd8 modification of Cul-1 Activates SCF$^{\beta TrCP}$-Dependent Ubiquitination of IκBα. Mol. Cell Biol. *20*, 2326-2333.

Richly, H., Rape, M., Braun, S., Rumpf, S., Hoege, C., and Jentsch, S. (2005). A series of ubiquitin binding factors connects CDC48/p97 to substrate multiubiquitylation and proteasomal targeting. Cell *120*, 73-84.

Rieder, C.L., Schultz, A., Cole, R., and Sluder, G. (1994). Anaphase onset in vertebrate somatic cells is controlled by a checkpoint that monitors sister kinetochore attachment to the spindle. J. Cell Biol. *127*, 1301-1310.

Rudner, A.D., and Murray, A.W. (2000). Phosphorylation by Cdc28 activates the Cdc20-dependent activity of the anaphase-promoting complex. J. Cell Biol. *149*, 1377-1390.

Russo, A.A., Jeffrey, P.D., Patten, A.K., Massague, J., and Pavletich, N.P. (1996). Crystal structure of the p27^{Kip1} cyclin-dependent-kinase inhibitor bound to the cyclin A-Cdk2 complex. Nature *382*, 325-331.

Salghetti, S.E., Kim, S.Y., and Tansey, W.P. (1999). Destruction of Myc by ubiquitin-mediated proteolysis: cancer-associated and transforming mutations stabilize Myc. EMBO J. *18*, 717-726.

Salghetti, S.E., Muratani, M., Wijnen, H., Futcher, B., and Tansey, W.P. (2000). Functional overlap of sequences that activate transcription and signal ubiquitin-mediated proteolysis. Proc. Natl. Acad. Sci. USA *97*, 3118-3123.

Sanger, F., Nicklen S. and Coulson, A. R. (1977) DNA sequ encing with chain-terminating inhibitors. Proc. Nat. Acad. Sci. USA *74*, 5463-7.

Schneffner, M., Nuber, U., and Huibregtse, J.M. (1994). Protein ubiquitination involving an E1-E2-E3 enzyme thioester cascade. Nature *373*, 81-83.

Schneider, B.L., Yang, Q.H., and Futcher, A.B. (1996). Linkage of replication to start by the Cdk inhibitor Sic1. Science *272*, 560-562.

Schulman, B.A., Carrano, A.C., Jeffrey, P.D., Bowen, Z., Kinnucan, E.R.E., Finnin, M.S., Elledge, S.J., Harper, W.J., Pagano, M., and Pavletich, N.P. (2000). Insights into SCF ubiquitin ligases from the structure of the Skp1-Skp2 complex. Nature *408*, 381-386.

Schwob, E., Bohm, T., Mendenhall, M.D., and Nasmyth, K. (1994). The B-type cyclin kinase inhibitor p40SIC1 controls the G1 to S transition in S. *cerevisiae*. Cell *79*, 233-244.

Sears, R., Leone, G., Degregori, J., and Nevins, J.R. (1999). Ras enhances Myc protein stability. Mol. Cell *3*, 169-179.

Sears, R., Nuckolls, F., Haura, E., Taya, Y., Tamai, K., and Nevins, J.R. (2000). Multiple Ras-dependent phosphorylation pathways regulate Myc protein stability. Genes Dev. *14*, 2501-2514.

Sedgwick, C., Rawluk, M., Decesare, J., Raithatha, S., Wohlschlegel, J., Semchuk, P., Ellison, M., Yates, J. 3rd, and Stuart D. (2006). Saccharomyces cerevisiae Ime2 phosphorylates Sic1 at multiple PXS/T sites but is insufficient to trigger Sic1 degradation. J. Biochem. *399*, 151-160.

Sherr, C.J. (1993). Mammalian G1 cyclins. Cell *73*, 1059-1065.

Sherr, C. J., and Roberts, J.M. (1999). CDK inhibitors: positive and negative regulators of G1-phase progression. Genes Dev. *13*, 1501-1512.

Shirane, M., Harumiya, Y., Ishida, N., Hirai, A., Miyamoto, C., Hatakeyama, S., et al. (1999). Down-regulation of p27Kip1 by Two Mechanisms, Ubiquitin-mediated Degradation and Proteolytic Processing. J.Bio.Chem. *274*, 13886-13893.

Shirayama, M., Toth, A., Galova, M., and Nasmyth, K. (1999). APC(Cdc20) promotes exit from mitosis by destroying the anaphase inhibitor Pds1 and cyclin Clb5. Nature *402*, 203-207.

Sim, K.G., Zang, Z., Yang, C.M., Bonventre, J.V., and Hsu, S.I.H. (2004). TRIP-Br links E2F to Novel Functions in the Regulation of cyclin E Expression during Cell Cycle Progression and in the Maintenance of Genomic Stability. Cell Cycle *3*, e92-e99.

Skowyra, D., Craig, K.L., Tyers, M., Elledge, S.J., and Harper, J.W. (1997). F-proteins are receptors that recruit phosphorylated substrates to the SCF ubiquitin-ligase complex. Cell *91*, 209-219.

Spruck, C.H., Won, K.A., and Reed, S.I. (1999). Deregulated cyclin E induces chromosome instability. Nature *401*, 297-300.

Spruck, C.H., Strohmaier, H., Sangfelt, O., Muller, H.M., Hubalek, M., Muller-Holzner, E., Marth, C., Widschwendter, M., and Reed, S.I. (2002). hcdc4 gene mutations in endometrial cancer. Cancer Res. *62*, 4535-4539.

Starborg, M., Brundell, E., Gell, K., and Hoog, C. (1994). A novel murine gene encoding a 216-kDa protein is related to a mitotic checkpoint regulator previously identified in Aspergillus nidulans. J. Biol. Chem. *269*, 24133-24137.

Stegmeier, F., Visintin, R., and Amon, A. (2002). Separase, Polo Kinase, the Kinetochore Protein Slk19, and Spo12 Function in a Network that Controls Cdc14 Localization during Early Anaphase. Cell *108*, 207-220.

Stillman, B. (1996). Cell Cycle Control of DNA Replication. Science *274*, 1659-1664.

Stoltze, L., Nussbaum, A.K., Sijts, A., Emmerich, N.P., Kloetzel, P.M., and Schild, H. (2000). The function of the proteasome system in MHC class I antigen processing. Immunol. Today *21*, 317-319.

Strohmaier, H., Spruck, C.H., Kaiser, P., Won, K.A., Sangfelt, O., and Reed, S.I. (2001). Human F-box protein hCdc4 targets cyclin E for proteolysis and is mutated in a breast cancer cell line. Nature *413*, 316-322.

Su, T.T., and O'Farrell, P.H. (1998). Chromosome association of minichromosome maintenance proteins in Drosophila endoreplication cycles. J. Cell Biol. *140*, 451-460.

Sudakin, V., Ganoth, D., Dahan, A., Heller, H., Hershko, J., Luca, F.C., Ruderman, J.V., et al. (1995). The cyclosome, a large complex containing cyclin-selective ubiquitin ligase activity, targets cyclins for destruction at the end of mitosis. Mol. Biol. Cell *6*, 185-197.

Suzuki, H. et al. (1999). IκBα ubiquitination is catalyzed by an SCF-like complex containing Skp1, cullin-1, and two F-box/WD40-repeat proteins, βTrcp1 and βTrcp2. Biochem. Biophys. Res. Commun. *256*, 127-132.

Tan, P., Fuchs, S.Y., Chen, A., Wu, K., Gomez, C., Ronai, Z., and Pan, Z.Q. (1999). Recruitment of a ROC1-CUL1 ubiquitin ligase by Skp1 and HOS to catalyze the ubiquitination of I kappa B alpha. Mol. Cell *3*, 527-533.

Tang, B., Bottinger, E.P., Jakowlew, S.B., Bagnall, K.M., Mariano, J., Anver, M.R., Letterio, J.J., and Wakefield, L.M. (1998). Transforming growth factor –β1 is a new form of tumour suppressor with true haploid insufficiency. Nat. Med. *4*, 802-807.

Tang, Z., Li, B., Bharadwaj, R., Zhu, H., Ozkan, E., Hakala, K., Deisenhofer, J., et al. (2001). APC2 Cullin protein and APC11 RING protein comprise the minimal ubiquitin ligase module of the anaphase-promoting complex. Mol. Biol. Cell *12*, 3839-3851.

Tang, Z., Shu, H., Oncel, D., Chen, S., and Yu, H. (2004). Phosphorylation of Cdc20 by Bub1 provides a catalytic mechanism for APC/C inhibition by the spindle checkpoint. Mol. Cell *16*, 387-397.

ter Haar, E., Harrison, S.C., and Kirchhausen, T. (2000). Peptide-in-groove interactions link target proteins to the β-propeller of clathrin. Proc. Natl. Acad. Sci. USA *97*, 1096-1100.

Tetsu, O., and McCormick, F. (2003). Proliferation of cancer cells despite CDK2 inhibition. Cancer Cell *3*, 233-245.

Tetzlaff, M.T., Yu, W., Li, M., Zhang, P., Finegold, M., Mahon, K., Harper, J.W., Schwartz, R.J., et al. (2004). Defective cardiovascular development and elevated cyclin E and Notch proteins in mice lacking the Fbw7 F-box protein. Proc. Natl. Acad. Sci. USA *101*, 3338-3345.

Tsunematsu, R., Nakayama, K., Oike, Y., Nishiyama, M., Ishida, N., Hatakeyama, S., Beesho, Y., Kageyama, R., Suda, T., et al. (2004). Mouse Fbw7/Sel-10/Cdc4 is required for Notch degradation during vascular development. J. Biol. Chem. *279*, 9417-9423.

Tugendreich, S., Tomkiel, J., Earnshaw, W., and Hieter, P. (1995). CDC27Hs colocalizes with CDC16Hs to the centrosome and mitotic spindle and is essential for the metaphaseto anaphase transition. Cell *81*, 261-268.

Tyers, M. (1996). The cyclin-dependent kinase inhibitor p40SIC1 imposes the requirement for Cln G1 cyclin function at Start. Proc. Natl. Acad. Sci. USA *93*, 7772-7776.

Ufano, S., San-Segundo, P., del Ray, F., and Vazquez de Aldana, C.R. (1999). SWM1, a developmentally regulated gene, is required for spore wall assembly in Saccharomyces cerevisiae. Mol. Cell Biol. *19*, 2118-2129.

Verma, R., Annan, R.S., Huddleston, M.J., Carr, S.A., Reynard, G., and Deshaies, R.J. (1997). Phosphorylation of Sic1p by G1 Cdk required for its degradation and entry into S-phase. Science *278*, 455-460.

Verma, R., McDonald, H., Yates III, J.R., and Deshaies, R.J. (2001). Selective degradation of Ubiquitinated Sic1 by purified 26S Proteasome Yields active S Phase Cyclin-Cdk. Mol. Cell *8*, 439-448.

Verma, R., Oania, R., Graumann, J., and Deshaies, R.J. (2004). Multiubiquitin Chain Receptors Define a Layer of Substrate Selectivity in the Ubiquitin-Proteasome System. Cell *118*, 99-110.

Vijay-Kumar, S., Bugg, C.E., Wilkinson, K.D., Vierstra, R.D., Hatfield, P.M., and Cook, W.J. (1987). Comparison of the three-dimensional structures of human, yeast, and oat ubiquitin. J. Biol. Chem. *262*, 6396-6399.

Vodermaier, H.C., Gieffers, C., Maurer-Stroh, S., Eisenhaber, F., and Peters, J.M. (2003). TPR Subunits of the Anaphase-Promoting Complex Mediate Binding to the Activator Protein CDH1. Curr. Biol. *13*, 1459-1468.

Vodermaier, H.C., and Peters, J.M. (2004). APC activators caught by their tails? Cell Cycle *3*, 265-266.

Von der Lehr, N., Johansson, S., Wu, S., Bahram, F., Castell, A., Cetinkaya, C., et al. (2003). The F-Box Protein Skp2 Participates in c-Myc Proteosomal Degradation and Acts as a Cofactor for c-Myc-Regulated Transcription. Mol. Cell *11*, 1189-1200.

Weinberg, R.A. (1989). Oncogenes, antioncogenes and the molecular basic of multi step carcinogenesis. Cancer Res. *49*, 3713-3721.

Weinberg, R.A. (1995). The retinoblastoma protein and cell cycle control. Cell *81*, 323-330.

Welcker, M., Singer, J., Loeb, K.R., Grim, J., Bloecher, A., Gurien-West, M., Clurman, B.E., and Roberts, J.M. (2003). Multisite Phosphorylation by Cdk2 and GSK3 Controls Cyclin E Degradation. Mol. Cell *12*, 381-392.

Welcker, M., Orian, A., Grim, J.A., Eisenman, R.N., and Clurman, B.E. (2004a). A nucleolar isoform of the Fbw7 Ubiquitin Ligase regulates c-Myc and cell size. Curr. Biol. *14*, 1852-1857.

Welcker, M., Orian, A., Jin, J., Grim, J.A., Harper, J.W., et al. (2004b). The Fbw7 tumor suppressor regulates glycogen synthase kinase 3 phosphorylation-dependent c-Myc protein degradation. Proc. Natl. Acad. Sci. USA *101*, 9085-9090.

Welcker, M., and Clurman, B. E. (2005). The SV40 Large T Antigen Contains a Decoy Phosphodegron that mediates its Interactions with Fbw7/hCdc4. J. Biol. Chem. *280*, 7654-7658.

Wendt, K.S., Vodermaier, H.C., Jackob, U., Gieffers, C., Gmachl, M., Peters, J.M., Huber, R., and Sondermann, P. (2001). Crystal structure of the APC10/DOC1 subunit of the human anaphase-promoting complex. Nat. Struct. Biol. *8*, 784-788.

Winston, J.T., Koeppp, D.M., Zhu, C., Elledge, S.J., and Harper, J.W. (1999). A family of mammalian F-box proteins. Curr. Biol. *9*, 1180-1182.

Won, K.A., and Reed, S.I. (1996). Activation of cyclin E/CDK2 is coupled to site-specific autophosphorylation and ubiquitin-dependent degradation of cyclin E. EMBO J. *15*, 4182-4193.

Wu, G., Xu, G., Schulman, B.A., Jeffrey, P.D., Harper, J.W., and Pavletich, N.P. (2003). Structure of a β-TrCP1-Skp1-β-Catenin Complex: Destruction Motif Binding and Lysine Specificity of the $SCF^{\beta\text{-}Trcp1}$ Ubiquitin Ligase. Mol. Cell *11*, 1445-1456.

Yada, M., Hatakeyama, S., Kumura, T., Nishiyama, M., Tsunematsu, R., Imaki, H., Ishida, N., Okumura, F., Nakayama, K., et al. (2004). Phosphorylation-dependent degradation of c-Myc is mediated by the F-box protein Fbw7. EMBO J. *23*, 1-10.

Yamada, H., Kumada, K., and Yanagida, M. (1997). Distinct subunit functions and cell cycle regulated phosphorylation of 20S APC/cyclosome required for anaphase in fission yeast. J. Cell Sci. *110*, 1793-1804.

Yamashita, Y.M., Nakaseko, Y., Samejima, I., Kumada, K., Yamada, H., Michaelson, D., and Yanagida, M. (1996). 20S cyclosome complex formation and proteolytic activity inhibited by the cAMP/PKA pathway. Nature *384*, 276-279.

Yao, T., and Cohen, R.E. (1999). Giant proteases: beyond the proteasome. Curr. Biol. *9*, R551-R553.

Ye, X., Nalepa, G., Welcker, M., Kessler, B.M., Spooner, E., Qin, J., Elledge, S.J., Clurman, B.E., and Harper, J.W. (2004). Recognition of Phosphodegron Motifs in human Cyclin E by the SCF^{FBW7} Ubiquitin Ligase. J. Biol. Cell *279*, 50110-50119.

Yeh, E., Cunningham, M., Arnold, H., Chasse, D., Monteith, T., Ivaldi, G., et al. (2004). A signaling pathway controlling c-Myc degradation that impacts oncogenic transformation of human cells. Nat. Cell Biol. *6*, 308-318.

Yoon, H.J., Feoktistova, A., Wolfe, B.A., Jennings, J.L., Link, A.J., and Gould, K.L. (2002). Proteomics Analysis Identifies New Components of the Fission and Budding Yeast Anaphase-Promoting Complexes. Curr. Biol. *12*, 2048-2054.

Yu, H., Peters, J.M., King, R.W., Page, A.M., Hieter, P., and Kirschner, M.W. (1998). Identification of a cullin homology region in a subunit of the anaphase-promoting complex. Science *279*, 1219-1222.

Yu, H. (2002). Regulation of APC-Cdc20 by the spindle checkpoint. Curr. Opin. Cell Biol. *14*, 706-714.

Yu, Q. and Sicinski, P. (2004). Mammalian cell cycles without cyclin E/CDK2. Cell Cycle *3*, 292-295.

Yudkovsky, Y., Shteinberg, M., Listovsky, T., Brandeis, M., and Hershko, A. (2000). Phosphorylation of Cdc20/fizzy negatively regulates the mammalian cyclosome/APC in the mitotic checkpoint. Biochem. Biophys. Res. Commun. *271*, 299-304.

Zachariae, W., Shin, T.H., Galova, M., Obermaier. B., and Nasmyth, K. (1996). Identification of subunits of the anaphase-promoting complex of Saccharomyces cerevisiae. Science *274*, 1201-1204.

Zachariae, W., Shevchenko, A., Andrews, P.D., Ciosk, R., Galova, M., Stark, M.J., et al. (1998). Mass Spectrometric Analysis of the Anaphase-Promoting Complex from Yeast: Identification of a Subunit Related to Cullins. Science *279*, 1216-1219.

Zariwala, M., Liu, J., and Xiong, Y. (1998). Cyclin E2, a novel human G1 cyclin and activating partner of CDK2 and CDK3, is induced by viral oncoproteins. Oncogene *17*, 2787-2798.

Zheng, J., Yang, X., Harrell, J.M., Ryzhikov, S., Shim, E.H., Lykke-Andersen, K., Wei, N., Sun, H., Kobayashi, R., et al. (2002). CAND1 binds to unneddylated CUL1 and regulates the formation of SCF ubiquitin E3 ligase complex. Mol. Cell *10*, 1519-1526.

Zheng, N., Wang, P., Jeffrey, P.D., and Pavletich, N.P. (2000). Structure of a c-Cbl-UbcH7 complex: RING domain function in ubiquitin-protein ligases. Cell *102*, 533-539.

Zheng, N., Schulman, B.A., Song, L., Miller, J.J., Jeffrey, P.D., Wang, P., Chu, C., Koepp, D.M., Elledge, S.J., Pagano, M., et al. (2002). Structure of the Cul1-Rbx1-Skp1-Fbox^{Skp2} SCF ubiquitin ligase complex. Nature *416*, 703-749.

7. Appendix

Table 7.1. Primer pairs used to clone the genes and DNA-fragments of interest.

Nr.	Primer pair	Sequence
1	5'-EcoR1+1_Fbw7_232 3'-Sal1_Fbw7_707	5-CCGGAATTCCATGACAGGCCTCCAGGAATGGCTA-3 5-ACGGTCGACTCACTTCATGTCCACATCAAAA-3
2	5'-EcoR1+1_Fbw7_263 3'-Sal1_Fbw7_707	5-CCGGAATTCCATGACACAAGTAAAACATATGATG-3 5-ACGGTCGACTCACTTCATGTCCACATCAAAA-3
3	5'-EcoR1+1_Fbw7_279 3'-Sal1_Fbw7_707	5-CCGGAATTCCATGGACTTCATTTCATTGCTCCCT-3 5-ACGGTCGACTCACTTCATGTCCACATCAAAA-3
4	5'-HindIII_hSkp1_1 3'-BglII_hSkp1_149	5-CCCAAGCTTATGCCTTCAATTAAGTTGCAG-3 5-GGAAGATCTTCACTTCTCTTCACACCACTG-3
5	5'-EcoR1_Fbw7_232 3'-BglII_Fbw7_707	5-CCGGAATTCATGACAGGCCTCCAGGAATGGCTA-3 5-GGAAGATCTTCACTTCATGTCCACATCAAAA-3
6	5'-EcoR1_Fbw7_279 3'-BglII_Fbw7_707	5-CCGGAATTCATGGACTTCATTTCATTGCTCCCT-3 5-GGAAGATCTTCACTTCATGTCCACATCAAAA-3
7	5'-Not1_scAPC1_1 3'-Xma1_scAPC1_1748	5-GCAGTTACGTGCGGCCGCATGACTTCTAAGCCGTCTACT-3 5-GCAGTTACGTGCCCCGGGTTATTCATCATGTGGTCCAAA-3
8	5'-Not1_scAPC4_1 3'-Xma1_scAPC4_652	5-GCAGTTACGTGCGGCCGCATGTCGTCTCCTATTAATGAT-3 5-GCAGTTACGTGCCCCGGGTCAAACATTTTGTTTTTCTTT-3
9	5'-BamH1_scAPC4_594 3'-Not1_scAPC4_652	5-CGCGGATCCATGCACGTCACCGATTATAGGGGAG-3 5-GCAGTTACGTGCGGCCGCTCAAACATTTTGTTTTTCTTT-3
10	5'-BamH1_scAPC4_599 3'-Not1_scAPC4_652	5-CGCGGATCCATGAGGGGAGAAAACTATGAAAAC-3 5-GCAGTTACGTGCGGCCGCTCAAACATTTTGTTTTTCTTT-3
11	5'-BamH1_scAPC4_602 3'-BamH1_scAPC4_652	5-CGCGGATCCATGAACTATGAAAACGAGGAAGAT-3 5-CGCGGATCCTCAAACATTTTGTTTTTCTTT-3
12	5'-BamH1_scAPC4_611 3'-Not1_scAPC4_652	5-CGCGGATCCATGACAATAGCTATTCCTGCTTAC-3 5-GCAGTTACGTGCGGCCGCTCAAACATTTTGTTTTTCTTT-3
13	5'-Not1_scAPC4_1 3'-Xma1_scAPC4_583	5-GCAGTTACGTGCGGCCGCATGTCGTCTCCTATTAATGAT-3 5-GCAGTTACGTGCCCCGGGTCAAATATCCCGAAGCAAGCTAT-3
14	5'-Not1_scAPC4_1 3'-Xma1_scAPC4_600	5-GCAGTTACGTGCGGCCGCATGTCGTCTCCTATTAATGAT-3 5-GCAGTTACGTGCCCCGGGTCATCCCCTATAATCGGTGACGTG-3
15	5'-Not1_scAPC4_1 3'-BamH1_scAPC4_115	5-GCAGTTACGTGCGGCCGCATGTCGTCTCCTATTAATGAT-3 5-CGCGGATCCTCAGTTACATGCAAAATCTCGATT-3
16	5'-BamH1_scAPC4_1 3'-Not1_scAPC4_110	5-CGCGGATCCATGTCGTCTCCTATTAATGAT-3 5-GCAGTTACGTGCGGCCGCTCATCGATTATTTGGTTCGTATCT-3
17	5'-Not1_scAPC4_116 3'-Xma1_scAPC4_652	5-GCAGTTACGTGCGGCCGCATGATCATTGATGATTTACCAA-3 5-GCAGTTACGTGCCCCGGGTCAAACATTTTGTTTTTCTTT-3
18	5'-Not1_scAPC4_210 3'-Xma1_scAPC4_652	5-GCAGTTACGTGCGGCCGCATGTATGAGGATGGAACTGTACAA-3 5-GCAGTTACGTGCCCCGGGTCAAACATTTTGTTTTTCTTT-3
19	5'-Not1_scAPC5_1 3'-Xma1_scAPC5_685	5-GCAGTTACGTGCGGCCGCATGAGTAAGTATGGTCCATTG-3 5-GCAGTTACGTGCCCCGGGTCAAGTCATCTGAACATCCCT-3
20	5'-Not1_scAPC6_1 3'-Xma1_scAPC6_840	5-GCAGTTACGTGCGGCCGCATGAAGTTTTGTCTTTATTGC-3 5-GCAGTTACGTGCCCCGGGTTATTCCAGTTCCATATCTGC-3
21	5'-Not1_scAPC8_1 3'-Xma1_scAPC8_626	5-GCAGTTACGTGCGGCCGCATGAATGACGACAGCCAGGAT-3 5-GCAGTTACGTGCCCCGGGCTACATATGCCTTCTGCACTC-3
22	5'-Not1_scAPC9_1 3'-Xma1_scAPC9_266	5-GCAGTTACGTGCGGCCGCATGAACCAAAATGGTGATAAG-3 5-GCAGTTACGTGCCCCGGGTCAGAGAAACGAACTATCCTC-3
23	5'-Not1_spAPC4_1 3'-BamH1_spAPC4_719	5-AAGGAAAAAAGCGGCCGCATGGTGTCAAAATCTTTCAAA-3 5-TTTCGCGGATCCTTAAAAAAGAGAATAAACGATA-3
24	5'-Not1_spAPC4_1 3'-BamH1_spAPC4_145	5-AAGGAAAAAAGCGGCCGCATGGTGTCAAAATCTTTCAAA-3 5-TTTCGCGGATCCTTAACCAAGTAAAGGCATATATGC-3
25	5'-Not1_spAPC4_146 3'-BamH1_spAPC4_719	5-AAGGAAAAAAGCGGCCGCATGACACTTCCTAGTTCGGCAAAA-3 5-TTTCGCGGATCCTTAAAAAAGAGAATAAACGATA-3
26	5'-Not1_spAPC4_1 3'-BamH1_spAPC4_494	5-AAGGAAAAAAGCGGCCGCATGGTGTCAAAATCTTTCAAA-3 5-TTTCGCGGATCCTTACTTGAGAGAATAATAATC-3
27	5'-Not1_spAPC4_495 3'-BamH1_spAPC4_719	5-AAGGAAAAAAGCGGCCGCATGGATTTTGCAAATCAAGAC-3 5-TTTCGCGGATCCTTAAAAAAGAGAATAAACGATA-3

Nr.	Primer pair	Sequence
28	5'-BamH1_hAPC2_497 3'-EcoR1_hAPC2_822	5-TTTCGCGGATCCATGCTCCAAGCGGCGTTCATC-3 5-CCGGAATTCTCAGCTGCAGTTCTTGGGCAG-3
29	5'-EcoR1+1_hAPC2_554 3'-EcoR1_hAPC2_822	5-CCGGAATTCCATGCACTTCTGTGAAGTCATG-3 5-CCGGAATTCTCAGCTGCAGTTCTTGGGCAG-3
30	5'-Nde1_hAPC11_1 3'-Not1_hAPC11_84	5-GCAGTTACGTCATATGATGAAGGTGAAGATTAAGTGC-3 5-GCAGTTACGTGCGGCCGCGGGCCTCACTCCTTGAACTTC-3
31	5'-Not1_hAPC4_1 3'-Xma1_hAPC4_809	5-GCAGTTACGTGCGGCCGCATGTTGCGTTTTCCGACCTGT-3 5-GCAGTTACGTGCCCCGGGTTAGGAGTCTAGCTCAGGGTC-3
32	5'-Not1_hAPC7_1 3'-Kpn1_hAPC7_565	5-AAGGAAAAAAGCGGCCGCATGAATGTGATAGACCACGTG-3 5-AAGGAAAAGGTACCTCACTGCATGCCGAACCAC-3
	Mutated primer pair	
33	5'-pABlOmut$^{M/I}$ 3'-pABLOmut$^{M/I}$	5-AACTTAAGAAGGAGATATACATATCAAGCTTTCTA-3 5-TAGAAAGCTTGATATGTATATCTCCTTCTTAAGTT-3
34	5'-BamH1_scCdc4_271 3'-scCdc4$^{S464A/T465V}$	5-CGCGGATCCATGAAGAGGGACCTAATAACG-3 5-TACTATATCTAGGCACCTCACCACAGCGTTATGACCTTTAAACACATG-3
35	5'-scCdc4$^{S464A/T465V}$ 3'-EcoR1_scCdc4_779	5-CATGTGTTTAAAGGTCATAACGCTGTGGTGAGGTGCCTAGATATAGTA-3 5-CCGGAATTCTCATGGTATTATAGTTGTCCTCG-3
36	5'-BamH1_scCdc4_271 3'-scCdc4$^{R443M/S464A/T465V}$	5-CGCGGATCCATGAAGAGGGACCTAATAACG-3 5-AATATCCCAAACTCGCACCGTCATGTCTGTAGAACCGCTGACTAAAAT-3
37	5'-scCdc4$^{R443M/S464A/T465V}$ 3'-EcoR1_scCdc4_779	5-ATTTTAGTCAGCGGTTCTACAGACATGACGGTGCGAGTTTGGGATATT-3 5-CCGGAATTCTCATGGTATTATAGTTGTCCTCG-3
38	5'-Not1_scAPC4_1 3'-scAPC4_Δ594-601	5-GCAGTTACGTGCGGCCGCATGTCGTCTCCTATTAATGAT-3 5-TCTTCCTCGTTTTCATAGTTGCTACTATGATAGTTACTAT-3
39	5'-scAPC4_Δ594-601 3'-Xma1_scAPC4_652	5-ATAGTAACTATCATAGTAGCAACTATGAAAACGAGGAAG-3 5-GCAGTTACGTGCCCCGGGTCAAACATTTTGTTTTTCTTT-3
40	5'-Not1_scAPC4_1 3'-scAPC4_Δ594-610	5-GCAGTTACGTGCGGCCGCATGTCGTCTCCTATTAATGAT-3 5-TAAGCAGGAATAGCTATTGTGCTACTATGATAGTTACTAT-3
41	5'-scAPC4_Δ594-610 3'-Xma1_scAPC4_652	5-ATAGTAACTATCATAGTAGCACAATAGCTATTCCTGCTTA-3 5-GCAGTTACGTGCCCCGGGTCAAACATTTTGTTTTTCTTT-3

Table 7.2. Vector constructs used in this work.

Vector	Description	Primer pair, (Table 7.1)	Reference
pABLOmut_Fbw7$^{232-707}$-Skp1	Skp1 contains two internal deletion (Schulman et al., 2000)	1, 4	this work
pABLOmut_Fbw7$^{263-707}$-Skp1	Skp1 contains two internal deletion (Schulman et al., 2000)	2, 4	this work
pABLOmut_Fbw7$^{279-707}$-Skp1	Skp1 contains two internal deletion (Schulman et al., 2000)	3, 4	this work
pMagE_Fbw7$^{232-707}$		5	this work
pMagE_Fbw7$^{279-707}$		6	this work
pVL1393_hSkp1	Skp1 contains two internal deletion (Schulman et al., 2000)	-	Schulman
pVL1393_scSkp1	Contains no deletions	-	Schulman
pAcG2T_scCdc4$^{271-779}$		-	Schulman
pAcG2T_scCdc4$^{271-779}$ (S464A/T465V)	Contains 2-point mutation	34, 35	this work
pAcG2T_scCdc4$^{271-779}$ (R443M/S464A/T465V)	Contains 3-point mutation	34, 35, 36, 37	this work
pET15b_Sic1$^{1-100}$	7 Cdk consensus sites	-	Hao
pMagE_hAPC2		-	Song
pAcG2T_hAPC2$^{497-822}$		28	this work
pABLO_hAPC2$^{554-822}$-hAPC11		29, 30	this work
pVLSO_hAPC4		31	this work
pMagE_hAPC7		32	this work
pMagE_hAPC10		-	Song
PMagE_hAPC11		-	Song
pVLSO_spAPC4		23	this work
pVLSO_spAPC4$^{1-145}$		24	this work
pVLSO_spAPC4$^{146-719}$		25	this work
pVLSO _spAPC4$^{1-494}$		26	this work
pVLSO _spAPC4$^{495-719}$		27	this work
pVLSO_scAPC1		7	this work
pMagE_scAPC2		-	Song
pVLSO_scAPC4		8	this work
pABLO_scAPC4$^{594-652}$		9	this work
pABLO_scAPC4$^{599-652}$		10	this work
pABLO_scAPC4$^{602-652}$		11	this work
pABLO_scAPC4$^{611-652}$		12	this work
pVLSO_scAPC4$^{1-583}$		13	this work
pVLSO_scAPC4$^{1-600}$		14	this work
pMagE_scAPC4$^{1-115}$		15	this work
pABLOmut_scAPC4$^{1-110}$		16	this work
pVLSO_scAPC4$^{116-652}$		17	this work
pVLSO_scAPC4$^{210-652}$		18	this work
pVLSO_scAPC4$^{\Delta 594-601}$	scAPC4 with internal deletion 594-601	38, 39	this work
pVLSO_scAPC4$^{\Delta 594-610}$	scAPC4 with internal deletion 594-610	40, 41	this work
pVLSO_scAPC5		19	this work
pVLSO_scAPC6		20	this work
pVLSO_scAPC8		21	this work
pVLSO_scAPC9		22	this work
pAcG2T_scAPC10		-	Song
pAcG2T_scAPC11		-	Song

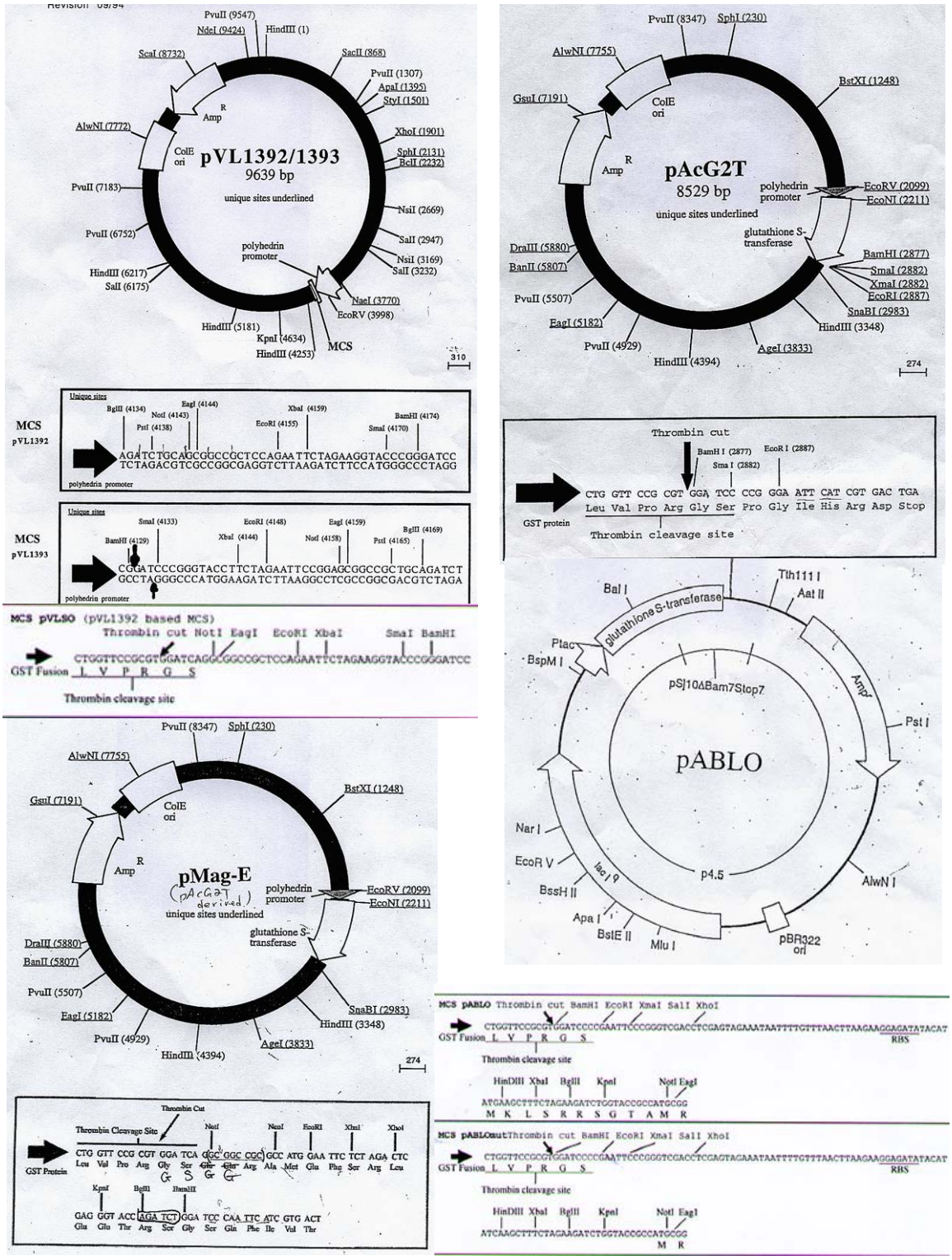

Figure 7.1. Vectors used in this work.

8. Curriculum vitae

Personal data

Family name:	Schumann
First name:	Stephanie
Date of birth:	13. 04. 1977
Place of birth:	Wippra, Germany
Nationality:	German
Personal status:	married (9.9.2006)
Children:	Sophie R.I. Oehlmann (18. 05. 2005),
	Albert G.B. Schumann (29. 12. 2006)

Education

1983-1991	Fritz-Weineck-Oberschule
1991-1995	Novalis-secondary school
06/1995	Abitur

Studies

1995-2000	Study of biochemistry/biotechnology at the Martin-Luther-University Halle/Wittenberg
	07/1998-10/1998 sommer student at the University of Toronto in the field of Protein crystallisation
	10/1999-09/2000 Diploma work on the "Characterization of two soft tissue sarcoma cell lines with p53 mutations in their response on radiation and chemotherapeutic treatment" in the research group of Prof. Dr. Taubert, Instiute of pathology, Martin Luther University.
09/2000	Dipl.Biochemikerin/Biotechnologin [mark:1,0]
11/2000-3/2006	Ph.D. Thesis on „Structure Determination and Biochemical Characterization of the Protein Ubiquitin Ligases SCF^{Fbw7} and APC" in the research group of Prof. Dr. Pavletich, Memorial Sloan Kettering Cancer Center.